Indoor Collaborative Positioning based on a Multi-sensor and Multi-user System

Hao Jing

B.Sc.

Thesis submitted to the University of Nottingham for the degree of Doctor of Philosophy

December 2015

Abstract

With recent developments in the Global Satellite Navigation Systems (GNSS), the applications and services of positioning and navigation have developed rapidly worldwide. Location-based services (LBS) have become a big application which provide position related services to the mass market. As LBS applications become more popular, positioning services and capacity are demanded to cover all types of environment with improved accuracy and reliability.

While GNSS can provide promising positioning and navigation solutions in open outdoor environments, it does not work well when inside buildings, in tunnels or under canopy. Positioning in such difficult environments have been known as the indoor positioning problem. Although the problem has been looked into for more than a decade, there currently no solution that can compare to the performance of GNSS in outdoor environments.

This thesis introduces a collaborative indoor positioning solution based on particle filtering which integrates multiple sensors, e.g. inertial sensors, Wi-Fi signals, map information etc., and multiple local users which provide peer-to-peer (P2P) relative ranging measurements. This solution addresses three current problems of indoor positioning. First of all is the positioning accuracy, which is limited by the availability of sensors and the quality of their signals in the environment. The collaborative positioning solution integrates a number of sensors and users to provide better measurements and restrict measurement error from growing. Secondly, the reliability of the positioning solutions, which is also affected by the signal quality. The unpredictable behaviour of positioning signals and data could lead to many uncertainties in the final positioning result. A successful positioning system should be able to deal with changes in the signal and provide reliable positioning results using different data processing strategies. Thirdly, the continuity and robustness of positioning solutions. While the indoor environment can be very different from one another, hence applicable signals are also different, the positioning solution should take into account

the uniqueness of different situations and provide continuous positioning result regardless of the changing datWith recent developments in the Global Satellite Navigation Systems (GNSS), the applications and services of positioning and navigation have developed rapidly worldwide. Location-based services (LBS) have become a big application which provide position related services to the mass market. As LBS applications become more popular, positioning services and capacity are demanded to cover all types of environment with improved accuracy and reliability.

While GNSS can provide promising positioning and navigation solutions in open outdoor environments, it does not work well when inside buildings, in tunnels or under canopy. Positioning in such difficult environments have been known as the indoor positioning problem. Although the problem has been looked into for more than a decade, there currently no solution that can compare to the performance of GNSS in outdoor environments.

This thesis introduces a collaborative indoor positioning solution based on particle filtering which integrates multiple sensors, e.g. inertial sensors, Wi-Fi signals, map information etc., and multiple local users which provide peer-to-peer (P2P) relative ranging measurements. This solution addresses three current problems of indoor positioning. First of all is the positioning accuracy, which is limited by the availability of sensors and the quality of their signals in the environment. The collaborative positioning solution integrates a number of sensors and users to provide better measurements and restrict measurement error from growing. Secondly, the reliability of the positioning solutions, which is also affected by the signal quality. The unpredictable behaviour of positioning signals and data could lead to many uncertainties in the final positioning result. A successful positioning system should be able to deal with changes in the signal and provide reliable positioning results using different data processing strategies. Thirdly, the continuity and robustness of positioning solutions. While the indoor environment can be very different from one another, hence applicable signals are also different, the positioning solution should take into account the uniqueness of different situations and provide continuous positioning result regardless of the changing data.

The collaborative positioning aspect is examined from three aspects, the network geometry, the network size and the P2P ranging measurement accuracy. Both theoretical and experimental results indicate that a collaborative network with a low dilution of precision (DOP) value could achieve better positioning accuracy. While increasing sensors and users will reduce

DOP, it will also increase computation load which is already a disadvantage of particle filters. The most effective collaborative positioning network size is thus identified and applied. While the positioning system measurement error is constrained by the accuracy of the P2P ranging constraint, the work in this thesis shows that even low accuracy measurements can provide effective constraint as long as the system is able to identify the different qualities of the measurements.

The proposed collaborative positioning algorithm constrains both inertial measurements and Wi-Fi fingerprinting to enhance the stability and accuracy of positioning result, achieving metre-level accuracy. The application of collaborative constraints also eliminate the requirement for indoor map matching which had been a very useful tool in particle filters for indoor positioning purposes. The wall constraint can be replaced flexibly and easily with relative constraint.

Simulations and indoor trials are carried out to evaluate the algorithms. Results indicate that metre-level positioning accuracy could be achieved and collaborative positioning also gives the system more flexibility to adapt to different situations when Wi-Fi or collaborative ranging is unavailable. a.

The collaborative positioning aspect is examined from three aspects, the network geometry, the network size and the P2P ranging measurement accuracy. Both theoretical and experimental results indicate that a collaborative network with a low dilution of precision (DOP) value could achieve better positioning accuracy. While increasing sensors and users will reduce DOP, it will also increase computation load which is already a disadvantage of particle filters. The most effective collaborative positioning network size is thus identified and applied. While the positioning system measurement error is constrained by the accuracy of the P2P ranging constraint, the work in this thesis shows that even low accuracy measurements can provide effective constraint as long as the system is able to identify the different qualities of the measurements.

The proposed collaborative positioning algorithm constrains both inertial measurements and Wi-Fi fingerprinting to enhance the stability and accuracy of positioning result, achieving metre-level accuracy. The application of collaborative constraints also eliminate the requirement for indoor map matching which had been a very useful tool in particle filters for indoor positioning purposes. The wall constraint can be replaced flexibly and easily with relative constraint.

Simulations and indoor trials are carried out to evaluate the algorithms. Results indicate that metre-level positioning accuracy could be achieved and collaborative positioning also gives the system more flexibility to adapt to different situations when Wi-Fi or collaborative ranging is unavailable.

Acknowledgements

I can still see myself walk through the front door of NGB on my first day in Nottingham. At last, this long journey has come to an end. With joy, with stress, with tears, but mostly, with gratitude.

I would like to sincerely thank my supervisors, Prof. Terry Moore, Dr. Chris Hill, Dr. James Pinchin, and also Dr. Chris Hide who had left Nottingham during my second year. Without their constructive advice and insightful suggestions, I would not be where I am today. Dr. Hide and Dr. Pinchin had spent many hours sitting with me, patiently going through problems and answering my bizarre questions. My supervisors have also allowed me the freedom to search in the field of my interest, giving me the opportunity of completing research independently and freely.

I would also like to thank my internal and external examiners, Dr. Xiaolin Meng and Dr. Ramsey Faragher, both of whom have helped me greatly through my PhD, giving me guidance and valuable advice.

Of course, I haven't forgotten all the people that I have met here in NGI and around the university. Without you, life in Nottingham would have been very different. Mrs Alison Mellor, who has helped me greatly with all the complicated forms and paperwork from day one. Mr. Sean Ince, Dr. Lukasz Bonenberg and Mr. Nick Kokkas have assisted me endlessly with all the dirty work of trials and experiments, preparing equipments, surveying and logging data. Mrs Jessica Shi, who has made lunchtime the best thing to look forward to. I would not forget all the helping hands from Mr. Yang Gao, Dr. Mustafa Amani...too many people that it just seems impossible to list every name here. But nevertheless, I sincerely thank everyone of you.

A very special thank you to my housemates, Dr. Xujuan Zheng and very-soon-to-be-Dr. Xiao Feng. I would never forget the many hours we have spent together in our home and the special treats after your "cooking operations". And the Chinese New Years that we have had together.

Finally, and most of all, I would like to thank my family. Without my parents I would not have had the courage to be here and achieve this PhD.

Mr Jieming Niu, my husband, who has helped me, supported me through my toughest times. Thank you for always being by my side.

September, 2015

Contents

List of Figures

List of Tables

Nomenclature

AOA Angle-of-arrival

AP Access Point

ARCP Adaptive Ranging Constraint Collaborative Positioning

BDS BeiDou Navigation Satellite System

BLE Bluetooth Low Energy

BU Base Unit

c-WiDB Collaborative Wi-Fi Fingerprint Database Training

cdf Cumulative Distribution Function

CFPM Collaborative Fingerprint Mapping Positioning

CHAIN Cardinal Heading Aided for Inertial Navigation

CP Collaborative Positioning

CPF Collaborative Positioning Particle Filter

CRLB Cramer Rao Lower Bound

CRS Coordinate Reference Systems

DOP Dilution of Precision

DP Direct Path

DR Dead Reckoning

ECEF Earth-Centred Earth-Fixed

EKF Extended Kalman Filter

FCC Federal Communications Commission

FIM Fisher Information Matrix

FP Fingerprinting

GAGAN GPS Aided Geo-Augmented Navigation system

GNSS Global Navigation Satellite Systems

GP Gaussian Process

GPR Gaussian Process Regression

GPX GPS Exchange Format

i.i.d. Indepedent and Identically Distributed

IEEE Institute of Electrical and Electronics Engineers

IERS International Earth Rotation Service

IMES Indoor Messaging System

IMU Inertial Measurement Unit

IPS Indoor Positioning System

IR Impulse Radio

ITRF International Terrestrial Reference Frame

k-NN k-Nearest Neighbour

KF Kalman Filter

LBS Location Based Services

LOS Line-of-sight

LQE Linear Quadratic Estimation

MC Monte Carlo

MC Multi-carrier

MDOP Modified Dilution of Precision

MEMS Micro-machined Electromechanical System

MU Mobile Unit

NDP Non-Direct Path

NGB Nottingham Geospatial Building

NGI Nottingham Geospatial Institute

NLOS Non-Line-of-Sight

P2P Peer-to-Peer

pdf Probability Density Function

PDR Pedestrian Dead Reckoning

PF Particle Filter

QZSS Quasi-Zenith Satellite System

RF Radio Frequency

RFID Radio Frequency Indentification

RQI Ranging Quality Indicator

RSS Received Signal Strength

RSSI Relative Signal Strength Indicator

RTOF Round-Time-Of-Flight

s-DB Static Fingerprint Database

SARCP Selective Adaptive Range Constraint Collaborative Positioning

SIS Sequential Importance Sampling

SLAM Simultaneous Localisation and Mapping

SMC Sequential Monte Carlo

SNR Signal-to-Noise Ratio

SOOP Signals Of OPportunity

TDOA Time-Difference-Of-Arrival

TOA Time-Of-Arrival

TP Training Points

UKF Unscented Kalman Filter

UWB Ultra-Wide Band

WARCP Wi-Fi integrated Adaptive Ranging Collaborative Positioning

WGS 84 World Geodetic System 1984

WLAN Wireless Local Area Network

WPAN Wireless Personal Area Network

ZUPT Zero Velocity Updates

Chapter 1
Introduction

1.1 Overview

The application of positioning technology has accelerated immensely during the past decades due the rapid development of global navigation satellite systems (GNSS). Following the American GPS and Russian GLONASS systems, many countries and regions have also begun building their own navigation satellite systems, such as the Chinese BeiDou Navigation Satellite System (BDS), European Galileo, Japanese Quasi-Zenith Satellite System (QZSS) and Indian GPS aided geo-augmented navigation system (GAGAN). Location based services (LBS), which rely greatly on positioning and navigation technology, have thrived and quickly extended from military and governmental applications to civil applications. From locating miners and firefighters during a rescue search, to searching for local restaurants and guiding passengers to the next terminal in an international airport, tracking goods on a delivery fleet or tracking people in special need, the interest in the "positions" of people and objects has greatly increased.

However, the working environment of GNSS positioning is limited to outdoors where the receiver has a clear view of the sky. To avoid interference to other wireless signals, satellite signals have a very low power. Therefore, signals can be easily disrupted or blocked when receivers are placed under thick foliage or amongst tall buildings, known as urban canyons. These disruptions can cause signal attenuation, refraction and multipath, which often lead to large positioning errors. Furthermore, if the receiver is placed inside a building or a tunnel, it will not be able to receive any signal at all. Even if some signals do manage to reach the receiver, it is very likely that it is contaminated by multipath and interference caused by the myriad of walls, furniture and moving pedestrians in the environment. These problems can be summarised as "indoor positioning" problems, even though the receiver may not really be "indoors". For example, for positioning purposes, being inside a tunnel or forest is very much like being inside a building. A wide range of research has been dedicated to the topic

with the aim of achieving ubiquitous positioning where systems would no longer be challenged by GNSS-denied environments.

Ubiquitous positioning consists two main problems: the transition between the outdoor and indoor positioning modes, and the lack of accurate indoor positioning solutions. The work in this thesis will mostly focus on the latter, indoor positioning. While indoor positioning has been researched from many different angles and many technologies have been proposed to provide positioning solutions, indoor positioning still remains a research problem due to its complexity and rapid changes in the environment.

1.1.1 Indoor positioning technologies

Due to the differences between indoor environments, there is currently no perfect solution for all conditions. Based on the equipment used, indoor positioning systems can be categorised into infrastructure-less positioning systems, ad-hoc infrastructure systems and infrastructure-based positioning systems.

Inertial navigation systems (INS) are popular infrastructure-less systems that can provide navigation solutions in any environment based on dead reckoning (DR) solutions. It is commonly integrated with GNSS and used in aircraft, marine, land vehicle navigation and a number of control systems (Gray and Maybeck, 1995; Hide et al., 2004). INS/GNSS integration enables INS to provide backup during occasional GNSS signal outage. In safety-of-life applications, high-grade INS is usually applied to ensure accuracy and robustness. However, the situation is very different indoors. GNSS signals are not available in indoor environments, therefore INS measurements would not be corrected by GNSS. On the other hand, most indoor positioning systems are not targeted at high-end users. Therefore low-cost inertial measurement units (IMU) are usually used to bring down the cost of the system. While high quality INS measurements will drift after a certain period of time, the drift of low-cost units is even worse. With an heading error of more than 1° every second, this could lead to severe positioning errors of hundreds of metres after a few minutes (Godha, 2006).

In IMU based pedestrian navigation, the IMU is most commonly attached onto the user's shoe (Foxlin, 2005). As the human walking phase consists of cycles of repeated movement which can be characterised and

detected; the measurements are collected at each step to provide an estimation of the step length and walking direction (Stirling et al., 2003; Kim et al., 2004; Beauregard, 2007). Recent work has also started to investigate mounting the IMU on to the waist, knees and other parts of the body (Lo et al., 2011; Altun and Barshan, 2012; Park et al., 2012; Rantakokko et al., 2014). The basic idea is to detect the body movement from the inertial measurements, identify step cycles and navigate the user based on the inertial measurements. While various correction algorithms have been proposed to correct the inertial measurement, several methods have also been applied to correct measurements through integration.

Wireless signal networks, such as the wireless local area network (WLAN), are regarded as ad-hoc infrastructure based systems as they are not originally positioning dedicated systems. But they can be applied in positioning and as the wireless network infrastructure is already implemented to provide internet connection, it is, therefore a low-cost method that is easy to maintain. Wi-Fi is a trademark name of the Wi-Fi Alliance, which defines a typical WLAN technology that connects devices onto the internet, based on the Institute of Electrical and Electronics Engineers' (IEEE) 802.11 standards. Over the past decade, Wi-Fi coverage has grown remarkably and is now found in many indoor environments. Researchers have taken advantage of this available signal and its applications in positioning are now almost as well-known as its applications for internet connections (Wang et al., 2003; Honkavirta et al., 2009; Jung et al., 2011). However, positioning accuracy is limited, as it was not designed for the purpose of positioning and navigation.

Meanwhile, other wireless signals such as Bluetooth, ZigBee and Ultra-Wideband (UWB) have been applied to indoor positioning with similar methods to Wi-Fi positioning (Hossain and Soh, 2007; Subhan et al., 2011; Alhmiedat et al., 2013; Koppanyi et al., 2014). Like Wi-Fi, the positioning accuracy of Bluetooth is rather limited due to signal instability. Although accurate positioning can be achieved from UWB systems, but a dedicated infrastructure has to be set up and this can be expensive to implement and maintain.

While GNSS navigation serves well outdoors, the barrier to implementing it indoors is that GNSS signals are lost inside. Regarding this problem, researchers have begun to look at different ways of bringing GNSS signals inside. Pseudolites, as their name suggests, are like GNSS satellites that are set up inside buildings and transmit GNSS signals to provide positioning in

similar ways to GNSS outside (Wang, 2002; Kennedy, 2005; Niwa et al., 2008). The Locata system is a pseudolite system, but instead transmits signals on the 2.4GHz frequency, which is the same as Wi-Fi and Bluetooth (Khan et al., 2010). However, a major problem with pseudolites is that because they transmit "fake" GNSS satellites signals, they can actually interfere with or even jam real GNSS signals which is a threat to many GNSS-dependent applications.

As so many different information sources are available indoors, less traditional signals have also been explored for positioning purposes, such as using light and sound (Minami et al., 2004; Medina et al., 2013; Fox, 2014; Jadhav, 2014). The recent introduction of Li-Fi, which provides wireless connection using visible light, has also drawn the attention of navigation researchers, and it is possible that this technology may also be applied to indoor positioning (Jadhav, 2014).

The wireless signal based methods mentioned above achieve positioning through range-based methods, i.e. positioning is achieved by measuring the distance between the receiver and transmitter unit. Another type of method is the proximity based positioning. Such methods are achieved by placing Radio Frequency identification (RFID) tags on objects or places of interest and trying to detect the tags using receivers or scanners (Bouet and dos Santos, 2008; Han et al., 2009; Hasani et al., 2014). Other proximity estimation techniques are provided by vision aided methods, such as scanning barcodes or QR codes to identify locations that have been marked by specific codes (Mulloni et al., 2009). Such methods require the provider to set up a dedicated infrastructure to perform positioning and the positioning accuracy is completely reliant on the density of the tags. Simultaneous localisation and mapping (SLAM) was originally developed for robotic navigation where navigation solution is vision based or high-accuracy ranging based. Robots, or the users, can estimate their location and measure its local environment at the same time. SLAM achieves navigation when no dedicated infrastructure is available.

As previously mentioned, indoor environments are complicated and prone to change. No sensor is able to provide positioning in all situations alone. To cope with the uncertainty of indoor environments and overcome limitations of any individual sensor, numerous multi-sensor integrated systems have been introduced. While INS can be integrated with GPS to provide continuous positioning in urban areas (Feng et al., 2013), a popular indoor positioning combination is INS and Wi-Fi integration (Evennou and

Marx, 2006). In urban areas, Wi-Fi has also been integrated with GPS and other sensors to provide aid when navigating in difficult environments (Weyn and Schrooyen, 2008; Spinella et al., 2010; Li et al., 2011). Multi-sensor systems have thrived due to their ability to provide positioning in a wider area. The combination of different sensors has extended the application range of the original single sensor system and has also provided measurement corrections to improve system robustness.

1.1.2 Indoor positioning applications

Indoor positioning systems comes in all shapes and sizes, depending on the requirements for accuracy, convenience and cost. For security and life-critical related applications, such as tracking firefighters and miners, a highly reliable and accurate infrastructure-less system is required. Such systems would depend on inertial measurements and reliable measurement corrections (Nilsson et al., 2014).

Commercial applications, such as those for airports, shopping malls, campuses and business sites, require a long-lasting and reliable system to provide users with sufficient accuracy. Therefore a dedicated infrastructure is usually required. The Bat system designed by AT&T Laboratories in Cambridge University is a 3D ultrasonic location system that achieves centimetre level positioning accuracy when sufficient "Bats" (which are hundreds or thousands of small transmitters) are placed in the building (Ward et al., 1997; Woodman and Harle, 2010). A similar indoor localisation system, Cricket, was also developed at MIT (Priyantha et al., 2000; Priyantha, 2005). Like the BAT system, Cricket also requires a number of beacons to be placed in the environment; these beacons transmit both on Radio Frequency (RF) channels and through ultrasonic pulses. Receivers listen to this information and achieve centimetre level ranging and positioning accuracy. The first Wi-Fi based localisation and tracking system, RADAR, was proposed by Bahl and Padmanabhan (2000). Authors here started looking at the localisation potentials by extracting information from wireless signal strength patterns. Following RADAR, further RF-based positioning systems have emerged, such as Horus and COMPASS. While Horus continues to look at fingerprinting with low computational requirements, COMPASS integrates information from a digital compass with fingerprinting (Youssef and Agrawala, 2005; King et al., 2006). These systems achieve accuracy of a few metres.

Following these research advancements, commercial companies like

Skyhook and Ekahau have started to provide Wi-Fi positioning solutions for dedicated locations such as business buildings, schools and hospitals (Skyhook, 2014; Ekahau, 2014). Google Maps has also enabled Wi-Fi sensors to locate mobile devices when GPS is not available. The wide variety of applications that have already been used gives us an indication of how fast this technology is developing. However, these applications only promise an accuracy of 20m. Add-on tags would need to be implemented if higher accuracy were to be required.

While the mass market for indoor positioning is the general public, positioning needs to be achieved with low-cost equipments, as well as being easy to understand and implement. The mobile phone would be the best solution in this digital world (Chincholle et al., 2002; Wang et al., 2011). According to GSMA statistics, more than 7 billion global mobile connections are to be expected by the end of 2014 (GSMA Intelligence, 2014). Modern smartphones are fully equipped with inertial sensors, GPS chips, Wi-Fi and Bluetooth sensors, as well as a number of other sensors that may be useful for positioning, such as cameras, barometers, magnetometers and light sensors (Serra et al., 2010; Weninger et al., 2011; Nguyen and Zhang, 2013). This means that everyone that has access to mobile phones should be able to achieve positioning solutions. While they can position themselves, they can also update information onto a central server to provide positioning aid to other people. Such crowd-sourcing approaches have become popular in the open source community, as shared information is beneficial to everyone. A crowd-sourced mapping method is provided by Sensewhere™ which achieves indoor positioning with 10m accuracy.

While the demand for accurate ubiquitous positioning continues to rise with the growing number of LBS-related applications, a robust low-cost real-time solution for accurate metre level indoor positioning solution is still yet to come.

1.1.3 Problem statement

The introduction of LBS brings great convenience into our lives, enabling us to locate ourselves or find directions with our own smartphones. However, as the application becomes more popular, many users now not only require location information when outside, but also when they are inside buildings. Problems arise as the satellite signals which they rely on for positioning are

no longer available indoors. Although the interest in indoor positioning problems has grown and numerous applications have become available, but current solutions still cannot completely meet the user demands. Most methods lack the required accuracy. While some solutions can achieve metre-level accuracy, they require a dedicated infrastructure to be set up beforehand. This becomes very costly, and, as soon as the user is outside the coverage of the infrastructure, positioning would fail. Current indoor positioning solutions lack the ability to provide high accuracy positioning and continuous positioning between different environments, while also ensuring low cost.

Looking at the developments of positioning applications, although much progress has taken place in the indoor positioning community, but current positioning solutions have not taken full advantage of the availability of local users for crowd-sourcing or collaborative aiding to enhance performance. Moreover, each positioning system is still limited to certain working conditions, even integrated systems. More flexibility is required for the systems to achieve accurate and reliable positioning under different conditions. Although many researchers have investigated the integration of different sensors and collaborative positioning, most previous applications focused on crowd-sourcing data and coarse location information sharing (Kurazume and Hirose, 2000; Chan et al., 2006; Garello, Samson, Spirito and Wymeersch, 2012; Thompson and Buehrer, 2012; Groves, 2013a; Rosa et al., 2014; Nilsson et al., 2014). There is little research concerning the collaboration of users and base stations through relative ranging, hence current collaborative positioning among pedestrians lacks the ability to share more detailed and accurate positioning data between users. There is also no detailed analysis on effective selection of required information and efficient application of the collaborative information, especially for indoor pedestrian positioning.

1.2 Aims and objectives

The research undertaken in this thesis aims to develop a robust collaborative indoor positioning solution that is able to adapt to different situations, i.e. when the signal environment or available sensors change, by integrating local existing measurements. Main aims of this work are:

- Carry out research to improve the performance of sensor and user integration for collaborative positioning;
- Develop and analyse the performance of collaborative indoor posi-

tioning based on low-cost IMU and wireless sensors for pedestrian navigation and positioning.

As more mobile users and positioning sensors are becoming available in the indoor environment, collaboration between different sensors and users will enable positioning systems to adapt to different conditions more smoothly and achieve better positioning accuracy. The main contributions of this work focus on developing methods to identify and apply useful location-based information in the surrounding environment to achieve collaborative pedestrian indoor positioning.

1.2.1 Research objectives

The collaborative positioning method proposed here brings together all of the available sensors in the local indoor environment, including wireless signals and local users. Inertial measurements, map information, Wi-Fi signals and peer-to-peer (P2P) relative ranging measurements are discussed and integrated in the proposed method. More specifically, the objectives of this research are:

1. To investigate the properties of different sensors for indoor pedestrian navigation, i.e. IMU, Wi-Fi and UWB signals, analyse and evaluate current indoor positioning methods, especially various integration methods to constrain the inertial measurement error, including integration of IMU/Wi-Fi, IMU/map, IMU/ranging and IMU/Wi-Fi/ranging, understanding their advantages and disadvantages;

2. Identify the most effective collaborative network according to theoretical lower bounds and develop indication factors to reflect different network conditions based on the relative ranging accuracy, the network size and the network geometry;

3. To develop adaptive collaborative positioning algorithms based on particle filtering, where the inertial error constraint threshold is adjusted based on the real network conditions;

4. To develop an efficient and improved Wi-Fi fingerprinting method, where the human effort during the training phase is greatly reduced and positioning is achieved according to signal and fingerprint reliability.

5. Carry out simulations and trials for each proposed algorithm.

The positioning algorithms proposed in this thesis demonstrates that the adaptive collaborative positioning algorithm achieves enhanced positioning performance in the indoor environment so that it is accurate, time efficient, robust, reliable and low-cost. It is capable of providing positioning even when the environment is changing. Furthermore, the training process for Wi-Fi fingerprint based on the adaptive collaborative positioning also becomes much more time efficient and reliable.

1.2.2 Contributions

A collaborative positioning method dedicated to pedestrian indoor navigation has been developed, which addresses three major issues of indoor positioning today: accuracy, continuity and cost effectiveness. The inertial measurement error is reduced by integrating a choice of map information, Wi-Fi signals or relative ranging, based on what is available.

A collaborative network analysis tool has been developed based on a modified DOP, which analyses the network geometry, size and measurement accuracy. An adaptive collaborative positioning has been proposed which constrains measurement errors based on the network conditions. This enables positioning without prior knowledge of the environment, hence eliminating the need for building information and a Wi-Fi fingerprint database.

Wi-Fi has been integrated with ranging to enable continuous positioning where the environment is changing. Furthermore, with collaborative positioning available, the required work for the training phase of Wi-Fi fingerprinting is reduced. A confidence factor is also produced in the improved fingerprint database. Higher positioning accuracy and reliability can be obtained when fingerprinting is performed with the confidence factor. Robustness is further enhanced when this is integrated with collaborative ranging.

1.3 Outline

The basic structure of this thesis is outlined below. The next chapter gives the theoretical background of positioning and navigation, including a description of positioning systems and coordinate frames, the basic positioning concepts of inertial systems, wireless network signals and collaborative positioning. Several popular Bayesian filtering methods applied in navigation are also introduced here, including Kalman filtering and Particle filtering.

Chapter 3 introduces several indoor navigation algorithms based on different sensors, including pedestrian dead reckoning, map matching and fingerprinting. Fingerprint mapping, a new method of integrating IMU and Wi-Fi fingerprinting is also explained.

Chapter 4 proposes the concept of collaborative positioning that integrates a number of different sensors and users. The performance of the collaborative network is analysed from three aspects, the measurement accuracy, the network geometry and network size. Simulations are presented for each situation as evidence of different network performance. Ranging based collaboration is applied to both IMU based PDR and Wi-Fi fingerprinting.

Two particle filter based collaborative positioning algorithms, adaptive ranging collaborative positioning (ARCP) and selective adaptive ranging collaborative positioning (SARCP), are proposed in Chapter 5. A collaborative Wi-Fi database training and improved adaptive fingerprinting (WARCP) method is also introduced based on the collaborative positioning performance. Figure 1.1 shows a flowchart of the algorithms discussed and introduced in this thesis. The arrows indicate the order of the development of each algorithm based on the previous one.

Chapter 6 presents trials using real data for each proposed algorithm, the SARCP, ARCP with Wi-Fi and WARCP. The performance of each trial is analysed according to the positioning accuracy and overall robustness. WARCP is applied in the final trial to enhance positioning performance by integrating all available sensors and users, allowing the system to select the appropriate algorithm based on the changing situation.

Chapter 7 summarises the proposed collaborative indoor positioning algorithms and methods applied in this thesis. The contributions of the algorithms are highlighted and some points for improvement are also given. Results indicate that collaborative sensors and users can constrain inertial measurement errors more effectively when it is applied adaptively according to the collaborative measurement quality itself. This concept is applied in each proposed algorithm, ARCP, SARCP and WARCP. The collaboration between users has also been found to be very useful for training fingerprint database.

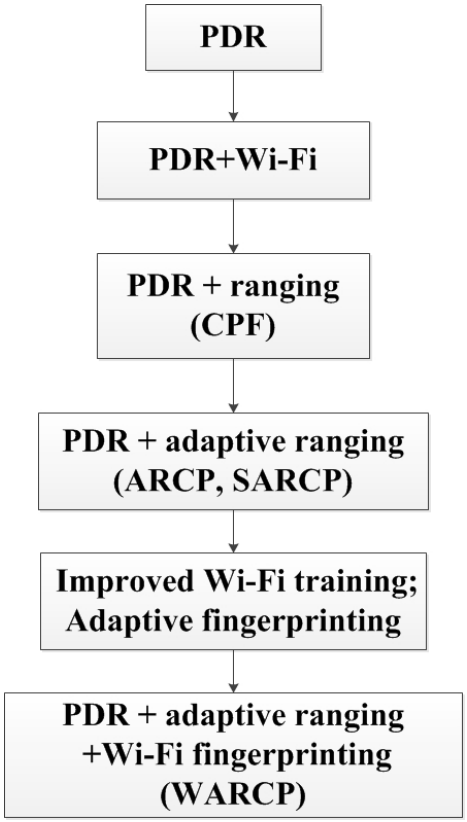

Figure 1.1: Summary of algorithms in the thesis

Chapter 2

Indoor positioning: An overview

2.1 Indoor positioning

While GNSS provides positioning and navigation solutions for outdoor environments, alternative methods must be used for indoor positioning due to lack of robust GNSS signals inside more complex environments. This is known as the indoor positioning problem and has become a highly popular topic within the navigation community. Indoor positioning refers to all positioning and navigation problems in GNSS-denied environments, i.e. inside buildings, under trees and in urban canyons etc. Indoor positioning systems (IPS) provide solutions that can achieve continuous real-time location of people or objects within a closed space through measurements relying on magnetic positioning, dead reckoning, other nearby anchors which either actively locate tags or provide ambient location or environment context for devices to get sensed (Youssef, 2008; Curran et al., 2011; Furey et al., 2012). While the positioning problem within indoor environments are the same regarding that there are no reliable GNSS signals, the actual problems for each environment and situation are unique and must be dealt with individually. Indoor positioning is generally more challenging than outdoor positioning due to this complexity. Different signals are found in different environments and the accuracy requirement will also differ for different applications. Some life critical situations will require high accuracy and reliability while high cost is acceptable. Other environment might consider low-cost low maintenance solutions only despite lower accuracy. This thesis aims to achieve a low-cost positioning solution for mobile device users with more promising accuracy.

The indoor environment is challenging for positioning because walls, furniture and other obstructions will disturb the signal due to multipath, non-line-of-sight (NLOS), signal attenuation and scattering, rapid variation due to moving pedestrian and changing furniture layout. On the other hand, due to the compact spacing inside buildings, higher positioning accuracy is required. Due to the complexity of indoor environments and

its problems, there is currently no available positioning solution in such environments that could compete with the performance level of GNSS positioning in an open outdoor environment, i.e. high accuracy, high availability, high integrity and low user cost (Rainer Mautz, 2012). With recent developments in manufacturing, computer technology and wireless communications, low-cost inertial sensors, e.g. accelerometer in mobile phones, and wireless network signals, e.g. RFID, Wi-Fi network and Bluetooth communication, have become widely available in most urban areas, i.e. GNSS-challenged environments. Therefore, these sensors are commonly used for indoor positioning. A brief introduction to all current indoor positioning methods are outlined in the following sections. The reference system is discussed first.

2.1.1 Coordinate systems

For a meaningful output, positioning and navigation results are expressed based on a common reference system, which defines the origin and the orientation of the axes of the system, as well as the mathematical and physical models. The reference frame is the realisation of a reference system through observations and measurements. Orthogonal reference systems are most commonly seen in positioning which has six degrees of freedom, including the position of the origin o, the orientation of the axes x, y and z. Reference systems commonly apply the *orthogonal right-handed convention*, where the three axes are always oriented in such a way that when the thumb and first two fingers of the right hand are extended perpendicularly, the thumb is the x-axis, the index finger is the y-axis and the middle finger is the z-axis.

Two fundamental reference systems are commonly applied in navigation problems and are specified here, i.e. the space-fixed celestial reference system and the Earth-centred Earth-fixed (ECEF) terrestrial reference system. The celestial reference system represents an approximation to an inertial system which describes the motion of the Earth and other bodies in space. It is not strictly an inertial system because it is affected by the annual revolution. We will only introduce the ECEF reference system here as it rotates with the Earth and is commonly used to describe motions on the Earth, as shown in Figure 2.1. This is a three dimensional geocentric coordinate system which is realised by the International Terrestrial Reference Frame (ITRF) that is maintained by the International Earth Rotation Service (IERS) (Seeber, 1993; Torge and Muller, 2012). The system orientation changes with respect to Earth's solid body as well as time. The

system origin is in the Earth's centre of mass, Z-axis directed towards a conventional mean North pole, X- and Y-axes lies on the mean equatorial plane that is perpendicular to Z-axis. The XZ-plane is generated by the mean meridian plane of Greenwich. Y-axis is directed so the system is a right-handed system.

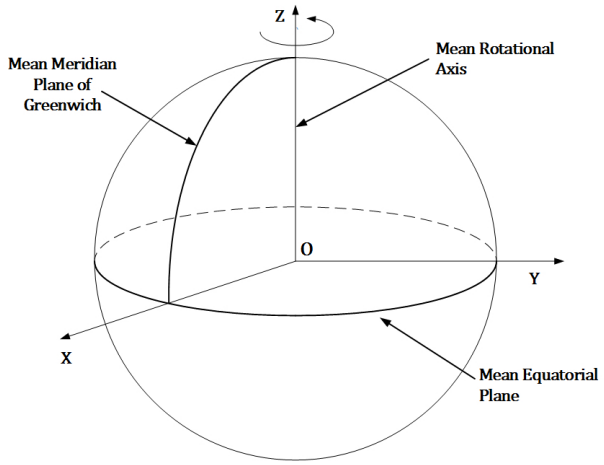

Figure 2.1: Earth-fixed terrestrial system (Source: Torge and Muller (2012))

To describe positions and locate geographical features in a reference system, coordinate reference systems (CRS) are defined that is coordinate-based regional or global systems which defines a specific map projection and the transformation between different reference systems. ECEF coordinates may be expressed by Cartesian coordinates (X, Y, Z) or ellipsoidal coordinates (φ, λ, r), which represent points in a three-dimensional space. The relationship between the two coordinates is as shown in Figure 2.2. φ and λ are the latitude and longitude from the ellipsoid and r is the ellipsoidal height. A note here is that as the Earth is an ellipsoid in reality, thus the centre of the ellipsoidal coordinates will not lie on the origin of the Cartesian coordinates.

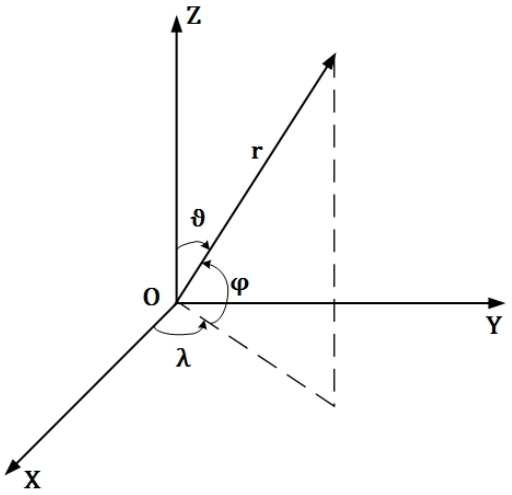

Figure 2.2: Cartesian and ellipsoidal coordinates (Source: Torge and Muller (2012))

Different reference frames are implemented for different positioning and mapping purposes. The World Geodetic System 1984 (WGS 84) is a geocentric terrestrial reference system used for GPS that was developed by the U.S. Department of Defence. It is globally consistent and consists of a standard coordinate system for the Earth, a standard spheroidal reference surface for altitude, and the geoid which defines the nominal sea level. GPS related position data are defined in the WGS 84 reference frame. The refined WGS 84 frame introduced in 2002 agrees with ITRF2000 at centimetre level. Local reference frames refers to a coordinate system that defines a consistent reference over a small region within the global coordinate system. The Ordnance Survey national grid reference system is a geographic grid reference used in Great Britain. The grid is based on the OSGB36 datum which is a coordinate system and set of reference points that is the regional best fit for Great Britain.

2.1.1.1 Inertial coordinate frames

To describe a navigation problem, at least two reference frames are usually applied: an object frame that describes the motion of the moving body and a reference frame that describes a known body relative to the moving body. To integrate positioning results from different systems, results must be expressed in the same reference frame and coordinates. Several common reference frames are listed here (Rogers, 2007).

- Earth-Centred Inertial frame (i-frame): the i-frame is a space fixed reference frame, centred at the Earth's centre of mass and axes are

non-rotating with respect to the fixed stars, defined by the axes Ox_i, Oy_i, Oz_i, with Oz_icoincident with the Earth's polar axis. $x-$ and $y-$axes lie within the equatorial plane, but do not rote with the Earth.

- Earth-Centred Earth-fixed frame (e-frame): origin at the centre of the Earth and axes are fixed with respect to the Earth, defined by Ox_e, Oy_e, Oz_e, with Oz_ealong the Earth's polar axis, Ox_e points from the centre to the intersection of the plane of the Greenwich meridian with the Earth's equatorial plane. The e-frame rotates with respect to the i-frame following the Earth's rotation Ω about the axis Oz_i, axes are shown in brown in Figure 2.3.

- Local Navigation frame (n-frame): the n-frame's origin is located at the navigation solution point P, i.e. navigation system or user etc. The down(D) axis is the local vertical which follows the ellipsoid normal pointing towards the Earth. The north(N) axis is the projection in the plane orthogonal to the D-axis of the line from P to the north pole. East(E) axis completes the orthogonal set by pointing East. The n-frame might rotate with respect to the Earth-fixed frame at a rate of ω_{en}, which is governed by the motion of P with respect to the Earth. This frame is important as it is useful in defining the users' attitude. Another common set of axes used in this frame is east-north-up (ENU). The relationship of n-frame to e-frame is shown in Figure 2.3.

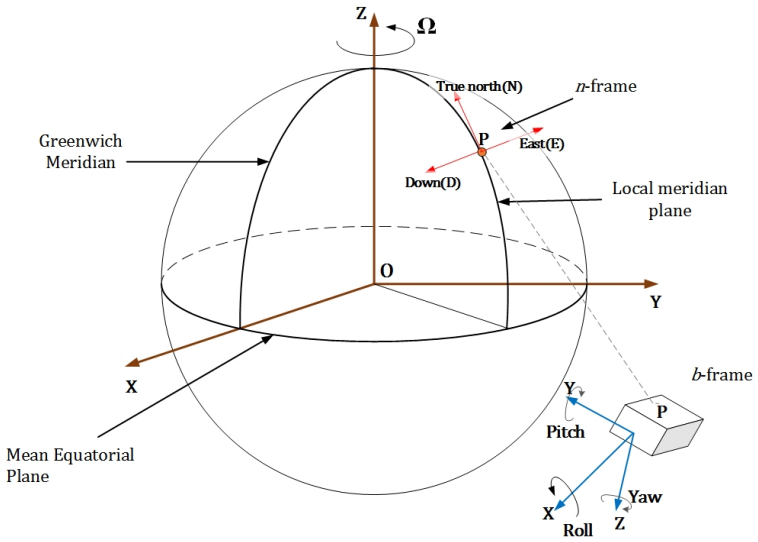

Figure 2.3: Relationship between the local navigation frame and body frame

- Body frame (b-frame): the origin is located at the origin of local nav-

igation frame and the orthogonal axis set remains fixed with respect to the body of the system. It is used to define the relative attitude of the object with respect to the location navigation frame. The $x-$axis commonly points towards the direction of travel, z-axis aligns with the direction of gravity and y-axis completes the orthogonal set. To describe angular motions of the body, the axes are also known as roll, pitch and yaw. The axes and its relationship to the local navigation frame is shown in Figure 2.3.

Usually, different systems will give results in different reference frames. For example, GNSS positioning results are expressed in the ECEF (WGS 84) frame by longitude λ, latitude φ and altitude h. IMU measurements are normally expressed with respect to the body frame. Terrestrial positioning and navigation results are usually given in the local navigation frame by ENU coordinates. To compare or integrate measurements from different systems requires the results to be converted to the same reference frame first. The positioning results throughout the work in this thesis will be given in a local reference frame of the experimental environment, referenced to the Ordnance Survey National Grid, expressed in ENU Cartesian coordinates.

2.1.2 Low cost inertial navigation

With the advancement in navigation technology in the last century, many systems that were either originally designed or not designed for positioning may now be applied for everyday civilian navigation and positioning. Inertial sensors, including both the gyroscope (or gyro) and the accelerometer, were used as guidance systems in rockets and aircrafts around the 1950s. Over the years, various high-grade and low-grade INS emerged for applications in a wide area of navigation for aircraft, vehicles and pedestrian navigation. The cost of inertial systems also vary greatly between high-grade and low-grade systems, as they are targeted at different users and give very different performance. Indoor positioning is mostly targeted at everyday civilian usage, therefore keeping the cost down has always been a big issue. For such applications, only low-grade inertial sensors can be applied.

Inertial navigation was originally applied by mounting inertial sensors onto a stable platform that is independent to the motion of the vehicle. This is still used in some systems where high accuracy is required. However

many systems have removed this complexity by attaching the inertial sensor on to the body of the moving object, so called the “strap down” system. This reduces cost, size and enhance reliability compared to equivalent platform systems (Titterton and Weston, 2004). Low-cost pedestrian inertial navigation systems are generally strapdown systems where we attach low cost sensors onto the user’s foot or waist, or any other body parts that can capture the motion of the pedestrian motion, such as attaching sensors onto the users’ knees (Rantakokko et al., 2014). This thesis will only discuss inertial measurements obtained from foot-trackers, i.e. a low-cost IMU sensor that has been attached to the pedestrian’s foot. The inertial measurements indicate the movement of the person’s foot and predict steps from such measurements.

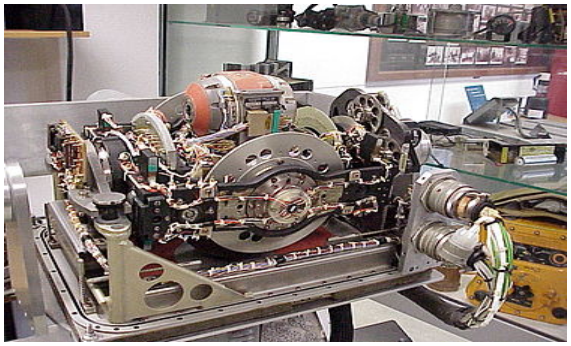

(a) LN3-2A gimballed inertial platform (developed by Litton Industries first equipped on Lockheed F-104 Starfighter)

(b) Optolink’s strapdown inertial system SINS-501

Figure 2.4: Inertial navigation systems

The classical laws of mechanics tell us that the motion of a moving body will continue to move uniformly in a straight line unless disturbed by an external force, which produces a proportional acceleration on the body. As a result, the change in velocity and position of the body could be worked out if the acceleration is known. Based on this concept, IMU measure the acceleration of the moving body using accelerometers and

gyros to navigate objects with respect to a local reference frame (Titterton and Weston, 2004). A typical INS consists of an IMU and a navigation processor to form a dead reckoning navigation system.

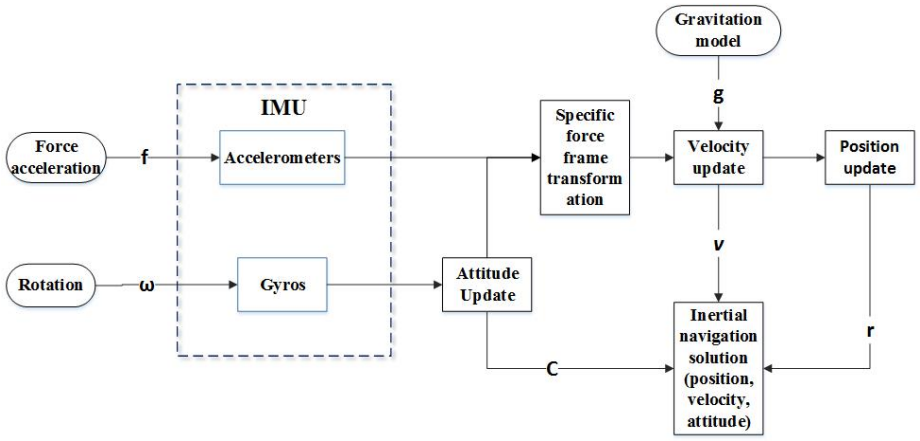

Figure 2.5: INS process

IMU will be introduced in more detail as it is the main measurement component in the system. A typical IMU is combined of three accelerometers and three gyros to provide 3-dimensional navigation measurements. Each accelerometer measures the force and detects acceleration in a single direction, while gyros detect the rotation of the body and determine the changes in the orientation of the accelerometers. The working process is as shown in Figure 2.5. The measurements of the sensors define the translational motion and rotational motion of the moving body at each epoch, which is then used to work out its current position relative to its previous position. Navigation solutions can be solved in any of the reference frames. Calculations below show how inertial measurements in the ECEF frame (Groves, 2013b), denoted by e, from time $t-\tau$ to t are used to update the attitude and positions with respect to the local navigation frame ($n-$frame) denoted by n,

$$\dot{\mathbf{v}}_e^n = \mathbf{f}^n - (2\omega_{ie}^n + \omega_{en}^n) \times \mathbf{v}_e^n + \mathbf{g}_l^n \tag{2.1}$$

where the superscripts of the vector denote the axis set in which the coordinates are expressed and the subscripts denote the the frame it is expressed with respect to. $\mathbf{g}_l^n$ is the local gravity vector in $n-$frame. $\mathbf{v}_e^n$ is the velocity with respect to the Earth expressed in $n-$frame, with components

$$\mathbf{v}_e^n = \begin{bmatrix} \nu_N & \nu_E & \nu_D \end{bmatrix}^{\mathrm{T}} \tag{2.2}$$

$\mathbf{f}^n$ is the specific force measured by accelerometers and expressed in

$n-$frame. ω_{ie}^{n} is the turn rate of the Earth expressed in $n-$frame and ω_{en}^{n} is the turn rate of $n-$frame with respect to the Earth-fixed frame, i.e. the turn rate of the navigation system, which may be expressed by the rate of change of longitude and latitude,

$$\omega_{en}^{n} = \begin{bmatrix} \dot{\ell}\cos L & -\dot{L} & -\dot{\ell}\sin L \end{bmatrix}^{T} \tag{2.3}$$

where L is the latitude, ℓ is the longitude. If the Earth is assumed to be perfectly spherical, the position of system in latitude, longitude and height is given by,

$$\dot{L} = \frac{\nu_N}{R_0 + h} \tag{2.4}$$

$$\dot{\ell} = \frac{\nu_E \sec L}{R_0 + h} \tag{2.5}$$

$$\dot{h} = -\nu_D \tag{2.6}$$

where R_0 is the radius of the Earth and h is the ellipsoidal height.

Eq.2.1 is known as the navigation equation because its first integral gives the velocity and the second integral gives the position of the system. Inertial navigation is commonly applied in the DR technique, which gives the user's motion and position with respect to the environment from relative measurements in the body frame. Pedestrian dead reckoning (PDR) is a navigation solution to resolve pedestrian navigation in challenging environments usually using step detection. Motion measurements are generally obtained from IMU or just accelerometers.

The advantage of inertial navigation is that it is completely self-contained hence do not rely on signals from external systems once initialised. However, such navigation errors are cumulative. Therefore, INS requires the correct knowledge of an initial position as well as periodic measurement corrections and aiding to prevent measurement error from accumulating.

Due to the continuous demand for low cost and lightweight features in new sensors and systems, current low-cost inertial sensors looks into micro-electromechanical system (MEMS) sensors. MEMS has been adapted to making small mechanical structures using silicon or quartz, with properties such as small size, low weight, low power consumption, low cost and low maintenance, etc. Although the performance from MEMS inertial sensors is less stable than high-end INS, but its measurement error is reasonable as a low-cost sensor with approximately $1^{\circ}/h$ for gyros and 50-100 micro-g for accelerometers, where $1g \approx 9.80665^{m}/s^{2}$ (Titterton and

Weston, 2004). It enables the mass production of inertial sensors to be implemented on less accuracy-demanding applications, such as mobile devices. However, the heading drift of low-cost inertial units can be so severe that it could accumulate up to hundreds of metres within a few seconds after initialisation. To compensate for this disadvantage, corrections must be implemented to provide accurate positioning results. While INS outputs a relative positioning result, it can be integrated with GNSS or some other sensor that provides absolute position solutions to enhance positioning accuracy (Grewal et al., 2013; Kempe, 2011).

2.1.2.1 IMU errors

Although IMU comes in different sizes and costs, from high-grade performance sensors that are used in military ships, spacecrafts and missiles to low-grade sensors that could be bought for $10, but this is not a perfect world and there will always be errors in measurements from all types of sensors, such as bias, scale factor, cross-coupling error or random noise. Despite the differences in hardware, all errors have some similar characteristics. Some main types of IMU sensor errors are explained and given below to illustrate a general idea of IMU performance.

System errors of any sensor generally consist of four types: a fixed bias, a temperature-dependent variation, a run-to-run variation and an in-run variation. The fixed component and temperature-dependent component can be calibrated and corrected in laboratory before put into actual utilisation. The run-to-run variation error remains the same throughout each run but varies between different runs. Therefore it should be calibrated each time the sensor is used. In-run variation error changes throughout each run and is very hard to observe. Usually, users hope to mitigate errors by calibrating the sensor before each run and also process the data by integrating with other sensors.

Bias is a constant error found in inertial sensors that is unaffected by the outside force or angular rate, which are also known as acceleration (or g) -independent bias, denoted as $b_a = (b_{ax}, b_{ay}, b_{az})$ and $b_g = (b_{gx}, b_{gy}, b_{gz})$ respectively for accelerometers and gyros. Accelerometer biases are described in the unit of milli-g (mg), gyro biases are described by degree per hour ($^\circ/_{hr}$) or degree per second for low-grade sensors. When describing a gyro bias, sometimes the term *drift* is used.

Scale factor errors relates the change in the output signal to a change in the input acceleration or rate, denoted as $s_a = (s_{ax}, s_{ay}, s_{az})$ and $s_g = (s_{gx}, s_{gy}, s_{gz})$ for accelerometers and gyros respectively.

Cross-coupling errors, also known as misalignment errors, are results of misalignment of the sensitive axes of the sensor to the orthogonal axes of the body frame. The accelerometer cross-coupling coefficient of β-axis specific force sensed by the α-axis accelerometer is denoted as $m_{a,\alpha\beta}$, while $m_{g,\alpha\beta}$ denotes the coefficient of β-axis angular rate sensed by the α-axis gyro. Both scale factor and cross-coupling error are expressed as parts per million (ppm) or a percentage.

Random noise, also known as random walk, come from various sources such electric noise which varies in inverse proportion to the square root of the averaging time, denoted as $w_a = (w_{ax}, w_{ay}, w_{az})$ and $w_g = (w_{gx}, w_{gy}, w_{gz})$ for accelerometers and gyros respectively.

Some other errors such as scale factor nonlinearity, anisoinertia error, acceleration-dependent bias and anisoelastic bias can be found in MEMS sensors which are affected by the applied force or angular rate. However, these errors are very small compared to the ones mentioned above. Therefore they are not of great concern when working with low-cost MEMS IMU sensors, hence will not be discussed.

2.1.2.2 Corrections

Errors in INS solutions can be categorised into three types: initialisation error, IMU measurement error and processing errors. Initialisation error can be reduced by integrating accurate sensors or providing external information during initialisation. Processing error is mainly due to the limitations of system iteration rate. This thesis will mainly focus on methods to reduce measurement errors, especially the heading bias which contributes to the position error cumulatively if uncorrected.

Zero Velocity Updates (ZUPT) has been used extensively in previous literature to correct the user's velocity as well as restrict position errors and estimate the sensor bias when wearing the IMU is worn on the user's foot (Foxlin, 2005; Godha and Lachapelle, 2008). The ZUPT is performed during the period when the foot is stationary on the ground. During this period, the velocity is assumed to be zero hence the force along the vertical direction should be approximately the negative gravity constant. Any measurements that does not agree with this can be assumed to be errors and thus corrected. Therefore, applying the ZUPT correction restricts the measurement error and improve navigation performance.

However, heading drifts cannot be completely eliminated even by applying ZUPT. Heading drifts has to be eliminated by external measurement corrections or sensors. The Cardinal Heading Aided for Inertial Navigation

(CHAIN) was proposed to restrict heading drifts by estimating headings from the knowledge of building orientations (Abdulrahim et al., 2011). The idea is based on the assumption that most buildings and the rooms within them are constructed in rectangular shapes and building layout information must be available.

Inertial measurements have become widely available in mobile devices therefore have been widely applied for indoor positioning solutions. Inertial measurements from low cost IMUs will provide the basic user position propagation model in this thesis. A number of external sensors and measurements are applied to correct the inertial sensor errors and produce more reliable and accurate positioning results.

2.1.3 Wireless signal based positioning

Wireless local area network or wireless personal area network (WPAN) are both wireless networks that links two or more devices using a wireless distribution method within a local area for data transmission or connecting to the Internet. The user can move around the coverage area and remain connected to the network or to the wider internet (IEEE Computer Society, 2012). WLAN and WPAN differs in their coverage range, where WPAN usually varies from centimetres to a few meters, WLAN can cover up to tens and hundreds of meters.

Wi-Fi, is defined by the Wi-Fi Alliance as any WLAN that is based on the IEEE 802.11 standards that provide data exchange or Internet connection at frequencies around 2.4GHz and 5GHz. Wi-Fi coverage has risen remarkably over the last decade in both office environment and homes. It has now become very common to use wireless network to connect to the internet (Cisco Systems, Inc, 2011; Curran et al., 2011; Farid et al., 2013). Due to its wide availability, we are able to use them as alternative positioning signals even though Wi-Fi signals were not specifically designed for positioning purposes. WPAN is carried over some common technologies such as Bluetooth and ZigBee have been used for indoor positioning in similar ways as Wi-Fi (Hossain and Soh, 2007; Chawathe, 2009).

Positioning based on wireless signals are achieved through estimating positions from either signal strength patterns or signal travelling time. Positioning can be achieved in any environment with the existence of wireless network. Positioning algorithms can be fairly simple or complicated depending on the required accuracy. However, as none of these common wireless technologies were originally dedicated to positioning, signal strength tend to fluctuate. This fluctuation causes uncertainties and error

in the positioning estimation. Signal travelling time could also be disturbed by obstructions in the environment which will result in errors. Several common wireless signal based positioning methods are introduced below.

2.1.3.1 Path-loss models

Wireless signal positioning fundamentally relies on measuring the signal strength at the location of interest. Given the transmitting power at the transmitting antenna, this can be used to work out the distance between two antennas based on the signal attenuation model, or path loss model. The power density of electromagnetic waves will weaken as it travels through space. This effect may be caused by a number of reasons, such as reflection, refraction, diffraction and absorption. But signal will attenuate even when travelling through a line-of-sight path through free space, known as free-space path loss (Cheung et al., 1998).

The power received by one antenna when the transmitting antenna at a certain distance away transmitting a known amount of power is described by *Friis' law* (Molisch, 2011):

$$P_{Rx}(d) = P_{TX} G_{TX} G_{RX} (\frac{\lambda}{4\pi d})^2 \tag{2.7}$$

where P_{TX} is the transmit power, G_{TX} is the antenna gain of the transmitting antenna and G_{RX} is the antenna gain of the receiving antenna. $(\frac{\lambda}{4\pi d})^2$ is known as the free-space loss factor, λ is the signal carrier wavelength, d is the distance between the transmitter and the receiver. This formula implies that signal attenuation increases with frequency in free space. For ranging and positioning, Eq.2.7 is most commonly written in the logarithmic form, known as the log-distance path loss model:

$$P_{RX}(d) = P_{d_0} + 10n \log \frac{d}{d_0} + X_\sigma \tag{2.8}$$

where $P(d_0)$ is the received signal strength (RSS) at reference distance d_0, typically 1m, $P_{RX}(d)$ is the RSS at distance d from the wireless access point (AP), n is the signal path loss exponent which defines how quickly the signal strength weakens as it travels through the air, X_σ is a Gaussian random noise with zero mean and standard deviation of σ (Bose and Foh, 2007).

Most real situations are much more complicated than free space path-loss therefore more complicated models have been developed to take into account parameters such as environment factor, number of obstructions,

even antenna and receiver heights etc. Other models such as Stanford University Interim (SUI) model, COST-231 Hata model, Hata-Okumara model and ECC-33 path loss model only to name a few, have also been proposed to predict signal strength (Hata, 1980; Abhayawardhana et al., 2005; Mardeni and Priya, 2010). However each model describes the characteristics of signals within a certain frequency range and certain models are more suitable for Wi-Fi signal frequencies at 2.4GHz and 5GHz. Several models discussed by Akl et al. (2006) and Cebula III, Stanley L. et al. (2011), for example the log-normal shadowing, the two-ray model and the JTC indoor path-loss model which all consider the indoor environment, are suitable for signals around the 2.4GHz frequency. The Motley-Keenan model not only models the free path loss but also the wall attenuation in urban and in building environments:

$$P_{Rx}(d) = P(d_0) - 10n\log(\frac{d}{d_0}) - \sum_{p=1}^{p} WAF(p) - \sum_{q=1}^{q} FAF(q) + X_\sigma \quad (2.9)$$

notations are the same as in Eq.2.8, WAF and FAF are the wall and floor attenuation factors respectively, p and q are the number of walls and floor between the receiver and transmitter. This model suggests that the signal attenuation can be anything between 1 and 20dB for Wi-Fi signals depending on the building material and even higher attenuation for higher frequencies.

If we could find the best fit model for the signal in a specific environment, we would be able to work out the travelled distance of the signal from the received signal strength by inversing the problem, i.e. calculating the distance between the transmitter and receiver d from $P_{RX}(d)$. However, indoor environments are complicated and very difficult to model accurately. Even with the most detailed model, signals can suffer unpredictable signal obstruction, multipath etc., causing signals to behave very differently, as well as having a large noise X_σ. Therefore it is very hard to find a very suitable signal path-loss model when we arrive in a new environment (Kaemarungsi and Krishnamurthy, 2012; Fet et al., 2013; Zhu and Feng, 2013). As a result, ranging estimation based on path-loss models are mostly inaccurate and corrections must be applied.

2.1.3.2 Time-of-arrival

The distance travelled by the signal can be estimated from measuring the time that the signal has taken to travel between two locations, known as

the time-of-arrival (TOA) approach. TOA is applied based on the principle that the distance should be proportional to the signal propagation time according to

$$s = ct \tag{2.10}$$

where c is the speed of light, t is the propagation time, s is the distance travelled. All units (both receivers and transmitters) within the system must be precisely time-synchronised to measure the one-way signal propagation time. To eliminate the clock synchronisation problem, sometimes the round-time-of-flight (RTOF) is used instead which measures the time of the signal travelling from the transmitter to the receiver and back.

The trilateration method can be applied to resolve for 2D or 3D positioning from TOA ranging. While one set of ranging equation is able to resolve for one unknown, three sets of ranging measurements is able to minimise measurement errors in 2D positioning, or produce a set of positioning estimation in 3D positioning. A simple scenario of trilateration is illustrated in Figure 2.6, where the user measures the signal travelling time to three transmitters and back. The solid line marks the true propagation distance, i.e. true propagation time for each receiver-transmitter pair. The middle circle around each transmitter marks all the possible positions of the receiver based on the true distance from the transmitter. The intersection point of the three circles should be the location of the receiver. However, due to signal variation and measurement error, the possible positions lie within a ring instead of the circumference of a circle. As a result, the intersection of the three rings would not be a single point but rather a small area of possibilities, representing the true location with error. More ranging measurements would result in more rings which should end up with smaller intersection area. Least square adjustment can be applied when redundant observations are available to reduce measurement error, i.e. the process of reducing the intersection area.

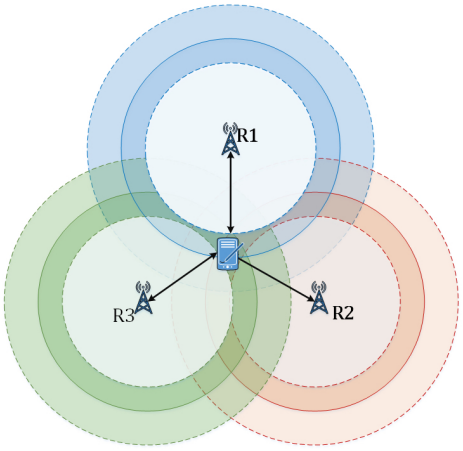

Figure 2.6: TOA ranging and positioning (solid line indicates the true range, dashed lines indicate the error range)

2.1.3.3 Time-difference-of-arrival

Multilateration, or Time-difference-of-arrival (TDOA) is a method to determine the position of a mobile receiver by measuring the time difference between several signals arriving from multiple transmitters. When two transmitters are known, one TDOA measurement would be achieved and the receiver can be determined to lie on a hyperboloid. Additional transmitters would produce additional hyperboloids and the intersection of them would narrow down the possible locations of the receiver. 2D positioning is achieved from at least three transmitters and 3D positioning from at least four transmitters. Signals should be time synchronised among the transmitters while synchronisation is not necessary on the receiver.

2.1.3.4 Angle-of-arrival

Angle-of-arrival (AOA) method obtains the location of the receiver by estimating the angle of the received signal from a number of transmitters. The receiver should lie on the intersection of the received angle direction lines. When AOA is combined with ranging solutions, such as TDOA from the two transmitters, a positioning solution could be obtained where no time synchronisation is required. However, in an indoor environment, wireless signals are often disrupted by walls resulting in multipath. Multipath signals change directions from its original signal thus cause errors in positioning.

2.1.3.5 Fingerprinting

The path-loss model introduced in earlier sections explains that accurate ranging estimation is hard to achieve due to obstructions and disturbance.

However, any ranging-based positioning method, e.g. TOA, relies on good ranging to achieve accurate positioning. Hence wireless signal based positioning should look into non-range based positioning methods. To overcome the problem of signal variation, the fingerprinting (FP) method is commonly applied which actually takes advantage of the fact that signals vary inside complicated areas. However it does depend on a recognisable pattern rather than unpredictable random fluctuation. As the name of this method suggests, a "fingerprint", i.e. the RSS pattern, is generated to represent each location within the area of interest and stored into a database. During positioning, the receiver compares its current RSS pattern to the fingerprints in the database and determines position based on the similarity between them. This method provides a position output directly through signal patterns rather than trying to work out the ranging estimations and perform multilateration (Farshad et al., 2013). The advantage of this method is that it ignores the signal fluctuation problem to a certain extent. Yet generating the fingerprints can be an arduous task and it does not cope with changes if the database is not updated properly.

2.1.4 Other indoor positioning signals and applications

Other than the well-known GNSS signals and Wi-Fi signals, many other radio signals have also been used for positioning purposes. Signals such as Bluetooth and ZigBee, which also lie on the 2.4GHz frequency band, can be applied in very similar ways as Wi-Fi signals to achieve positioning.

Furthermore, Ultra-wideband (UWB) signals have also begun to be applied to positioning and localisation in more recent work since the introduction of regulations in 2002 (Koppanyi et al., 2014), although the UWB technology was introduced much earlier. UWB signals are signals that are sent out with a fractional bandwidth[1] equal to or greater than 0.20 or has a bandwidth equal to or greater than 500MHz. As developments in UWB arise, the IEEE 802.15.4a standard was first setup for UWB-based low-rate WPANs with localisation ability (Dardari et al., 2009). Typical UWB systems work at a bandwidth more than 1GHz within the frequency range of 3.1-10.6GHz at a power spectral density emission of -41.3dBm/MHz due to established regulations by the Federal Communications Commission (FCC) (Federal Communications Commission (FCC), 2002; Breed, 2005). Specific channel regulations may differ slightly depending on the country or region it is been applied. UWB has become popular for precise indoor localisation

[1]Fractional Bandwidth: the bandwidth of a device divided by its centre frequency.

as it resolves a major problem in indoor environments: multipath (Win and Scholtz, 1998; Suwansantisuk et al., 2005). If the signal pulse repetition rate was 2×10^6 pulses per second, then up to 0.5μs of multipath spread could be observed. This means that sub-meter accuracy may be achieved. However, accurate UWB positioning requires a dedicated infrastructure to be setup beforehand which is expensive to implement and maintain. Yet, precise UWB ranging measurements can be obtained even without the infrastructure. This is particularly useful for collaborative positioning where relative ranging measurements can be applied to constrain other measurement errors (Multispectral Solutions, Inc., 2006; Ward, 2010).

Other various short-range wireless communication technologies have also been implemented for indoor positioning, such as RFID tags, where the positioning solutions are based on proximity and accuracy depends on a fully operational infrastructure and its network density.

Pseudolites are ground-based GNSS-like signal transmitters which operate under the same principles as GNSS systems. The LocataLite system consists of pseudolite transceivers which is intended to work indoors and use signals on the 2.4GHz frequency band (Bonenberg et al., 2010; Khan et al., 2010). However a major problem with pseudolites is that they can be so similar to GPS signals that it could potentially block the reception of real GNSS signals. Therefore it has been restricted from real application in the United Kingdom.

Indoor messaging system (IMES) is implemented as part of the QZSS system in Japan for indoor positioning. It transmits proximity location messages to GPS-enabled mobile devices when they are no longer able to receive GPS signals. Transmitters operate on the GPS L1 band and the data structure is very similar to that of L1 C/A code while the power level lies between -158.5dBw and -94dBw (Dempster, 2009). The system can achieve better accuracy than A-GPS when IMES signals are received and should at least locate itself within tens of metres of the true location. However, it does require a dense indoor network and could cause GNSS jamming much like pseudolites.

Bluetooth® has introduced a low energy technology in its Bluetooth Low Energy (BLE) or Bluetooth Smart as part of Bluetooth v4.0 so that it only consumes a fraction of the power of previous Bluetooth devices while increasing the possible range of over 50m (Kalliola, 2011; Cinefra, 2012; Bluetooth, 2014). BLE works on the 2.4GHz frequency which is the same frequency as Wi-Fi and classic Bluetooth, but applies adaptive frequency

hopping to avoid interference. Apple Inc. implements this technology to its trademark technology iBeacon which derive proximities between the beacon and receiver from relative signal strength indicator (RSSI) (Mubaloo Ltd, 2014).

While this thesis cannot cover all the applications that are available in both research or on the market, this short introduction gives an idea of how many different technologies and applications can be applied for indoor positioning. A reason to why so many technologies can be found is that there is no single solution that could solve the problem in every indoor positioning scenario. There are both pros and cons to applying each different signal and method. However, users constantly look for systems that could adapt easily in different environments and provide seamless positioning even when situations change. Therefore, recent works start looking at how different methods could be integrated to achieve better positioning in various different environments.

2.2 Collaborative positioning

2.2.1 Basic concepts

The complexity of indoor positioning comes from the fact that, unlike outdoors, the indoor environment are very different from each other in terms of available signals. The previous section provides a background knowledge on sensors and systems that can be used in different indoor positioning situations independently. While GNSS is able to provide accurate positioning in all weather and all year round in outdoor open areas, it is almost impossible to use GNSS in any indoor environment. With signal power as low as -150dBw, its weak signal makes it very hard to penetrate not just buildings walls but foliage as well, which is why forests are also considered as “indoor positioning” problems (Borre, 2007; Petovello and Joseph, 2010). While so many indoor positioning techniques have been proposed, each technique relies on different signals which are suitable in different environments. Therefore, different indoor positioning methods must be tailored to suit the specific conditions of an indoor environment.

While Wi-Fi fingerprinting provides absolute positioning results, wireless signals naturally fluctuate and signal strength are easily disturbed by interference, obstruction and environmental factors which makes its positioning accuracy unstable (Tarrio et al., 2011; Fahed and Liu, 2013; Luo et al., 2013). Inertial navigation can achieve reliable relative positioning based on consecutive inertial measurements which works in almost

any environment. However, the major disadvantage is that heading drift accumulates very quickly and must be constrained by some kind of other measurement.

Another problem that often occurs in indoor positioning is the biased measurements reaching the receiver simply caused by the disturbance at the location of the receiver. While the measurements obtained by a single user could be restricted by its location, multiple measurements from a number of users could eliminate some the error and bias.

The idea of collaborative positioning (CP) is introduced here which integrates a selection of different sensors and information from different users to minimise individual system limitations and enhance overall positioning performance. CP enable users to share and utilise the location information among its surroundings and neighbours over communication links. It initially extends the positioning network boundary as it implements signals and data that cannot be acquired directly to assist the determination of positioning solutions that would not have been possible otherwise. Further work on CP also suggests that it is able to increase positioning and navigation accuracy and robustness (Patwari et al., 2005; Chan et al., 2006; Alsindi and Pahlavan, 2008; Thompson and Buehrer, 2012; Nilsson et al., 2013, 2014). CP benefits from opportunistic navigation which takes advantage of any environmental features and measurements available to the system, e.g. broadcasting signals, mobile signals, visual landmarks, magnetic anomalies, light, sound, temperature, etc (Groves et al., 2014). The concept of signals of opportunity (SOOP) has been introduced as part of opportunistic navigation in (Yang et al., 2009) which utilises available signals that were not originally intended for positioning. The collaboration of signals is enhanced through multiple users within the CP network that can share data amongst each other. This data can be information of the surrounding environment, clock data, mapping information or relative ranging measurements (Groves, 2013a,b).

Positioning based on collaboration of nodes (users and transmitters) within a network is fairly new among all methods of positioning and navigation. This is mainly because the concept of collaboration between nodes among the network relying on direct communication between each node rather than an infrastructure has only been introduced in recent years (Aspnes et al., 2006). CP only started emerging since then. Collaborative positioning was first applied in intelligent transport systems where roadside beacons and vehicle clusters helped to maintain reliable positioning when

the vehicle could not receive sufficient satellite signals (Alam et al., 2011; Yao et al., 2011; Tang et al., 2012; Amini et al., 2014; Tsai et al., 2014). CP improves navigation performance through correcting GNSS observations and positioning errors are reduced by vehicle-to-vehicle ranging.

This thesis mainly discusses collaborative positioning from two aspects: integration of multi-sensors to provide positioning for a single system and integration of multi-users to enhance the positioning accuracy among the whole network. Multi-sensor systems have been discussed in literature as it is considered as the future trend to provide robust ubiquitous positioning (Hide et al., 2007; Groves, 2014). However, the characteristics of a multi-user system is still relative new and lacks comprehensive understanding.

As ranging measurements between the nodes within the network is an important piece of information in collaborative positioning, it is also referred as peer-to-peer (P2P) positioning in some literature (Groves, 2013a; Garello, Presti, Corazza and Samson, 2012). However, because the more broader aspect of CP discussed in this thesis, P2P will only be used when referring to the relative ranging scenarios here.

2.2.2 Network optimisation

The next generation of CP aims to bring together a range of different sensors and environmental information to provide more robust solution which potentially overcomes interference and enables seamless navigation when moving between indoor and outdoor environments. To achieve such solutions, appropriate information should be selected for integration so that the system has enough measurements while not been burdened with too much information. Moreover, not all information is essential to improving positioning performance. Yang and Soloviev (2014) have investigated the spatial and temporal effects of collaborative positioning and find that there is an equalising point which marks out the number of users when the inclusion of more measurements begin to improve performance. The optimisation of collaborative network performance is also explored among various works based on geometric positions and lower bound estimations (Jia and Buehrer, 2010; Lei, 2014).

In this thesis, we look at the critical point where CP performance improvement begins to reduce when increasing measurements are being included. We try to find the balance point where enough information is integrated to achieve accurate positioning while also taking care not to

reduce efficiency.

2.3 Performance evaluation metric

A good positioning system should be able to constantly provide accurate and reliable results. The positioning performance in this thesis is evaluated from the three aspects listed below.

2.3.1 Accuracy

Accuracy is the offset between the estimated value and the true value. Higher accuracy indicates a smaller offset. In many cases of positioning, we are unable to acquire the absolute truth. Usually, results from a positioning system that is able to achieve higher accuracy than the currently measured system can be regarded as the ground truth and used to evaluate the accuracy of the current system. In this thesis, most of the ground truth is provided by surveying total stations which achieve measurement accuracy of up to millimetre level.

2.3.2 Reliability

Reliability reflects the confidence in the estimated result. It is derived from the variation of the positioning accuracy over a period of time and also the accuracy of each implemented measurement.

2.3.3 Robustness

Robustness in computer science is the ability to cope with errors during execution. In positioning, it is the ability to provide continuous positioning solutions in different situations. A robust positioning system should maintain high level positioning results when the available information and conditions around the receiver changes.

2.4 Navigation filters

In navigation problems, measurements are processed through navigation algorithms to minimise errors and achieve optimal estimation. Different navigation algorithms are suitable for processing different problems. Therefore, to achieve better positioning and navigation performance, the most suitable navigation algorithm should be applied. Normally a mathematical model describing the current physical conditions of a system and its parameters, usually time variant, is known as the state model, and the obtained measurements from surrounding sensors are known as the observation

model. An algorithm that tries to estimate the current state value based on previous and current observations is also known as filtering.

In a navigation problem, a prediction model is generally given which describes how the system state model change over time. Recursive Bayesian estimation, also known as Bayes filter, is a probabilistic approach for estimating the probability density functions of the state recursively over time based on the observation and the prediction model. In the real world, obtaining a perfect positioning measurement is impossible no matter what system we choose. Therefore, measurement errors and biases are usually minimised or smoothed through appropriate filtering.

Bayes filters estimate and optimise the dynamic system states from given prediction models and the noisy measurements, i.e. estimating the position and orientation of a moving body to output accurate positioning (Fox et al., 2003). Some of the most commonly applied filters are introduced below.

2.4.1 Kalman filters

The Kalman Filter (KF) or linear quadratic estimation (LQE) was proposed by Rudolf E. Kalman in 1960 to deal with discrete dynamic linear filtering problem (Kalman, 1960; Faragher, 2012). It continuously measures and estimates the navigation system state variable, e.g. the position and velocity, while the estimates can be updated with new measurements. The navigation system state at time k can be derived from the state at time $k-1$ by the form:

$$x_k = A_k x_{k-1} + B_k u_k + w_k \tag{2.11}$$

where x_k is the system state at time k, A_k is the transition model, B_k is the control input model, u_k is the control input vector for each time step, w_k is the process noise which is usually assumed to be independent white Gaussian distribution. At each time step, a new measurement z_k of the true state x_k is obtained:

$$z_k = H_k x_k + v_k \tag{2.12}$$

where H_k is the observation model, v_k is the measurement noise that is assumed to be zero mean Gaussian noise with covariance R_k, i.e. $v_k \sim \mathbb{N}(0, \mathrm{R_k})$.

Basic procedures in a KF include two phases known as the prediction phase and update phase. During prediction, the current *a prior* state is estimated from the previous time step state estimate. In the update step,

the *a posteriori* state is estimated by including the current observation information with the *a prior* prediction. An outline of the specific steps in the KF algorithm is given below:

1. Predict *a prior* state estimate $\hat{x}_{k|k-1}$ and the *a prior* estimate covariance matrix $P_{k|k-1}$ which measures the estimated accuracy of the state estimate, where Q_k is the covariance of the process noise;

$$\hat{x}_{k|k-1} = A_k \hat{x}_{k-1|k-1} + B_k u_k \tag{2.13}$$

$$P_{k|k-1} = A_k P_{k-1|k-1} A_k^T + Q_k \tag{2.14}$$

2. Calculate the measurement residual, the noise covariance matrix and the Kalman gain K_k;

$$K_k = P_{k|k-1} H_k^T (H_k P_{k|k-1} H_k^T + R_k)^{-1} \tag{2.15}$$

3. Formulate the measurement z_k;

4. Update the *a posteriori* state estimate and *a posteriori* estimate covariance using the measurement data that is weighted by the Kalman gain.

$$P_{k|k} = P_{k|k-1} - K_k H_k P_{k|k-1} \tag{2.16}$$

KF is very efficient to implement. However, it is normally limited to linear problems and performs best with low state uncertainty. It is commonly applied for the integration of GNSS and INS systems (Hide et al., 2003; Ding et al., 2007; Abdulrahim et al., 2012).

2.4.1.1 Extended Kalman filter

Many navigation systems are non-linear systems and do not behave in such a predictable way as high-end inertial systems. The extended Kalman Filter (EKF) extends the applications of KF to nonlinear systems by applying a linear expansion of the Taylor series expansion to the nonlinear system functions (Welch and Bishop, 1995; Faruqi and Turner, 2000; Zhao et al., 2003; Julier and Uhlmann, 2004; Feng et al., 2013).

A nonlinear system dynamic model is described as

$$\dot{x}_k = f(x_{k-1}, u_{k-1})) + w_{k-1} \tag{2.17}$$

where $\dot{x}$ is the linear function of x, f is the nonlinear function of the state vector, u_{k-1} is the control vector and w_{k-1} is the process noise. The EKF state vector propagation equation is as below

$$\hat{x}_{k|k-1} = \hat{x}_{k-1|k-1} + \int_{t_k-\tau}^{t_k} f(\hat{x}_{k-1|k-1}, t_k)\tau_s \tag{2.18}$$

where τ_s is the time difference between $k-1$ and k. EKF assumes that the error in the state vector estimate is much smaller than the state vector and that f is constant over the propagation period. The measurement model is expressed as

$$z_k = h(x_k) + v_k \tag{2.19}$$

where h is the nonlinear function of the state vector and v_k is the measurement noise. The state vector is updated with the measurement vector as

$$\hat{x}_{k|k} = \hat{x}_{k|k-1} + K_k(z_k - h(\hat{x}_{k|k-1})) \tag{2.20}$$

EKF works on the basis that the linearised system and measurement models about the state vector estimate is very close to the true values and it has the advantage of being very efficient computation-wise (St-Pierre and Gingras, 2004; Afonso, 2008; Myers et al., 2012). However, some limitations are that f and h cannot be applied to the covariance directly. Their Jacobian matrix[2] is computed instead. Linearisation can only be applied when the Jacobian matrix exists and that it is only reliable when the error propagation can be approximated by a linear function. Even so, the Jacobian matrix calculation can be a difficult and complex process. When linearised, the error covariance matrix P and Kalman gain K become functions of the state estimates, which may lead to stability problems.

2.4.1.2 Unscented Kalman filter

Due to the difficulties of applying EKF in real situations, several nonlinear filtering algorithms were further proposed to address such problems. Unscented Kalman Filter (UKF), or also named sigma-point Kalman filter, was proposed to deal with more complex systems that is hard to linearise. In UKF, the mean and covariance information of the system state is

[2]Jacobian matrix is the matrix of all first-order partial derivatives of a vector-valued function.

described by a set of sample points and propagated directly through an arbitrary set of nonlinear equations (Julier et al., 1995, 2000; Chen, 2003). The set of sample points $O(n)$, known as sigma points, is used to represent the system state with the desired mean $\hat{x}_{k|k}$ and covariance $P_{k|k}$. These points propagate through the nonlinear system and their transformations are assumed to be an estimation of the posterior distribution. The basic procedure is as follows:

1. compute the set of points $2n$ from the columns of the matrices $\pm\sqrt{nP_{k|k}}$;
2. translate the set of point so that the sigma points represent the mean and covariance;
3. transform each points through the dynamic equation following

$$x^i_{k|k-1} = x^i_{k-1|k-1} + f(x^i_{k-1|k-1}, t_k)\tau_s \tag{2.21}$$

4. compute the propagated mean $x_{k|k-1}$and covariance $P_{k|k-1}$

$$\hat{x}_{k|k-1} = \frac{1}{2n}\sum_{i=1}^{2n} x^i_{k|k-1} \tag{2.22}$$

$$P_{k|k-1} = \frac{1}{2n}\sum_{i=1}^{2n}(x^i_{k|k-1} - \hat{x}_{k|k-1})((x^i_{k|k-1} - \hat{x}_{k|k-1})^{\mathrm{T}} + Q_{k-1} \tag{2.23}$$

5. update measurements, calculate the measurement innovations and obtain the Kalman gain, the state vector update and error covariance update.

UKF is able to predict the mean and covariance accurately up to the fourth term of the Taylor series. It predicts the covariance with the same level of accuracy as EKF, while eliminating the requirement of computing the Jacobian matrices. However, UKF still remains a sub-class of the linear filters, as it still tries to estimate system states by linearising the state measurements. It can only be applied to models driven by Gaussian noises. Moreover, it is not a truly global approximation as it is only based on a small set of sample points.

2.4.2 Monte-Carlo methods

To tackle real non-linear non-Gaussian tracking and navigation systems, Particle Filtering (PF) was proposed to estimate state models through sequential Monte Carlo (SMC) estimations based on a large number of sample points (or particles) whose distribution represents the state probability density (Doucet et al., 2001). Among numerous literatures, it has been known as bootstrap filtering, Monte Carlo (MC) filters, the condensation algorithm, interacting particle approximations and survival of the fittest. The MC methods are a broad class of computational algorithms that rely on repeated random sampling to obtain optimal numerical results. It is often considered as a stochastic sampling approach to tracking purposes. SMC is flexible and easy to implement for computing the posterior distribution (Gordon et al., 1993; Crisan et al., 1999; Doucet et al., 2000; Arulampalam et al., 2002). The basis of MC integration takes the form of

$$I = \int g(x)dx = \int f(x)\pi(x)dx \tag{2.24}$$

where $g(x)$ is factorised so that $\pi(x)$ could be regarded as the probability density where $\pi(x) > 0$ and $\int \pi(x)dx = 1$. It is assumed that if $N \gg 1$ samples are drawn according to $\pi(x)$, the sample mean which is

$$I_N = \frac{1}{N}\sum_{i=1}^{N} f(x^i) \tag{2.25}$$

should converge to I if samples x^i are independent and I_N would be unbiased. However in reality, drawing an infinite number of samples is infeasible. Instead a finite number of N samples are generated from a density $q(x)$ to achieve a weighted approximation of the true posterior density. $q(x)$ is known as the *importance density* and weights w^i are chosen based on *importance sampling* where the sum of weights is 1.

Importance sampling is the fundamental concept of the particle filters.

2.4.2.1 Particle filters

PF, or sequential importance sampling (SIS) algorithm, performs system state estimation by applying the recursive Bayesian filter to a set of weighted particles drawn from the importance density to represent the desired posterior probability density function (pdf). If the number of particles is sufficient, their representation of the state converges very closely to the required posterior pdf $p(x)$ and the filter is assumed to be the optimal

Bayesian estimator. Similar to the KF introduced above, the system state vector x_k is given by a discrete-time stochastic model:

$$x_k = f_{k-1}(x_{k-1}, v_{k-1}) \tag{2.26}$$

where k is the time index, f_{k-1} is a nonlinear function of the state x_{k-1} and noise v_{k-1} which is an independent and zero-mean process noise. x_k is recursively updated from measurement z_k

$$z_k = h_k(x_k, n_k) \tag{2.27}$$

where $h_k$is a known non-linear function and n_k is the independent and zero-mean measurement noise.

For further description and understanding on PF, let $\{x_k^i, w_k^i\}_{i=1}^N$ denote a set of random particles x_k^i and their associated weight w_k^i to characterise the posterior pdf of a system state. The particles $x^i \sim q(x), i = 1, ..., N$ are samples drawn from an *importance density* $q(.)$, which is a weighted approximation to the true density $p(.)$. The density is approximated as

$$p(x) \approx \sum_{i=1}^{N} w^i \delta(x - x^i) \tag{2.28}$$

where $\delta(.)$is the Dirac delta function and

$$w^i \propto \frac{\pi(x^i)}{q(x^i)} \tag{2.29}$$

is the normalised weight of the ith particle. The MC estimation is obtained through integration of the independent samples and their associated importance weights,

$$I_N = \frac{1}{N} \sum_{i=1}^{N} f(x^i) \widetilde{w}(x^i) \tag{2.30}$$

The state estimation depends greatly on how particles are drawn and the associated weight. While the particle weights are recursively updated by observation measurements, it is hard to avoid the problem of increasing variance of the importance weights over time (Doucet et al., 2000; Tulsyan et al., 2013). As a result, particle filtering often faces two common problems, *degeneracy* and *impoverishment*. Degeneracy tends to happen after a several iterations when only very few particles will have a significant weight (Ristic et al., 2004). A resampling procedure is thus introduced to

overcome this problem. However, another problem may arise from insufficient resampling, i.e. sample impoverishment. During the resampling process, new particles are only regenerated from particles with significant weighting. A problem this might lead to is that the diversity of the particles can decrease very quickly after a few iterations. An extreme situation would be when the whole distribution is actually only represented by the state of one particle (Li et al., 2014). To balance this trade-off, the resampling procedure is applied at steps only when a specific requirement is met, e.g. when the variance of the non-normalised weights is over a certain threshold.

The basic procedures of a typical PF is outlined as below.

1. Initialisation: N particle samples x_0^i are drawn from the known prior distribution $p(x_0)$ to represent the system state.

2. Prediction: the state is propagated through a prediction model, and the prior probability density function (pdf) of the state at time step k is obtained,

$$p(x_k|Z_{1:k-1}) = \int p(x_k|x_{k-1})p(x_{k-1}|Z_{1:k-1})dx_{k-1} \tag{2.31}$$

   where $Z_{1:k-1}$ is a set of all available measurements z_i up to time k, $p(x_k|x_{k-1})$ is the probabilistic model of the state propagation defined by the system equation and estimation of noise v_{k-1}, while it is assumed that $p(x_k|x_{k-1}, Z_{1:k-1}) = p(x_k|x_{k-1})$.This step changes the state estimates of the particle cluster.

3. Update: a new measurement z_k is obtained to update the prior via Bayes rule and obtain the posterior of the state

$$p(x_k|Z_{1:k}) = \frac{p(z_k|x_k)p(x_k|Z_{1:k-1})}{p(z_k|Z_{1:k-1})} \tag{2.32}$$

   where

$$p(z_k|Z_{1:k-1}) = \int p(z_k|x_k)p(x_k|Z_{1:k-1})dx_k \tag{2.33}$$

   The conditional pdf of z_k given x_k, $p(z_k|x_k)$, is defined by the measurement model and the known statistics of n_k

$$p(z_k|x_k) = \int \delta(z_k - h_k(x_k, n_k))p(n_k)dn_k \tag{2.34}$$

The likelihood of each particle, the weight, is also obtained and normalised through

$$w_k^i \propto \frac{p(z_k|x_k^i)p(x_k^i|x_{k-1}^i)p(x_{0:k-1}^i|z_{1:k-1})}{q(x_k^i|x_{0:k-1}^i, z_{k-1})q(x_{0:k-1}^i|z_{1:k-1})}$$
$$= w_{k-1}^i \frac{p(z_k|x_k^i)p(x_k^i|x_{k-1}^i)}{q(x_k^i|x_{0:k-1}^i, z_{k-1})} \tag{2.35}$$

$$w^i = \frac{p(z_k|x_k^i)}{\sum_{j=1}^N p(z_k|x_k^j)} \tag{2.36}$$

This step updates the state probabilities but not the estimates.

4. Resample: any particle that has a weight w_i which is below the weight threshold is "killed", i.e. $w_i = 0$. The sample size is measured by the number of "live" particles, i.e. particles whose weight $w_i > 0$. If the effective sample size N_{eff} is below a threshold N_{thresh}, which is defined according to particular system estimation requirements, resampling is carried out where new particles are generated by replicating the remaining particles to maintain the total sample size.

5. Return to step 2 or end process, a weighted mean of the particles is computed to obtain the state estimation at time step k by

$$p(x_k|Z_{1:k}) \approx \sum_{i=1}^{N} w_k^i \delta(x_k - x_k^i) \tag{2.37}$$

The resampling procedure is crucial during the process of PF to maintain the effective number of particles as well as ensuring that particles which no longer contribute to the approximation of posterior distribution are replaced by new particles. Therefore, choosing the appropriate particle size and the right resampling method are the two fundamentals of achieving the optimal result at the end of the process. A widely accepted measurement of degeneracy is the effective particle cluster size N_{eff}, introduced in (Arulampalam et al., 2002) as

$$N_{eff} = \frac{N}{1 + var_\pi(w) * (x_{0:k})} \leqslant N \tag{2.38}$$

In most applications, a simpler estimate of N_{eff} is given by

$$\hat{N}_{eff} = \frac{1}{\sum_{i=1}^{N} (\widetilde{w}_k^i)^2} \tag{2.39}$$

PF seems to be very similar to UKF in some ways. However the two filters differs in several aspects. One of the most significant difference is that the sigma points in UKF are deterministically selected so that they represent certain specific properties while the particles in PF are generated randomly. The sigma points are weighted in a way so that they can be inconsistent with the distribution. Interpretation of sample points in UKF and their weights are not restricted to a certain range.

Chapter 3

Indoor positioning with selected sensors

3.1 Introduction

When one mentions indoor positioning, one often refers to the general idea of positioning in a GNSS-denied environment, which could be indoors, in forests, underwater, in tunnels or in urban canyons. People are so used to using GNSS positioning now that they would expect positioning could be achieved anywhere on the planet. What they may not realise is that a huge gap actually still remains between indoor- and outdoor-based positioning. It is the lack of a robust indoor positioning solution that prevents us from bridging this gap and providing seamless positioning to all users. This is becoming a growing concern as most people spend more than 70% of their time indoors but normal devices can only achieve very poor positioning accuracy while indoors (Benford, 2005; Zandbergen, 2009). Due to the complications of urban and indoor environments, there is still no one single solution that could solve all positioning problems under such conditions.

Based on the accuracy requirements and number of users as well as the cost that users are willing to pay, three different levels of positioning systems can be found where each solution provides a different level of accuracy and robustness for different situations and environments (Harle, 2013).

- Dedicated infrastructures implemented for the general public or specific staff in environments, such as airports and school campuses, where a high demand for positioning and navigation can be anticipated. Robust and accurate positioning is usually required in these places not only for its commercial potentials, but also due to life-and-safety critical applications.

- High accuracy but non-infrastructure based positioning systems in environments where dedicated infrastructure is hard to implement but accuracy is vital, e.g. for search and rescue teams in a mining tunnel or firefighters on a rescue mission. In such cases, users must perform positioning and navigation from the information provided

by sensors carried on themselves as well as the information obtained autonomously or collaboratively.

- Environments where accuracy requirements are less demanding and cost is the major factor. Ad hoc methods can be applied where users take advantage of available sensors and information that were not originally dedicated for positioning and apply them to enhance the positioning solution, such as wireless network signals, cameras and building mapping information. These sources of information are generally easy to acquire and require relatively lower costs than other solutions.

Depending on the specific situations and requirements, different sensors and algorithms should be applied. This thesis aims at providing indoor positioning solutions for mobile users which inevitably has to be low cost, easy to use and implement. Sections below will give several common indoor navigation algorithms that only require navigation measurement from low-cost equipments and is easily found in urban areas.

3.2 Pedestrian dead reckoning

Dead reckoning (DR), also known as Deduced Reckoning, is the process of measuring the position of a moving body based on its relative position or velocity to its previous state (Hofmann-Wellenhof et al., 2003). The concept of DR is simple and it is commonly applied in different areas of navigation, such as vehicle navigation, robotic tracking, aircraft navigation as well as pedestrian navigation (Fry and Wells, 1954; Azenha and Carvalho, 2008; Duan et al., 2014; Bao and Wong, 2014). Pedestrian dead reckoning (PDR) algorithms are DR applied to navigating or tracking a pedestrian based on the measurements that are obtained from walking patterns. PDR typically consist of three steps: step detection, step length estimation and position update. PDR requires the relative distance and direction measurement between two consecutive steps which is usually obtained by low-cost inertial sensors or even just accelerometers (Godha and Lachapelle, 2008; Kim et al., 2014). The analysis of acceleration measurements is also known as gait cycle detection, common step detection methods are autocorrelation, peak detection and zero crossings where all of them rely on identifying the frequency pattern of a typical step (Kim et al., 2004; Weimann et al., 2007; Zampella et al., 2011; Altun and Barshan, 2012).

A MicroStrain 3DM-GX3®-25 IMU is used throughout this thesis as a

low-cost foot-tracker to measure inertial measurements by fixing the unit on the user's foot during walking (Abdulrahim et al., 2012). Inertial data can be logged by any mobile device which is able to connect to the unit through Bluetooth or USB connector. A Raspberry Pi single-board computer is used here which provides a more portable solution for obtaining inertial measurements from IMUs. Figure 3.1 plots the total acceleration of the foot movement measured by the foot-tracker during a normal walk. A random noise can be observed at the beginning when the sensor is just turned on. To stabilise the sensor, an initialisation phase is carried out each time the sensor is turned on and before the actual data collection. Any still body on the Earth will experience the *g*-force, which is approximately $9.8m/s^2$, thus the detected step acceleration starts off just above $-10m/s^2$. The acceleration of the walking phase consists of cycles of very similar patterns with few minor jumps where each cycle represents a step.

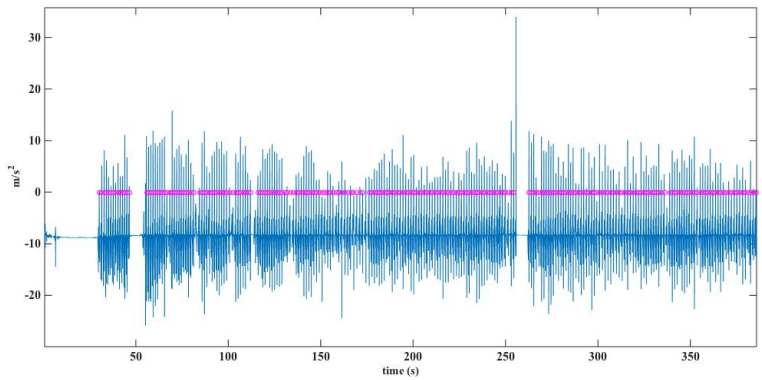

Figure 3.1: ZUPT step detection

In INS navigation, ZUPT correction is applied to minimise sensor errors. During ZUPT, a step detection has to be carried out to find the moment when the velocity of the foot should be $v_{foot} = 0m/s$. Step detection is also the first major requirement for PDR navigation. In the ZUPT applied here, steps are detected by comparing and correlating the foot acceleration measurements with a model of a single step acceleration model which is modelled prior to the navigation phase. Any cycle that matches with the step model is detected as a step, as indicated by magenta circles in Figure 3.1. However, human behaviours are not always predictable, and neither is the environment that we walk in. Any unexpected turning, foot swaying, slipping or jumping will cause anomalies in the acceleration pattern which could cause step detection errors. Figure 3.2a gives an example of under-detection during the walking phase, when the foot movement may have

suddenly reduced. Figure 3.2b is an example of over-detection when the foot may have swayed in the air while no step was taken. While small anomalies in the step acceleration pattern are hard to model, we can only detect steps that follow typical patterns. The number of mis-detections should be minimised to achieve better IMU based positioning. However, it is hard to completely eliminate such errors. To produce better positioning results, corrections should be applied based on the situation.

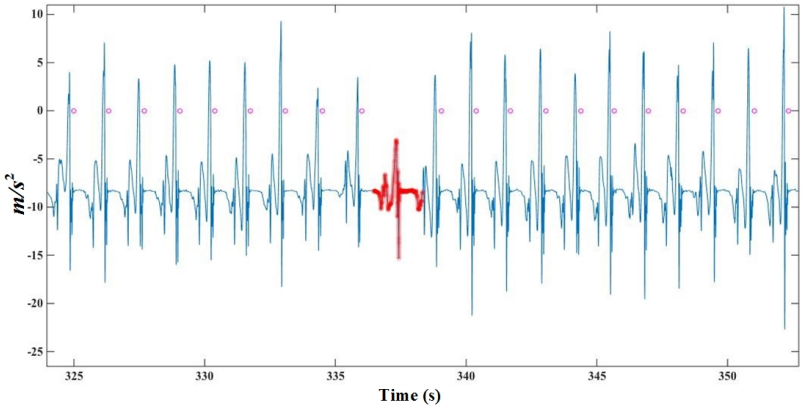

(a) Under-detection

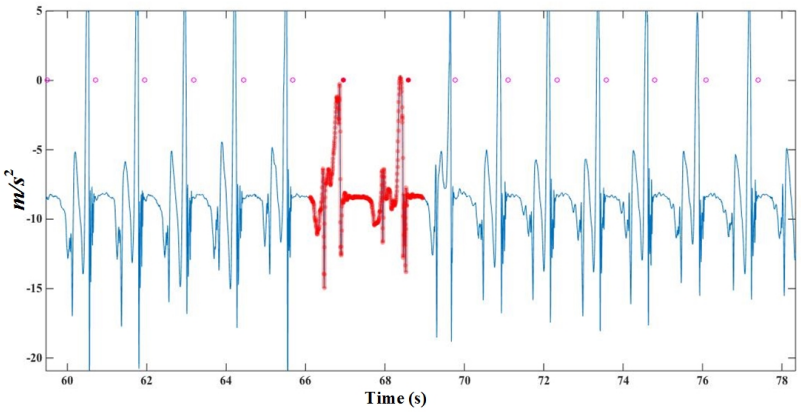

(b) Over-detection

Figure 3.2: Mis-detection of steps during ZUPT

The estimation of the actual step length is a more difficult task as it is highly dependent on different height and weight of the person wearing the foot-tracker as well as the actual step pace and the terrain. Even if the details of the environment are fully available, it will still be hard to correctly estimate the exact step length. To simplify the process, a constant step length model which assumes the step length is a constant value with a zero mean Gaussian noise is usually applied (Ladetto, 2000; Kim et al., 2004; Khan, 2011; Zampella et al., 2011; Nishiguchi et al., 2012; Valentin

and Mahesh, 2013). When a step is detected, the estimated step length with a directional measurement is fed into the DR model in Eq.3.1 to update the pedestrian position.

$$\begin{bmatrix} \hat{x}_k \\ \hat{y}_k \end{bmatrix} = \begin{bmatrix} \hat{x}_{k-1} + \hat{s}_{k|k-1} \cos \hat{\theta}_{k|k-1} \\ \hat{y}_{k-1} + \hat{s}_{k|k-1} \sin \hat{\theta}_{k|k-1} \end{bmatrix} \tag{3.1}$$

where $[\hat{x}_k, \hat{y}_k]$ is the estimated position at time step k, $\hat{s}_{k|k-1}$is the estimated length of the step taken from time $k-1$ to k, $\hat{\theta}_{k|k-1}$ is the measured heading from time $k-1$ to k. The procedure of the application of the DR model during a step is as shown in Figure 3.3.

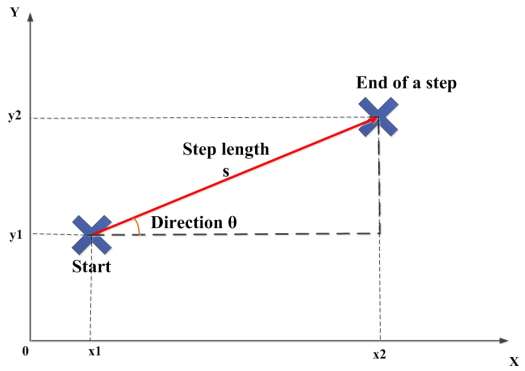

Figure 3.3: Dead reckoning during a step

3.3 Map matching

As maps are widely available in urban areas, they are commonly implemented in the navigation filter through map matching. Maps provide the details of roads, junctions, construction sites and natural landscape, etc. Map matching integrates this information into the positioning system to aid navigation performance as the moving user is only allowed to travel according to certain rules according to the map (Morisue and Ikeda, 1989; Quddus et al., 2007; Bao and Wong, 2013). It was introduced in military aviation for terrain contour matching and later widely applied in road based transport navigation. Map matching minimises and constrains positioning errors by eliminating estimations that fall outside the road boundary or any other features that allow the vehicles to travel on.

In pedestrian navigation, map matching is applied based on the general rule that humans must walk on the ground and the only possible way to get from one side of the wall to the other is by going through doors. This means that if the navigation estimation of a pedestrian is crossing walls or jumping through floors then something must be wrong. When map

information is known beforehand and ready to be integrated in positioning systems, it provides a good constraint on pedestrian navigation by preventing estimations going to the wrong places (White et al., 2000). Indoor maps can be expressed by many different methods, such as schematic maps, CAD maps or polygons. Polygons are the most straightforward representation of rooms and corridors while directions could be easily extracted as well.

The map information applied throughout this thesis is based on polygons that are stored in a matrix format. The rooms are represented by polygons which describe the coordinates of each corner of the room and the doorways in the sides of the polygon. Doors are represented by the coordinates of the middle point of the door. In the matrix, the ID of the wall that it sits in and the rooms that are on either side of the door are given. An example of the polygon matrix is shown below.

Table 3.1: Example of a map matrix

(a) Room polygon-wall relationship

Polygon No.	Wall position	Door No.
1	$\begin{bmatrix} x^1_{w1} & y^1_{w1} \\ x^1_{w2} & y^1_{w2} \\ \vdots & \vdots \\ x^1_{wn} & y^1_{wn} \end{bmatrix}$	$[1]$
2	$\begin{bmatrix} x^2_{w1} & y^2_{w1} \\ x^2_{w2} & y^2_{w2} \\ \vdots & \vdots \\ x^2_{wn} & y^2_{wn} \end{bmatrix}$	$[2, \quad 4]$
$\vdots$	$\vdots$	$\vdots$
m	$\begin{bmatrix} x^m_{w1} & y^m_{w1} \\ x^m_{w2} & y^m_{w2} \\ \vdots & \vdots \\ x^m_{wn} & y^m_{wn} \end{bmatrix}$	$[k]$

(b) Door-room relationship

Door No.	Door position	Linked Rooms
1	$[x_1, y_1]$	$[1, 11]$
2	$\begin{bmatrix} x_2 & y_2 \\ x_4 & y_4 \end{bmatrix}$	$[2, 11]$
$\vdots$	$\vdots$	$\vdots$
k	$[x_k, y_k]$	$[m]$

This is a simple way to store the building map information and apply it to different platforms. This format can be stored as a *kml* file and used for visualisation in Google Map as well as Matlab. The user can easily find its position within the building matrix and extract useful information, such as

the location of walls and the heading of the corridors. The building map of Nottingham Geospatial Building (NGB) on the University of Nottingham campus is surveyed and stored as polygons in *kml* format. The map can be loaded onto Google Earth and is shown as below.

Figure 3.4: KML Map loaded in Google Earth

3.4 Wireless signal positioning

Wireless Fidelity, or commonly known as Wi-Fi, is the WLAN product based on the IEEE 802.11 standards and currently operates on the 2.4GHz and 5GHz radio wavebands. However, according to studies and surveys, the 2.4GHz frequency band is much more heavily occupied than the 5GHz band (AEGIS Engineering and Quotient Associates, 2013; Farshad et al., 2014). The 2.4GHz band operates on the 802.11b standard with a limited radio power of 20 dBm (100 mW) in Europe. This band is divided into eleven 5MHz wide channels by the Federal Communications Commission (FCC). To avoid interference, networks must be separated by five channels. The 802.11b and 802.11g standards were released in 1999 and 2003 respectively to enhance data rate for 2.4GHz band. The 5GHz band operates on both the 802.11a and 802.11n standard where the bandwidth for 802.11a is 20MHz and bandwidth for 802.11n is 20 and 40MHz (Molisch, 2011). A few of the earlier and most commonly used protocol standards are listed in Table 3.2.

Table 3.2: Summary of 802.11 network standards

802.11 protocol	Frequency (GHz)	Bandwidth (MHz)	Indoor range (m)	Outdoor range (m)
a	5/3.7*	20	35	120
b	2.4	22	35	140
g	2.4	20	38	140
n	2.4/5	20/40	70	250

*3.7GHz will not be discussed here

Originally designed for wireless connection to the internet from personal computers, phones and other mobile devices, its widespread applications promotes the growing coverage of Wi-Fi signals in urban areas. From Table 3.2, we can see that each Wi-Fi access point (AP) has an average range of around 30m indoors and more than 100m outdoors. This technology has promoted a growing number of mobile device users which leads to a general growth in data traffic in all mobile networks. Statistics show that mobile data traffic will grow more than 500-fold between 2010 and 2020 (Chin et al., 2014). Therefore, while GNSS signals are blocked in urban areas, the dense Wi-Fi and mobile network is a good compensation. Although these wireless signals were not initially designed for positioning purposes, they have enabled the development of many indoor positioning solutions based on Wi-Fi signal characteristics.

A common problem for all wireless signals in urban environments is obstructions which cause multipath, shadowing and interference. However, unlike GNSS signals, there is no positioning data or code to extract and we can only rely on the received signal physical characteristics for positioning. Due to obstructions, wireless signals typically come in two types, line-of-sight (LOS) and non-line-of-sight (NLOS) signals. LOS signals that travel between the transmitter and the receiver in a straight line with no obstruction are also referred to as Direct Path (DP) measurements, e.g. signal between Tx and Rx1 in Figure 3.5. NLOS is caused by either DP excess delay or non-direct path (NDP). DP excess delay is experienced if the signal reaches the receiver by travelling in a straight line but penetrating through some kind of obstruction, e.g. signals from Tx penetrate the wall to reach Rx2. If the DP signal is completely blocked, the receiver would only be able to detect the signal from a reflected or refracted path, which is referred to as NDP, e.g. the signal between Tx and Rx3. In both cases, the signal propagation times are extended and the signal strength weakened, partial changes in the signal physical characteristics may be experienced as well. Meanwhile, wireless signals also have a natural fluctuation regardless of everything else. Wireless signal based positioning errors result from a contribution of all these related factors.

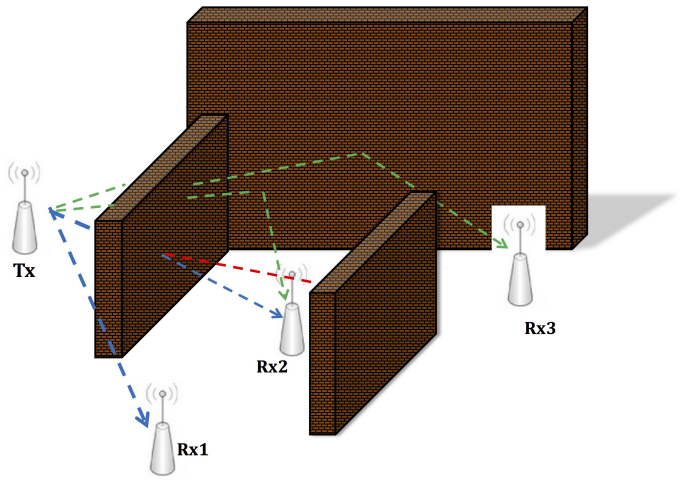

Figure 3.5: Diagram of NLOS and LOS signal

3.4.1 Wi-Fi fingerprinting

Wireless signals are widely popular for indoor positioning as they are commonly found inside buildings. However, as a result of path-loss and other disturbances, signals are unstable even when the receiver remains static at one location. As already introduced, fingerprinting (FP) is a solution that aims to overcome the signal variation problem in complicated areas. FP is solved by identifying the actual received signal patterns rather than relying on a theoretical path-loss model.

The Radar system was among the first systems to provide localisation based on FP (Bahl and Padmanabhan, 2000) and many others followed in more recent years, addressing some of the shortcomings of the basic FP method (Youssef and Agrawala, 2008; Bolliger, 2008; Rai et al., 2012). FP typically consists of two steps. The first step is the training phase, where the received signal strength (RSS) from all observable APs at a number of chosen training points (TP) is scanned and recorded in a database. To train for an accurate database, a large number of TPs should be selected covering the entire area of interest. These RSS vectors are known as *fingerprints*. Fingerprints are typically structured as $\{(x,y)|(MAC_1, R\bar{S}S_1),(MAC_2, R\bar{S}S_2)...(MAC_n, R\bar{S}S_n)\}$, where (x,y) is the accurate position of the TP, MAC_n is the identification (MAC address) of the nth AP, $R\bar{S}S_n$ is the RSS from the AP at the location of the TP, which is usually the mean of the RSS over a period of time. In the second step, also known as the positioning phase, the user measures the RSS from all the detectable APs at an unknown location and compares

the vector to the fingerprints in the database. The position of the best matched fingerprint is regarded as the current location. The performance of fingerprinting depends on the quality of the trained database. However, training for a high quality fingerprint database can be a very time consuming job. Therefore, many studies try to address these shortcomings by trying to reduce the pre-training workload and achieve positioning from less training data while providing the same level or enhanced positioning accuracy (Mok and Cheung, 2013; Alhmiedat et al., 2013; Dutzler, Roland et al., 2013; Luo et al., 2013).

3.4.2 Data collection

3.4.2.1 24hr data at specified locations

To develop a comprehensive understanding on the behaviour of Wi-Fi signals inside modern office buildings, several datasets were collected in different places inside the NGB. The selected experiment locations were a store room (referred to as Location1), a small office room (referred to as Location2) and an open plan area (referred to as Location3) respectively, shown in Figure 3.6. A Toshiba laptop was placed at each location and data was collected for 24 hours using an open source software inSSIDer Version 2.1.1.13 (Metageek, 2012). The computer wireless adapter hardware is an Intel® Centrino® Advanced-N 6200. All APs are fitted on to ceilings and their locations are marked out as red stars on all three floors of the NGB floor plan as shown in Figure 3.7. Green triangles indicate the three data collection points.

(a) Store room (Location1)

(b) Small office (Location2)

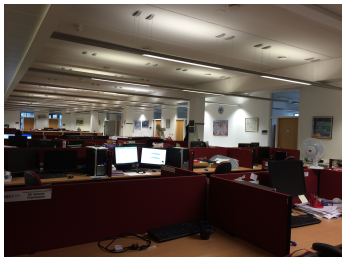

(c) Open plan area (Location3)

Figure 3.6: Data collection locations

(a) Floor A

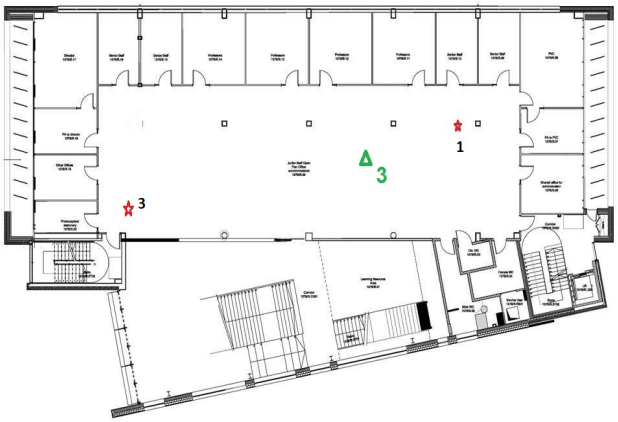

(b) Floor B

(c) Floor C

Figure 3.7: AP locations in NGB (all hardware are fitted on the ceiling)

The data logging software is shown in Figure 3.8. The RSS from all

visible APs are logged in GPS Exchange Format (GPX) file. All required data are extracted from the original file and put into an ascii text file to reduce file size and enhance processing efficiency.

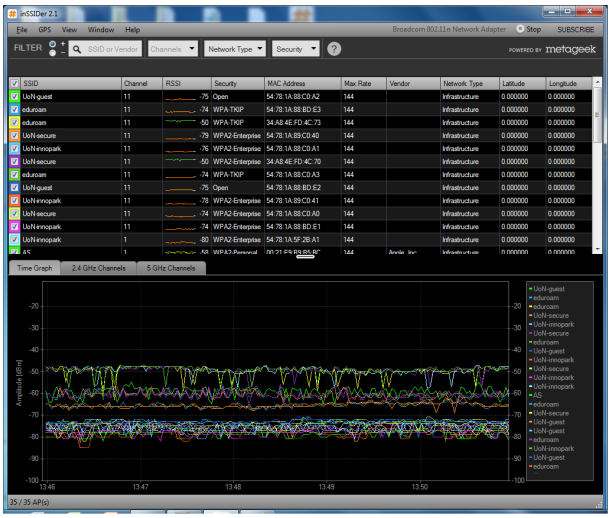

Figure 3.8: inSSIDer logging software

Cisco 1142 series (802.11a/b/g/n) wireless APs were installed in the NGB. All were equipped with internal omnidirectional antenna and provide coverage on both 2.4GHz (802.11b/g/n) and 5GHz (802.11a/n) radio bands, with auto Radio Frequency (RF) power setting (Convergis and Logicalis, 2011; Cisco Systems, Inc, 2012). APs provide wireless coverage with a minimum of 25dB signal-to-noise ratio (SNR) on 2.4GHz band and maximum transmit power is 20dBm on both frequencies. Antenna power gains are 4.0dBi and 3.0dBi for 2.4GHz and 5.0 GHz respectively. Usually the power is kept at a low level to gain extra capacity and reduce interference. For an overview of the signal pattern over a period of time, the 24 hour RSS data from four of the APs in the building at data collection location 1 are plotted in Figure 3.9. The RSS data from all APs collected at other data collection locations are plotted in Figure A.1, A.2 and A.3 in Appendix A.1. Signal fluctuation can be observed throughout the entire data collection period from all APs which is indicated by the spikes in the plots. Furthermore, a slight change in the average signal strength could be observed during the 24 hours of the collection period. This illustrates that the signal strength is time dependant which might be due to change during working hours when there is more disturbance and more users. If we zoom in onto any of these plots and try to extract the RSS for a very short period of time, we can see that the signal strength could vary up to more than 10dB due to fast fading, as shown in Figure 3.10. However, if the fast

fading is filtered out in the signals, we can still clearly identify a mean signal strength, indicated by the red box in Figure 3.10, which is relatively stable over periods of hours. Slow fading may also occur over time. As its effect may not be permanent, the characteristics of the signal needs to be derived from data collected over a longer period rather a short instant of time. However, unless there is permanent change in the environment, the statistics of the signal strength from a 30 minute dataset can sufficiently characterise the RSS pattern for a longer period without having to collect data for hours and days.

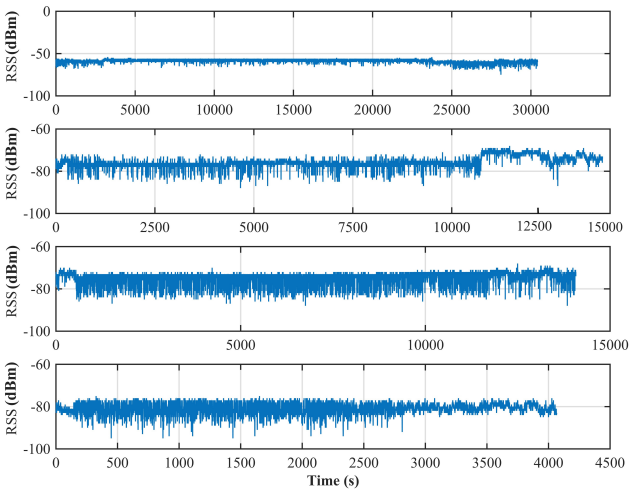

Figure 3.9: 24Hr RSS data pattern of four APs at Location 3

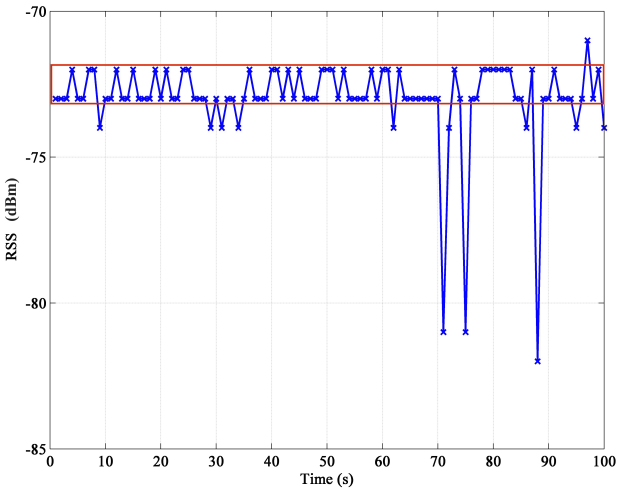

Figure 3.10: Extract of 100s from 24Hr RSS data

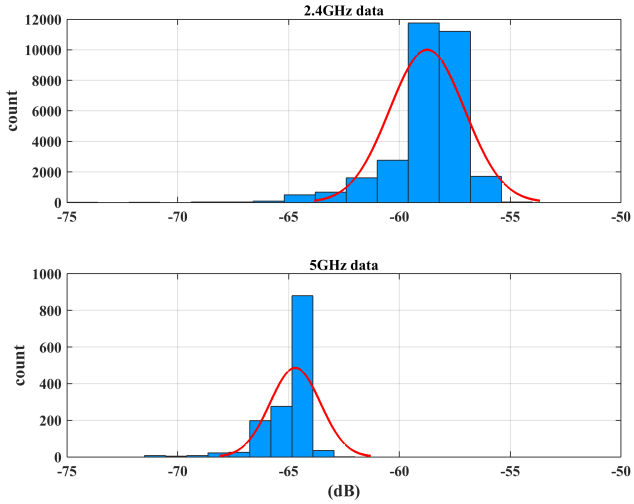

Figure 3.11: RSS data histogram

Figure 3.11 shows the histogram of RSS data for both 2.4GHz and 5GHz data over a period of time. Both signals are slightly skewed and not strictly normally distributed. Therefore, Table 3.3 list the mean, median and standard deviation of RSS from all APs in the building at each location. As the median remains close to the mean, hence the distribution can be regarded as a Gaussian distribution. This is a main reason why in later sections, the Gaussian process can be used to derive RSS from collected data. The signal strength is higher when the receiver is located closer to the AP. Yet the signal variance is not so much related to the distance nor the specific AP hardware. The standard deviation of the RSS at Location3, which is the open plan area, is actually larger than the other two locations on average.

Table 3.3: Wi-Fi RSS 24Hr observation (dB)

AP	MAC address	Location1			Location2			Location3		
		Mean	Median	Sd	Mean	Median	Sd	Mean	Median	Sd
1	34:A8:4E:FD:4C:70/1/2/3	-84.7	-85	1.2	-82.9	-83	1.0	-55.6	-56	2.2
2	34:A8:4E:FD:7D:80/1/2/3	-73.5	-74	1.4	-81.9	-82	1.7	-64.9	-65	1.9
3	54:78:1A:21:DA:60/1/2/3	-74.3	-74	1.4	-72.8	-73	1.1	-58.7	-59	1.7
4	54:78:1A:5F:2B:A0/1/2/3	-66.2	-66	1.0	-66.0	-65	1.7	-79.2	-80	2.2
5	54:78:1A:72:E1:00/1/2/3	-60.0	-60	1.6	-68.5	-68	1.6	-75.8	-76	2.4
6	54:78:1A:88:C0:A0/1/2/3	-78.2	-78	1.5	-81.3	-81	1.3	-74.4	-74	2.4
7	54:78:1A:88:BD:E0/1/2/3	-46.5	-47	1.4	-42.4	-44	4.0	-79.1	-79	1.5
8	54:78:1A:89:C0:40/1/2/3	-67.9	-68	0.9	-72.0	-72	1.4	-81.1	-81	2.9

3.4.2.2 RSS data at varying distances

Even though the RSS tends to change very rapidly over the 24 hours, the average signal remains relatively stable and the fluctuation usually stays within a certain range with occasional jumps. The RSS still follows the general pattern of the path loss model, i.e. the RSS reduces as the distance between the receiver and AP increase. To further investigate the relationship of signal strength path loss and the distance, several different environments where selected and RSS was collected at various distances from the AP. A Samsung Galaxy GT-P1000 tablet was used as the receiver with more mobility to move around in different places. WifiLogger, software developed at Nottingham Geospatial Institute (NGI) for Android devices, was used to log Wi-Fi RSS data on the tablet. A BT Voyager wireless ADSL router was used as the AP enabling us to place the router outdoors and investigate Wi-Fi signal patterns in different environments. As the device used here is different to the receiver and AP used previously, the absolute signal strength values may vary due to different hardware offsets. But the offset between different equipments should remain the same and the relative change is more influenced by the environment which is what we are interested in here.

(a) Corridor (b) Roof (c) Open outdoor

Figure 3.12: Data collection locations

The first selected location for data collection is a corridor on Floor A of NGB. The router is placed at one end of the corridor and the tablet is placed at every 10cm until 50cm, then every 25cm until 2m, every 50cm until 5m and every metre until 10m away from the AP. Data is collected for a period of 10 minutes at each distance. The second location is on the roof of NGB where there is less disturbance. The router is placed at a fixed point and the receiver is placed in the same pattern as the first trial. The third environment is a large meadow with no obstructions. This is an open outdoor environment where the nearest wall or tree is at least

200m away making this the environment with the least multipath and signal interference. RSS was measured up to 300m away from the AP. The collected RSS data is plotted in Figure 3.13 as well as the mean and standard deviation of the signals at each location from the AP.

From Figure 3.13, we can identify the general pattern of signal path-loss as the receiver moves away from the AP. However, such path-loss is not a smooth drop. We can identify several stages where as the distance increases the RSS does not continue to reduce or may even increase slightly. Within a short distance, we can see this stage begins at around 2m. When the observation distance increases, the RSS drops rapidly for the first 30 meters while remaining around the same level for almost 100m after that. However, the signal fluctuation in all environments can be so large that the same RSS could be indicating distances that are different by 3-5m. Also, the RSS reduction slows down as the distance grows longer. This causes more ambiguity in RSS-based ranging as the distance from the AP grows as the same RSS could indicate any distance that are 10m apart. This also implies that the RSS at a single location is unstable and is prone to change even in short periods. Therefore, even if we apply fingerprinting instead of path-loss based ranging, we still have to be aware that the current RSS vector may differ to the previously collected fingerprint from the same location. This is one of the major error sources hence it is important to know how much signal strength difference to expect at different locations.

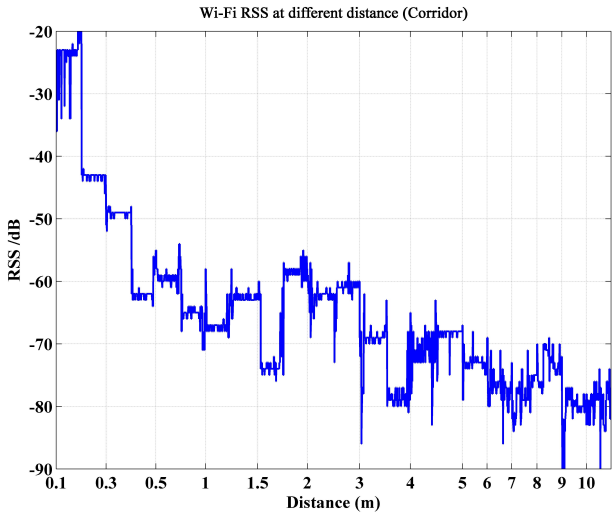

(a) RSS in corridor

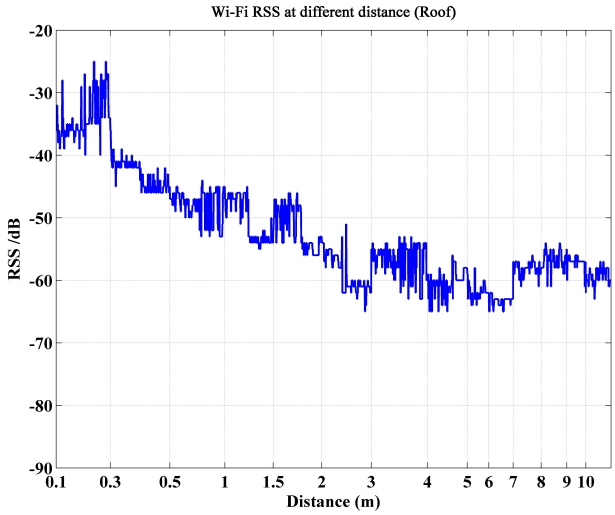

(b) RSS on the roof

Figure 3.13: RSS at varying distance to the AP

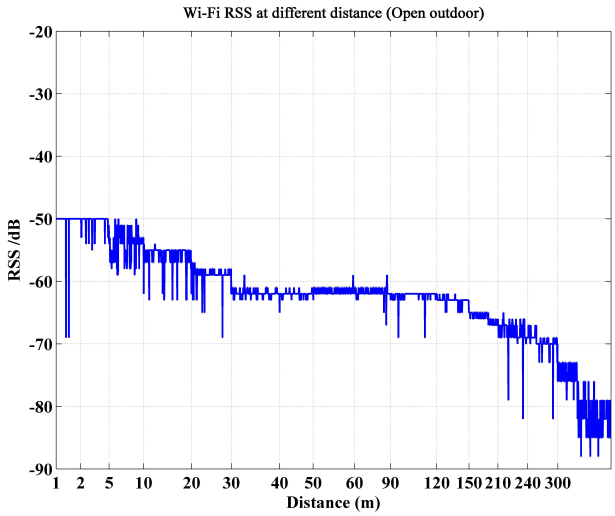

(c) RSS outdoors

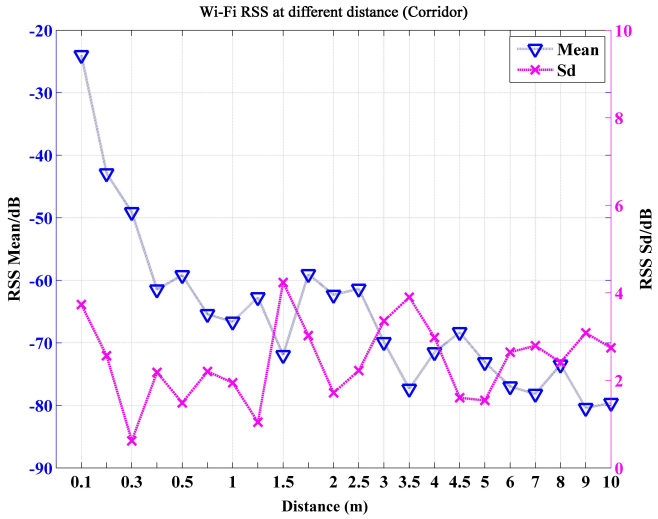

(d) RSS mean and std in corridor

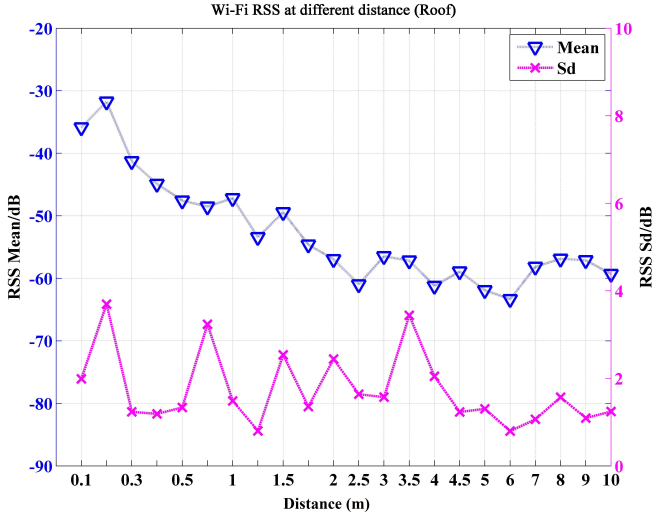

(e) RSS mean and std on the roof

Figure 3.13: RSS at varying distance to the AP(Cont'd)

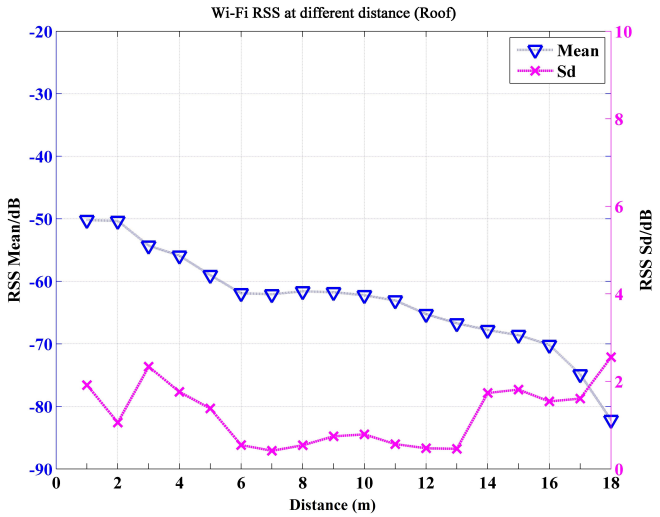

(f) RSS mean and std outdoors

Figure 3.13: RSS at varying distance to the AP(Cont'd)

3.4.3 Building the fingerprint database

The conventional method for training the database is by placing the receiver at a selected number of TPs as described in Chapter 2. The smaller the fingerprint grids are, the more training points are required, which means the more detailed the database would be. However this would also increase the training cost from the time aspect, equipment requirement and human labour.

3.4.3.1 Training data

During the positioning phase based on conventional fingerprint training, the observed RSS at an unknown location will be compared to each of these fingerprints and the position is returned usually based on the location of the fingerprint that has the most similar set of RSS or mean of the first *k* fingerprints, also known as *k-nearest neighbour* (*k*-NN). The distance in signal strength between the observed RSS and the fingerprints is found by

$$D_m = \sqrt{\sum_{i=1}^{n}(RSS_i - FP_i)^2} \tag{3.2}$$

where RSS_i is the observed RSS from AP_i at the unknown location, FP_i is the RSS of the *m*th fingerprint from AP_i. The first *k* fingerprints with the smallest D_m are returned as the *k* nearest fingerprints and the position is obtained by averaging their position. The way that positions are obtained implies that if the TPs are 5m apart, then the final position will have an

ambiguity of 5m due to lack of fingerprints. Therefore selecting more TPs will reduce the ambiguity in the final positioning result.

To start the training process, 56 TPs are selected to cover the entire accessible area in NGB Floor A, as shown in Figure 3.14. A laptop is used throughout the trials and data is logged by inSSIDer. Two rooms are trained in particular detail, i.e. a meeting room (denoted as R1) with no obstruction, and a heavily obstructed store room with metal shelves (denoted as R2). Another 56 TPs are selected to cover these two rooms with 1m$\times$1m grids. Training for all TPs is done by placing the laptop at each location and data is collected for around 15 to 30 minutes until at least 100 vectors are received from each AP. During the time of this trial, each AP transmits signals on both the 2.4GHz and 5GHz frequencies. Therefore, the data from each AP is separated into “a” and “b”, where “a” represents 2.4GHz signals and “b” represents 5GHz signals. The mean and standard deviation of the entire collection of data from all eight APs at each TP is obtained and stored in the training database.

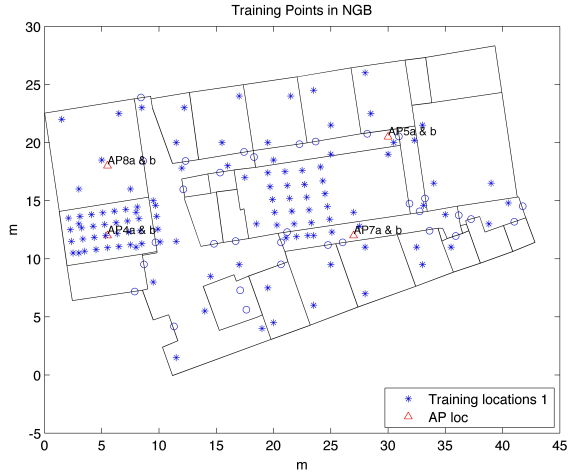

Figure 3.14: Static database training points

The signal strength difference between the 2.4GHz and 5GHz is listed in Table 3.4. Results show quite a significant difference between the signals on the two frequency bands thus they should be treated separately during the positioning phase. Fingerprinting algorithms can be based on either one of the three different databases, i.e. 8-AP database of 2.4GHz signal, 8-AP signal database of 5GHz signal or 16-AP database of both frequencies.

Table 3.4: RSS difference between 2.4GHz and 5GHz

	AP1	AP2	AP3	AP4	AP5	AP6	AP7	AP8
ΔRSS	7.42	2.15	5.00	-6.11	10.32	2.82	4.40	5.22
σ	7.19	5.17	8.38	5.54	5.56	4.31	6.39	6.41

3.4.3.2 Gaussian process regression generated database

Figure 3.14 provides a general idea of the density of TPs selected within the building. Although these points cover most of the critical locations and the total training time lasts for several days, this is still far from a "detailed" database. However, based on the trained fingerprints for the TPs, we can generate further fingerprints for locations that were not selected as TPs through a machine learning process. We can assume that the Wi-Fi signal noise follows the Gaussian distribution and the RSS of the fingerprint is correlated with the distance between the AP and location of the fingerprint. This process of generating new data from known data applied here is through a machine learning method known as Gaussian process regression.

Gaussian process (GP**)** is a stochastic process where the random variables can be described by the Gaussian probability distribution. It is a generalisation of the Gaussian probability distribution at each point of a certain range of space or time from the training data (Rasmussen and Williams, 2006). A Gaussian process can be realised through classification or regression, depending on whether the output is discrete or continuous. Gaussian Process Regression (GPR) is applied here as we need to create a continuous map of fingerprints covering the entire building based on the data from trained fingerprints. The basic concept of the process is explained below. Let $D = \{(x_i, y_i), i = 1, 2, ..., n\}$ be a set of training observations drawn from a real noisy process,

$$y_i = f(x_i) + \varepsilon \tag{3.3}$$

where x_i is the the input training data and y_i is the target observation or output values. ε is an independent and identically distributed (i.i.d.) Gaussian distribution noise that follows $\mathbb{N} \sim (0, \sigma_n^2)$. GPR estimates the posterior distribution over functions f from training data D. GPR is plausible under the conditions that the function values on the specified space are correlated, hence the function values $f(x_i)$and $f(x_j)$ depend on the input values x_i and x_j. Therefore, the GP can be fully specified by a mean function $m(x)$ and covariance function $k(x, x')$,

$$m(x) = E[f(x)] \tag{3.4}$$

$$k(x, x') = E[(f(x) - m(x))(f(x') - m(x'))] \tag{3.5}$$

The covariance function is also known as the *kernel*. Gaussian process is then denoted as

$$f(x) \sim GP(m(x), k(x, x')) \tag{3.6}$$

The key predicative equations for the regression process expand Eq.3.4 and Eq.3.5 into

$$\bar{\mathbf{f}}_* \triangleq E[\mathbf{f}_*|X, \mathbf{y}, X_*] = K(X_*, X)[K(X, X) + \sigma_n^2 I]^{-1}\mathbf{y} \tag{3.7}$$

$$cov(\mathbf{f}_*) = K(X_*, X_*) - K(X_*, X)[K(X, X) + \sigma_n^2 I]^{-1}K(X, X_*) \tag{3.8}$$

where X_* is a vector of the test input points, $\mathbf{f}_*$ is the corresponding function value, X is the training input, $\mathbf{y}$ is the training output or observed values, and σ_n^2 is the noise variance. The covariance function is a crucial part of the GPR prediction as it defines the similarity or the closeness of the trained dataset. Generally, three types of covariance functions can be applied to determine the prediction depending on the relationship between training data and predictive data. A *stationary* covariance function is a function of $\mathbf{x} - \mathbf{x}'$, such process is invariant to translations in the input space. An *isotropic* covariance function is a function of $|\mathbf{x} - \mathbf{x}'|$ where the process is invariant to rigid motions. A *dot product* covariance function is when the covariance is only dependent on $\mathbf{x}$ and $\mathbf{x}'$ through$\mathbf{x} \cdot \mathbf{x}'$.

The covariance function is typically specified by some free parameters, known as hyperparameters. A common form of the covariance function is the square covariance function, expressed as,

$$k_y(x_p, x_q) = \sigma_f^2 \exp(-\frac{1}{2\ell^2}(x_p - x_q)^2) + \sigma_n^2 \delta_{pq} \tag{3.9}$$

The hyperparameters here consist of the characteristic length scale ℓ, the signal variance σ_f^2 and the noise variance σ_n^2, denoted as $\theta = (\sigma_n^2, \ell, \sigma_f^2)$. The characteristic length-scale defines how far you can move in the input space for the function values to stay correlated.

The *marginal likelihood* is given here which refers to the marginalisation over the function values $\mathbf{f}$, which is the product of the integral of the

likelihood and the prior,

$$p(\mathbf{y}|X) = \int p(\mathbf{y}|\mathbf{f}, X)p(\mathbf{f}|X)d\mathbf{f} \tag{3.10}$$

where X are the inputs, $\mathbf{y}$ is the target vector, $\mathbf{f}$ indicates the function values. The log marginal likelihood conditioned on the hyperparameters can be derived from the integration as

$$\log p(\mathbf{y}|X, \theta) = -\frac{1}{2}\mathbf{y}^T(K + \sigma_n^2 I)^{-1}\mathbf{y} - \frac{1}{2}\log|K + \sigma_n^2 I| - \frac{n}{2}\log 2\pi \tag{3.11}$$

Training for a Gaussian process actually refers to the selection of the covariance function and its parameters. These parameters, i.e. the hyperparameters, are found by maximising the marginal likelihood which is achieved through the partial derivative of Eq.3.11. The hyperparameters define the specific mean and covariance functions which are then applied for prediction.

3.4.3.3 GPR database quality

The density of the fingerprints in the conventional fingerprint training method is greatly constrained by the number of TPs selected, which directly impacts the length of dedicated working hours. However, signal strength observation trials show that the RSS follows the general pattern of the path-loss model hence RSS relates to the distance and the number of obstructions, i.e. walls, between the training location and the AP. This allows us to increase the fingerprint density by applying GPR based on the collected training data, as introduced in many literatures (Ferris et al., 2006; Huang et al., 2011; Faragher et al., 2012).

The GPR generated fingerprint database will be referred to as the static fingerprint database, denoted as s-DB. This is regarded as the best possible fingerprint database as the generated fingerprints cover the entire training area in high density. Hence it is regarded as the "ground truth" database throughout this thesis. However, to generate this database with high confidence level, a large amount of TPs have to be selected. Although GPR has helped to reduce a huge amount of training time, but training for this database is still very time consuming. If the training time for each TP lasts for 30 minutes, then the entire training time for 112 points is more than two days if training continues nonstop. s-DB for both the 2.4GHz and 5GHz frequency band of the eight APs are shown in Figure 3.15 and Figure 3.16.

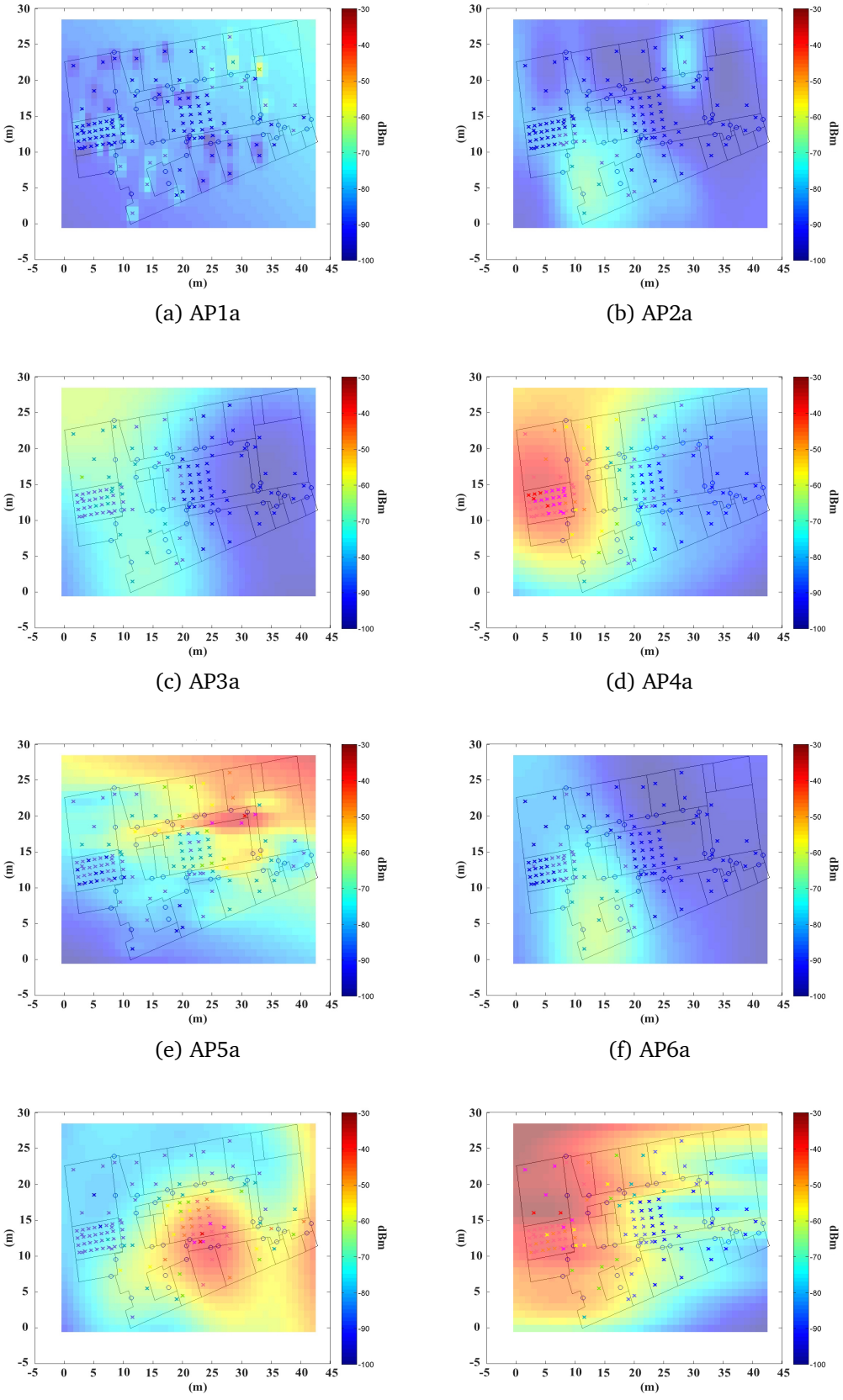

(a) AP1a (b) AP2a

(c) AP3a (d) AP4a

(e) AP5a (f) AP6a

(g) AP7a (h) AP8a

Figure 3.15: Static fingerprint database for AP1 - 8 (2.4GHz)

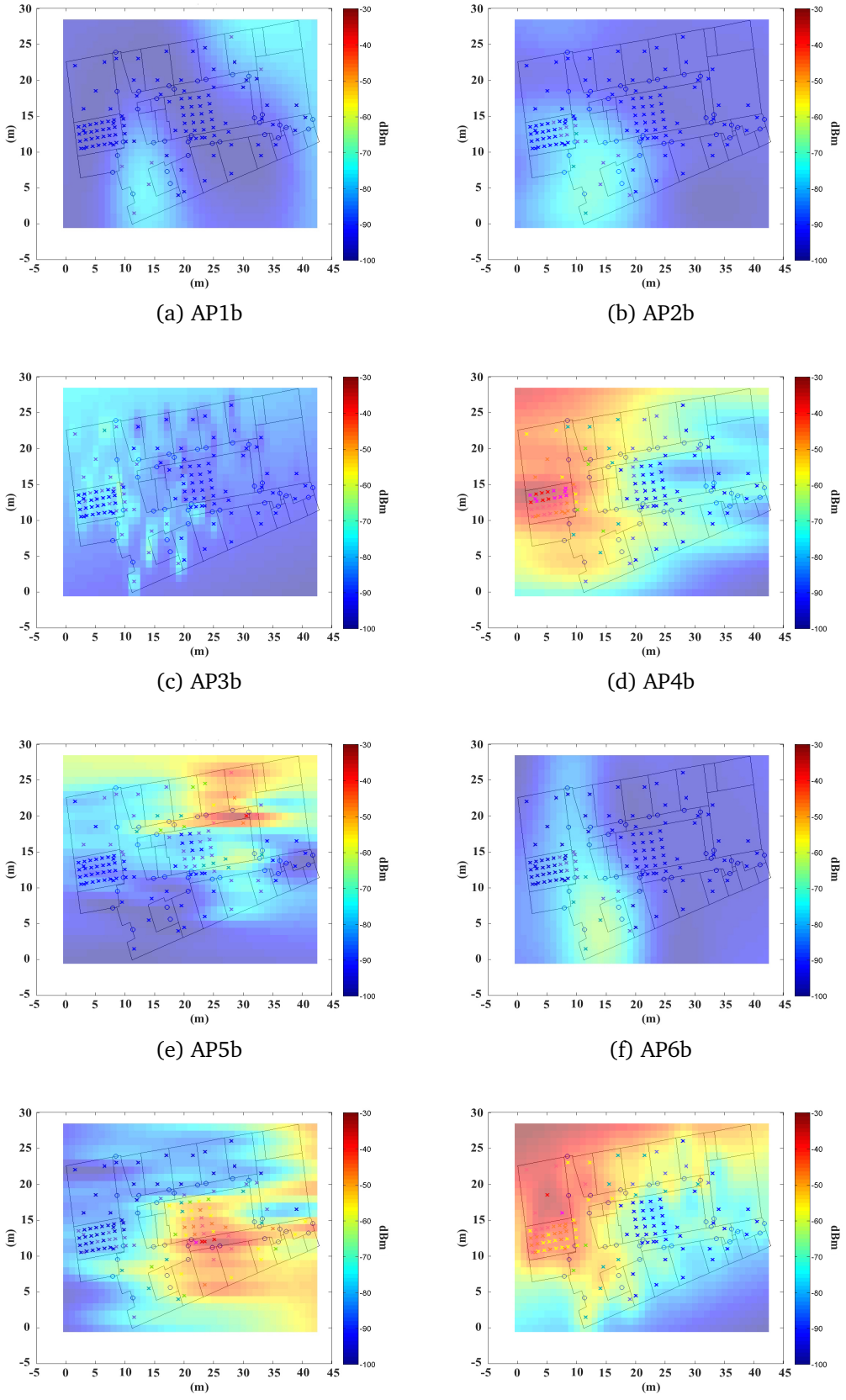

(a) AP1b (b) AP2b

(c) AP3b (d) AP4b

(e) AP5b (f) AP6b

(g) AP7b (h) AP8b

Figure 3.16: Static fingerprint database for AP1 - 8 (5GHz)

The s-DB divides the building into 1m×1m grid cells. Fingerprints are generated at the mid-point of each grid cell based on the collected fingerprints and it is assumed that the RSS remains the same within each grid cell. To verify the accuracy of the s-DB, the difference of the RSS (ΔRSS), between the trained fingerprints and the generated fingerprints of the s-DB at distances from 1m up to 8m apart are compared. The mean and standard deviation of the ΔRSS at 1m, 3m and 6m are listed in Table3.5.

Table 3.5: ΔRSS of static TP and GPDB

(a) RSS difference of static TP and GPDB 2.4GHz (dB)

	AP1a		AP2a		AP3a		AP4a		AP5a		AP6a		AP7a		AP8a	
	m	Sd	m	Sd	m	Sd	m	Sd	m	Sd	m	Sd	m	Sd	m	Sd
1	3.2	2.8	3.2	2.4	3.4	3.0	4.3	3.8	1.4	1.2	3.7	2.8	2.6	2.4	13.0	7.7
3	5.5	5.8	3.6	2.8	3.4	3.1	4.4	3.9	4.7	4.3	3.7	2.9	2.8	2.7	13.2	8.5
6	5.6	5.6	5.2	4.1	3.6	3.2	5.6	4.4	5.1	4.7	4.5	3.1	4.6	3.8	13.2	9.1

(b) RSS difference of static TP and GPDB 5GHz (dB)

	AP1b		AP2b		AP3b		AP4b		AP5b		AP6b		AP7b		AP8b	
	m	Sd	m	Sd	m	Sd	m	Sd	m	Sd	m	Sd	m	Sd	m	Sd
1	2.9	2.8	4.4	2.6	3.9	2.6	11.1	7.5	2.2	2.0	3.6	2.4	1.9	1.2	14.1	8.6
3	3.4	2.6	4.5	2.7	4.1	2.7	11.4	8.0	6.6	6.0	3.8	2.6	4.5	4.3	13.7	10.3
6	5.3	2.3	5.4	3.1	4.8	3.1	12.5	8.8	7.1	6.2	4.9	3.3	5.9	5.1	13.6	11.9

The overall increase in ΔRSS could be seen from Figure 3.17. We can see here that when the GP generated RSS stay within a distance limit of 3m from the TP location, the RSS is only slightly different from the training data. However, the ΔRSS does not increase linearly when the distance between the TP and the generated fingerprint is over 6m. In some cases, it remains the same level or might even reduce slightly. However, this does not mean that a fingerprint generated based on the fingerprint of a TP that is more than 8m away is still reliable. It simply indicates that this distance has crossed over the correlation threshold as the distance between the training data and predicted data is too long. s-DB will be used as the primary database for fingerprint positioning in this chapter and Chapter 5. The positioning results and performance of other fingerprint database will be compared to this database.

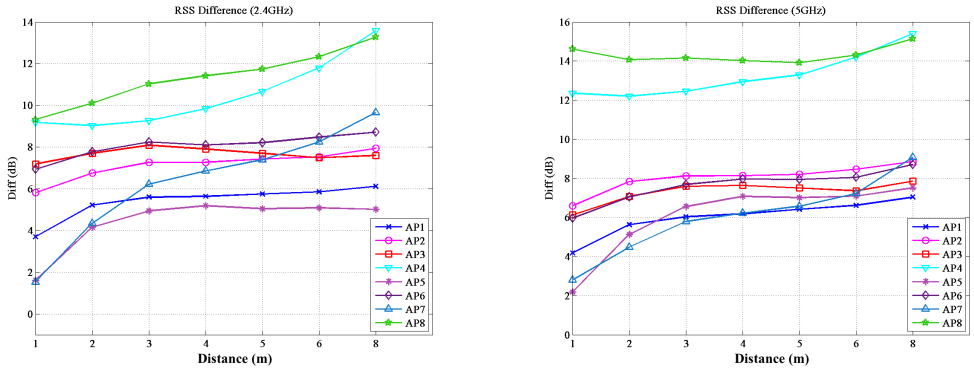

(a) 2.4GHz (b) 5GHz

Figure 3.17: ΔRSS between fingerprints and training data at different distances (dB)

3.5 Dead reckoning and Wi-Fi integration

We can see from Figure 3.15 and Figure 3.16 that a large area or even very different places may have the same RSS leading to ambiguity in positioning. We could eliminate part of this ambiguity by telling the system that a person can only travel so far on foot thus restricting the distance between consecutive positions. The distance between each step can be achieved through DR models as introduced in Section 3.2.

The behaviours of the errors from DR and Wi-Fi positioning are quite different as the DR measurement error increases as a function of time while Wi-Fi signals fluctuate randomly and invariant with time. Therefore integrating Wi-Fi fingerprinting and PDR can restrict the random error found in fingerprinting and in return provide more stable navigation results. A PDR/Wi-Fi integrated fingerprint mapping (FPM) algorithm is introduced here to provide navigation based on simulated low-cost IMU and Wi-Fi fingerprint data.

The algorithm is based on particle filtering and the fingerprint database is simulated using Eq.2.9. PDR is applied for the prediction of the system state which is represented by the particles. Simulated RSS data is generated at each epoch and treated as observations to update the state model. The whole procedure is as below:

1. Initialisation: initialise particles within 10m of the true initial position;

2. Prediction: particles propagate forward according to Eq.3.1 where the measurements consist of a 0.5m noise in velocity and a heading

variance of $\pm 30^{\circ}$ as well as a heading drift bias of $0.5^{\circ}/s$ (values are simulated to the same error level of the low-cost IMU);

3. Weighting and normalisation: the observed Wi-Fi RSS RSS_k is received. Potential fingerprint locations $P(x_p, y_p)$ are found by

$$|RSS_P - RSS_k| \leq \tau_{FP}(dB) \tag{3.12}$$

τ_{FP} is set to 10dB here based on the variation of real RSS data. Each particle is weighted by its average distance to the locations of all the potential fingerprints,

$$w_{pt} = \begin{cases} \frac{1}{\frac{1}{P}\sum_{FP=1}^{P}\sqrt{(x_{pt}-x_{FP})^2+(y_{pt}-y_{FP})^2}}, & \text{did not cross wall} \\ 0, & \text{cross a wall} \end{cases} \tag{3.13}$$

where (x_{pt}, y_{pt}) is the coordinate of the particle, (x_{FP}, y_{FP}) is the coordinate of the potential fingerprint, P is the total number of potential fingerprints. The particle weights are then normalised so that very small weight are assigned 0 and $\sum w_{pt} = 1$;

4. Resampling: the effective size of the particle cluster is acquired through Eq.2.39 which reflects the number of nonzero weighted particles. If the effective size falls below a threshold N_{eff}, new particles are resampled by drawing from the remaining old particles following Eq3.14,

$$pt_{new} = pt_{old} + \varepsilon \tag{3.14}$$

where pt_{old} is the location, weight and all other characteristics of previous live particles, ε is an additional noise to avoid distribution impoverishment. If the effective size becomes zero, particles are reinitialised around the last position.

3.6 Simulations

3.6.1 Fingerprint positioning simulation

The performance of Wi-Fi signal propagation and its influence on fingerprinting in a controlled environment is simulated in Matlab. As previous work suggests, wireless signals should give stable performance when the

appropriate propagation parameters are selected (Zhou and Pollard, 2006; Pei et al., 2010; Subhan et al., 2011). A building of 20 m $\times$ 12 m is defined with an AP at each corner, i.e. located at (12,0), (0,0), (12,20) and (0,20). Four rooms are designed along two sides of the wall as shown in Figure 3.18.

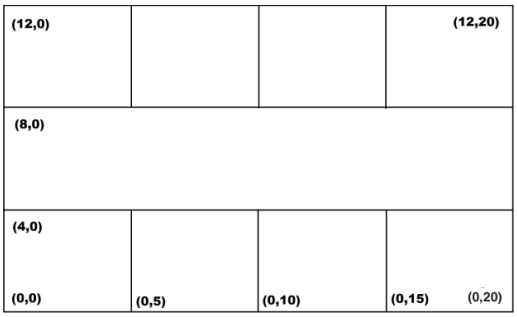

Figure 3.18: Simulated building layout

Parameters for the path loss model Eq.2.9 are set to $n = 3.5$ and $WAF = 6$ which is extracted from real data collection trials as well as other work such as discussed by Sandeep et al. (2008). The model is applied to generate the RSS vectors for the signal strength of the fingerprint database for each AP throughout the building. The fingerprint maps for the four APs are simulated without error as shown in Figure 3.19, where red indicates the strongest signal and dark blue the weakest. This database is built up from simulating RSS at 20 cm intervals. To compare the performance of fingerprinting, the database resolution is reduced to 1 m, 2 m and 5 m respectively.

Weighted *k*-NN positioning is applied here so that the first *k* positions with the smallest ΔRSS between the fingerprints and the observed RSS_k are selected and then each is weighted by their exact ΔRSS. More weight is given to fingerprints with smaller ΔRSS as in Eq.3.15, where $(x_k, y_k)$is the coordinate of the *k* nearest neighbour fingerprints.

$$(\tilde{x}, \tilde{y}) = \frac{\sum_{k=1}^{N} w_k (x_k, y_k)}{\sum_{k=1}^{N} w_k} \tag{3.15}$$

Two factors are used to evaluate the performance of the positioning algorithm with different noise levels: the mean and standard deviation of the positioning error. The positioning error is the difference between the the true position (defined randomly for each simulation) and the estimated

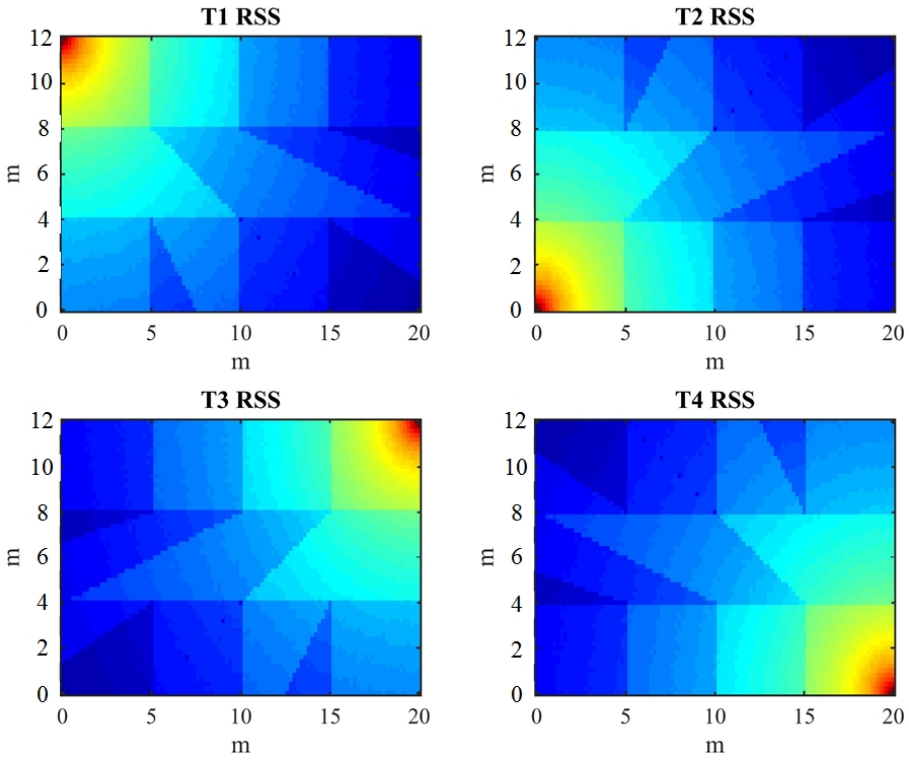

Figure 3.19: Wi-Fi signal strength map

position from fingerprinting,

$$error = \sqrt{(x_{true} - \tilde{x})^2 + (y_{true} - \tilde{y})^2} \tag{3.16}$$

Positioning for each set of parameters is simulated for 300 times with a different (x_{true}, y_{true}) each time. The mean performance is given by the mean error $mean_{err}$ and error standard deviation sd_{err},

$$mean_{err} = \frac{\sum_{k=1}^{N} error_i}{N} \tag{3.17}$$

$$sd_{err} = \sqrt{\frac{\sum_{k=1}^{N} error_i^2}{N-1}} \tag{3.18}$$

For each database of different resolutions, the k is set to 2,3,4,5 and 10 respectively for *k*-NN positioning. Figure 3.20 shows the positioning error for each database when $k = 2$. Table 3.6 lists the mean and error standard deviation (SD) for each different resolution database and different k. It can be clearly identified that the positioning error reduces as the database resolution increases with 5 m resolution giving the worst results. For resolutions of more than 1 m, the positioning error is the smallest when $k = 3$. Increasing the number of k may not help here due to that the

grid size is very large, and picking out more "neighbour" fingerprints will actually include fingerprints which are quite far away from the truth. $k = 3$ performs better than $k = 2$ as three fingerprints can surround the true location and the weighted mean will bring the final estimation to within the three fingerprints and closer to the truth from both x and y directions, whereas two fingerprints can only estimate to along a line between the two. However, when the resolution is 0.2 m, the number of k no longer has much affect on the positioning result.

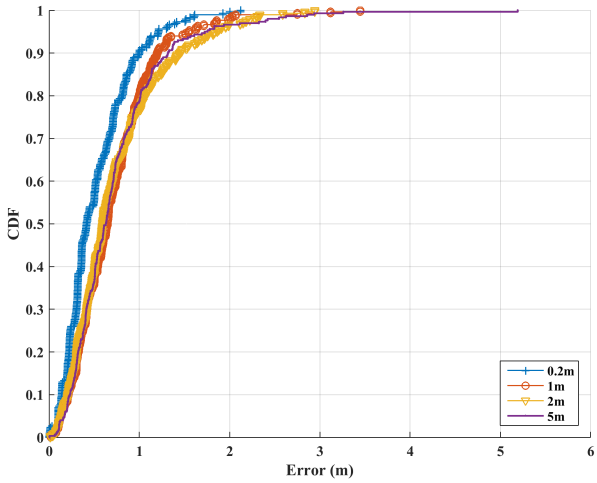

Figure 3.20: Fingerprint positioning error for different database resolutions ($k = 2$)

Table 3.6: Fingerprint positioning error for different database resolutions (m)

	k=2		k=3		k=5		k=10	
Res	Mean	SD	Mean	SD	Mean	SD	Mean	SD
0.2	0.52	0.37	0.52	0.36	0.54	0.34	0.51	0.32
1	0.70	0.47	0.68	0.45	0.76	0.51	0.86	0.57
2	0.73	0.53	0.66	0.46	0.83	0.55	0.85	0.55
5	0.73	0.57	0.65	0.40	0.80	0.54	0.84	0.53

The RSS of the fingerprints in reality are usually disturbed, hence the database is simulated to a resolution of 0.2 m with different noise levels here.The standard deviation of the database fingerprint noise is $\sigma_{FP} = 1$ dB and $\sigma_{FP} = 5$ dB respectively. The noise of the observed RSS_k during the positioning phase is also set to $\sigma_{Rx} = 1$dB, $\sigma_{Rx} = 2$ dB,$\sigma_{Rx} = 3$ dB and $\sigma_{Rx} = 5$ dB respectively.

Although the positioning error increases as the observation noise σ_{Rx} increases, but increasing the fingerprint noise σ_{FP} and choosing different k does not have a big effect when the resolution is high. As a result, using

Table 3.7: Fingerprinting positioning error ($\sigma_{FP} = 1$) (m)

	k=2		k=3		k=5		k=10	
σ_{Rx}	Mean	SD	Mean	SD	Mean	SD	Mean	SD
1	0.58	0.43	0.56	0.42	0.56	0.36	0.52	0.37
2	1.01	0.65	0.98	0.74	1.05	0.81	0.92	0.70
3	1.36	0.93	1.29	0.93	1.41	0.96	1.38	1.01
5	1.87	1.20	1.99	1.29	1.86	1.20	1.88	1.24

Table 3.8: Fingerprinting positioning error ($\sigma_{FP} = 5$) (m)

	k=2		k=3		k=5		k=10	
σ_{Rx}	Mean	SD	Mean	SD	Mean	SD	Mean	SD
1	0.58	0.36	0.58	0.40	0.55	0.39	0.52	0.32
2	0.97	0.66	0.98	0.73	0.97	0.70	0.93	0.67
3	1.37	0.94	1.26	0.87	1.23	0.86	1.19	0.77
5	1.92	1.30	1.88	1.24	1.77	1.25	1.82	1.22

the *k*-NN positioning method is not so necessary when the database can be generated based on Gaussian process to a high resolution which greatly improves both positioning accuracy and efficiency.

3.6.2 Fingerprint mapping navigation simulation

To evaluate the Wi-Fi fingerprint mapping performance, the navigation algorithm based on particle filtering is simulated in Matlab. A single trajectory is simulated as the ground truth. The initial position of the mobile user is simulated near the start of the trajectory. The user step length and heading for DR propagation is simulated as described in Section 3.5, a Wi-Fi RSS vector RSS_k is also simulated at each epoch based on Eq. 2.9. Standalone DR, conventional fingerprint positioning (FP) and fingerprint mapping navigation (FPM) are applied at each epoch respectively to update the user position based on inertial and Wi-Fi observations. FP weights the particles based on their distance to the average position of the *k*-NN fingerprints at each epoch, while FPM weights the particles based on the their mean distance to the location of all potential fingerprints. The positioning result for the three different positioning methods is compared while taking measurements from different numbers of APs, i.e. from 1 AP up to 6 APs.

The DR is simulated to the same accuracy level for each scenario. Positioning results are plotted in Figure 3.21. Green lines indicate the true trajectory for each user. Red lines indicate the DR standalone solution. Blue lines in Figure 3.21a and 3.22b show the PF performance based on the

integration of DR measurement and Wi-Fi RSS_k from 6 APs and 1 AP. Blue lines in Figure 3.22a and 3.22b show the path of FPM positioning based on RSS_k measurements from 6 APs and 1 AP. Black circles highlight the doorways in the building. Red stars indicate the simulated AP locations.

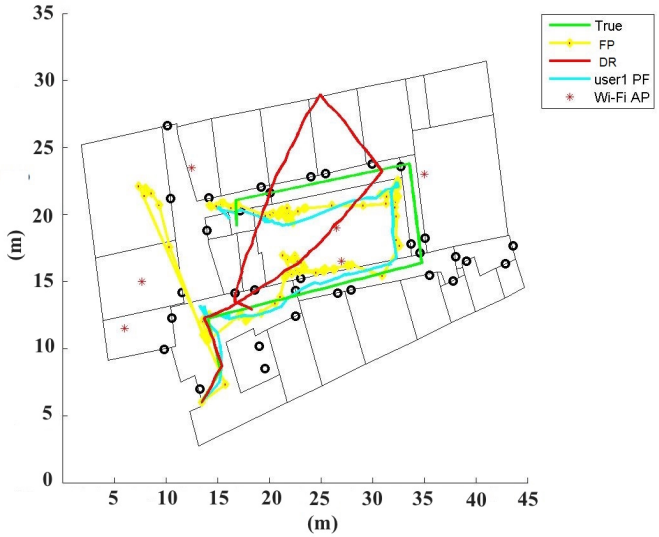

(a) FP (6AP)

Figure 3.21: Conventional fingerprinting result with varying APs

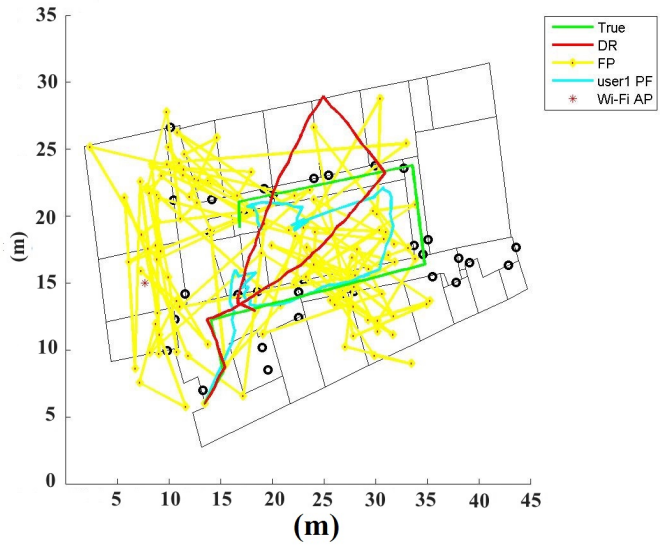

(b) FP (1AP)

Figure 3.21: Conventional fingerprinting result with varying APs (Cont'd)

The positioning errors when different numbers of APs are applied are listed in the columns of FP and FPM in Table 3.9. The error in the each

column of the table shows the average distance of the different solutions, i.e. DR, FP and FPM, from the simulated truth.

Table 3.9: Mean positioning error of different navigation solutions (m)

AP no.	PDR	FP	FPM
6	4.80	2.12	1.72
3	4.80	1.50	1.77
2	4.80	2.56	1.59
1	4.80	2.79	1.52

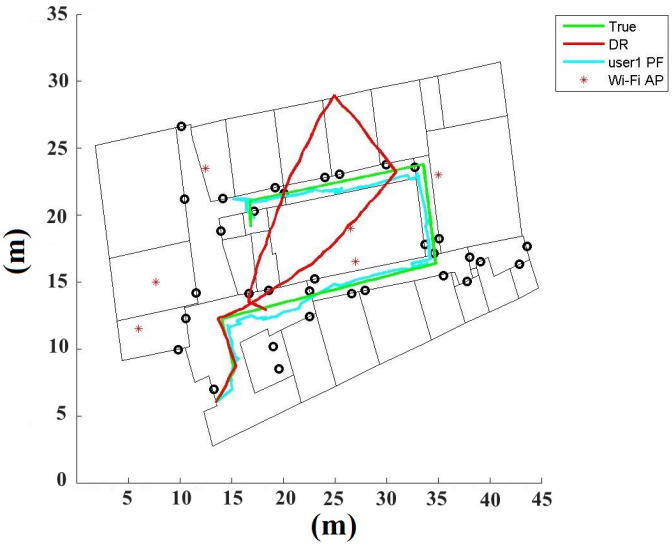

(a) FPM (6AP)

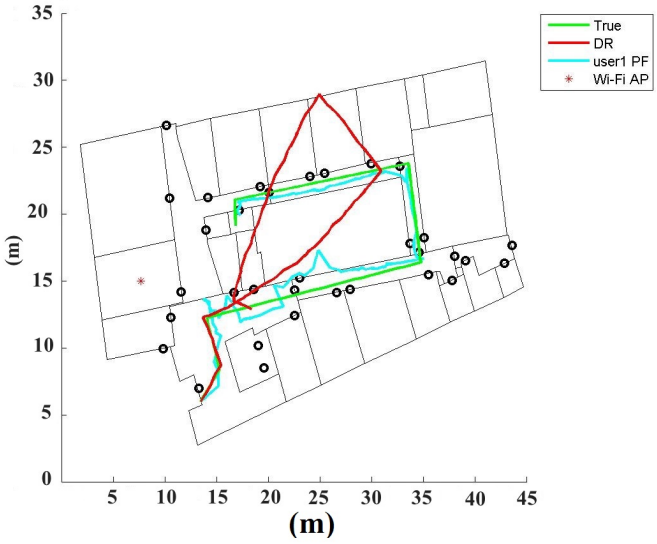

(b) FPM (1AP)

Figure 3.22: Fingerprint mapping result with varying APs

While the positioning error increases as AP numbers drop for the FP method, the number of APs does not affect the positioning performance so much for the FPM method. FP is highly dependent on the stability and the number of existing APs. FPM shows more resilience to a changing wireless network environment. Results in Section 3.6.1 show that averaging more *k* neighbours for fingerprinting give better performance, FPM also shows a similar pattern. The particles in the FP method are weighted by a single fingerprint solution (the mean of *k*-NN) thus if the solution at a certain epoch is biased from the truth, the FP solution would be contaminated as well. Due to the large fluctuation shown in Wi-Fi signals, this may occur quite often during the FP method. On the other hand, the particles in FPM are weighted by all potential fingerprints, therefore the positioning solution would not be affected too much if only very few fingerprints of the total potential fingerprints are biased. Hence a larger number of fingerprints should be counted as potential locations. Although this may mean a large ambiguous area of fingerprints alone, at least the fingerprints around the true location would not be discarded. FPM proves to be more appropriate for the DR/Wi-Fi integrated navigation solution as it averages out the error and proves to be more resilient to Wi-Fi signal variation.

However it must be remembered that this result is based on simulated Wi-Fi RSS and real data tend to be much more noisier. Thus to tackle the complexity of a real environment and the potential failure of Wi-Fi network, collaborative algorithms are developed by bringing in ranging measurements from a number of collaborative users in a local network.

3.7 Summary

This chapter gives details to some popular indoor positioning methods, including PDR using foot mounted inertial sensors, Wi-Fi fingerprinting and indoor map matching. To reduce fingerprint database training time, Gaussian Process regression is applied to generate the database. Trials show that GPR reduces training time by reducing the number of required training points and the time for training each point. A particle filtering based PDR and Wi-Fi integrated pedestrian navigation algorithm is also introduced here for more stable positioning results.

Simulations of the basic Wi-Fi fingerprinting procedure is presented in this chapter to develop understandings of positioning performance under different conditions, i.e. setting different measurement error and different number of nearest neighbour, k. The PDR and Wi-Fi integration navigation

is further developed into a fingerprint mapping navigation (FPM) solution to reduce positioning error and noise. The performance of FPM simulation is analysed with different number of APs. Its performance is compared to PDR solutions and conventional fingerprinting solutions and obvious improvement can be seen in FPM, especially when the number of APs reduce and conventional fingerprinting becomes less reliable.

Chapter 4

Collaborative positioning with ranging constraint

4.1 Introduction

The first aspect of collaborative positioning has already been considered in the previous chapter, i.e. the integration of inertial measurements and Wi-Fi signal measurements into a single system. This chapter will take a step further and look into the other aspect of collaborative positioning which involves the integration of multiple systems, or users, through ranging measurements between multiple users and transmitters.

A typical collaborative network consists of a number of fixed transmitter nodes, known as *anchors* (denoted as Tx), and a number of unknown moving nodes, known as *rovers* (denoted as Rx). In collaborative positioning, the heading drift of each rover can be constrained by integrating ranging to other rovers and anchors. Accurate ranging measurements can push the state estimation of rovers towards the true position by providing information on the geometry of the network. This fixes the rover and other nodes into the geometry with a certain distance between each other (i.e. the ranging measurement). By sharing this collaborative information between each other, the positioning results of all rovers within the network are improved.

Signals of opportunity provides a major opportunity for collaborative positioning. Our environment is filled with a variety of opportunistic signals, e.g. GNSS, Wi-Fi, cellular signals, radio signals etc. Usually, GNSS signals would not be considered opportunistic, however different signals behave differently in different environments and each is suitable for positioning in different environments. While GNSS provides very accurate positioning outdoors, they are not reliable inside, where Wi-Fi signals work best. In this rapidly developing modern era where we are constantly facing a mass of information, it is more about selecting the right and valid information than simply searching for information. In collaborative

positioning, the selection of signals should be aimed at seamless transfer between different positioning environments, achieving high positioning accuracy with relatively low computation cost. The authors in Yang et al. (2009) demonstrate that while a number of signals of opportunity are available, not all of them improve the positioning accuracy. The authors search for an optimal collaborative network among users and signal sources based on differential ranges.

As already discussed in Chapter 3, each navigation method has its own strengths and weaknesses. Wi-Fi and IMU integration has been introduced to compensate the drift of inertial sensors as well as the unstable signals from Wi-Fi sensors. Yet low-cost inertial sensors used for pedestrian navigation can have a very large gyro drift that leads to errors of hundreds of meters in a few seconds. Even with corrections from Wi-Fi signals, such positioning instability cannot be easily overcome. Relative ranging, i.e. the implementation of P2P ranging, can restrict such measurement bias when integrated efficiently.

4.2 Theoretical ranging constraint

4.2.1 CRLB

To properly understand when and how to apply the ranging constraint in collaborative positioning, the actual performance of the ranging measurements and the relative network conditions must be understood. Different levels of ranging and network conditions could change the effect of collaborative positioning performance dramatically. Therefore, some kind of indicator should be identified to assess the collaborative network conditions and its positioning performance. Identifying the lower bound of the achievable variance is useful in assessing the estimator performance.

Various lower bounds can be applied to introduce network positioning performance, of which Cramer Rao Lower Bound (CRLB) has been used extensively (Patwari and Hero, 2002; Chang and Sahai, 2004; Patwari et al., 2005; Venkatesh and Buehrer, 2006; Wymeersch et al., 2009). CRLB provides a lower boundary on the achievable variance of any unbiased location estimator for unknown parameters (Kay, 1993). It is useful for justifying how well an estimator can perform and help to decide whether it is outputting the desired performance (Ziv and Zakai, 1969; van den Bos, 1994; Jacobson, 2004).

Authors of Penna et al. (2010) introduce the application of CRLB analyses to the ranging measurement from anchors, pseudorange measure-

ments from satellites and P2P ranging measurements. The factor specifies the *a priori* information on the network configuration when integrating P2P cooperation with satellite-based positioning.

CRLB states that the variance of an unbiased estimator $\hat{\theta}$ must satisfy

$$var(\hat{\theta}) \geq \frac{1}{-E[\frac{\partial^2 \ln p(x;\theta)}{\partial \theta^2}]} = I^{-1} \tag{4.1}$$

reflect where the derivate is evaluated at the true value of θ and the expectation is taken with respect to the pdf $p(x;\theta)$. The CRLB states the minimum achievable variance,

$$CRLB = I^{-1}(\theta) \tag{4.2}$$

where $I(\theta)$ is the Fisher Information Matrix (FIM). Consider a measurement model that maps measurements Z to estimate θ, e.g. the positioning result,

$$Z = h(\hat{\theta}) + w \tag{4.3}$$

where w is assumed to be a zero-mean Gaussian noise with a variance of σ^2, Z is a Gaussian distributed measurement that follows $\mathbb{N}(h(\theta), \sigma^2)$. The FIM $I(\theta)$ can be written as,

$$\begin{aligned} I(\theta) &= E\left\{ \left[\frac{\partial}{\partial \theta} \log p(Z|\theta) \right] \left[\frac{\partial}{\partial \theta} \log p(Z|\theta) \right]^T \right\} \\ &= (\frac{\partial}{\partial \theta} h(\theta))^T R^{-1} (\frac{\partial}{\partial \theta} h(\theta)) \end{aligned} \tag{4.4}$$

where $\frac{\partial}{\partial \theta} h(\theta)$ is the Jacobian matrix of $h(\theta)$ with respect to every element in the parameter vector θ.

Since we are interested in ranging measurements here, Z can be expressed more specifically as,

$$r_i = \sqrt{(\hat{x}_u - X_i)^2 + (\hat{y}_u - Y_i)^2} + \varepsilon \tag{4.5}$$

where $(\hat{x}_u, \hat{y}_u)$ is the estimated user location, (X_i, Y_i) is the ith reference node, r_i is the ranging measurement with a Gaussian noise ε that has a mean of b_i and variance of σ^2, where b_i is a measurement bias. If there were m nodes in the network, the Jacobian matrix of the measurements

would be

$$H = \frac{\partial}{\partial \theta} h(\theta) = \begin{bmatrix} \frac{x_u - X_1}{r_1} & \frac{y_u - Y_1}{r_1} \\ \vdots & \vdots \\ \frac{x_u - X_m}{r_m} & \frac{y_u - X_m}{r_m} \end{bmatrix} \tag{4.6}$$

The theoretical lower bound, CRLB, at location (x, y) can be given by Atia (2013),

$$CRLB(x, y) = \sqrt{tr((H^T R^{-1} H)^{-1})} \tag{4.7}$$

where $R = diag(\sigma_1^2, \sigma_2^2, ..., \sigma_m^2)$, σ_i^2 is the variance of ith measurement. The resulting CRLB is an indication of how well a positioning system can perform under the best circumstances. It is used to analyse and compare the positioning performance of different networks.

To evaluate the positioning error level of multilateral positioning at different locations with different ranging measurement error levels, four anchors are set up on each corner of a $100 \times 100m$ square area. The entire area is divided into 1m by 1m grids and the CRLB of each grid is calculated respectively for different noise levels, i.e. variances of $\sigma^2 = 1$, $\sigma^2 = 3$ and $\sigma^2 = 5$ while ranging measurement bias is $b = 1m$ and $b = 5m$ respectively. Figure 4.1 indicates the CRLB at different measurement accuracy levels and different locations within the test area, dark blue indicates low CRLB values, i.e. good performance, and red indicates high CRLB values, i.e. poor performance.

CRLB increases with the signal variance and measurement bias. As a result, more uncertainty in the positioning accuracy will be found in those locations with high CRLB. Figure 4.1 reflects that CRLB increases more significantly when the variance increases compared to when the bias is increasing, indicating that the impact of the variance is larger than the bias. The CRLB also increases faster when the variance is larger. This simple simulation models the effect of the variance of the measurement signals on collaborative positioning.

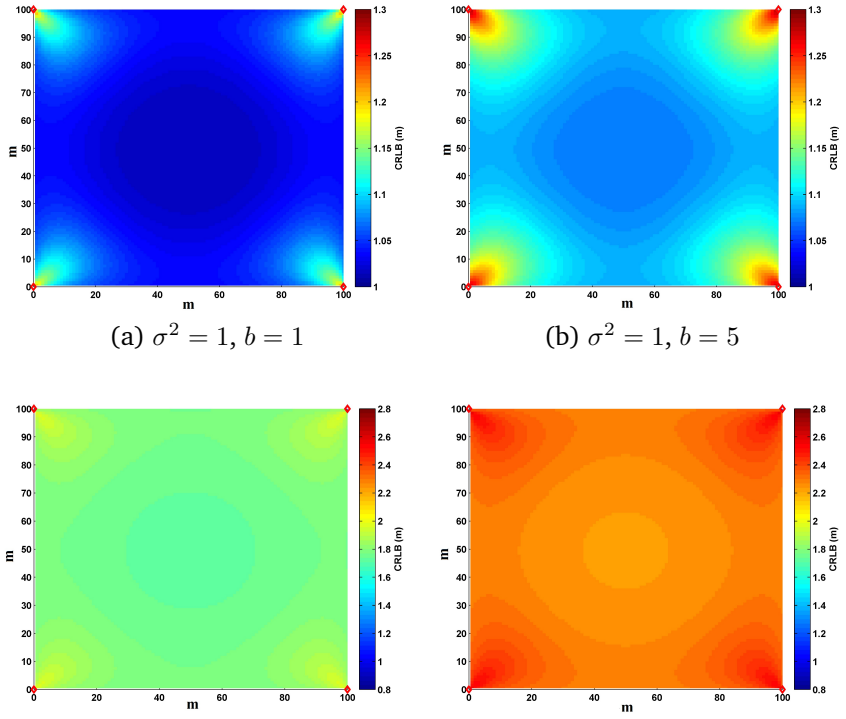

(a) $\sigma^2 = 1, b = 1$ (b) $\sigma^2 = 1, b = 5$

(c) $\sigma^2 = 3, b = 1$ (d) $\sigma^2 = 5, b = 1$

Figure 4.1: CRLB with different noise variance and bias

4.2.2 Ranging constraints

Before we start integrating real ranging information into the system, the constraint effect on two system state estimations based on ranging measurements with different noise levels and biases is examined. In particle filtering, each system state is represented by a cluster of particles scattered around the true location with a certain level of noise representing the uncertainty. Suppose the ranging measurement obtained between the two systems is characterised by two parameters, bias and noise. Bias is the difference between the true distance and the actual ranging measurements, which could be caused by a system error (system bias) or a measurement error (measurement bias). The system noise is reflected by the variance of the particles cluster and the measurement noise is reflected in the estimation between each pair of particles. P2P ranging constrains the positioning uncertainty by comparing the difference between the ranging measurement and the distance between each pair of particles representing the two system states. A constraint boundary is defined which specifies the upper threshold of the difference, usually reflecting the assumed measurement noise level (the bias is always assumed to be 0 as in reality users never know when the measurement might be biased). When the difference between a particle

of one user and each particle of the other user falls outside this boundary, it will be killed. Hence the error reflected in this particle will also be eliminated. The remaining particles will be a better representation of the system state.

To carry out the examination of different ranging measurements, a pair of particle clusters each representing Rover 1 (R1) and Rover 2 (R2) with varying noise level and bias from the true location are simulated to represent a pair of system states. The ranging measurements between the two states are also simulated with different noise and bias levels. The effectiveness of the relative ranging constraint for each different setting is evaluated by the mean of the live particles after applying the constraint.

In the first set of simulations, the noise level of the ranging measurement is examined by fixing the particle cluster size to 500 and ranging measurement bias to 0m. The measurement is simulated around the true distance with a zero mean Gaussian noise where the standard deviation is $\sigma = 1$m, $\sigma = 0.1$m, $\sigma = 0.01$m and $\sigma = 0.001$m respectively, as shown in Figure 4.2. The green line indicates the true distance between the two rovers (the true location is indicated by a red * and the green clusters are the 500 particles used to represent their current state). The red line indicates the measured range, the blue Xs indicate the killed particles of R1 and the magenta Xs indicate the killed particles of R2.

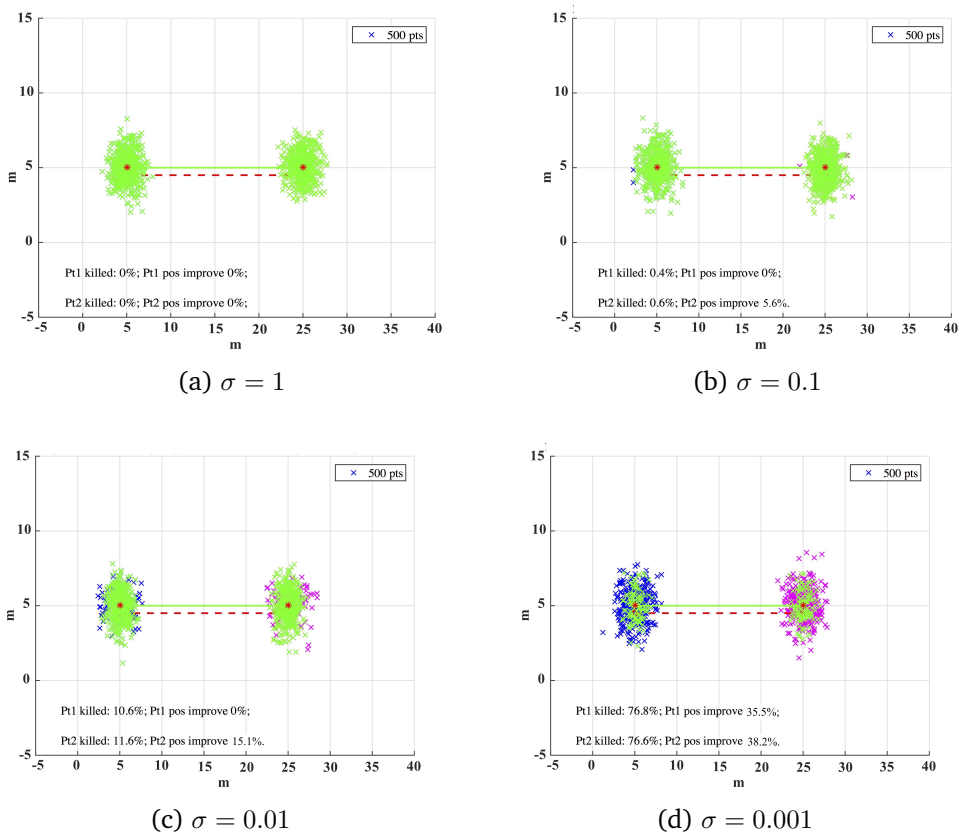

(a) $\sigma = 1$ (b) $\sigma = 0.1$

(c) $\sigma = 0.01$ (d) $\sigma = 0.001$

Figure 4.2: Ranging constraint with different measurement variance

For a small particle cluster, very few particles will be killed if the measurement noise standard deviation is relatively large. On the other hand, if the noise level is very small, too many particles may be killed because of the uncertainty contained in the particles. Hence the measurement noise level plays an important role in keeping the effective particles alive, i.e. keeping only the particle closest to the true position alive.

However in some situations, even if we know the fixed range measurement bias and noise level, the system state estimation may already be biased from previous state estimations. It would take a great effort to pull the biased state back to the true location. Different system bias states are examined to test their impact on the relative ranging constraint while the ranging measurements have no bias. From Figure 4.3, we can see that it is not easy to pull the estimation back just by one ranging constraint when the system is already biased. Although the red line indicating the measured range is consistent with the truth distance, but the cluster of particles for R2 is always biased as it sits a distance away from the true location. The P2P ranging between two rovers gives a better constraint on the unbiased system state than the biased state. When the system bias is very large, the

ranging may have a negative effect on the unbiased system state by killing too many particles, especially the ones nearer the true location. Thus relative ranging is not capable of constraining the system error when it is already biased. In such cases, absolute positioning solutions are required.

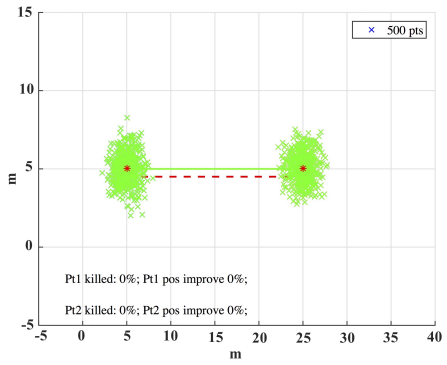

(a) system bias = 0m

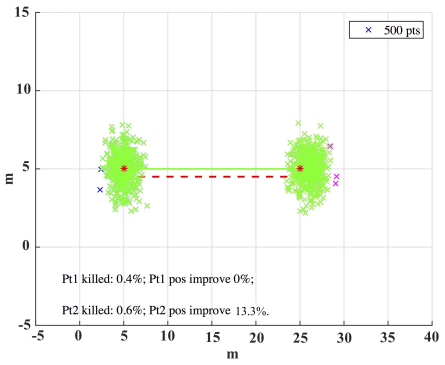

(b) system bias = 1m

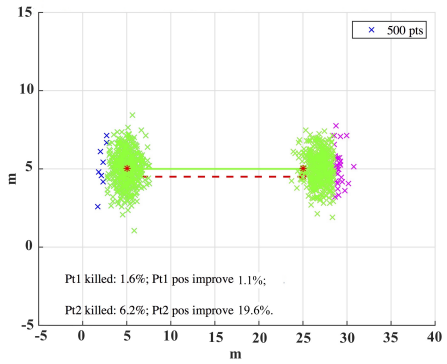

(c) system bias = 2m

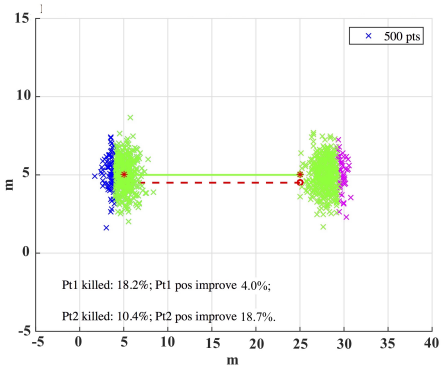

(d) system bias = 3m

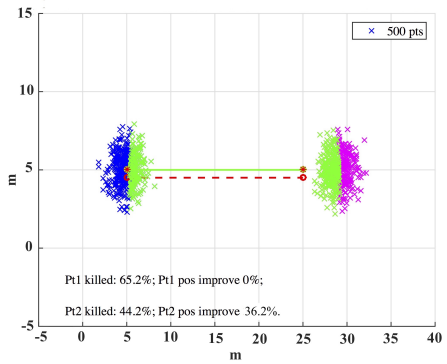

(e) system bias = 4m

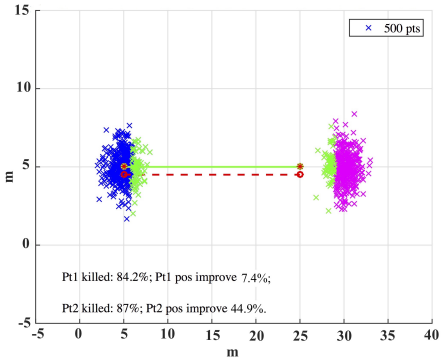

(f) system bias = 5m

Figure 4.3: Ranging constraint with different system bias

The influence of different ranging bias on the system constraint is then examined with different noise level of the particle scatter, a group of particles are scattered at a standard deviation of 1m around the true loca-

tion and a second group of particles are scattered at a standard deviation of 2m around a second true location. Results are shown in Figure 4.4 and Figure 4.5.

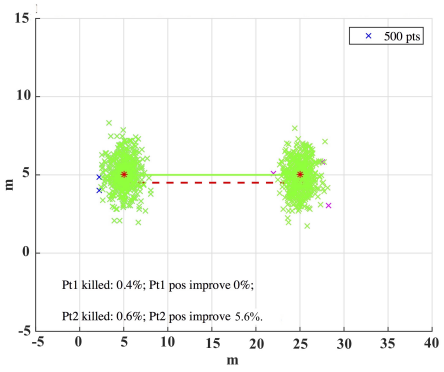

(a) Ranging bias = 0m

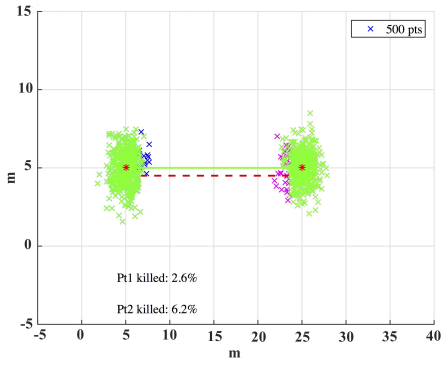

(b) Ranging bias = 1m

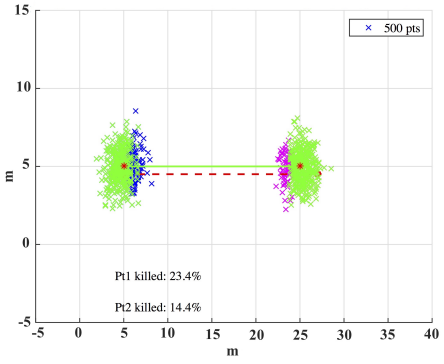

(c) Ranging bias = 2m

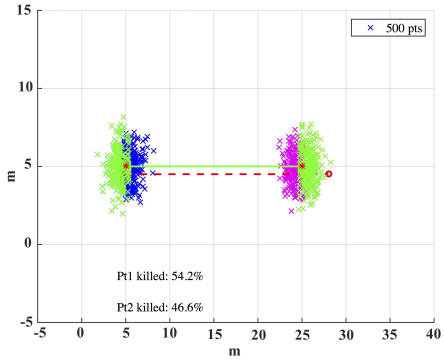

(d) Ranging bias = 3m

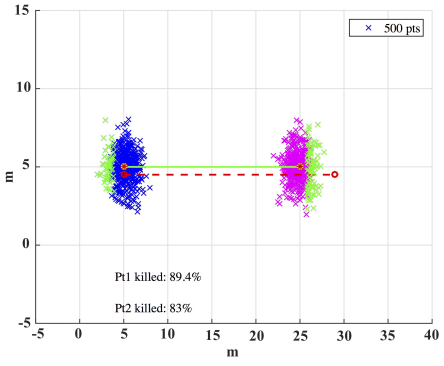

(e) Ranging bias = 4m

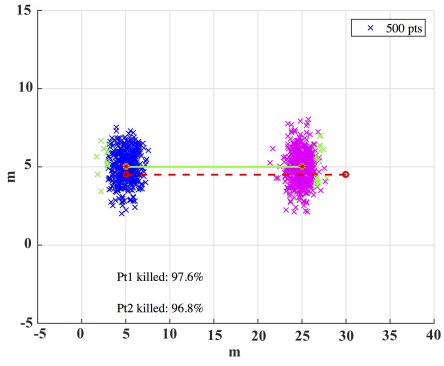

(f) Ranging bias = 5m

Figure 4.4: Ranging constraint with different ranging bias (particle sd = 1m)

Due to the uncertainty of particles, perfect ranging measurement may not give the best constraint performance. In reality, we only intend to integrate ranging constraints because we are unsure of the accuracy of the system state estimation, such as in Figure 4.5, where particles are scattered

with a large variance indicating more uncertainty in the system state. Thus in fact, the required level of ranging accuracy may change with the actual system estimation uncertainty itself and perfect ranging measurement is not required.

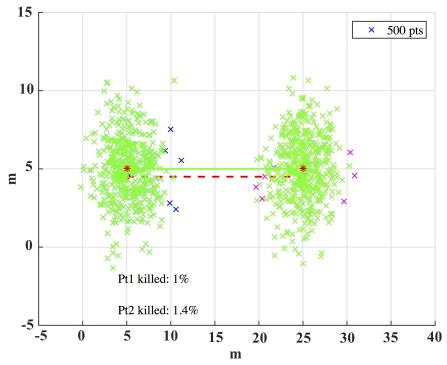

(a) Ranging bias = 0m

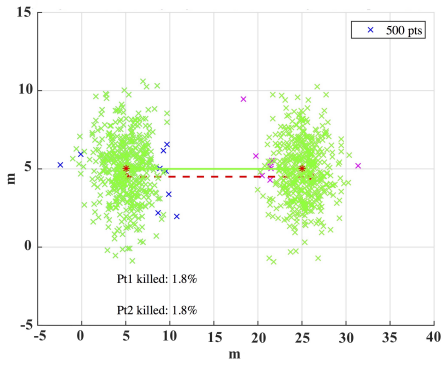

(b) Ranging bias = 1m

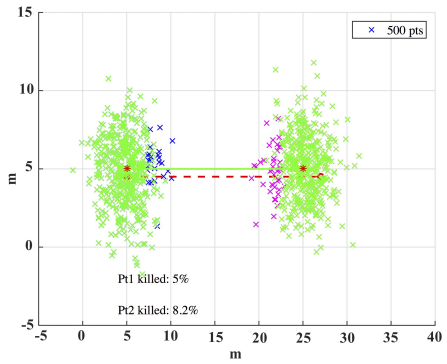

(c) Ranging bias = 2m

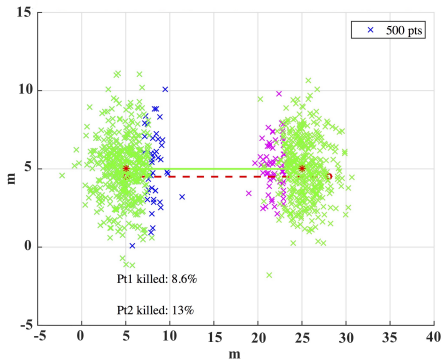

(d) Ranging bias = 3m

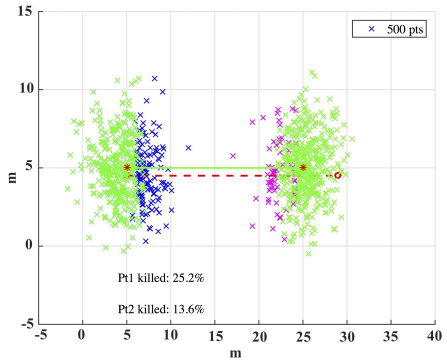

(e) Ranging bias = 4m

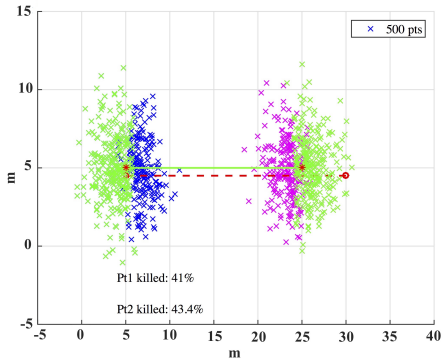

(f) Ranging bias = 5m

Figure 4.5: Ranging constraint with different ranging bias (particle sd = 2m)

These simulations provide a better understanding of the relative ranging constraint on system state errors. The constraint performance is related to the system state bias, the particle cluster noise, the ranging measurement

bias and variance. Perfect ranging is not required to constrain system errors. In fact, most of the time, ranging measurements with a certain noise level provide the best constraint on state estimations that contain errors and noise.

4.3 UWB signals

Integrating P2P ranging measurements between users is an important aspect of the collaborative positioning discussed in this thesis. Due to the complexity of indoor environments, users that are close together achieve higher accuracy ranging measurements as there is less disturbance (Rosa et al., 2014). Hence close-by users can form a collaborative positioning network where relative ranging is measured to correct and mitigate the measurement bias of each user in the collaborative network.

Popular ranging methods use TOA or RSS measurements from wireless signals, e.g. Wi-Fi, Bluetooth and UWB sensors. A major issue of wireless signal ranging is identifying the correct signal features such as the propagation time or the RSS of the LOS signal. However, most narrowband communication wireless signals are very noisy due to signal strength fluctuation. Therefore, ranging usually results in large errors and tends to be unreliable.

For time-based ranging, the ranging estimation resolution is related to the bandwidth of the signal (Ghavami, 2004),

$$d = \frac{c}{B} \tag{4.8}$$

where B is the bandwidth of the signal, d is the ranging resolution. Although this can be affected by disruption and disturbance in the environment. Yet even so, UWB ranging performance is still better than conventional narrowband ranging (Saleh and Valenzuela, 1987; Molisch et al., 2006; Schroeder et al., 2007; Choliz et al., 2011). Therefore UWB signals achieve better ranging as they have better time resolution (Ingram et al., 2004; Mahfouz et al., 2008). The boost in UWB applications has enabled even further development in wireless signal ranging accuracy.

4.3.1 UWB based ranging

With up to 7.5GHz bandwidth between the 3.1-10.6GHz spectrum, UWB signals were originally used for radar and military communications. UWB applications were boosted after the documentations released by FCC

in 2002 which noted that UWB can be applied in data communication (Federal Communications Commission (FCC), 2002). However the power output were restricted to a very low level to prevent interference with other signals in the overlapping bands. If the entire bandwidth is utilised, the maximum allowed power is 0.5mW. Thus the UWB signal can only either achieve high data rates but short-range communications, usually indoors, or longer distances but with very low data rate (Oppermann et al., 2004).

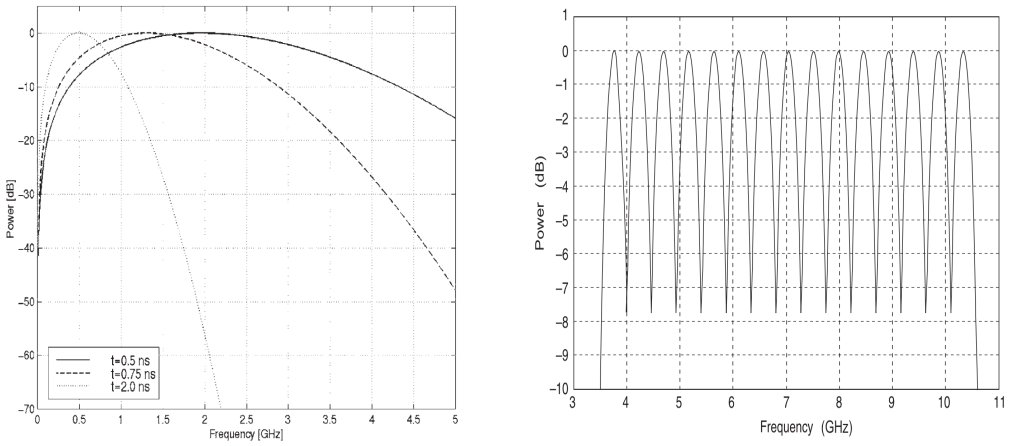

(a) Single band UWB pulse in frequency domain (b) Multiband

Figure 4.6: Examples of UWB pulses (Source: Oppermann et al. (2004))

In existing literatures, two main types of modulation methods for UWB systems can be found: time modulated impulse radio (IR) and multi-carrier (MC) schemes (Oppermann et al., 2004; Ghavami, 2004). Some applications of MC are frequency hopping (FH) UWB and multiband UWB. IR-UWB systems transmit wideband signals at sub-nanosecond pulses (Molisch et al., 2006) and ranging measurements are obtained by amplitude modulating the pulse train. MC-UWB systems transmit data over hundreds of regularly spaced frequency bands simultaneously. Due to the signals being spread across a wide bandwidth, TOA measurements can be obtained from the received phase difference between successive bands. FH-UWB systems broadcast a signal on a frequency band for a short period and then hop onto a different frequency every few microseconds to achieve a wider bandwidth over a period of time. Multiband UWB systems transmit overlapping signals where each signal has a bandwidth of 500MHz. The advantage of multiband systems is the potential efficient utilisation of the frequency spectrum.

As UWB signals have very fine time resolution and frequency resolution,

it becomes easier to distinguish noise and disturbance. As a result of the signal characteristics, UWB positioning systems have the advantage of low interference from other wireless signals, low sensitivity to fading, possible strong penetration ability (Molisch et al., 2006) and ability to overcome multipath (Win and Scholtz, 1998; Foerster, 2001; Lee and Scholtz, 2002). Due to these advantages, a number of localisation systems using UWB have been investigated over recent years (Mahfouz et al., 2008; Koppanyi et al., 2014). UWB's potential ability to achieve ranging measurements of decimetre or centimetre level boosts its popularity in positioning systems.

A received UWB signal can be expressed as

$$r(t) = a_d s(t - \tau_d) + \sum_{l=1}^{L} a_l s(t - \tau_l) + n(t) + i(t) \tag{4.9}$$

where a_d is the direct path (DP) signal strength, τ_d is its arrival time; a_l,τ_l is the signal strength and arrival time of the lth non-direct path (NDP) signal, i.e. the multipath components (MPC). $n(t)$ and $i(t)$ denote the noise and interference. $s(t)$ is the channel response of a transmitted signal pulse. The signal strength a_l and time delay τ_l of the MPC are closely related to the material and thickness of the obstruction as well as the travelling distance (Wang et al., 2003). For narrowband signals, the time difference between τ_l and τ_d is barely detectable. Yet this detection becomes possible for UWB signals, as well as the signal strength difference. Therefore, the ranging estimation can be achieved by just extracting the characteristics of the first arriving signal. However, if there is NLOS disruption even in the first arriving signal, measurements would be contaminated. Therefore, identifying and mitigating the error caused by NLOS becomes the main task of improving UWB ranging results.

The UWB system used in the trials discussed throughout this thesis is the Thales UWB system which utilises a combination of Frequency Hopping and Direct Sequence Spread Spectrum signal covering 4760MHz to 6200MHz with output power level of -41.3dBm/MHz. Positioning is achieved through TDOA techniques. A full UWB positioning network consists of two types of units: base units (BU) which should be static and setup over known positions, mobile units (MU) whose positions are unknown and needs to be determined. One of the BUs must be setup as a master BU to provide time synchronisation among the whole network as well as setting a fixed point for the network local coordinate system. Therefore, when setting up the system, at least one BU must be set up for the network to function

properly. Several factors are discussed below.

- *Ranging error*: the distance difference between the UWB ranging measurement and the truth.
- *Ranging difference*: the difference between the ranging measurements of the two MUs.
- *Data strength (DS)*: indicating the signal strength of the peak signal in 10^{-2} dB, where 0 is approximately 0 dB code-to-noise-ratio. All signal strengths given below are $\frac{1}{100}th$ of the original value.
- *Led strength (LS)*: indicating the signal strength of the signal leading edge in 10^{-2} dB. Offsets and the given values below are the same as DS.

4.3.2 Data collection

The Thales UWB units are setup in several different environments to test their ranging performance when different settings are applied. A static trial is first carried out in an indoor environment. Another four sets of trials are carried out to examine UWB ranging results in a dynamic environment, i.e. where the MU or both MU and BU are moving. In each trial, the ground truth of the UWB units is provided by Leica TS30 robotic total stations (TS) which can track and measure the position of the units.

4.3.2.1 Static trials

The first trial is carried out in a laboratory room to demonstrate the UWB systems indoor positioning accuracy in its normal working environment and setting. Six BUs are placed around the perimeter of the room at different heights to form a 3-D geometry network and an MU is placed at a fixed position in the middle of the room as shown in Figure 4.7.

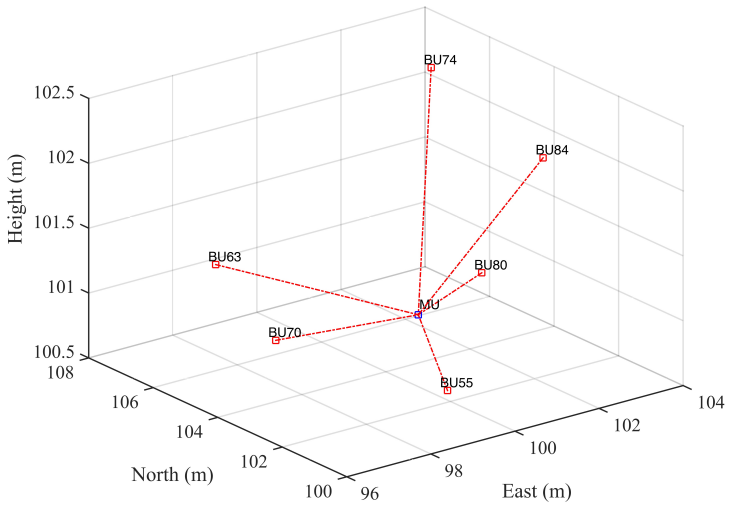

Figure 4.7: UWB system setup

Each unit position is measured by a total station to millimetre accuracy. The true ranging distance from the MU to each BU is obtained from the total station measured positions. The UWB ranging measurements from the MU to each BU are logged for a period of 7 minutes and their differences to the true distance are regarded as the ranging errors. The ranging error over the logging period is plotted in Figure 4.8 where the red line indicates the mean error throughout the data collection period. The mean error and standard deviation are listed in Table 4.1.

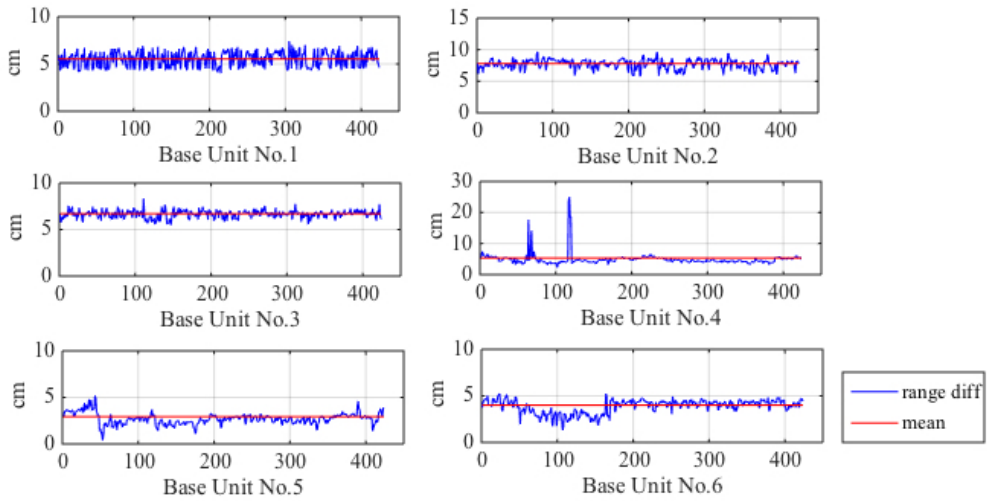

Figure 4.8: Static UWB system ranging error

With very precise timing and wide frequency band, the UWB system performs very accurate ranging in an open indoor environment with the

Table 4.1: Static UWB system ranging error

MU - BU no.	Mean (cm)	Standard Deviation (cm)
1	5.5	0.8
2	7.8	0.9
3	6.7	0.5
4	5.3	1.7
5	2.9	1.7
6	4.0	0.6

units setup in a good geometry. We intend to apply this ranging information in a dynamic indoor positioning scenario where the environment might not always be open and can become more complex. Its ranging accuracy in other less ideal environments will be investigated in the next sections.

The static trial proves UWB's ability to provide very accurate positioning and ranging. However, it is anticipated that disturbance may occur when the MU is moving as its relative position to the other units in the network will change. The system performance is tested by including two MUs in the network and allowing the MUs to move freely within the network coverage area. The dynamic ranging performance of the UWB system is tested in two environments, an open outdoor football pitch and a modern office building (NGB), at University of Nottingham.

4.3.2.2 Outdoor trials

The first set of dynamic trials are based in an open outdoor environment in the middle of a large football field as shown in Figure 4.9. A full network of four BUs is set up on the four corners of a square. The MUs will be tracked while they are moving and in order for the MU to be tracked with logical coordinates, the UWB system is referenced to a local coordinate system. The origin of the coordinate system is setup just outside the square and each unit is measured to the local system. As long as the BUs remain static, the local system will be maintained and the referenced MU position will be logical. The football pitch should be an ideal environment for UWB ranging, even though the units will not have a very good 3D setting as it is very hard to vary the height of units on an open field. But we will only be examining the 2D positioning and ranging performance thus this is not too much of a problem.

(a) Experiment Location

(b) UWB unit

Figure 4.9: Outdoor UWB setup environment

The first MU, MU1, is placed on a fixed point in the middle of the square. The second MU, MU2, is allowed to move within the square so that the connection between the units is always maintained. All static unit positions are measured by the total station to provide the ground truth. The moving MU is tracked by the robotic total station throughout the trial. The true distance between the two MUs is obtained from the total station tracked positions.

The ranging measurement from MU1 to MU2 and the measurement from MU2 to MU1 are each logged onto laptops which are connected to the units. The ranging errors for both units are obtained from comparing the UWB measurements to the total station measurements. The ranging measurement from both units as well as their ranging error is plotted in Figure 4.10.

The ranging results in the outdoor environment indicate that most measurements still maintain an accuracy of decimetre, or even centimetre level. Throughout the 8 minutes, only one large error of occurred which went over 1m. Even though the measurements from UWB mobile units are much more accurate than other wireless systems, we should note that the measurement error of the moving MU is slightly larger than that of the static MU. Further MU ranging performance is investigated in the indoor environment.

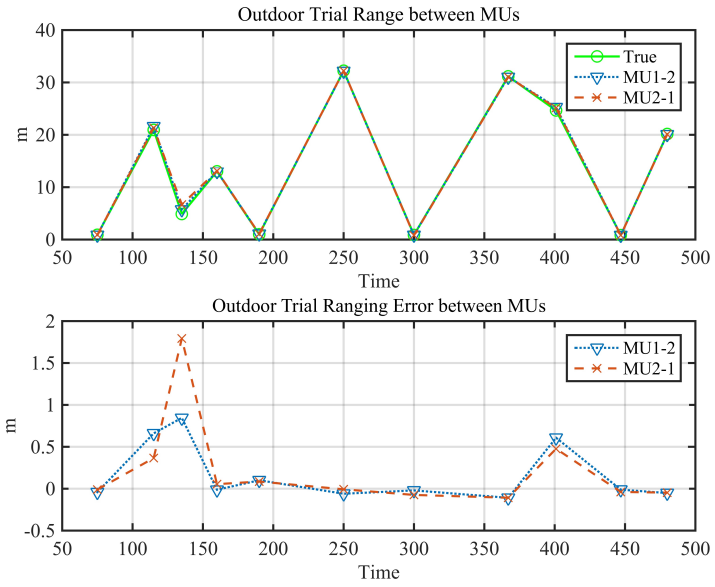

Figure 4.10: UWB outdoor ranging results

4.3.2.3 *Indoor trials*

The indoor environment chosen for the UWB trials is Floor A of NGB, as shown in Figure 4.11. Although the true orientation of the building is slightly turned towards the west, to simplify the description of directions and locations, the building orientation is adjusted to a local coordinate system so that the corridors are strictly along the east-west and north-south direction. This is a modern office building with office rooms, narrow corridors and equipment store rooms. The small rooms alongside of the corridors are normal office rooms. The two big rooms on the left-hand side are a meeting room and a lecture room. The large room in the middle is an equipment store room with metal shelves loaded with equipment. The large room on the east end is the garage. Examples of the corridor, office rooms and the store room have been shown in Figure 3.6.

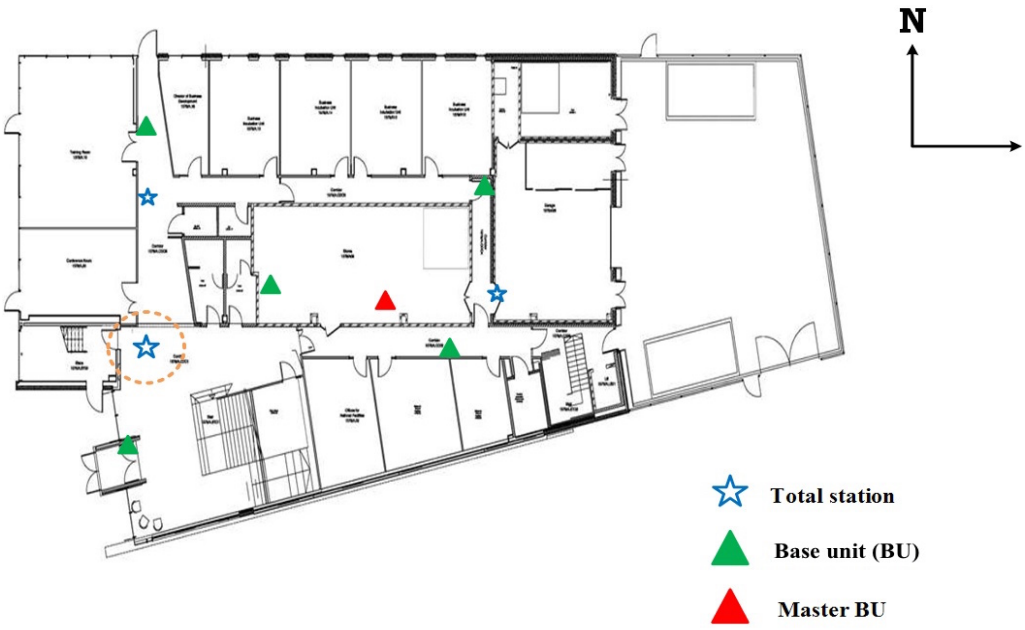

Figure 4.11: NGB Floor A building map

Three scenarios are carried out to test the ranging quality of UWB systems in such an indoor environment. The ranging network consists of two moving pedestrians, Rover 1 and Rover 2, who will carry UWB units on them to measure the range to other units in the network. To observe the effect of different network setting on the ranging performance, the ranging quality is tested with different combinations of the units, i.e. setting up the full network and setting up the network partially. Each performance will be explained in detail below. A local coordinate system is setup with its origin at the TS placed over the blue star highlighted in an orange circle. All positions and ranging measurement are given with reference to this local system.

1. Scenario 1 (Non-network based ranging):
   In the first scenario, only two units will be used in total. A master BU must be setup to provide network synchronisation, thus it will be carried by Rover 1. Ranging measurements can only be provided by MUs, thus Rover 2 carries an MU which collects the ranging data between the two units which is connected to a laptop. This scenario is an example of the basic P2P ranging provided by UWB units. Due to the metal structure of modern office buildings, wall obstructions and metal shelves in the store rooms, the UWB signals are easily blocked and disrupted causing frequent disconnection between units. Therefore in Scenario 1 and 2, the two units will only be separated by

one wall at the most to maintain connection. The designated route for the two users is that Rover 2 walks along the corridor next to the store room while Rover 1 walks inside the store room in parallel with Rover 2. At the end of each trial, Rover 2 remains static at the end of the corridor while Rover 1 moves along the corridor perpendicular to Rover 2 so that the two rovers are in LOS of each other during the last few minutes. The Easting and Northing of the trajectory is plotted in Figure 4.12 as a reference of positions.

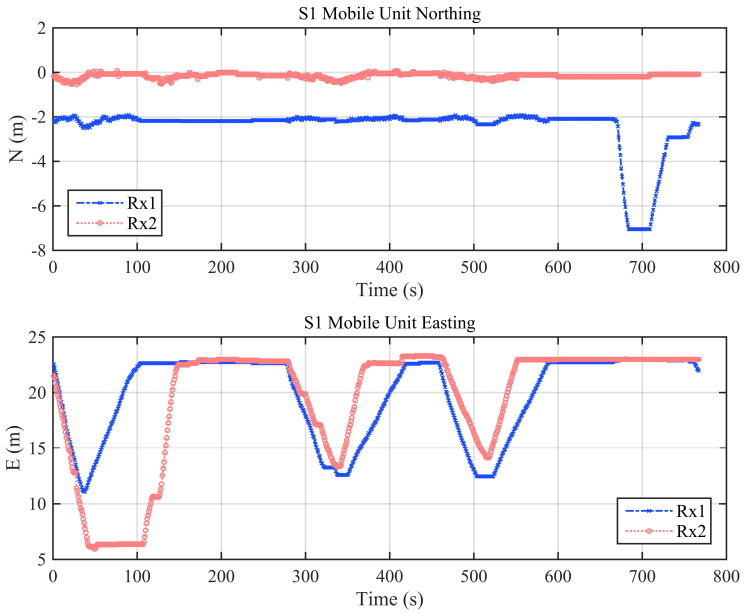

Figure 4.12: Scenario 1 Easting and Northing

Each rover is tracked by a total station to provide the ground truth. The ranging error is plotted against the distance between the two units in Figure 4.13 which shows the relationship between the two. There is no obvious correlation between ranging error and the distance. However, no ranging information could be found when the distance is over 8m thus it is hard to say if this pattern will continue for even longer distances. This is most probably because in indoor environments, the signal would hit many walls in its 8m of travelling and as it is hard for signals to penetrate so many obstructions, signals can only travel so far in complicated indoor environments.

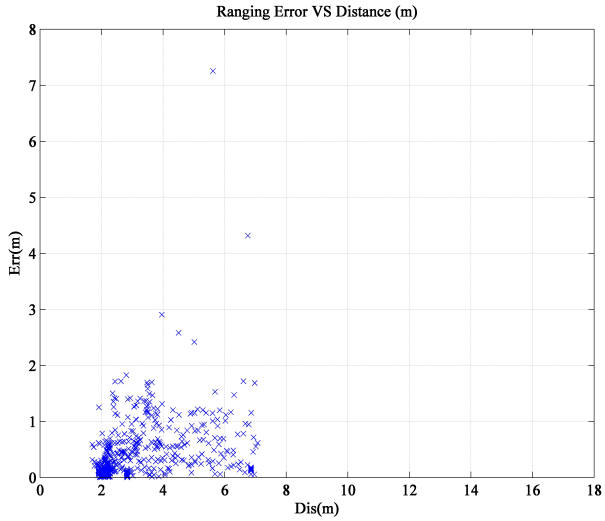

Figure 4.13: Scenario 1 Ranging error and distance correlation

The DS and LS of the received signals are extracted and plotted against the ranging error in Figure 4.14. LS never exceeds the power level of DS as DS is the strongest signal strength while LS is the signal strength of the first signal. For the majority of the time, LS is the same or at least very close to DS. However, when a signal penetrates an obstruction, the drop in LS is more significant than DS. During this period, the transmission time is delayed causing the ranging measurement to be positively biased, while the signal strength is weakened as well. From Figure 4.14, we can see that the ranging error increases dramatically when both DS and LS values drop.

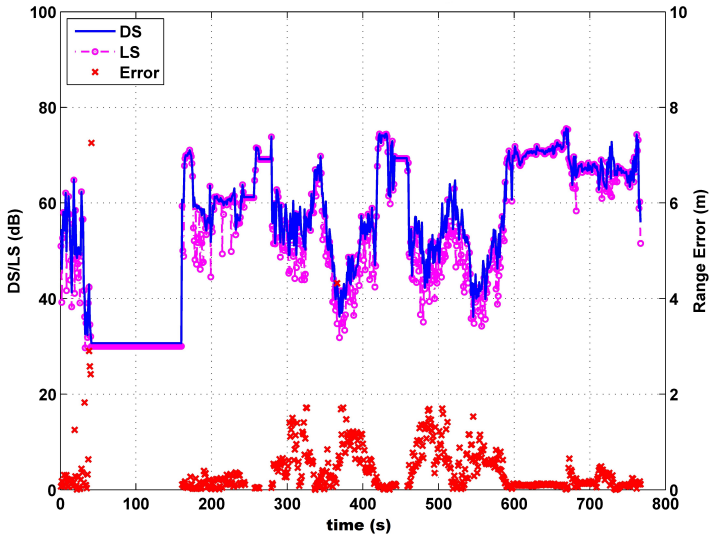

Figure 4.14: Scenario 1 DS and LS values

2. Scenario 2 (Ranging between MUs)
   In this scenario, the master BU is setup in the central location of the trial location indicated by a red triangle in Figure 4.11. Rover 1 and Rover 2 both carry MUs to collect the ranging measurement to each other. Two rovers walk in parallel path almost identical to the first scenario. The only difference between this path and the previous is the introduction of body obstruction (at around 400s). This is asking one of the users carrying the MU to deliberately walk in such a way that his body obstructs the signal between the two MUs while the two rovers are walking in parallel, one in the corridor and the other on the other side of wall in the store room.

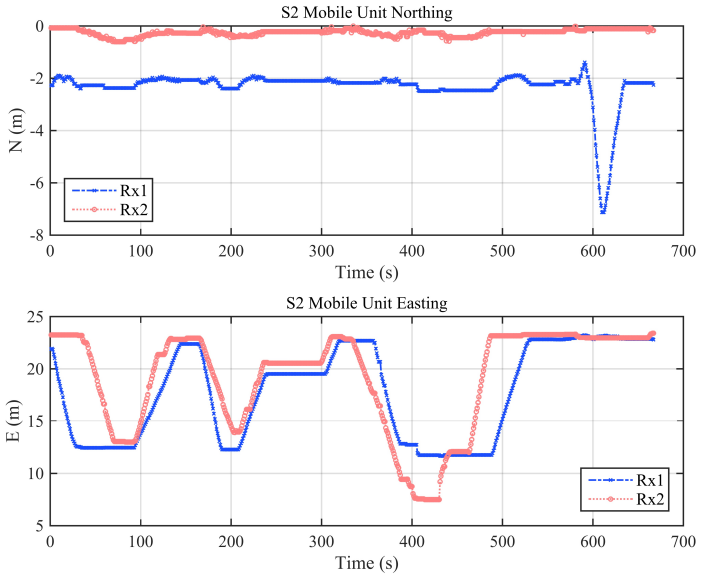

Figure 4.15: Scenario 2 Easting and Northing

The ranging error and distance correlation is plotted in Figure 4.16. Even though ranging measurements could be obtained at a longer distance than the previous scenario. But again, no obvious relationship can be found in the observed distance. However a hint of linear correlation could be observed as the distance increases over 6m and the ranging error increases as well. Figure 4.17 shows the difference between the ranging measurements collected by the two MUs. Their ranging patterns are almost identical where the difference between the two measurements only shows when body obstruction is introduced.

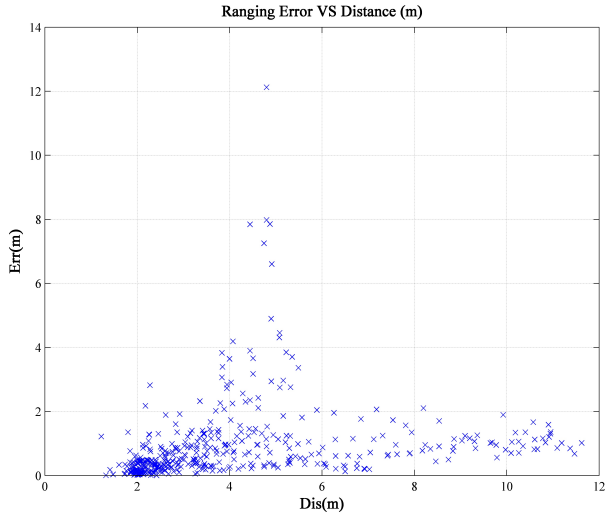

Figure 4.16: Scenario 2 Ranging error and distance correlation

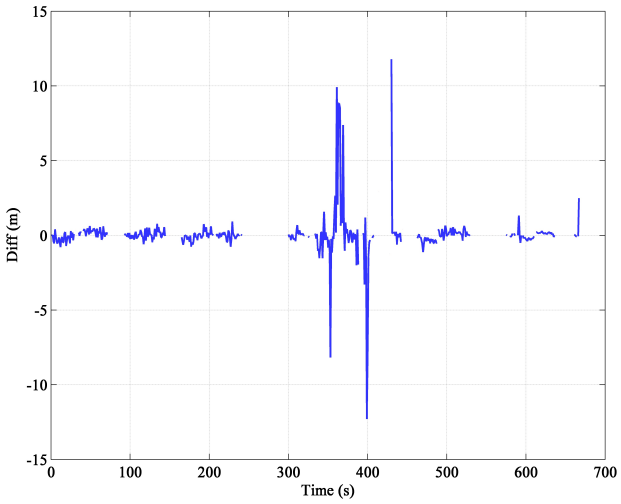

Figure 4.17: Scenario 2 Ranging difference

The DS and LS values are plotted in Figure 4.18. Again, we could see in this scenario that the periods with low LS and DS as well as large difference between DS and LS coincides with the period of large ranging error.

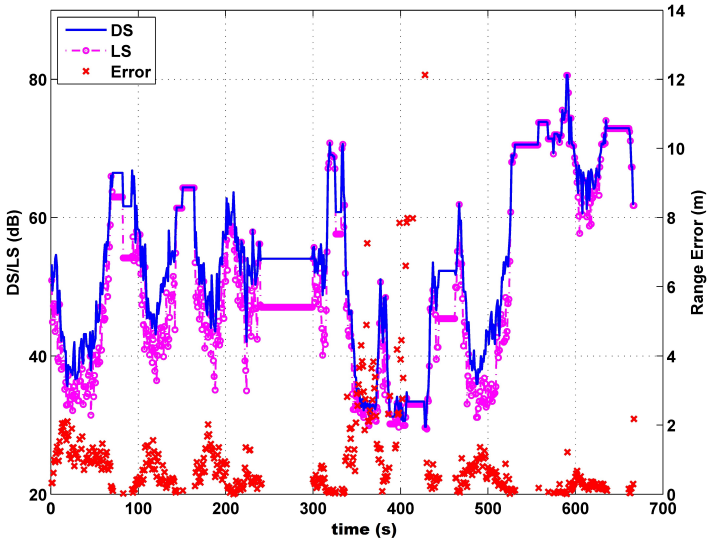

Figure 4.18: Scenario 2 DS and LS values

3. Scenario 3 (Network based ranging)
   The full UWB network is setup in this scenario where BUs are placed at known locations as indicated in Figure 4.11. Two rovers each carry an MU and start at one of the corners of the square corridor. The designated route for both rovers is to walk around the store room by following the corridor in two opposite directions, coordinates as shown in Figure 4.19. The received DS/LS at the MU carried by Rover 2 is plotted along with its ranging error in Figure 4.20. The two rovers are separated by a longer distance in this scenario and more obstruction is experienced. As a result, larger ranging error is observed. Both DS and LS values are significantly lower in this scenario than previous trials due to the obstructions experienced in this trial (e.g. walls, shelves).

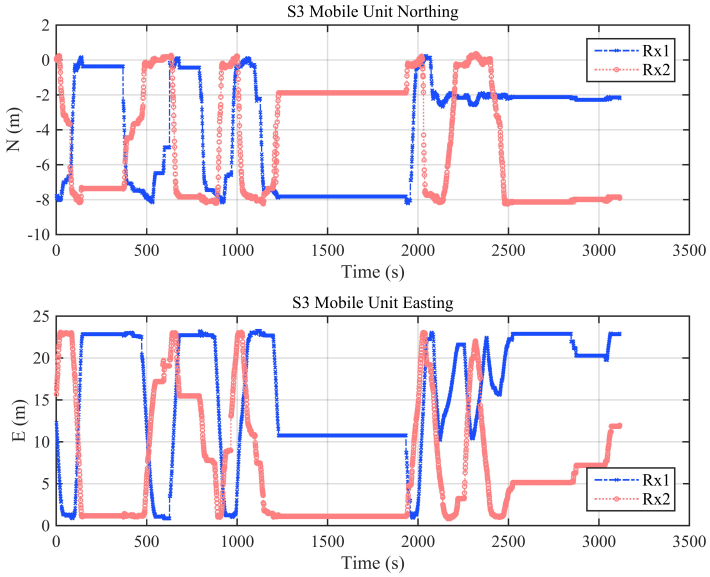

Figure 4.19: Scenario 3 Easting and Northing

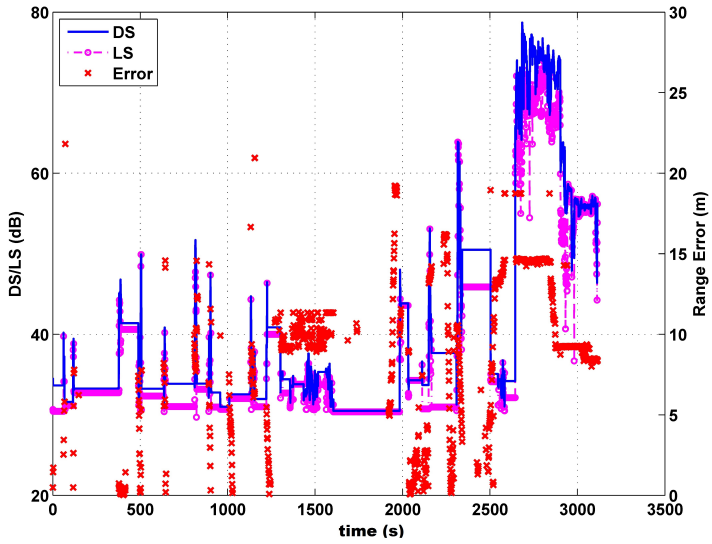

Figure 4.20: Scenario 3 DS/LS values

Table 4.2 lists the maximum and minimum ranging error of each scenario. As the power of the applied UWB system is limited and more suitable for open environments, the modern building structure and metal shelves caused frequent signal obstruction and data outage while it was implemented indoors. Thus 79% of the collected data in Scenario 1, 66% in Scenario 2 and 36% in Scenario 3 contained valid ranging information and only those data have been used for error evaluation. All evaluated data are

collected from Rover 2 for comparison. Of the valid data, 85%, 71% and 65% of the ranging errors were within 1m in Scenario 1, Scenario 2 and Scenario 3 respectively.

Table 4.2: Indoor trial ranging error (m)

	Mean		Min		Max	
	R1	R2	R1	R2	R1	R2
S1	\	0.41	\	0*	\	7.25
S2	0.95	0.90	0*	0*	10.88	12.13
S3	2.40	2.60	0*	0*	17.32	26.64

*sub-millimetre value

4.3.2.4 *Mine trial*

Another indoor trial was conducted in the tunnel of the Janina Mining Plant, about 60km from Krakow, Poland to examine the DS/LS pattern. The field work was not carried out by the author of this thesis, but authors in Skulich et al. (2013). However, data was shared for analysis as a colleague from NGI was involved in this trial. A UWB network consisting of four BUs was setup within the mine tunnels with one MU as the rover that measures positions and obtains ranging results while moving along the tunnels. If less than three BUs could be detected from the MU then no position output would be recorded but trials were carried out until no ranging measurement could be recorded. The tunnels stretched from 25m to 70m in length and 4m in width with steel shorings fixed on arches for stability.

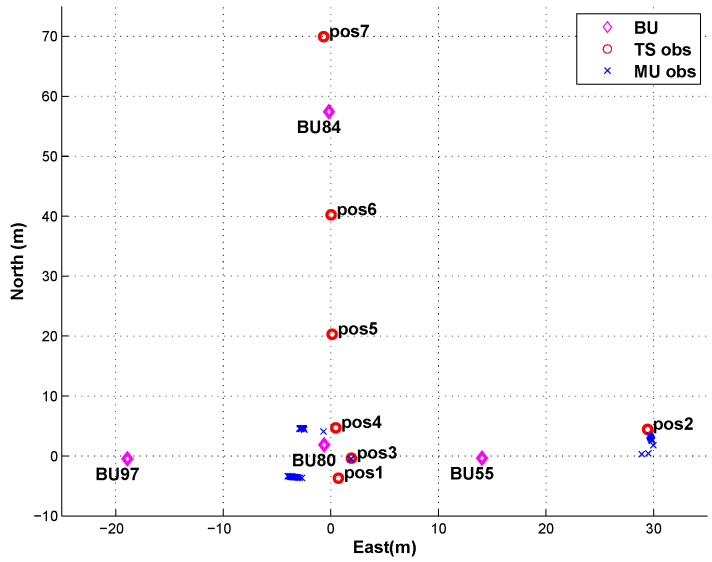

Figure 4.21: UWB network tunnel setup diagram

Positions of the BUs and the MU measured by a total station are shown in Figure 4.21. The MU travelled from Pos1 to Pos7 respectively as labeled in the diagram. The positions of the MU at each location were measured using a total station by remaining static for 20-80 seconds. The UWB ranging accuracy is achieved by comparing the UWB observations to the total station measurements. The actual distance between the MU and BU, the ranging measurement error, DS and LS values are listed in Table A.1 for each location.

This trial is based in a very different environment compared to previous ones. Tunnels are assumed to an indoor environment, however they differ to indoor buildings due to their restricted space and unique spatial geometry. Although units were sometimes obstructed by thick rock walls up to several tens of metres, but signals were able to reach the receiver in most cases and data outage rarely happened. This is most probably because the special geometry of tunnels allow the signals to travel along its path. However in such cases, the ranging measurement from the received signals tend to be biased, as it has travelled a further distance. Measurements are listed in full in Appendix A.2. Some data are extracted and listed in Table 4.3. Again, like the previous trial, a general pattern of the ΔDLS values indicates that a high ΔDLS value correlates with a low ranging error and vice versa. A large difference between the DS and LS values usually correlates with the NLOS periods between MU and BU with low ranging accuracy, except for a few outliers, such as Pos2 for Unit 84 and Pos7 for Unit 55, where the DS is relatively high but there is still a very large ranging error. This may be a result of the different wall structures on the left and right hand side of Pos5, Pos6 and Pos7. But the effects on data acquisition and measurement accuracy of different materials are not the main concern of this study.

Table 4.3: UWB ranging in mine trial (extracted)

MU location	Pos4	Pos5	Pos6	Pos4	Pos1	Pos7
BU No.	84	80	80	97	97	55
Dist (m)	52.72	18.47	38.38	20.66	19.89	71.82
Error (m)	0.48	0.13	0.38	4.28	5.13	31.45
DS (dB)	40.22	56.42	51.42	32.59	33.08	46.52
LS(dB)	39.80	56.31	51.25	31.33	31.79	44.78
ΔDLS (dB)	0.42	0.11	0.16	1.26	1.28	1.74

For the purpose of giving better ranging constraints, an appropriate ranging accuracy indicator should be given with each measurement. The

system can then constrain particles based on the assumed error level. While the system cannot know for sure how much error is in the measurement, it has been found that the error level can be estimated from the DS and ΔDLS values which arrives together with the ranging measurement. The data collected in the tunnels further indicate this, i.e. the pattern of the DS and ΔDLS values can be applied to estimate the ranging measurement accuracy.

4.3.2.5 Ranging quality

By observing the signal strength plots and data in the trials described above, we could see that the DS and LS values will decrease for two reasons: either the signal penetrating an obstruction or when the distance between the receiver and transmitter is increasing. When an obstruction is experienced, both DS and LS decrease, but not by the same amount. The separation between the DS and LS values depend greatly on the type of obstruction experienced. As Figure 4.13 and 4.16 indicate, in the short ranging distances that is observed in an indoor environment, the ranging error is not affected too much by the distance. Thus, a large difference in the DS and LS values are more likely to reflect a larger error in the ranging measurement. Further attention should be given to body obstruction as it could cause more significant unstableness in ranging.

With its broader bandwidth and fine timing properties, UWB provides ranging accuracy of decimetre level in an open environment. In indoor environments, ranging measurements are contaminated by obstructions and disturbances from passing pedestrians. If these disturbance periods could be identified, the remaining ranging measurements can still maintain a high level of accuracy.

Accurate P2P ranging is vital information in a collaborative positioning system to constrain the measurement error of each individual user. Yet if the ranging information itself is biased, the system state would still be biased after integrating the collaborative constraint. Or even worse, a biased constraint may push the system state error further away from the truth and increase positioning error. Therefore, it is important to know the ranging measurement quality so accurate ranging could be integrated and poor ranging could be neglected or corrected before integration.

4.4 Predicting the ranging quality

From the measurements collected in the open environments, we see that UWB systems can provide very accurate ranging measurements when there is no disturbance in the surrounding environment. However the results shown in the indoor trial results indicated that UWB signals are easily disturbed in such environments due to limited signal power. However, the system ranging performance can be identified from a clear pattern of the collected DS/LS values and their corresponding ranging error in the trials. Higher DS and LS values indicates less disturbance, hence ranging measurements with smaller error. Yet if a large difference exists between the DS and LS values or if the DS value is relatively low, this suggests a high probability of NLOS which leads to low ranging accuracy. Many previous studies have discussed the identification and classification of LOS and NLOS signals from extracting information on the channel statistics of the physical properties of the received signal such as the root mean square delay spread[1], the kurtosis [2] and mean excess delay [3] etc (Casas et al., 2006; Benedetto et al., 2007; Guvenc et al., 2008; Alsindi et al., 2009; Dardari et al., 2009; Marano et al., 2010; Montorsi et al., 2011; Wymeersch et al., 2012; Yan et al., 2013).

However, many of these algorithms depend on extracting physical information that requires more sophisticated methods which are not easy to implement in real time positioning systems. Furthermore, these works focus on identifying whether the signal is LOS or NLOS and this is not the primary concern here. We are more interested in the actual ranging measurement accuracy so that we can apply a collaborative constraint more effectively according to its accuracy. A ranging measurement quality indicator (RQI) is introduced here based on the patterns described above. The indicator does not categorise the signals into LOS or NLOS, but instead provides the probability of high accuracy measurement. An RQI is assigned to each received measurement based on its DS, LS and difference between

[1]Root mean square delay spread: the delay spread is a measure of the multipath richness of a communications channel. In general, it can be interpreted as the difference between the time of arrival of the earliest significant multipath component (typically the line-of-sight component) and the time of arrival of the latest multipath component.

[2]Kurtosis: any measure of the "peakedness" of the probability distribution of a real-valued random variable.

[3]Mean excess delay: time delay during which multipath energy falls to X dB below the mean.

DS and LS. This indicator is a value between 0 and 1, where 1 indicates high accuracy and 0 indicates low accuracy.

4.4.1 Detection method

Gaussian Process (GP) was introduced in Chapter 3 which is able to predict data based on given training data. It is applied here to learn and predict the RQI from a given categorising rule. As a supervised machine learning approach, GP generalises a mapping from a given pair of DS/LS values and its corresponding ranging error to a theoretical ranging error indication (RQI). This is then applied to predict the RQI for other DS/LS pairs.

To train for the hyperparameters of the specified GP, 5474 sample data from the previously collected UWB indoor ranging measurements are applied for analysis. These data are sorted into two datasets, 10% of the data are sorted as a test dataset and used for validation testing, the rest are used as a training dataset. The data which contains invalid data or an obvious measurement outlier will not be included in the training dataset as we want only the "clean" data during training to produce the most suitable hyperparameters. The applied covariance function is the squared exponential covariance function,

$$k_{SE}(x_p, x_q) = \sigma_f^2 \exp(-\frac{(x_p - x_q)^2}{2\ell^2}) + \sigma_n^2 \delta_{pq} \tag{4.10}$$

where x_p and x_q are the input data, i.e. sets of DS, LS values and the ranging error. The hyperparameters are $\theta = (diag(\ell)^{-2}, \sigma_n^2, \sigma_f^2)$, ℓ is the characteristic length scale, σ_f^2 is the variance of the input signal, σ_n^2 is the noise variance, δ_{pq} is the Kronecker delta, such that $\delta_{pq} = 1$ if $p = q$ and $\delta_{pq} = 0$ otherwise.

Each training data input vector consists of $\{DS, LS, \triangle DLS, err_r\}$, whereas $\triangle DLS$ is the difference between the DS and LS of a single received data vector, err_r is the ranging error in metres. As DS, LS values and the ranging error change quite rapidly, the relationship between them cannot be established in a straightforward way. Moreover, the accuracy in a low-cost indoor positioning scenario is mostly metre level. Therefore, error changes in the centimetre level is not a main concern. As it is not easy to identify the correlation between the signal strength values and the ranging error, ranging errors are sorted into groups and each group is assigned an RQI. The range of errors in each group is identified by the level of accuracy the system is trying to achieve and its effect on the positioning performance.

By analysing the data obtained in trials, it can be seen that small measurement errors give good positioning performance but the performance can be changed by even a slight change in the measurement accuracy. Larger errors will result in poor performance but larger changes in the measurement error will be needed before it changes the positioning performance level significantly. Therefore, the range of errors increase as the errors become larger. The collected measurements have been sorted into different groups for trial and test to give the best positioning performance based on the ranging measurement accuracy level. The following rules for assigning RQI values to err_r are given based on tests,

$$if \begin{cases} err_r \geq 15\text{m}, & RQI = 0 \\ 8\text{m} \leq err_r \leq 15\text{m}, & RQI = 0.1 \\ 5\text{m} \leq err_r \leq 8\text{m}, & RQI = 0.2 \\ 3\text{m} \leq err_r \leq 5\text{m}, & RQI = 0.35 \\ 2\text{m} \leq err_r \leq 3\text{m}, & RQI = 0.5 \\ 1\text{m} \leq err_r \leq 2\text{m}, & RQI = 0.75 \\ 0.5\text{m} \leq err_r \leq 1\text{m}, & RQI = 0.9 \\ err_r \leq 0.5\text{m}, & RQI = 1. \end{cases} \tag{4.11}$$

The aim of the training procedure is to learn how each pair of received DS and LS values can be mapped to an RQI. With the trained hyperparameters, we would be able to predict the RQI based on the received signal parameters, which indicates the ranging accuracy.

4.4.2 Detection results

As introduced, 90% of the collected data are applied to train for the hyperparameters. Once this is obtained, the remaining data is used as the test data to perform RQI prediction. All ranging data are measured by UWB units and each moving unit is tracked by total stations, thus we know the real ranging error for each pair of received DS/LS data, hence the true RQI. The training quality of the prediction algorithm is first evaluated by comparing the detected RQI from the DS/LS input and the actual ranging error, as shown in Figure 4.22 where the detected RQI value for the test dataset is plotted with the ranging error. The training quality is also evaluated by comparing the detected RQI and the true RQI derived from the actual ranging error. The detected RQI is plotted along with the true

RQI in Figure 4.23.

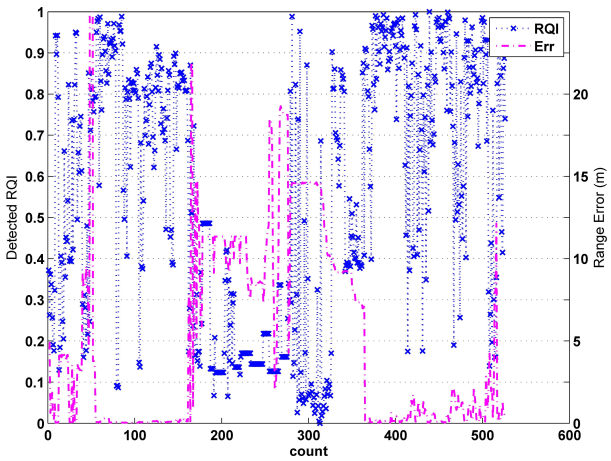

Figure 4.22: Comparing the detected RQI and the corresponding true ranging error

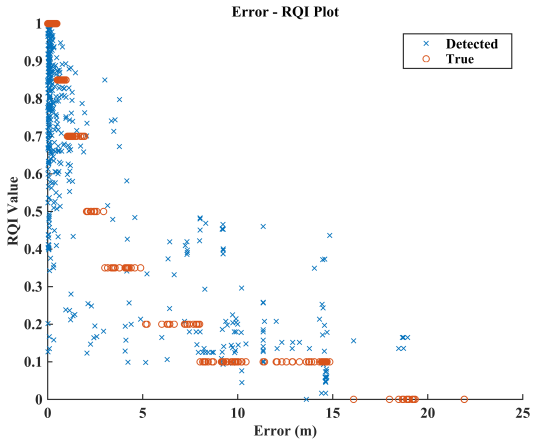

Figure 4.23: Comparing the detected RQI with the RQI derived from true ranging error

Results indicate that most of the detected RQIs are very close to the true RQI and reflect the ranging error accurately. According to the given RQI assignment rules above, the real ranging error is quantised into eight different categories each assigned with a unique RQI. However the ranging error is a real number which is continuous. Therefore if there is a measurement error during the training phase, the DS/LS pair could be mapped to the wrong RQI, which will result in biased training parameters. Likewise, a small error in the RQI detection will result in a different category which indicates a ranging error that could be several metres different. Furthermore, the detected RQI is the training output of the continuous DS/LS input, which is also continuous. Thus a small difference between the detected

and the true RQI should be acceptable. From Figure 4.23, the detected RQI follows the pattern of the proposed RQI categories. The overall result of the ranging error detection shows that the probability of Type I Error, where a high accuracy measurement is assigned a low RQI value, is 11%; the probability of Type II Error, where a low accuracy measurement is assigned a high RQI value, is 6%.

The detected RQI value is intended to act as a weighting factor in the collaborative positioning algorithm, reflecting the confidence in the relative ranging measurement. Ranging measurements with high RQI would be given a higher weighting factor implying that the system has higher confidence that the measurement is accurate, while low RQI measurement would be given lower weights. To achieve better collaborative constraints, it is vital to identify measurements with low ranging accuracy. Therefore, maintaining a low Type II Error is important as the positioning performance relies integrating accurate ranging constraints and neglecting low accuracy ranging measurements. If a low accuracy ranging measurement is assigned a high RQI, the system would be misled to believe a measurement with a large error and the system measurement errors would be incorrectly constrained, hence producing wrong estimations in the system state. On the other hand, if a low RQI is given to a high accuracy ranging measurement, the resulting problem would be that the measurement error is not properly constrained and eliminated. But the state estimation would not immediately be affected. Further description on applying the RQI to the collaborative positioning algorithm will be given in Chapter 5.

4.5 Network geometry

Collaborative network performance is affected by many factors and even with good quality ranging, other environmental factors can still prevent the ranging from constraining measurement errors properly and increase the system estimation error. Besides, when there are a number of ranging measurements available, it is not necessary to integrate all measurements even if they were all perfect measurements. Even though integrating more data will provide more information on the positioning confidence and error corrections, it can also cause information overload and reduce computation efficiency which is a crucial problem in real time pedestrian positioning and navigation. This section discusses the efficiency of a collaborative network from the aspects of network geometry. The corresponding effects of different network geometric structures as well as other measurement

properties on the system state estimation is analysed.

4.5.1 DOP

A useful indicator of the network geometry is the dilution of precision (DOP) (Dempster, 2006). Originating from the Loran-C navigation system, DOP describes the geometric layout of the system transmitters by a single value (Langley, 1999). It later became widely applied in range-based positioning systems to state how the geometry of the ranging measurement will affect the positioning estimation, especially in GNSS systems, where it is used to predict and analyse the positioning performance based on the satellite geometry. With this information, users have a general idea of the expected accuracy from the Standard Positioning Service, which specifies the minimum performance level based on the current satellite constellation.

Given the measurement error of a system, DOP scales this error and reflects the relationship between the error and the positioning error. In a way, it relates the network geometry and the potential positioning result for range-based positioning systems. Therefore, authors have applied it to analyse the positioning performance of wireless networks and their integration with other sensors. Zirari et al. (2009) have modified the DOP to reflect both geometric and signal strength characteristics to act as a signal quality criterion for the integration of GPS and Wi-Fi positioning systems. Chen et al. (2013) presents a weighted geometric DOP that may be applied to select the optimal measurement devices for GPS, WSN or cellular communication systems.

Consider an example of a ground based radio positioning system, this is used to further explain how geometry can be reflected by DOP. A rover measures the radio signals received from all the surrounding base stations (BS) of the system and estimates the range between the rover and each BS based on the received signal measurements. Like the example given in the explanation of TOA, if two perfect ranges have been received from two separate BSs, the receiver would be able to position itself on one of the two intersection points of the two circles each with a radius of the measured range and centred at the two BSs. If we further increase the number of BSs to three, the receiver would be able to pinpoint its location to a single intersection point of three circles formed by the ranging measurements. Unfortunately, all ranging measurements contain errors.

Therefore, we would not be able obtain a perfect positioning estimation from the ranging measurements. Instead, each circle would actually be a ring of possible locations where the width of the ring is dependent on the variance of the measurement. Therefore positioning estimations will actually be within a bounded area formed by the intersection of the rings as shown in Figure 4.24. In such cases, the relative position of the intersection rings will affect the size of the bounded area, where smaller areas reflect smaller uncertainty in the estimation, thus smaller positioning error, as the geometry in Figure 4.24a. Figure 4.24b is an example of a bad geometry where the intersection is much larger.

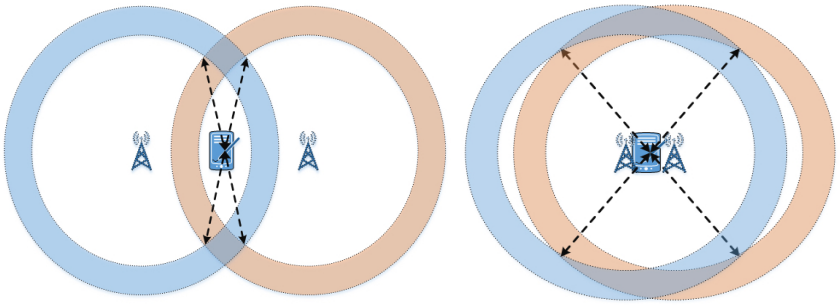

(a) Example of good geometry (b) Example of bad geometry

Figure 4.24: Diagram of positioning geometry

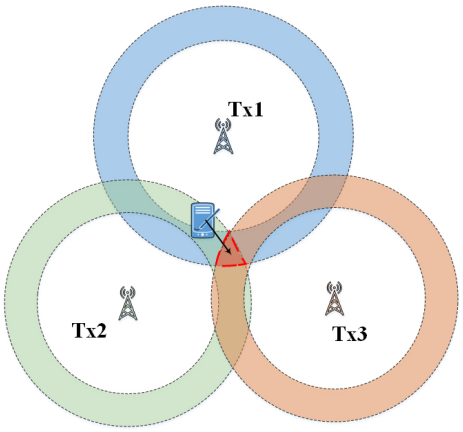

Figure 4.25: Positioning from the intersection of three stations

If three or more ranges are received, the rover would narrow down its position estimation to a single possible area where the three “estimation rings” intersect, as in Figure 4.25. As we can see, the relative geometry of the rings plays a critical role in the final position estimation. Ideally, in order to to form the smallest possible intersection area from the rings, the BSs should to be evenly spread out around the rover. DOP can be applied

to describe this spread. If we denote the rover position as $(\hat{x}_u, \hat{y}_u, \hat{z}_u)$, its ranging measurement to each BS may be expressed as

$$\hat{r}_i = \sqrt{(\hat{x}_u - X_i)^2 + (\hat{y}_u - Y_i)^2 + (\hat{z}_u - Z_i)^2} + c\delta_t + v_i \tag{4.12}$$

where (X_i, Y_i, Z_i) is the position of the ith BS, δ_t is a time offset, c is the speed of signal transmission, and v_i is a random noise. The ranging measurement can be linearised through Taylor series expansion to obtain the measurement error,

$$\triangle r = r_i - \hat{r}_i \cong \frac{\hat{x}_u - X_i}{\hat{r}_i}\delta_x + \frac{\hat{y}_u - Y_i}{\hat{r}_i}\delta_y + \frac{\hat{z}_u - Z_i}{\hat{r}_i}\delta_z + c\delta_t + v_i \tag{4.13}$$

For all ranging measurements, Eq.4.13 can be simplified as

$$z = A\delta + v \tag{4.14}$$

whereas $z = \begin{bmatrix} r_1 - \hat{r}_1 \\ r_2 - \hat{r}_2 \\ \vdots \\ r_n - \hat{r}_n \end{bmatrix}$, $\delta = \begin{bmatrix} \delta_x \\ \delta_y \\ \delta_z \\ c\delta_t \end{bmatrix}$, $v = \begin{bmatrix} v_1 \\ v_2 \\ \vdots \\ v_n \end{bmatrix}$, and $A = \begin{bmatrix} \frac{\hat{x}_u - X_i}{\hat{r}_i} & \frac{\hat{y}_u - Y_i}{\hat{r}_i} & \frac{\hat{z}_u - Z_i}{\hat{r}_i} & 1 \\ \frac{\hat{x}_u - X_2}{\hat{r}_2} & \frac{\hat{y}_u - Y_2}{\hat{r}_2} & \frac{\hat{z}_u - Z_2}{\hat{r}_2} & 1 \\ \vdots & \vdots & \vdots & \vdots \\ \frac{\hat{x}_u - X_n}{\hat{r}_n} & \frac{\hat{y}_u - Y_n}{\hat{r}_n} & \frac{\hat{z}_u - Z_n}{\hat{r}_n} & 1 \end{bmatrix}$ (known as the geometry matrix). If we apply least squares adjustment to Eq.4.14 with the constraint $v^T P v = min$, where P is a weight associated with each measurement, a matrix of the errors of each parameter can be derived,

$$\hat{\delta} = (A^T A)^{-1} A z \tag{4.15}$$

where $(A^T A)$ is also known as the normal equation matrix. The covariance matrix of the error estimations is then expressed as

$$\Sigma_{\hat{\delta}} = \hat{\sigma}_0^2 (A^T A)^{-1} = \hat{\sigma}_0^2 Q_{\hat{\delta}_0} \tag{4.16}$$

where $\hat{\sigma}_0^2$ is the variance of the unit weight. The diagonal elements of $\Sigma_{\hat{\delta}}$ contain the position error, i.e. σ_x^2,σ_y^2,σ_z^2. The off-diagonal elements describe the correlation between the position errors in the three directions. Thus the cofactor matrix $Q_{\hat{\delta}}$ is written as

$$Q_{\hat{\delta}} = \begin{bmatrix} \sigma_{xx}^2 & \sigma_{xy}^2 & \sigma_{xz}^2 & \sigma_{xt}^2 \\ \sigma_{xy}^2 & \sigma_{yy}^2 & \sigma_{yz}^2 & \sigma_{yt}^2 \\ \sigma_{xz}^2 & \sigma_{yz}^2 & \sigma_{zz}^2 & \sigma_{zt}^2 \\ \sigma_{xt}^2 & \sigma_{yt}^2 & \sigma_{zt}^2 & \sigma_{tt}^2 \end{bmatrix} \tag{4.17}$$

DOP is calculated from the diagonal elements of Eq.4.17. For different positioning situations, several different DOPs can be derived. The geometric DOP is defined as

$$GDOP = \sqrt{\sigma_{xx}^2 + \sigma_{yy}^2 + \sigma_{zz}^2 + \sigma_{tt}^2} \tag{4.18}$$

Positional DOP is defined as

$$PDOP = \sqrt{\sigma_{xx}^2 + \sigma_{yy}^2 + \sigma_{zz}^2} \tag{4.19}$$

When x and y correspond to the Eastings and Northings of the a local horizontal coordinate, the horizontal DOP is defined as

$$HDOP = \sqrt{\sigma_{xx}^2 + \sigma_{yy}^2} \tag{4.20}$$

Generally in GNSS positioning applications, low PDOP values indicate good satellite geometry, hence accurate positioning, and vice versa. In an indoor positioning network, we usually only consider 2D scenarios as people mostly stay on floors where the height is constrained and relatively easy to estimate. HDOP can reflect the number and the relative spread of the units in the network. HDOP will be applied throughout this thesis to describe the 2D geometry of the collaborative network consisting of both rovers and anchors on the same floor level.

Two aspects of collaborative positioning will be investigated based on the DOP value of the positioning network. The first is the network geometry with a constant number of units. With a fixed number of units, a low DOP usually indicates that the units are more evenly spread about the receiver, hence signals give better constraint. The second is the network size, i.e. the number of units in the network. If all units were evenly spread out around the receiver, a denser network with more units would reduce the DOP value and produce more constraint on the rover.

In a multi-user collaborative network, both rovers and anchors can provide ranging measurements to the specific rover that is in the positioning phase. DOP reflects the relative position of the units in the local area. Thus by calculating the DOP of each network combination, we are able to evaluate whether a unit is in a good location to be included in the network and if they can constrain the rover's measurement error through relative ranging. DOP also allows the rover to balance the number of units in the network so that computation is not slowed down by integrating too many

measurements.

4.5.1.1 Network geometry

Most measurement types contain some random error which produces a level of uncertainty in the positioning result. The advantage of collaborative positioning is that it should be able to effectively reduce this uncertainty given useful collaborative information. However, only measurements in a good geometry can reduce that uncertainty and produce positioning results with a small error variance, whereas a bad geometry will not be able to give a good boundary to the positioning error. While DOP reflects the network geometry, it provides the relationship between the geometry and its effect on how the measurement error will reflect on the final positioning performance. Thus when all ranging measurements are at the same accuracy level, a good geometry, i.e. low DOP network, will generate a high accuracy positioning result whereas a bad geometry will result in low positioning accuracy.

To examine the relationship between positioning accuracy and the network geometry, the CRLB as well as DOP is computed and compared for all locations inside the simulated area described in Section 4.2.1 with different network settings. First of all, a network of two anchors is examined where the two anchors are placed at different locations on the perimeter of the square area, numbered from 1 to 6, to form different network geometry. The CRLB and DOP of each network is then calculated and indicated in the heatmap shown in Figure 4.26. The anchors are marked as red diamonds. Dark blue indicates low CRLB values and red indicates high values. The DOP for each location within each network is also computed and shown in Figure 4.27.

The plots indicate that locations that are almost in-line with the two anchors have the highest CRLB which means that there is more uncertainty in those areas, and locations that are farther out have much lower CRLB, indicating better accuracy.

The DOP plot follows the same pattern as CRLB. In fact, if we examine the derivation of DOP and CRLB closely, we will notice that CRLB and DOP only differ in that

$$CRLB = \sqrt{\text{tr}(A^T R^{-1} A)^{-1}} \tag{4.21}$$

while

$$DOP = \sqrt{\text{tr}(A^T A)^{-1}} \tag{4.22}$$

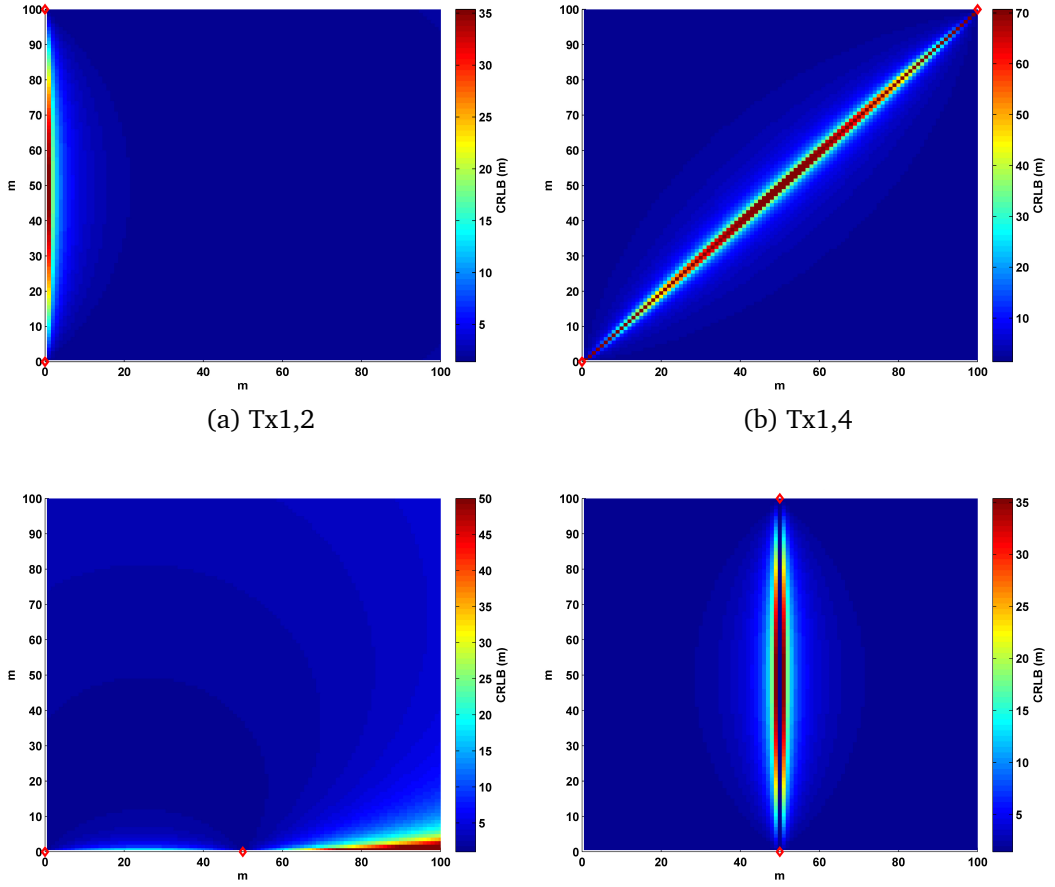

(a) Tx1,2 (b) Tx1,4

(c) Tx1,5 (d) Tx5,6

Figure 4.26: CRLB for different geometry settings

where R is the measurement variance. This is based on the assumption that the noise in each of the measurements is uncorrelated and DOP assumes that all measurements have the same noise variance. DOP is able to reflect the network positioning quality without prior knowledge of the system measurement variance.

To examine how DOP can help to improve collaborative positioning, a rover is simulated within a 100m $\times$ 100m square area, as shown in the green line in Figure 4.28. The rover moves along a straight line propagated by dead reckoning based on particle filtering. The step length of the rover propagation model is a constant value with a uniformly distributed random noise and the heading is simulated according to the trajectory with a constant bias as well as a random noise. The DR navigation result without corrections is shown in the magenta line in Figure 4.28. Anchors can be placed at any of the eight designed locations marked by red diamonds.

A pair of anchors are simulated at five different locations to form five

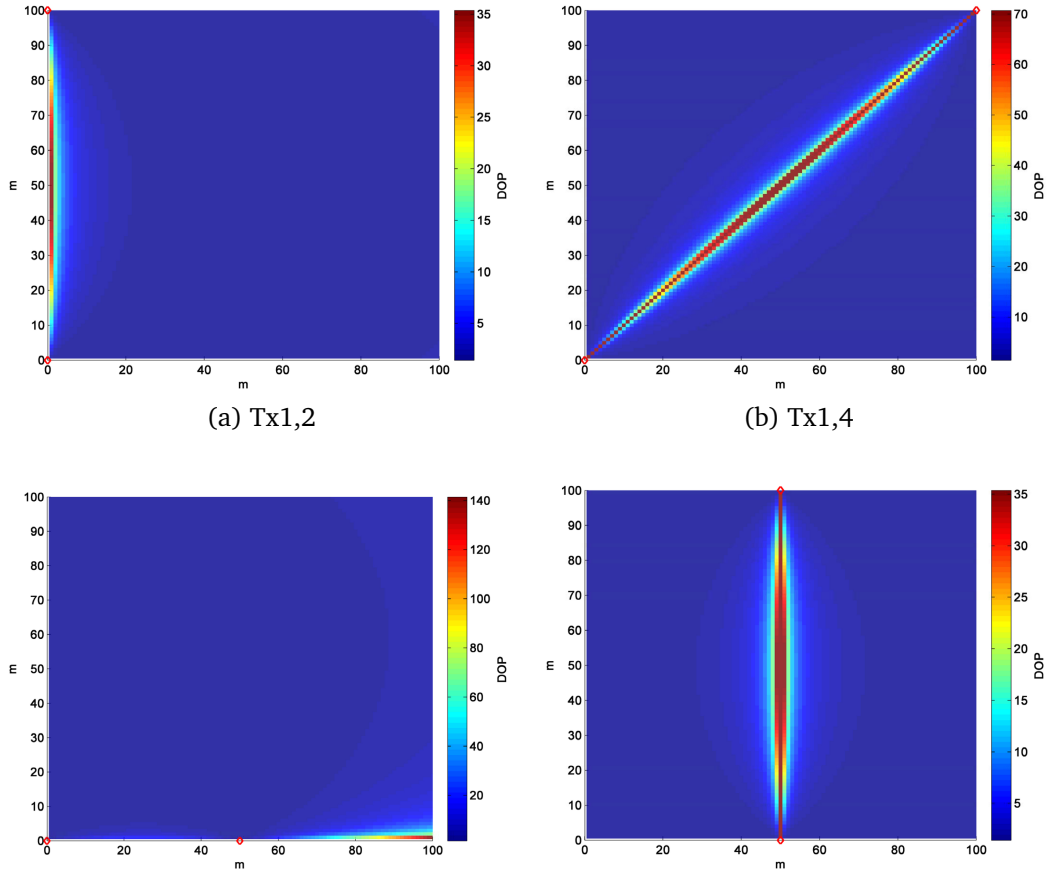

(a) Tx1,2

(b) Tx1,4

(c) Tx1,5

(d) Tx5,6

Figure 4.27: DOP for different geometry settings

different networks to evaluate the positioning accuracy of different geometries. The ranging measurements between the rover and each surrounding transmitter are obtained for each network. Particles that do not fall inside the ranging measurement constraint will be killed. The position of the rover is then updated by estimating the mean of the particles.

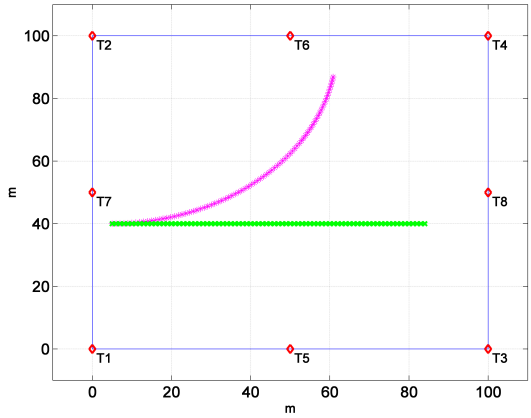

Figure 4.28: Simulated trajectory and network

The HDOP is calculated during each epoch of propagation for all five networks and the mean DOP during the entire propagation period is computed to indicate the overall network geometry. The DOP at each epoch of all five networks is plotted in Figure 4.29b. The positioning errors of each network are shown in box-plots in Figure 4.29a, x-axis is the mean DOP value of each network and y-axis indicates the positioning error. The central mark in the box is the median, the edge of the box is the 25th and 75th percentiles, the whiskers extend to the most extreme data not considering outliers. The box plot clearly shows that the networks with low DOPs have smaller positioning error while the error is also more concentrated. As DOP increases, the large errors increase much more than the small errors as we see the box start to stretch out a long range. This increases the mean error and also indicates that most positioning results during the propagation are inaccurate. Therefore, the network geometry makes quite a significant difference on positioning. Hence DOP should be take into consideration when analysing collaborative positioning network.

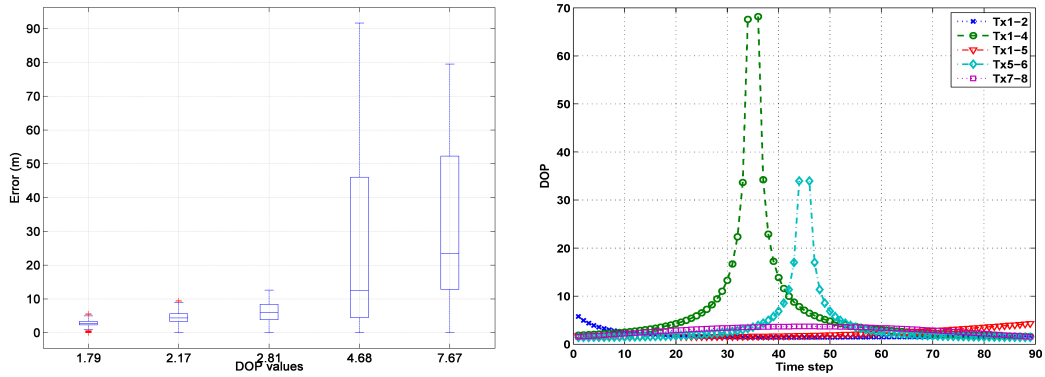

(a) Positioning errors for five different networks (the average DOP for each network is given on x-axis)

(b) DOP measured at Rx for each network

Figure 4.29: Positioning error for networks of the same size but different DOP values

4.5.1.2 *Network capacity*

The other factor that affects the DOP of a network is the network size. As DOP is correlated to $(A^T A)^{-1}$where A is the geometric matrix describing the ranging vector of each measurement, thus increasing the number of units in the network will increase the product of $(A^T A)$ hence decrease the final DOP value. Authors in Yang and Soloviev (2014) suggest that increasing the number of rovers or anchors will give better collaborative positioning performance. If the overall network density is increased by adding new units to the network, then the relative location of the units will become a less dominating factor for positioning performance. However, to balance the computation efficiency of the network, we cannot expand the network size limitlessly. Several questions should be raised when we include units into the network, such as how including an additional unit will affect the computation speed, and how the positioning accuracy improves with every additional unit.

The heat map of DOP values throughout the same simulated square area is plotted in Figure 4.30 to give a general idea of the DOP at different locations when the network size changes. Dark blue indicates low DOP and red indicates high DOP. The efficient network capacity is examined carefully to ensure that each selected anchor contributes to improving accuracy. To evaluate the relationship between the network size, DOP and positioning accuracy, the potential positioning accuracy for the locations in the square area is evaluated by the CRLB for different networks. Different numbers of anchors are placed at various locations on each side of the

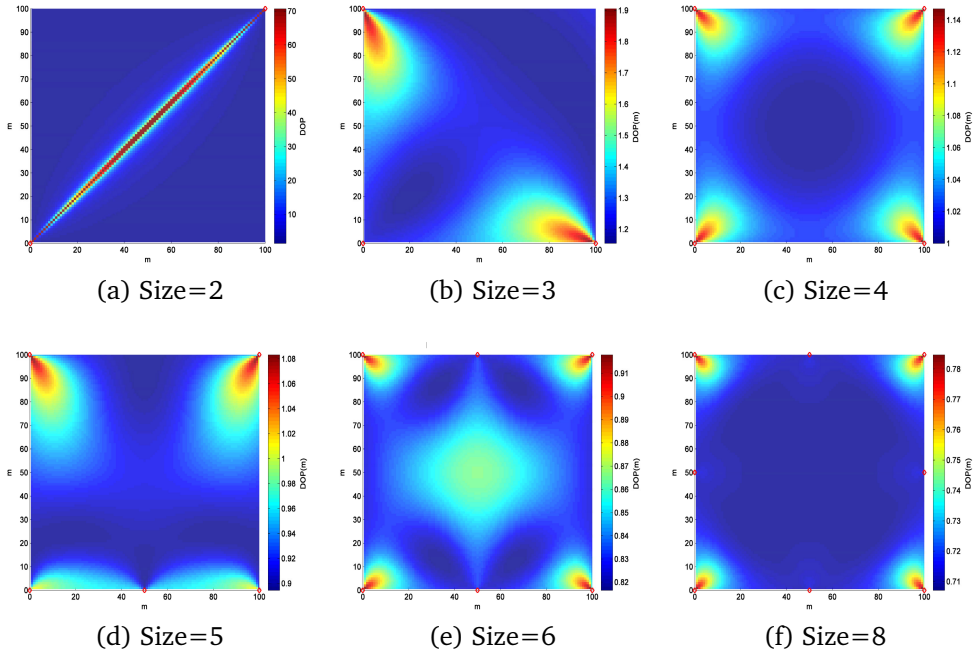

(a) Size=2 (b) Size=3 (c) Size=4

(d) Size=5 (e) Size=6 (f) Size=8

Figure 4.30: DOP for different network sizes

test area to examine the CRLB for the entire area. The network increases gradually from three anchors on the three corners up to eight anchors, as marked in red diamonds in Figure 4.31. The measurement noise level remains $\sigma^2 = 1$. Dark blue indicates low CRLB values and red indicates high CRLB.

An obvious decrease in CRLB could be seen when the network size increases, but the deduction rate is not linear as the decrease slows down when the number of units continues to grow. In this case, a network capacity threshold should be identified where additional units begin to have less obvious impact on improving the positioning performance, i.e. the least number of units required to make a significant improvement on the system performance.

The same positioning algorithm as in Section 4.5.1.1 is applied here to examine the positioning accuracy of different sizes for three different levels of ranging accuracy. The number of anchors in the network increases from 2 to 10, and the standard deviation of the ranging error σ_{err} is set to 3, 5 and 15. The rover positioning error in each network is plotted in Figure 4.32. We can see a distinct improvement in positioning when the number of anchors increases from three to four when the ranging error $\sigma_{err} = 3$ and $\sigma_{err} = 5$, hence the effective size is regarded as 4. The effective size becomes 5 when $\sigma_{err} = 15$ as the distinctive drop in positioning error

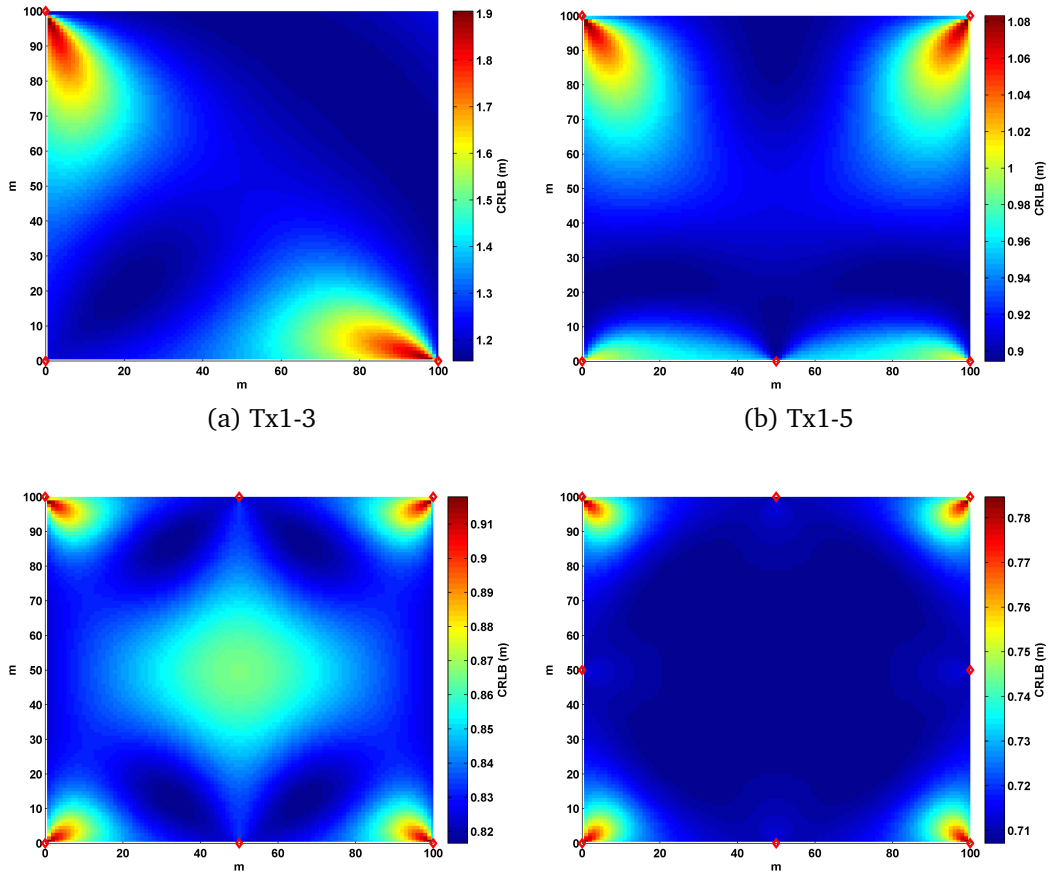

(a) Tx1-3

(b) Tx1-5

(c) Tx1-6

(d) Tx1-8

Figure 4.31: CRLB for different network sizes

is seen when the number of units increases from four to five. Once the effective size is reached, the improvement in positioning becomes less evident when more anchors are added to the network. In some occasions, there may be no improvement at all. Yet if we continuously add more anchors into the network, the additional units would soon become a burden for computation. The number of ranges we can obtain between n units is $n(n-1)$. This would mean that each additional unit increases $2(n-1)$ computation steps, For a rover state that is represented by 500 particles, this would be an extra $1000(n-1)$ calculations for each added unit, i.e. 5000 steps if $n = 5$. Thus after reaching the effective size, the increase in computation cost overtakes the increase in accuracy. To keep a balance between the network capacity and computation efficiency, the number of units in a collaborative positioning network should be kept within four even if more units are available. However, it should be kept in mind that the units in this scenario are simulated within a rectangular shaped space. Irregular shaped scenarios will not be discussed here as they can be split

into more regular shapes and the network can be analysed within the regular shape.

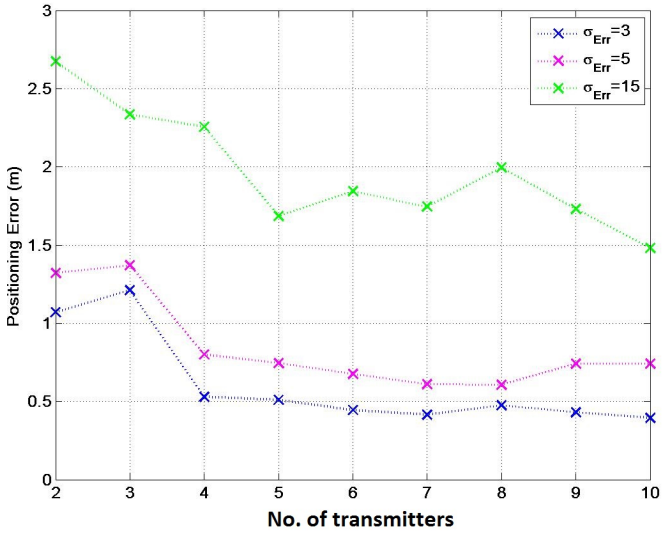

Figure 4.32: Positioning error for different network sizes

4.5.2 Modified DOP

Although DOP is the most straightforward method of reflecting the geometry effect on positioning performance, it is not sufficient to reflect all details within the network, especially directional and system related bias. It might also be unfit to reflect non-ranging based network conditions, e.g. fingerprinting, which will not be discussed here. DOP is only used in this thesis to analyse the network conditions of ranging based networks when units are in LOS. When units are in NLOS, either the environment is separated into different LOS areas, or the influence on the ranging measurement between NLOS units will have to be considered, e.g. longer ranging measurement with lower accuracy between NLOS units.

The first factor that DOP cannot take into account is the accuracy of the ranging measurements between the rover and other units. However, the ranging accuracy directly influences the effectiveness of the ranging constraint in collaborative positioning while it is also one of the most influential factors on positioning accuracy. The states of the users within the collaborative network are constrained by the relative constraint, which is the ranging measurement plus an “error bound”. However, if this bound is set to a value smaller than the measurement error itself, i.e. the constraint is too “tight”, the state estimation would be pushed towards a wrong location. On the other hand, if the bound is much larger than the error, i.e.

constraint too "weak", then it would not be able to sufficiently eliminate the observation noise and error. While the ranging measurements are used to calculate the DOP of each network, the quality of ranging would affect whether or not the DOP reflects the true geometry. Therefore, a modified DOP (MDOP) which integrates the ranging quality is applied here to reflect the network geometry that is weighted by the measurement precision. The modified geometry matrix A_{mod} is computed as below,

$$A_{mod} = \begin{pmatrix} \frac{\hat{x}_u - X_1}{a_1 \cdot \hat{r}_1} & \frac{\hat{y}_u - Y_1}{a_1 \cdot \hat{r}_1} & 1 \\ \frac{\hat{x}_u - X_2}{a_2 \cdot \hat{r}_2} & \frac{\hat{y}_u - Y_2}{a_2 \cdot \hat{r}_2} & 1 \\ \vdots & \vdots & \vdots \\ \frac{\hat{x}_u - X_n}{a_n \cdot \hat{r}_n} & \frac{\hat{y}_u - Y_1}{a_n \cdot \hat{r}_n} & 1 \end{pmatrix} \tag{4.23}$$

where $a_i (i = 1, 2, ..., n)$ is a measurement accuracy coefficient derived from RQI, hence a value between 0 and 1. Reliable measurements produce a closer to 1 and A_{mod} would be close to A. On the other hand, less reliable measurements produce a closer to 0 and A_{mod} would be much be larger than the actual A. MDOP is computed from A_{mod} as in Eq. 4.24, thus the produced MDOP is usually larger than the original DOP.

$$MDOP = \sqrt{\text{trace}((A_{mod}^T A_{mod})^{-1})} \tag{4.24}$$

Another problem with applying just DOP is that the information on the relative "spread" of a network is condensed into a single value. However when observing the DOP equation, we can see that the DOP is the same when the product of the distance between the rover and the other two units are the same. This indicates that the same DOP can indicate two completely different networks where anchors are on different sides of the rover, as in Figure 4.33. Under normal circumstances, the two anchors in both situations will give the same restriction on the positioning precision in the diagonal direction along the line of the anchor and the rover (↗↙) and unable to determine the position in the other diagonal direction (↖↘). Hence correctly indicated by the DOP value. However, in most ranging-based positioning scenarios, the ranging measurement are always positively biased, i.e. the ranging measurement is usually longer than the real distance due to disturbance in the propagation path. Given these conditions, the two scenarios in Figure 4.33 will no longer give the same restriction. Network 1 is able to constrain the error along the diagonal direction, but it is likely to be biased to one side of the rover due to the positive bias

in the ranging measurement (as indicated by the eclipse in Figure 4.33a). Yet network 2 can further constrain the error in both directions along the diagonal line as the ranging is coming from two different directions (error uncertainty is indicated by the eclipse in Figure 4.33b). Therefore, even with the same DOP, network constraints behave differently when the ranging measurement is known to be positively biased.

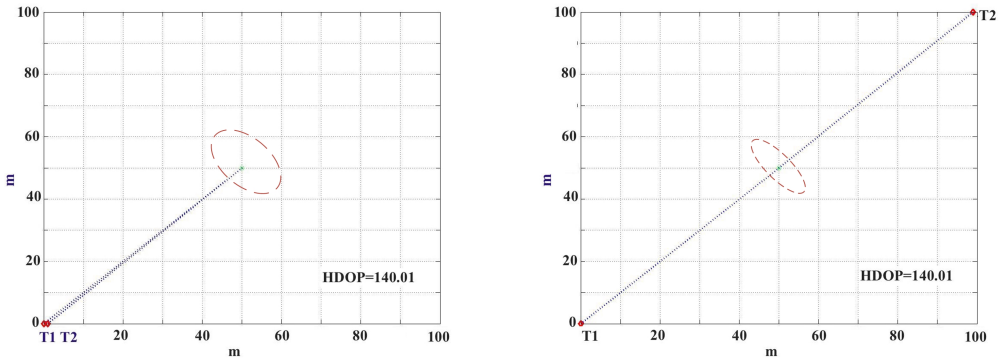

(a) Network 1 (b) Network 2

Figure 4.33: Examples of different network with same DOP (eclipse with dashed line indicates the error uncertainty in each network)

Moreover, when the two anchors are aligned, equation $\Delta x_1 \cdot \Delta y_2 = \Delta x_2 \cdot \Delta y_1$ holds true. Hence the geometry matrix will be a singular matrix where no valid DOP could be derived. Taking the example in Figure 4.33 one step further, there would be no valid DOP value if the two anchors in the first example are both located on the same corner , or if the anchors in the second example are located on the two corners but aligned with the rover. However as discussed, the network is able to provide relative constraint along the diagonal line. Therefore when the system detects an invalid DOP value, different situations are treated separately.

The third factor that DOP cannot reflect is the dynamic information during navigation, especially the directional information, e.g. the relative direction of the moving rover to the anchors as well as the rover system bias. Yet, this is also hard to detect if no prior knowledge is given. As an example, the simple simulation as shown in Figure 4.28 is applied here again. North direction is defined as upwards from the origin of the coordinate along the y-axis, East is defined as rightwards from the origin along the x-axis. Three scenarios are shown in Figure 4.34 where each network consists of two anchors at two of the selected locations. Scenario 1 is a network where the rover system bias is drifting northwards and

consists of anchor Tx1 and Tx4 (positioning results shown in magenta line). Scenario 2 shows a network of rover bias drifting southwards and anchors Tx1 and Tx4, and the bias of the rover is drifting downwards (shown in blue line). Scenario 3 shows a network of rover bias drifting northwards and anchor Tx2 and Tx3 (shown in cyan line).

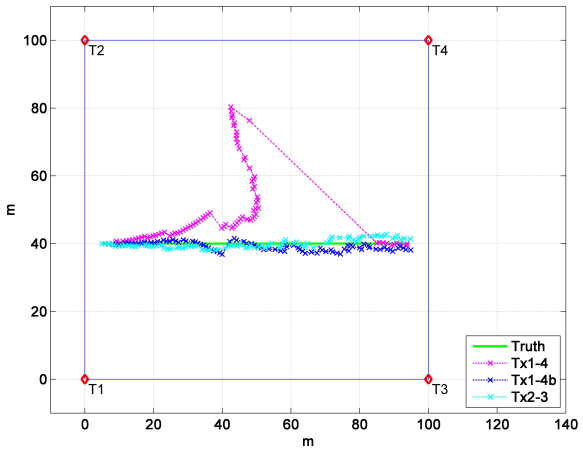

Figure 4.34: Relative constraint effects on different system bias

Gyro drift is one of the largest error source in inertial measurements which pulls the rover offtrack from its original trajectory. This bias is almost always at an angle to the direction of the travelling trajectory and seldom follow the direction along the trajectory. Thus constraints along the direction of the actual bias direction are more useful in restricting the measurement error and preventing the bias from pulling the positioning estimation away from the truth. The relative constraint of two different networks and their effect on the measurement error in two directions are examined, where Network1 consists of Tx5, Tx6 and the rover, Network2 consists of Tx7, Tx8 and the rover, the location of each anchor is as shown in Figure 4.28. Figure 4.35 shows the cumulative distribution function (cdf) of the error distribution in both the East and North directions when applying the collaborative constraint from the two networks. As Tx5 and Tx6 are located on either side of the rover, the network constrains the error in the North direction better than the East direction, which is the travelling direction of the rover. Tx7 and Tx8 are located on either end of the travelling trajectory, thus constrains the error in the East direction better than the North direction.

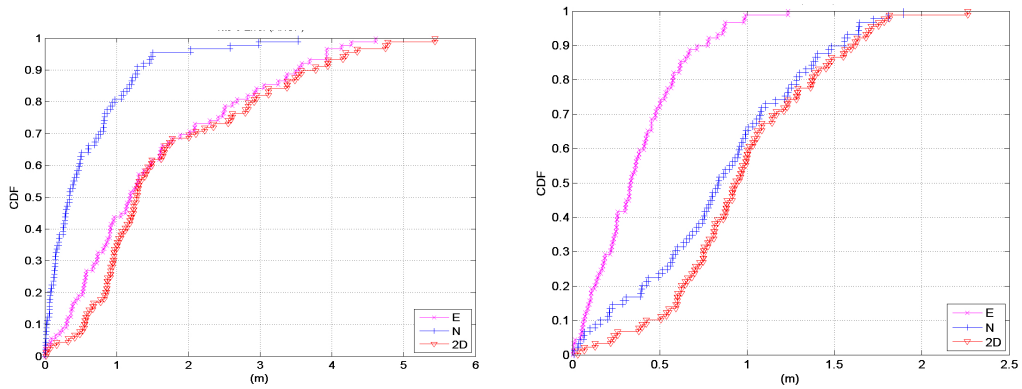

(a) Tx5-6 network (b) Tx7-8 network

Figure 4.35: Positioning CDF of different relative position network

As the rover is moving within the network, its relative direction to other units is always changing. Constraints from different directions are required when the rover is travelling in different directions even if the relative network remains unchanged. While DOP is only capable of reflecting the geometry at a single epoch in time, MDOP includes a relative directional factor to treat the dynamic relative motion of the network geometry.

4.6 Simulations and analysis

4.6.1 Simulations

In this chapter, the basic form of collaborative constraint is simulated. The proposed collaborative positioning algorithm is based on particle filtering as it provides more a flexible integration of different numbers of units and sensors, hence known as collaborative positioning (CPF). CPF can be applied to constrain and update inertial and wireless signal measurements based on current requirements and adjust weighting accordingly. The basic procedures of CPF is outlined as below:

i. Initialisation: generate N_p particles around the initial position for each rover $[x_0, y_0]$, all particles are assigned an equal weight $w_k^i = \frac{1}{N_p}$, indicating that each particle contributes the same amount in the position estimation at the beginning;

ii. Prediction: particles propagate forward based on the PDR prediction model Eq.3.1. Since there is no knowledge of how the model will propagate in the next step before the step is actually taken, thus the step length is assumed to be a constant value sl with a uniformly distributed random noise $U \sim (0, n_s)$, the heading $\hat{\theta}_{(t|t-1)}$ is simulated

with a constant heading bias of b_h and a uniformly distributed random noise $U \sim (-n_h, n_h)$. Therefore, the particles will propagate equally to all possible directions and distances before further measurements are taken to constrain the particles and estimate where the current position is after the step.

iii. Update and weighting: map information can be integrated so that particles which cross walls are "killed", i.e. $w_k^i = 0$; Wi-Fi RSS measurements is obtained when available and particles are weighted by fingerprint mapping; ranging measurements $\hat{r}$ are obtained between the rover and available units in the surrounding network to constrain measurement errors.
In such cases, the distance from each particle of the rover (i.e. user) to the position of the M rovers and anchors $\hat{d}_m^i$ is calculated and compared to $\hat{r}$ which is assumed to be the "true distance". For a particular particle i, if the distance difference Δ_{dis_i} between the particle and every particle of the other unit is over a threshold $thres_r$

$$\Delta dis_i^m = \left| \hat{d}_m^i - \hat{r} \right|_{m=1,2,\ldots,M} \geq thres_r \tag{4.25}$$

the particle is "killed", i.e. $w_i = 0$. $thres_r$ is defined by the error variance of ranging measurements. If the $\hat{d}_m^i$ is measured between the rover and an anchor, there would be N_e distance estimations each from one particle, where N_e is the number of the effective particles in the current epoch; if it is measured between two rovers, each with N_{e1} and N_{e2} effective particles, the distance is obtained between each pair of particles, hence $N_{e1} \cdot N_{e2}$ estimations.

iv. Resampling: if the number of "live" particles, N_e falls below a threshold, new particles are generated by replicating the live particles with an additional noise to replace the killed particles in order to maintain a total number of N_e particles. If the cluster of particles all get "trapped" in a wrong location and no longer able to propagate to a valid location, all old particles will be "killed" and a new cluster will be regenerated at a previous location with a large variance (usually the same as the variance used for initialisation).

v. Return to step ii or end iteration.

This is the fundamental CPF algorithm applied in the following sections and chapters. As discussed in Chapter 2, the selection of the effective

particle size can affect the performance of the filter. The variance of the particle weights will increase over time and reduce the accuracy (Merwe et al., 2000). Therefore, resampling is normally carried out as often as possible. However, there are many uncertainties in the measurements in the discussed simulations. Hence a certain level of variance among the particle weights is needed to maintain the diversity of the particles and cope with measurement noise and errors. Therefore, the threshold of effective particle size used is $N_e = \frac{N_p}{2}$ before resampling is carried out.

4.6.1.1 Simple implementation of ranging constraint

A simple scenario of collaborative ranging is simulated in this section to understand how collaborative ranging can improve positioning results. Two rovers are simulated to move along designed trajectories in a 50$\times$50m square area. Each rover is propagated forward following a basic dead reckoning algorithm with Wi-Fi RSS measurements from one AP as well as ranging measurements between each other at every epoch. Two different set of trajectories, T1 and T2, each with four different sets of DR bias directions are simulated to observe the effect of ranging constraints.

The first simulated trajectory is as shown in Figure 4.36 and 4.37. Figure 4.36a shows case 1 for T1, where the two rovers move in the same direction both $90^{\diamond}$ to the x-axis and their DR drift are in the same direction. Case 2 shows two users both moving $90^{\diamond}$ to the x-axis but with drifts in the opposite direction, as shown in Figure 4.37a when no ranging measurement is integrated and Figure 4.37b when ranging measurement is used to constrain measurements. Figure 4.36b shows case 3 where the two rovers move in opposite directions as indicated by the arrows and bias is also shown by the red line. In case 4, the rovers move in the same directions but with opposite drift directions as case 3.

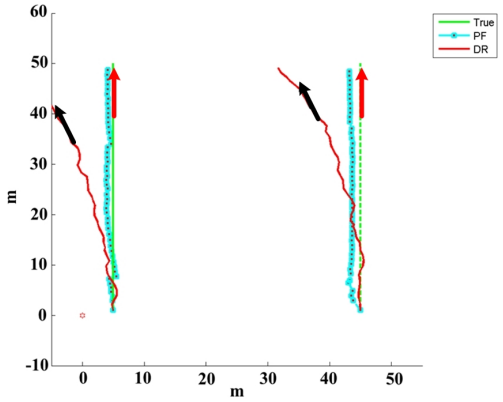

(a) T1 case 1

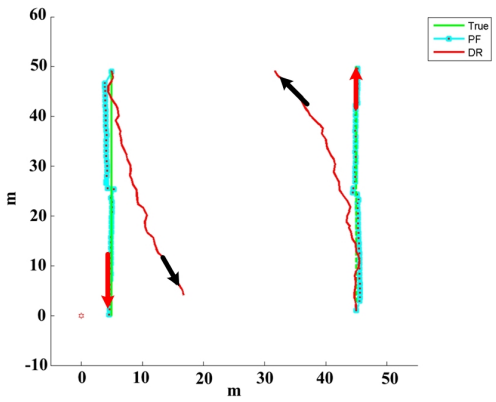

(b) T1 case 3

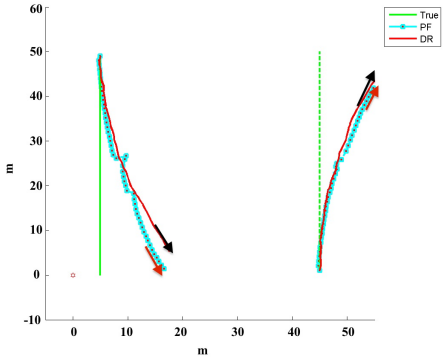

(c) T1 case 4

Figure 4.36: Positioning results for Trajectory 1 with ranging (moving directions are indicated by arrows)

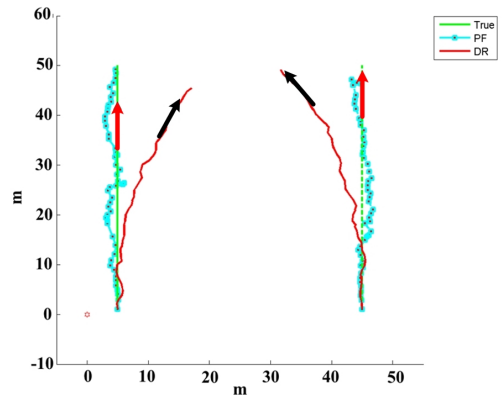

(a) T1 case 2 without ranging

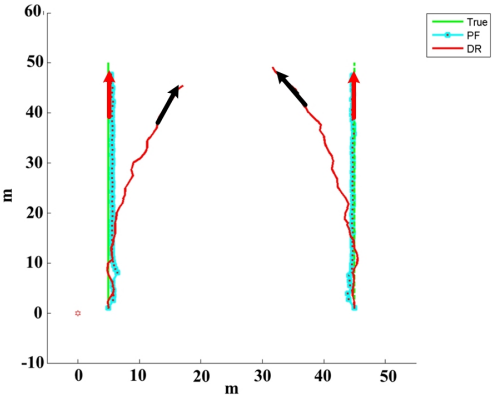

(b) T1 case 2 with ranging

Figure 4.37: Positioning results for Trajectory 1 Case 2 with and without ranging(moving directions are indicated by arrows)

Table 4.4: Positioning error for Trajectory 1

	User 1			User 2		
	DR	No ranging	Ranging	DR	No ranging	Ranging
Case 1	4.71	1.71	1.48	3.88	1.83	1.61
Case 2	4.71	1.61	1.25	5.31	1.54	1.31
Case 3	4.29	1.85	0.87	5.31	1.42	0.95
Case 4	4.29	1.83	0.93	3.88	1.67	0.80

The positioning error for each different case of Trajectory 1 is listed in Table 4.4. The positioning error is reduced by 30% on average when the ranging constraint is applied.

Trajectory 2 is simulated so that the two rovers are moving perpendicular to each other with four different DR bias cases as well. In case 1 and 2, Rover 1 moves $90^{\diamond}$ to the x-axis while Rover 2 moves $90^{\diamond}$ to the y-axis, drift directions are set to two situations, as indicated in Figure 4.38 and 4.39.

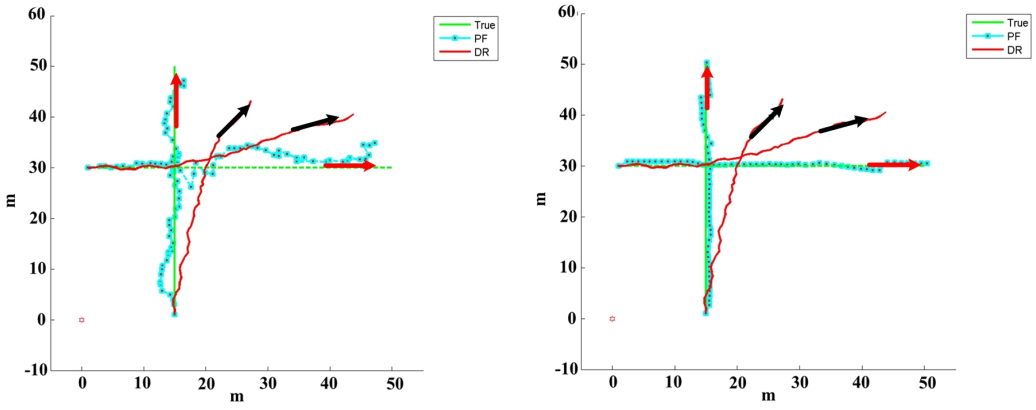

(a) T2 case1 without ranging

(b) T2 case1 with ranging

Figure 4.38: Positioning results for Trajectory 2 Case 1 with and without ranging (moving directions are indicated by arrows)

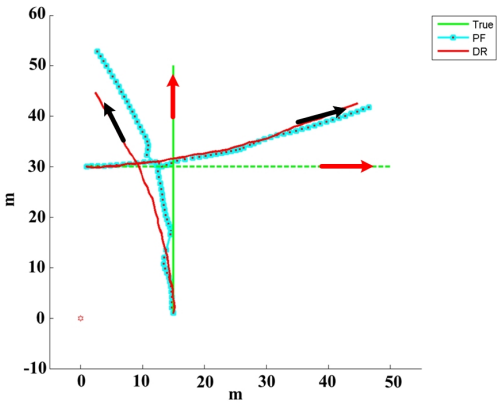

(a) T2 case 2

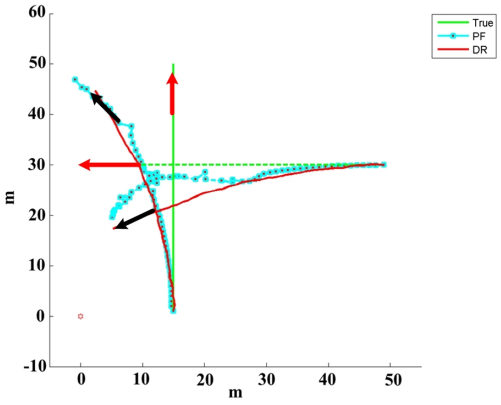

(b) T2 case 3

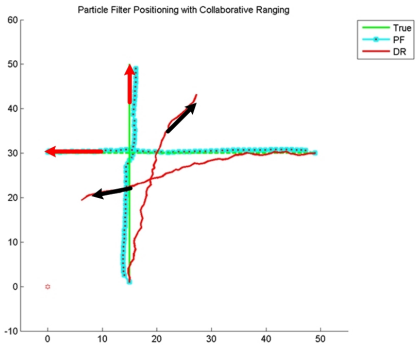

(c) T2 case 4

Figure 4.39: Positioning results for Trajectory 2 with ranging (moving directions are indicated by arrows)

In case 3 and 4, Rover 1 moves in the same direction while Rover 2 moves $-90^{\diamond}$ to the y-axis, bias directions are set to two different situations as previous situations. Ranging is only able to constrain rovers to remain a relative distance from each other, hence both users could still follow the wrong trajectory.

Table 4.5: Positioning error for Trajectory 2

	User 1			User 2		
	DR	No ranging	Ranging	DR	No ranging	Ranging
Case 1	4.77	2.15	0.66	4.77	2.48	1.01
Case 2	4.77	2.40	0.69	5.20	1.56	1.02
Case 3	5.20	1.55	0.88	5.20	1.70	0.74
Case 4	5.20	1.56	1.12	4.77	1.49	0.64

From the positioning error results listed in the two tables above, we could see an overall 30% improvement for the two users when moving parallel to each other and an overall 50% improvement when moving

perpendicular to each other. It could be identified that implementing the collaborative ranging between users helps to improve positioning accuracy. This improvement becomes more significant when the heading drifts are in opposite directions compared to same scenario with the heading drift in the same direction. This is due to the opposing effects of the drift bias when ranging is implemented which eventually pulls the trajectory in the right direction. Yet if the bias is in the same direction, the rovers could maintain the same relative distance while both are pulled offtrack by the bias.

4.6.1.2 Simple collaborative ranging

A second simple CPF simulation is carried out based in NGB between two mobile users, Rover 1 and Rover 2. Six fingerprint databases are simulated from six APs that are located across the entire floor plan. The RSS is as shown in Figure 4.40 where solid yellow triangles indicate the location of the APs on the same floor as the floor plan shown on the map and transparent yellow triangles show the location of APs which are on a floor above.

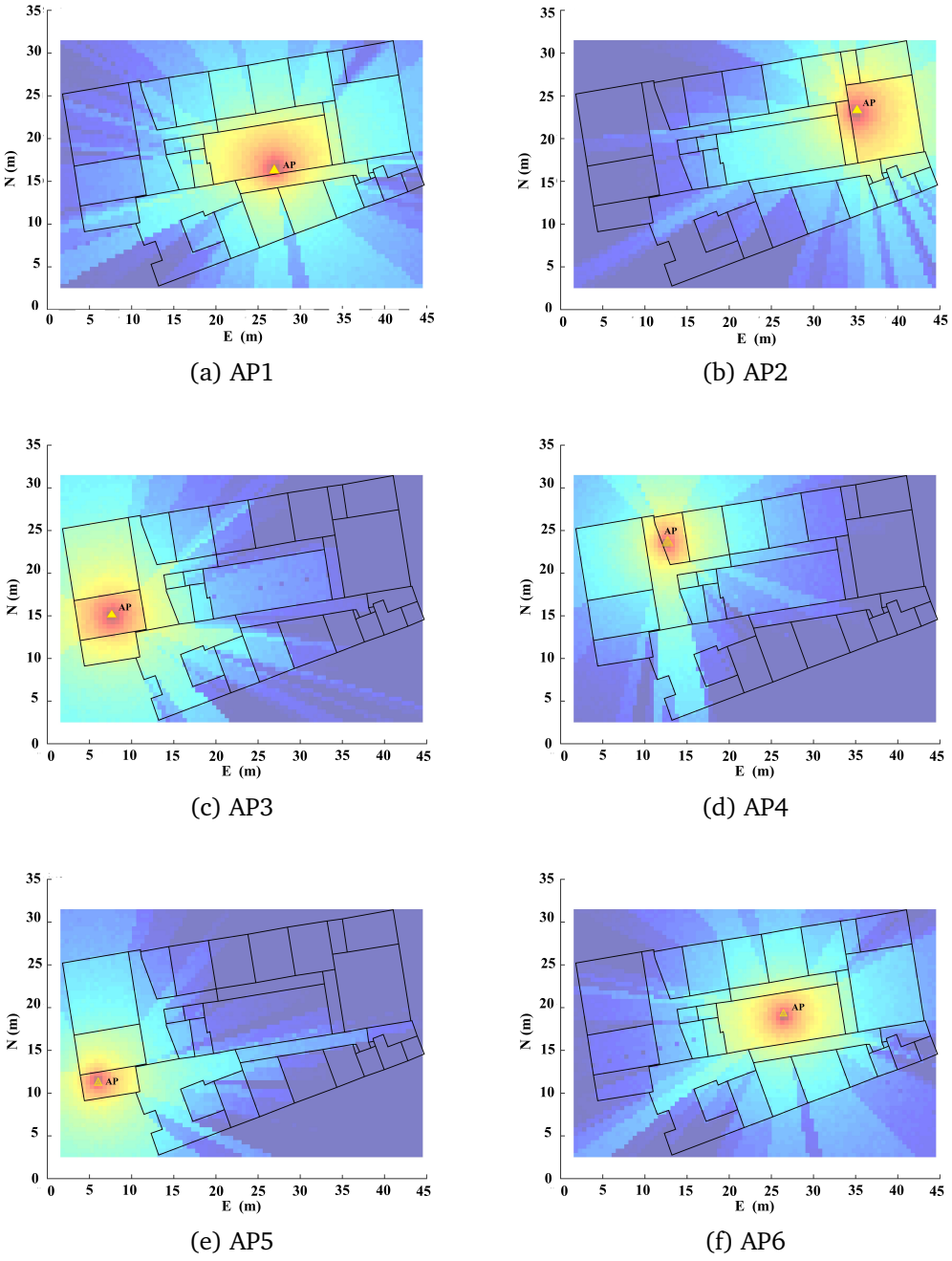

(a) AP1 (b) AP2

(c) AP3 (d) AP4

(e) AP5 (f) AP6

Figure 4.40: Simulated Wi-Fi fingerprints in NGB

Each rover travels along a different path following the PDR propagation model and collects Wi-Fi RSS measurements at every epoch. Figure 4.41a plots the positioning result when both users propagate based on DR/Wi-Fi integrated PF and there is no collaborative ranging involved. In the scenario shown in Figure 4.41b, ranging measurements r_{12} are obtained between the two users to constrain their DR and Wi-Fi measurements. Green lines indicate the true trajectory, red lines indicate the DR trajectory

if no constraints are applied. During the update phase of CPF, the particle of each rover tries to find particles from the other rover that fall inside the ranging threshold defined in Eq.4.25. More specifically, the difference between the ranging measurement and the particle distance is computed by

$$diff_m = \left| \sqrt{(x_{1m} - x_{2n})^2 + (y_{1m} - y_{2n})^2} - r_{12} \right| \tag{4.26}$$

where (x_{1m}, y_{1m}) is the position of the mth particles of Rover 1 and (x_{2n}, y_{2n}) denotes the nth particle of Rover 2. If no particle from the other rover fits the constraint $diff_m < thres_r$ for this particular particle, it would be killed. After each particle of the rover is evaluated against the constraint, the remaining live particles are weighted by their distance to the fingerprints and the final position is obtained by taking the weighted average of all live particles. The threshold $thres_r$ is set to 3m here. Hence when all $diff_m$ for particles of Rover 1 is over 3m, it will be killed. Blue and magenta lines indicate the CPF result of each user.

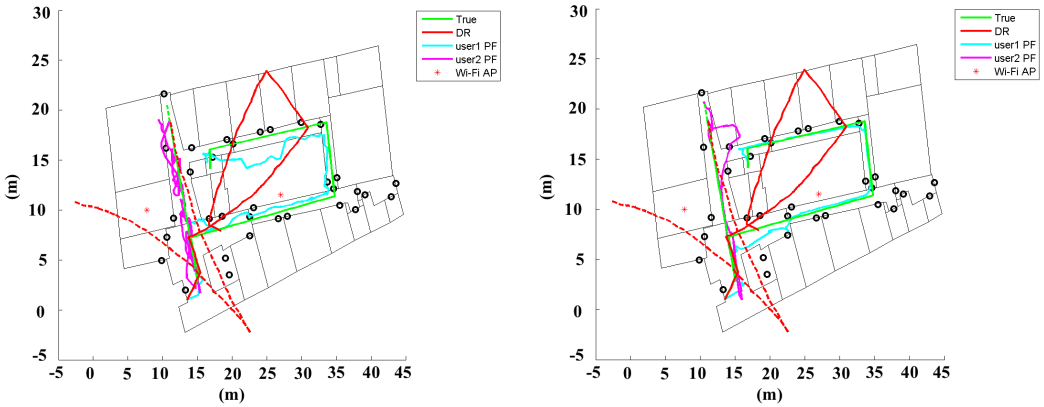

(a) Without collaborative ranging (b) With collaborative ranging

Figure 4.41: Indoor positioning based on DR and Wi-Fi fingerprinting

To examine the influence of the ranging constraint on a positioning system with insufficient Wi-Fi data, Wi-Fi APs are gradually reduced from 6 to 0. The positioning error of each setting is listed in Table 4.6.

The positioning accuracy improves by 70% for both users when compared to DR positioning results. By comparing the result of Rover 1 to its non-collaborative Wi-Fi positioning result in Chapter 3, an improvement of 25% can be seen. What should be noticed is that when ranging constraint is integrated, reducing or even eliminating the Wi-Fi infrastructure does not affect the system performance too much. Therefore, when collaborative positioning is applied, the system can provide continuous navigation even

if Wi-Fi infrastructure fails or changes.

Table 4.6: Positioning error for network with different Wi-Fi data (m)

	Rover 1		Rover 2	
AP no.	DR	CPF	DR	CPF
6	4.80	1.22	6.69	1.67
2	4.80	1.16	6.69	1.51
1	4.80	1.27	6.69	1.75
0	4.80	1.34	6.69	1.82

4.6.1.3 Collaborative constraint on Wi-Fi fingerprints

In this section, the collaborative constraint is applied to the FPM method introduced in Section 3.6.2, denoted as CFPM. During the update process of each epoch, the measured Wi-Fi RSS are compared to the database and a group of potential fingerprints that have similar RSS to the current measurement is returned as in FPM. The distance r_{ij} between each rover i and j is measured during the update phase and applied as the ranging constraint. The distance between the location of the mth fingerprint of rover i and the nth fingerprint of rover j ($diff_{FP_m}$) is also measured and each fingerprint is weighted by computing the difference between the rover-rover range r_{ij} and fingerprint-fingerprint range $diff_{FP_m}$, as in Eq.4.27.

$$diff_{FP_m} = \sqrt{(x_{im} - x_{jn})^2 + (y_{im} - y_{jn})^2} - r_{ij} \tag{4.27}$$

Fingerprints with a smaller difference in the distance measurements will be given higher weights. Ideally, these fingerprints should be close to the true position, i.e. the green locations in Figure 4.42.

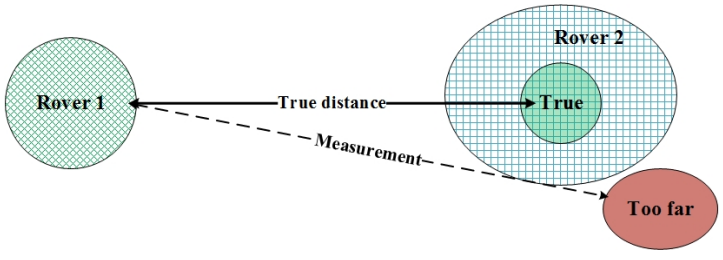

Figure 4.42: Extracting potential fingerprints with FPM ranging

Fingerprints that do not fall inside the constraint, i.e. the red locations, will be neglected and not considered as potential fingerprints. Particles of rover i are then weighted by their distance to the remaining m fingerprints

as in Eq.4.28 and positions are obtained by taking the weighted average of the particles.

$$wt_{pt} = \frac{1}{\sqrt{(x_i - x_{FP_m})^2 + (y_i - y_{FP_m})^2}} \tag{4.28}$$

Users follow three different trajectories designed on Floor A, NGB, denoted as T1, T2 and T3. DR measurements are collected from the Microstrain foot-tracker and real Wi-Fi RSS is logged onto a laptop. All data are time-tagged with UTC time for synchronisation. To perform CFPM in a controlled environment, the ranging measurements between users are simulated by forming a true distance from the true position and adding a zero mean Gaussian noise with standard deviation of 1m.

During the update phase of the positioning algorithm, fingerprints with $diff_{FM} < 1m$ are highly weighted and weights gradually reduce for any fingerprints that have a difference larger than 1m. The collaborative positioning performance between users following T1 and T2, T1 and T3, T1, T2 and T3 is plotted in Figure 4.43 respectively. In Figure 4.44b and 4.44c, T1 is cut short as the travelling time for rover following T3 is shorter. Although particles are not allowed to cross walls during consecutive updates, since no history information is taken into account, the weighted mean of the particles may have crossed walls and ended up in the wrong room for a short period before the resampling procedure brings the particles back into the right location.

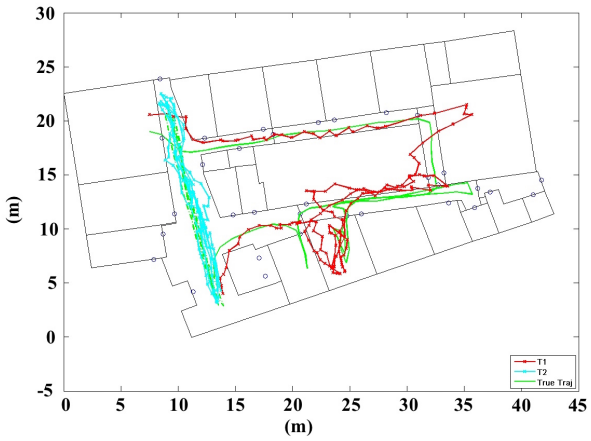

(a) Scenario a

Figure 4.43: CFPM positioning result

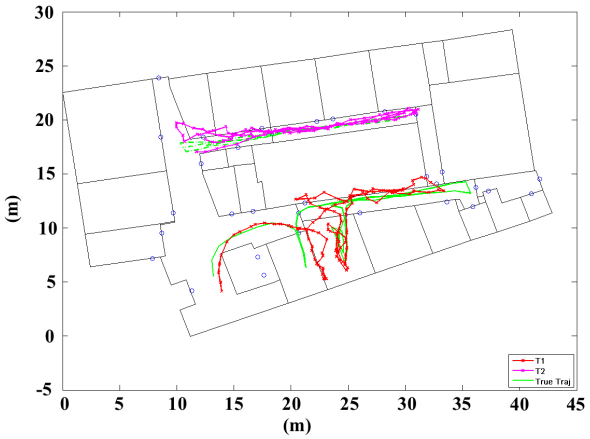

(b) Scenario b

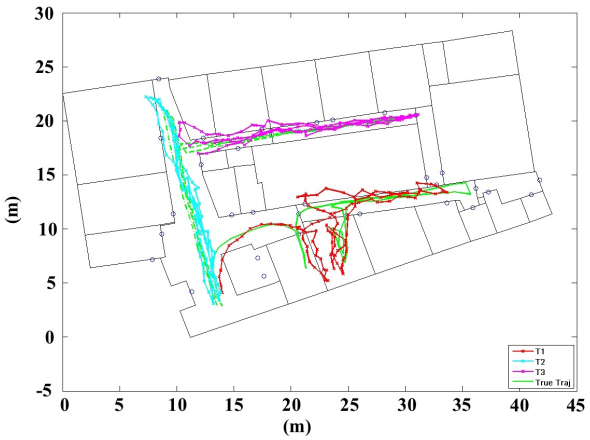

(c) Scenario c

Figure 4.43: CFPM positioning result(Cont'd)

The positioning error is obtained by finding the distance between the CFPM position to the true position. The performance of the algorithm is evaluated by the maximum error throughout the whole trajectory and listed in Table 4.7 for each scenario.

Table 4.7: CFPM maximum positioning error (m)

Scenario	T1	T2	T3
a	4.32	3.2	/
b	3.31	/	3.08
c	3.48	2.7	2.88

The cdf of the positioning error for DR/Wi-Fi integration and CFPM for rovers following T1 and T2 is plotted in Figure 4.44a and 4.44b respectively. T1 is more complicated than T2 with more turnings and entering rooms and Wi-Fi signals can become quite messy in such places. Yet its positioning

accuracy is greatly improved by integrating the collaborative constraint on fingerprint mapping.

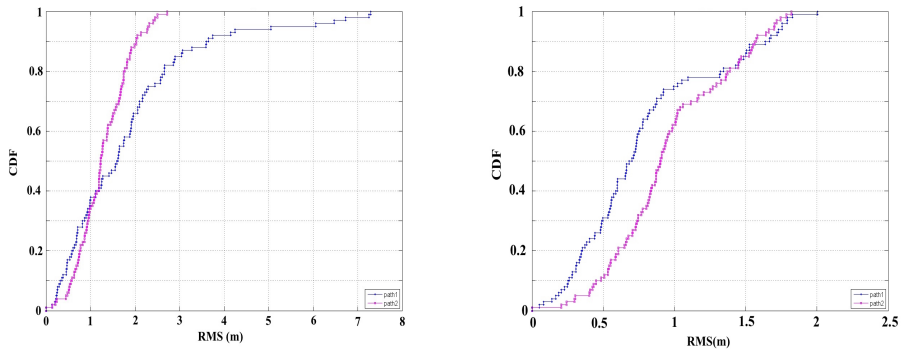

(a) DR/Wi-Fi integration (b) CFPM

Figure 4.44: Positioning error CDF

Results for the user following T2 are shown to be quite accurate in all scenarios. However this is mainly because that particles are not allowed to cross walls. With not very many doors to wander through, the paths of the particles are constrained by the corridor walls. Therefore, any particles that are biased by the gyro drift will be killed off, thus enabling more accurate positioning accuracy. As the trajectory becomes more complicated in T1 and more doors are seen along the path of T3, the positioning accuracy decreases evidently. Ranging constraints help to exclude the fingerprint outliers that may be caused by signal fluctuation. The two-user collaboration improves positioning accuracy by 40% compared to DR/Wi-Fi integrated positioning, three-user collaboration improves accuracy by 50%. Further trials were also carried out by increasing the ranging measurement noise standard deviation to 3m, yet the positioning error remained at the same level.

4.7 Discussions and summary

This chapter discusses and analyse the possibility of integrating relative ranging measurements between anchors and rovers in a local positioning network to improve indoor positioning results using low-cost devices.

Different network conditions, i.e. measurement quality, number of users included and network geometry, are compared by their CRLB and DOP values. The ranging measurements in this work is obtained from UWB systems. Hence the UWB ranging performance when the mobile unit is static and moving in both outdoor and indoor environments are analysed.

A Gaussian process tool is applied to predict the measurement accuracy from received signal strength patterns by producing an RQI indicator. The prediction method achieves prediction accuracy to more than 80%.

Both theoretical and simulation analysis show that the positioning accuracy is related to the network size and geometry when the measurement accuracy is known. As DOP is able to reflect the network size and geometry, it therefore also indicates the effect of the measurement error on the positioning error. To include the effect of the measurement error, MDOP is applied to indicate network conditions which weights the DOP by the predicted measurement accuracy. Based on the MDOP, the positioning system can then set the threshold which kills off particles and predict the performance of the current network.

The initial implementations of collaborative ranging positioning are demonstrated in this chapter through simulating simple trajectories as well as collecting real IMU and Wi-Fi data in indoor environments. However, because UWB ranging is easily disrupted in this building, all ranging measurements are simulated to ensure the continuity of ranging data.

The CPF algorithm which integrates ranging with inertial measurements for PDR, demonstrates that the ranging measurement obtained between two moving rovers is able to constrain measurement errors by eliminating particles which fall outside the relative constraint. CFPM integrates the ranging constraint with fingerprint mapping and inertial measurements. The simulation that implemented CFPM demonstrates that the ranging measurement could constrain measurements by eliminating outlier fingerprints before particles are weighted. Wi-Fi signals are unstable and the selected fingerprint locations are not always close to the true position. Sudden signal changes in the environment, either when setting up the database or during the positioning phase, could both lead to fingerprinting outliers. Ranging constraints would eliminate those that do not obey the measured geometry. In this case, particles would not need to be weighted to those outlier fingerprints anymore. This improves positioning accuracy.

Due to the fingerprint outlier elimination from ranging constraints, the quality requirement for the Wi-Fi fingerprint database is reduced and allows for faster database training methods. The map information and RSS measurement constrains the heading bias while the ranging information corrects the RSS positions. As a result of the constraint on each measurement, the proposed multi-sensor multi-user positioning algorithm provides improved positioning accuracy and stability for mobile users with access to

inertial and Wi-Fi measurements.

However, real life situations are far more complicated. More users could be available in the designated area; users could be walking in random directions. In the two rover ranging simulation, there are periods were ranging did not improve result significantly. Failure could also occur when both inertial measurement and RSS information are dragging particles into the wrong room on the other side of the wall, causing new particles to be eventually resampled in the wrong room.

However, as also introduced in this chapter, the actual effect of the ranging measurement integration is heavily influenced by ranging accuracy, network geometry and network size. The following chapter will discuss this in detail and also look into a collaborative fingerprint training method.

Chapter 5

Adaptive collaborative indoor positioning

5.1 Introduction

Collaborative positioning has been widely applied in intelligent transport systems so that vehicles are aware of the situation of other vehicles and infrastructure in the surrounding area. It integrates positioning related measurements from multiple sensors and users to reduce positioning errors and enhance robustness. Both sensors and users consist of two types of systems, those whose positions are known, i.e. anchors, and those whose positions are unknown, i.e. rovers. The collaborative positioning algorithm proposed in this thesis is applied for pedestrian navigation which integrates multiple sensors and users adaptively from two aspects: the integration of multi-sensors into a single positioning system and the integration of multi-users (or multi-systems) to form a collaborative network based on measurement quality and geometry. The integration of multi-systems enables information to be shared among the users in the network and improve the positioning accuracy of each user by constraining the measurement error of each system through relative ranging between users.

The implementation of collaborative positioning is convenient in indoor positioning scenarios as many users and sensors can be found in such environments. However, while many units can be found, it is important to identify the rovers and anchors before integration and only pick out the units that will contribute the most to enhance positioning for effective performance improvement. For each rover, its own network of rovers and anchors are selected based on the three aspects discussed in Chapter 4, the ranging measurement accuracy between the units, the collaborative network geometry and size. Based on these aspects, two adaptive collaborative positioning algorithms are developed and introduced in this chapter. The application of collaborative positioning also introduces to a collaborative Wi-Fi fingerprint training and positioning method that is

discussed here as well.

5.2 Collaborative ranging

During each epoch of collaborative positioning, the rover selects a number of rovers and anchors obtains measurements from them to perform positioning. The selected units make up the collaborative network at the current epoch. The collaborative network is influenced by several factors, i.e. the number of units, including both rovers and anchors, in the network, the ranging information between each unit and the position of the units. However the basic collaborative positioning particle filtering (CPF) algorithm applies the relative ranging constraint on all units regardless of what the actual ranging accuracy is or what the geometry of the network is like. In CPF, the particles are weighted based on the difference between the ranging measurement between units and the distance between the pair of particles. A fixed difference threshold is applied to kill the particles that do not fall inside the constraint hence eliminate the noise in the ranging measurement. However, the fixed threshold cannot cope with changes in the ranging measurement error. When the actual ranging measurement error is larger than the threshold, the algorithm does not know that the boundary should be stretched hence killing particles more than necessary.

The previous chapter introduced the ranging accuracy prediction method based on received signal characteristics, which provides a general idea of the reliability of the ranging measurement to the system. The system then adjusts the ranging confidence boundary based on this prediction, thus the threshold increases if the predicated accuracy is low, which potentially kills less particles during the measurement update. If the predicated accuracy is high, the threshold would be reduced so that particles which contains representation of large errors would be killed and the remaining particles would be more concentrated nearer to the true position.

In a network where the number of units are fixed, the relative position of the units, reflected by the horizontal dilution of precision (HDOP), would affect the positioning performance of the collaborative network. The ranging constraint threshold is therefore also set according to the DOP of the network. A network with low DOP is able to constrain the measurement error of each unit in the network more effectively thus a smaller constraint threshold is applied. If a large number of units, including all rovers and anchors that can provide ranging measurements, are visible in the environment, each rover would then select the appropriate collaborative units that is able to provide effective constraint on its measurement errors

while integrating the least number of units altogether.

If these specific network conditions are not taken into account during collaborative positioning, the applied constraints may not be effective which will produce no improvement on the positioning accuracy or even push the system state estimation into the wrong place. To mitigate such problems and enhance performance, two weighted adjustment algorithms are developed and applied accordingly based on real time network situations.

5.3 Collaborative ranging with adjusted weighting

5.3.1 Adaptive range constraint collaborative positioning (ARCP)

Both algorithms are developed on the basis of the CPF algorithm introduced in Section 4.6.1. The adaptive ranging constraint collaborative positioning (ARCP) method is introduced first which improves the positioning performance for a collaborative network consisting a fixed number of units. Although we do not have the freedom to choose the location of the units here, but the ARCP benefits from the adaptiveness by enabling the network to adjust the relative constraint threshold with more flexibility based on the predicted ranging accuracy and theoretical network geometry at each epoch, which immediately improves the system performance compared to the conventional non-adaptive CPF method. As a result, the positioning process is more robust as well as providing improved accuracy.

The constraint boundary $thres_r$ is adjusted at each epoch based on the modified DOP (MDOP) factor of the network. The MDOP reflects the HDOP of the selected network, the predicted ranging accuracy level from the units as well as the position of the selected units relative to the navigation bias of the current rover. The ideal network should have a low MDOP, indicating that the HDOP of the network is low and the position of the collaborative units are located at positions where the measurement bias of the rovers can be constrained. If the network is not ideal, the system would be allowed to adjust to a larger constraint threshold which fundamentally gives a smaller weight to the ranging constraint. Figure 5.1 shows a flowchart of the procedures of the particle filter based ARCP algorithm.

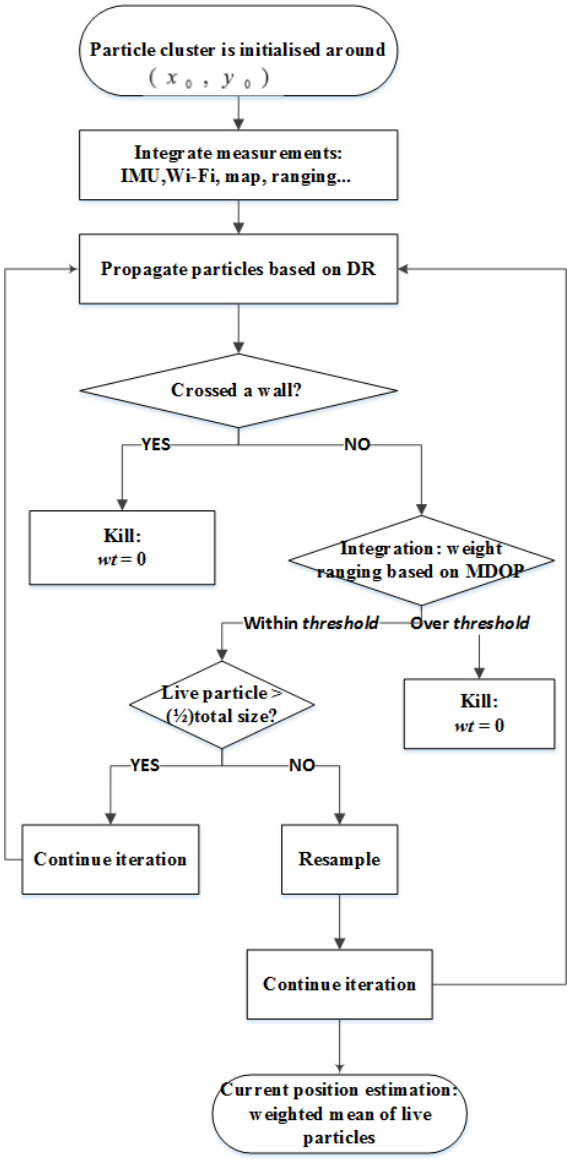

Figure 5.1: Flowchart of ARCP

The simple simulation presented in Chapter 4 is applied here again to compare the CPF and ARCP positioning results. Eight different locations can be used to place anchors and a trajectory is simulated in the middle of the square area. Six different pairs of locations are set for a pair of anchors and the rover follows the same trajectory propagated by a PDR model. Figure 5.2 plots the positioning result and cdf of the positioning error of applying CPF and ARCP for each different network setting. The green line indicates the true trajectory and the magenta line shows the positioning result.

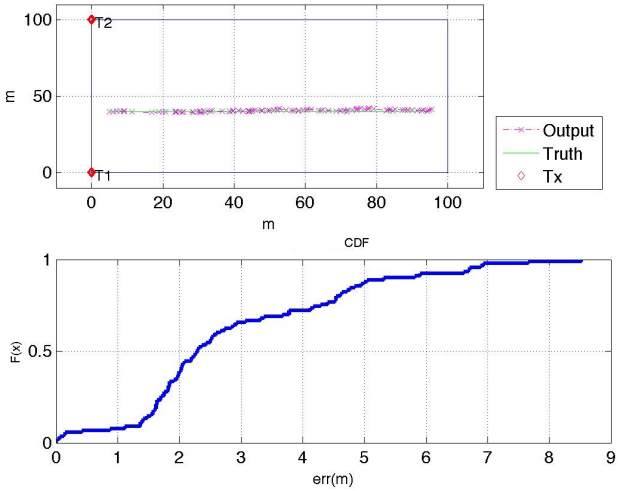

(a) CP (Tx1,2 used)

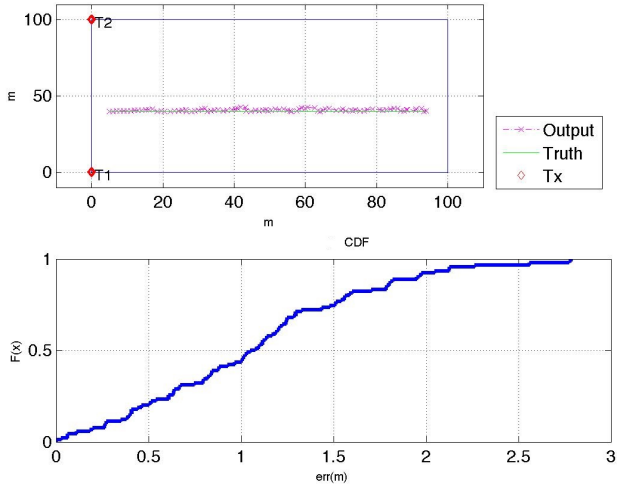

(b) ARCP (Tx1,2 used)

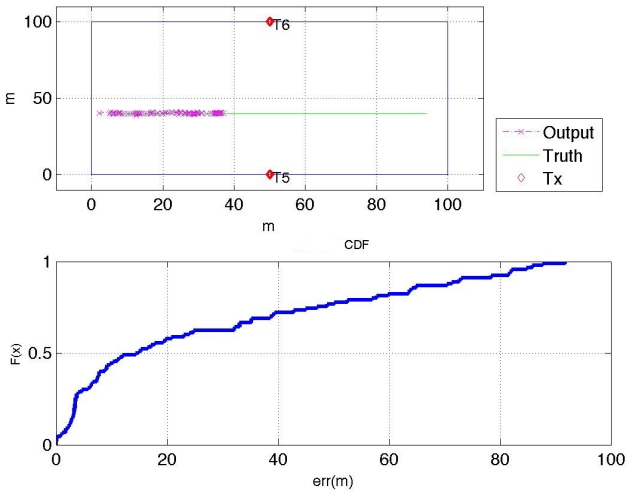

(c) CP (Tx5,6 used)

Figure 5.2: CP and ARCP Positioning Results using different Tx (Top plot of each subplot shows the trajectory, bottom plot shows the positoning error cdf)

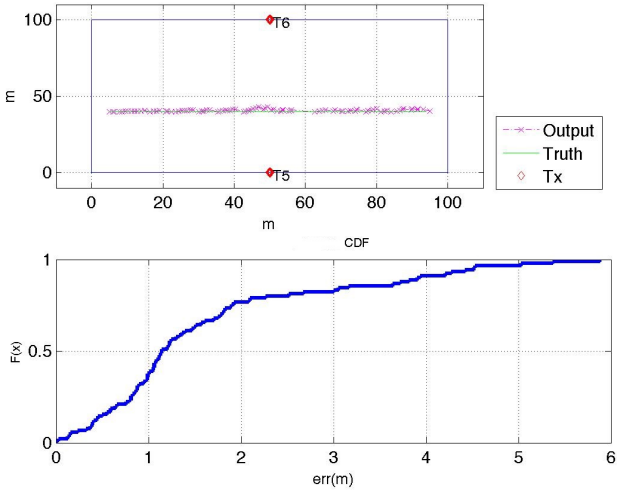

(d) ARCP (Tx5,6 used)

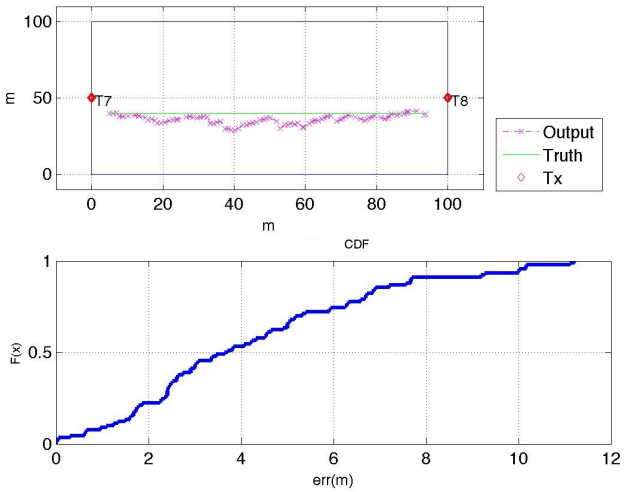

(e) CP (Tx7,8 used)

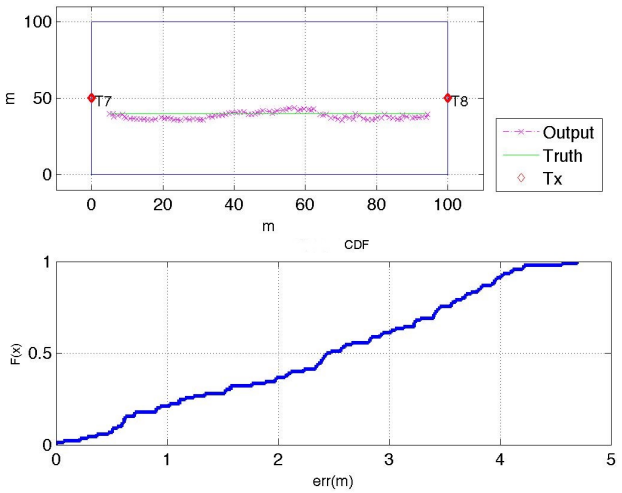

(f) ARCP (Tx7,8 used)

Figure 5.2: CP and ARCP Positioning Results using different Tx (Top plot of each subplot shows the trajectory, bottom plot shows the positoning error cdf)(Cont'd)

Four out of the six network combinations see improvement in positioning accuracy when ranging constraint is applied by CPF. The network consisting of Tx5 and 6, denoted as network Tx5,6, is a typical situation where the constraint pushed the positioning estimation further away from the truth due to the symmetry of the network, as in Figure 5.2c. In such cases, the positioning output fits into the constraint whether it follows the trajectory in the correct direction or goes the opposite direction. Without additional information, the system is unable to judge the correct direction. Hence as a combined result of the pull of the heading bias and the insufficient constraint, the relative constraint seems to be useless in constraining measurement error and drives the particles in the wrong direction.

For all network combinations, applying the adaptive ranging constraint improved the positioning performance. ARCP loosens the relative constraint when it learns that the network is not optimal. As a result, the particles are allowed to wander. Although errors are not well constrained at the beginning of the positioning phase, but the positioning estimation is eventually able to follow the right direction. Furthermore, the adaptive collaborative constraint is the most effective when the anchors are aligned with the direction of the bias.

In most collaborative situations, the rover positioning is improved the most when collaborative units lie on either sides of its trajectory. Figure 5.3 plots the positioning error cdf in both the East and North direction for network T1-2 when applying CPF and ARCP. As the bias direction pulls the positioning estimation towards north, thus it is natural that the position accuracy in the East direction is better, as indicated in Figure 5.3a. However, ARCP is able to constrain and improve the positioning in both directions, especially the North direction. As the anchors are perpendicular to the trajectory, one located on the northeast side of the trajectory and one located to the southeast, the error in the North direction is improved most effectively when constraint is applied adaptively.

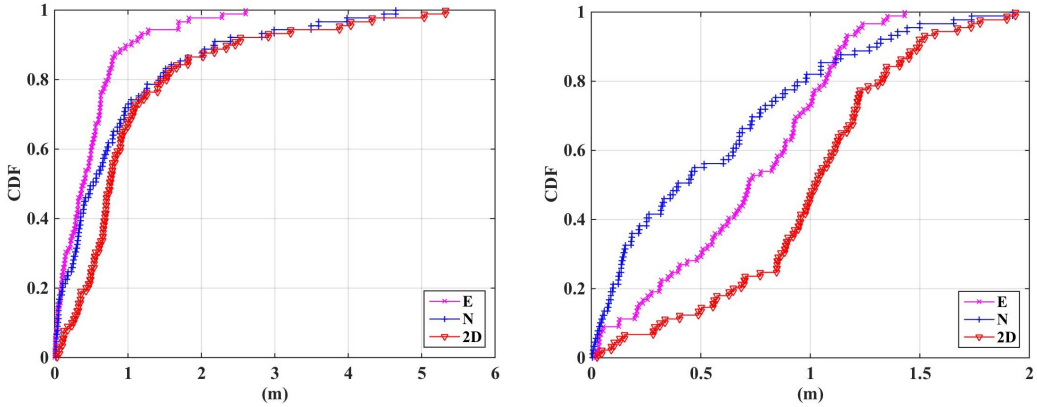

(a) CPF error cdf (b) ARCP error cdf

Figure 5.3: Ranging constraint in East and North directions for collaborative positioning with non-adaptive and adaptive ranging

5.3.2 Selective adaptive range constraint collaborative positioning (SARCP)

Many indoor environments are usually filled with a number of fixed wireless signal transmitters (the anchors) and moving users (the rovers). During the positioning phase of each rover, the problem becomes a question of which anchors and rovers should be included in the positioning network and which should be neglected. The application of a multi-rover-anchor collaborative positioning network is discussed here. Based on the MDOP of each different network formed by different units, the appropriate units are selected to output the optimal positioning results with high computation efficiency while ensuring system performance robustness throughout the whole positioning process. The robustness of the system ensures that positioning is not interrupted as the available units in the environment and the relative geometry change.

The selective adaptive range constraint collaborative positioning (SARCP) is applied to tackle situations where the rovers are required to make a decision on which units to include in the collaborative positioning network when sufficient units, i.e. more than four units (including rovers and anchors), are available. In such cases, the estimated accuracy level of the ranging measurement from each unit is obtained. Units whose ranging measurement accuracy coefficient a is larger than 0.5 are considered as potential units. As the effective network size is identified as four, potential units are combined with the current rover to form a network of four units in total to obtain the optimal units and the MDOP of each network is com-

puted. The relative positions of the units are also considered by sharing the position of the anchors and the estimated position of the other rovers. The network with the smallest MDOP value and most spread out units is selected as the optimal network. The relative constraint threshold $thres_r$ for each ranging measurement is set according to the smallest MDOP value, which reflects both the ranging quality indicator (RQI) and DOP. If less than four units are available, the units would simply be included in the collaborative network and $thres_r$ set according to MDOP. The procedure of SARCP is plotted in Figure 5.4.

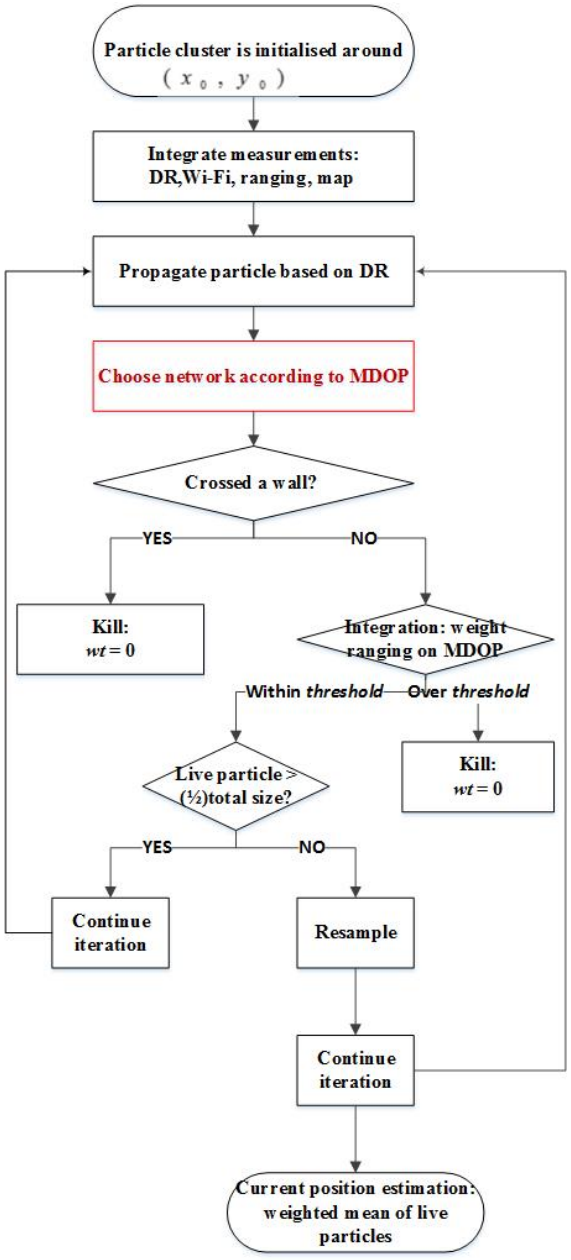

Figure 5.4: Flowchart of SARCP

To evaluate the performance of SARCP when a number of units are around, a network of three rovers and two anchors is simulated in the square area providing a number of different network combinations. The locations of the two anchors, Tx1 and Tx2, are given beforehand. All three rovers, Rx1, Rx2 and Rx3, positions are unknown and move along three simulated trajectories. For Rover 1, three networks could be formed from the units if we set the network size to three, i.e. Rx1-Rx2-Rx3, Rx1-Rx2-Tx1 and Rx1-Rx2-Tx2. During the positioning phase, Rx1 selects the optimal network for collaborative positioning by computing the MDOP of each possible combination. The HDOP is computed at each epoch and plotted in Figure 5.5a. ARCP is then applied where the ranging constraint boundary is adjusted based on the DOP value. The positioning error cdf of Rover 1 is plotted in Figure 5.5.

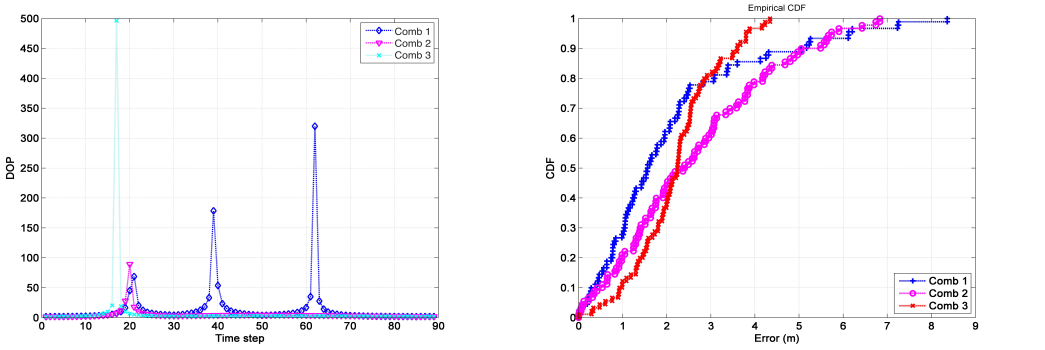

(a) DOP of the three networks

(b) Positioning error for Rover 1 based on ARCP

Figure 5.5: DOP for three different collaborative positioning networks and the corresponding positioning error cdf

Figure 5.6 plots the positioning result of SARCP and the corresponding positioning error for each rover. During positioning, each rover selects its own network at each epoch consisting the units which result in the lowest MDOP. As a network size of three or four is the most optimal size, here we keep the network size within three, consisting the rover itself and two other units. For comparison, CPF is also applied where all units are integrated to provide collaborative positioning regardless of actual ranging measurement quality or network geometry.

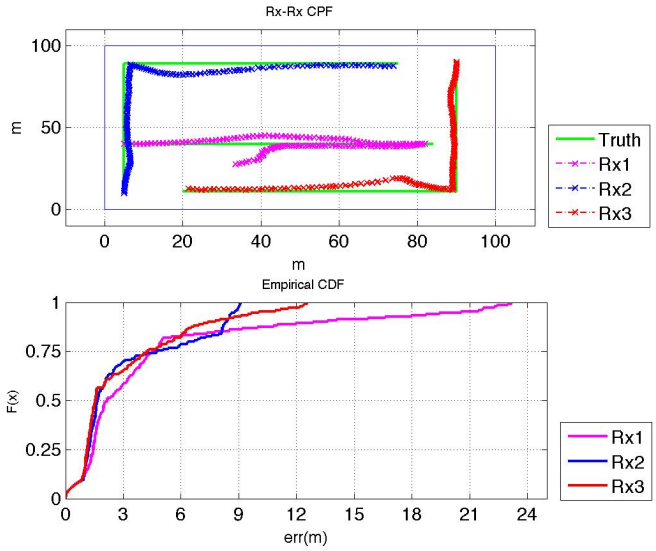

(a) CPF result

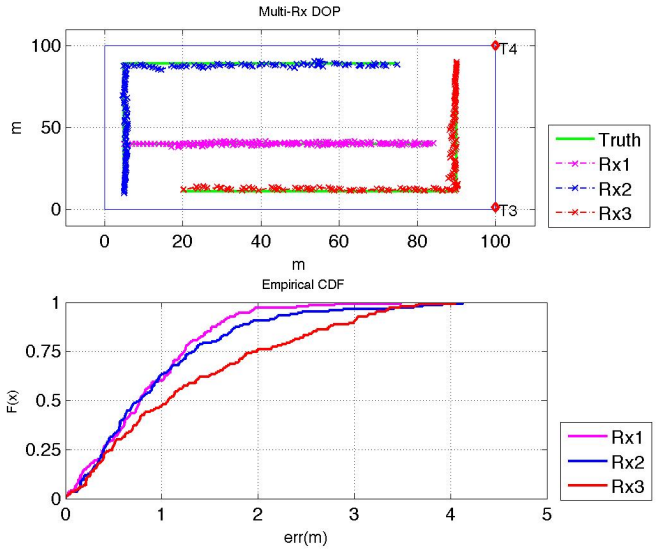

(b) SARCP result

Figure 5.6: Positioning result for network Rx1-2-3/Tx3-4 (Top plot of each subplot shows the trajectory, bottom plot shows the positioning error cdf)

Comparing the positioning error of SARCP and the basic CPF method, results indicate that positioning accuracy is increased by 60%. The positioning accuracy for Rx1 improves by 45% compared to the ARCP positioning results shown in Figure 5.5.

5.4 Simulations

A collaborative positioning scenario of two rovers is simulated in NGB, University of Nottingham, to test the performance of adaptive ranging collaborative positioning with a combination of real data and simulated

data. The low-cost MicroStrain 3DM-GX3®-25 IMU is worn on the users' foot to collect inertial measurements. Raw data from the MicroStrain foot-tracker is logged in a binary file which is then processed through a Matlab script to extract the inertial measurements while applying ZUPT corrections as well. ZUPT helps to correct the velocity and restrict position and sensor errors through consecutive step detection and process through Kalman filter. However, while the IMU roll and pitch can be obtained by comparing to the local gravity vector, ZUPT is unable to estimate yaw error (primary cause of heading drift). Therefore ZUPT cannot eliminate heading drifts and external heading measurements must be provided. Figure 5.8 shows the inertial data output from Rover 1 after applying ZUPT. The first 120 seconds of the data from Rover 1 is extracted to integrate with the data collected from Rover 2 through SARCP. The heading at the beginning of each step and the time when each step is taken is extracted to perform PDR.

(a) Building foyer (b) Corridors

Figure 5.7: Nottingham Geospatial Building indoor environment

Three anchors are simulated at three different locations inside the building to provide extra ranging constraint. The ranging measurements between the rovers and anchors are simulated with a noise level that changes with the number of walls observed in between the pair of units, i.e. the variance of measurement noise is smaller when the two rovers are in LOS of each other and larger when there is obstruction. The interior building map of NGB Floor A was surveyed by a Leica TS30 robotic total station and loaded into Matlab as polygons (representing rooms and polygons) and points (representing doors), shown as the background layout in Figure 5.8.

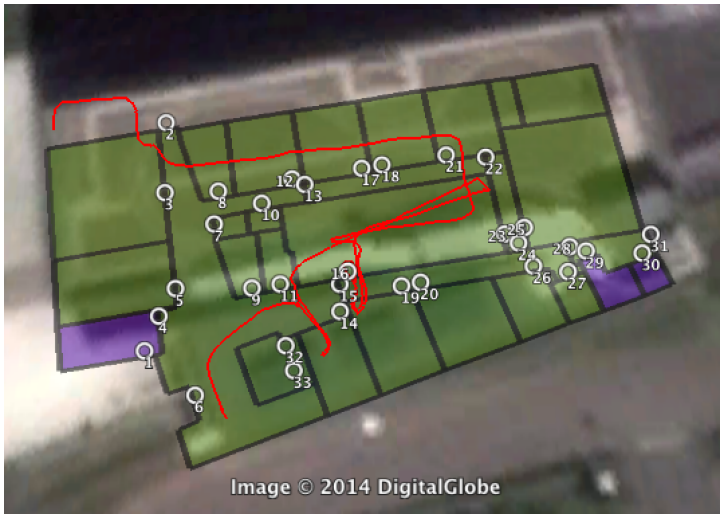

Figure 5.8: Raw IMU output with ZUPT

The IMU data for the two rovers are first processed only through PDR. Results are plotted in dark blue and cyan line in Figure 5.9. The green line indicates the true trajectory. Although wall constraint can restrict particles from passing through walls and reduce bias from doing so. But due to the amount of noise and error in the raw heading measurement, particles can be driven to the wrong room easily and the wall constraint will no longer be useful is the particles are in the wrong room.

The basic CPF algorithm is then applied to the same set of data. Ranging measurements are integrated between the units at each epoch. However, a constant constraint threshold is applied thus it does not change with the varying ranging accuracy. Therefore, particles representing the rover state can be constrained into the wrong distance when the ranging accuracy level does not agree with constraint threshold. Figure 5.9 plots the CPF results for the two rovers, where the green solid line indicates the ground truth, the circle dot line indicates the PDR results for both rovers and the cross dot line indicates the CPF outputs. The positioning results improves for Rover 1 when CPF is applied. However, not much improvement can be seen in Rover 2's results. This is due to that Rover 2's trajectory is fairly simple as it is a straight line along the same direction of the corridor it is in. While the inertial heading bias pushes the positioning estimation to be biased so that it seems like it is turning left, the wall constraint is applied in the particle filtering of PDR to restrict inertial errors from increasing. As we can see, the effect of wall constraint is greatly related to the geometry of the walls and the pedestrian's trajectory. For Rover 1, the wall constraint was not as useful.

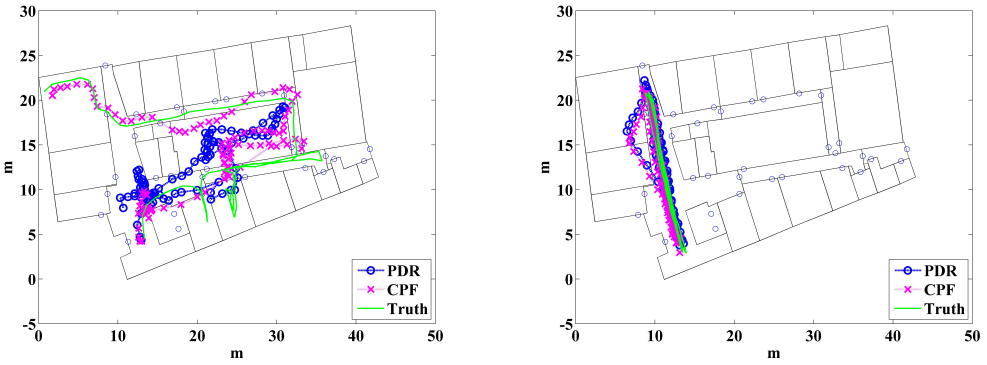

(a) Rover 1 (b) Rover 2

Figure 5.9: Positioning result from PDR and non-adaptive collaborative positioning (CPF) for two rovers

The performance of ARCP is evaluated by integrating the measurement data from one of the three anchors, Tx1, Tx2 and Tx3, respectively to form three different networks with the two rovers. As each anchor is located in relatively different places, their effects on the collaborative network are also quite different. The positioning results of each network is shown in Figure 5.10. Tx1 is placed on the east-side of the building and its signal to Rover 2 is directed in such a way that it is able to restrict the inertial heading bias of Rover 2. Therefore Rover 2's positioning estimation is greatly improved. But the geometry of Rover 1's trajectory is much more complicated with more heading changes and the measurements from Tx1 cannot fully eliminate the errors hence a large part of Rover 2's positioning estimation remains biased. On the other hand, Tx3 is located to the north of Rover 1's trajectory. Due to the relative position of the units and the direction of the trajectory, Tx3 corrects most of Rover 1's measurement error. However its corrections on Rover 2 is rather limited. Tx2 performs better constraint on both rovers as its relative position to both rovers is along the direction of the bias hence eliminates the heading bias. The average positioning error of each network is given in each plot. Results show that ARCP can improve positioning by adjusting the ranging constraint threshold. However, rovers at different positions requires constraint from anchors at different locations, e.g. Tx1 is more suitable for constraining the error of Rover 2 while the network formed by Tx3 is better for Rover1. Yet ARCP can only integrate all that is available and does not have the freedom to choose appropriate units for a better network.

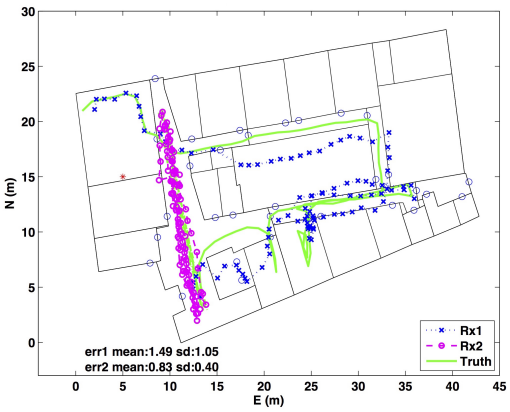

(a) Network with Tx1

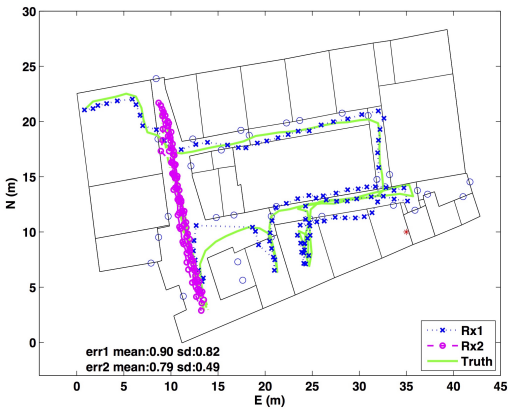

(b) Network with Tx2

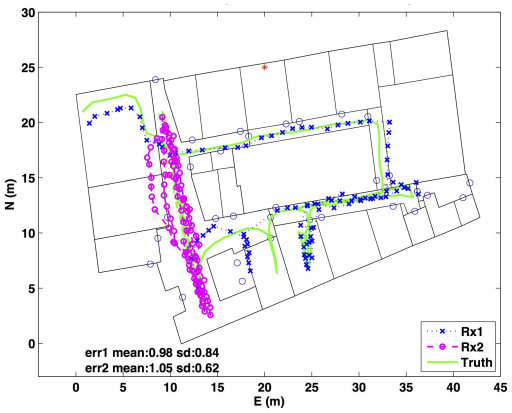

(c) Network with Tx3

Figure 5.10: Different anchors applied in positioning network for ARCP

The network consisting of all three anchors and the two rovers is processed through SARCP with wall constraint to achieve positioning results. By applying SARCP, each rover will have the freedom of choosing a suitable network independently. At each epoch, each rover integrates ranging between the other rover as well as one of the anchors to form a collaborative network. The selected anchor should produce the minimum MDOP for the current epoch. Particles are also constrained by the ranging measurement with an adaptive threshold that is adjusted according to the measurement accuracy. Therefore when a low accuracy measurement is obtained, a larger threshold will be applied and particles will be less likely to get killed. Results are shown in Figure 5.11, where the green line indicates the ground truth, the cross dot line represents the mean position of Rover 1 and circle dash line represents the mean position of Rover 2.

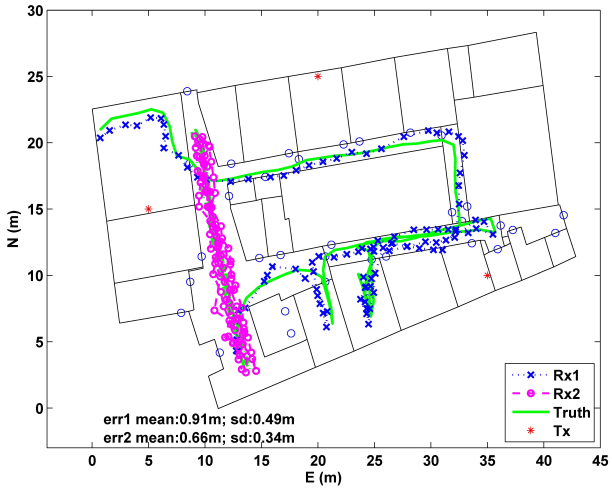

Figure 5.11: Positioning result of SARCP (Network: Rx1,2 and Tx1,2,3)

Finally, in the last scenario, the SARCP is applied to the positioning network without the building map information. Therefore, the particles can cross walls and is no longer limited to move along the direction of walls inside the building as they no longer have information on where the walls and rooms are. In this case, the inertial measurement error is bounded only by the ranging constraint. Results are shown in Figure 5.12.

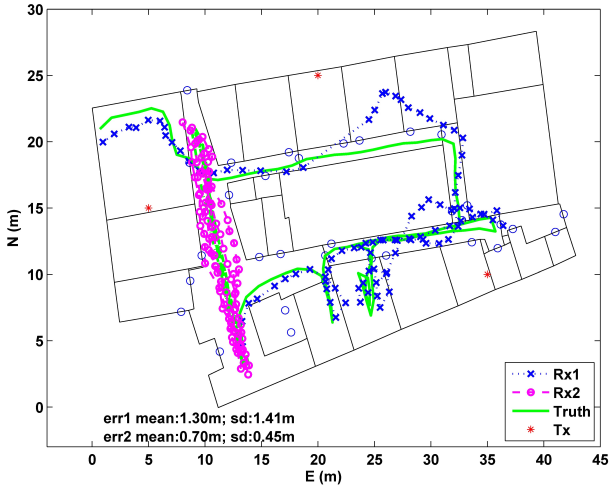

Figure 5.12: Positioning result of SARCP without map matching (Network: Rx1,2 and Tx1,2,3)

The positioning error which is the distance between the estimated position and the true position is obtained for each set of results. Table 5.1 lists the mean of the errors as well as the observed maximum error throughout the whole trajectory for each different algorithm. The mean positioning accuracy is improved by more than 60% for both rovers when

SARCP is applied, regardless of applying the wall constraint or not. Although it seems that the PDR error for Rover 1 is smaller than the CPF result, but it does not indicate a better positioning result here as both results are in a completely wrong place. SARCP provides the system with better adaptiveness to the different ranging measurements. As a result, the positioning system is more robust as it can deal with both high and poor quality ranging measurements. Regardless of ranging situations, the state estimation will not be driven to the wrong location due to the wrong constraint. With confident ranging constraint, the wall information can also be discarded, just as Wi-Fi fingerprinting, which we have not applied at all here. In a sense, all infrastructure-based positioning methods can be neglected when collaborative ranging is integrated between units within a local network.

Table 5.1: Positioning error for simulation trials (NGB) (m)

	PDR		CPF		SARCP (wall)		SARCP (no wall)	
	mean	max	mean	max	mean	max	mean	max
Rover 1	2.95	7.87	3.27	6.25	1.17	2.83	1.18	3.12
Rover 2	8.95	12.94	2.37	6.40	0.71	1.71	0.70	2.24

5.5 Collaborative Wi-Fi fingerprint training

With the positioning accuracy achieved from ARCP and SARCP, any mobile system with some kind of inertial measurement and ranging sensor would be able to achieve accurate positioning in an indoor environment. However, indoor environments are complicated and prone to change unpredictably. Therefore, to maintain robustness, the positioning system should be able to adapt to the changing situation, e.g. availability of signals, sensors and collaborative units. Although collaborative positioning can be performed without Wi-Fi signals, but as Wi-Fi signal is one the most popular and widely available signal inside buildings, the fingerprint database should be maintained so that continuous positioning can be provided when collaborative units are not available.

Conventional Wi-Fi fingerprint database training is a very time and effort consuming task. Furthermore, it is an on-going task where fingerprint information needs to be updated frequently to maintain positioning reliability and accuracy, especially when known modification to the hardware or building has taken place. To reduce the time and human labour required for training, GPR was applied in Chapter 3 which reduces the training time by decreasing TPs and then generating denser fingerprints by machine

learning the RSS pattern.

Simultaneous localisation and mapping (SLAM) has been applied in a variety of tracking and navigation applications which the system learns and constructs a map of the the surrounding environment based on the observed signal pattern, location information during its positioning phase, hence positioning data is updated so further positioning is more accurate (Ferris et al., 2006; Faragher and Harle, 2013). SLAM was originally applied in robotic navigation where robots learn the relative environmental features during navigation and enable quicker and more accurate positioning as the process carries on (Dissanayake et al., 2001). It allows the system to navigate in a new environment with no *a prior* knowledge of the environment. Features could also be learned with respect to available maps. Wi-Fi SLAM enables the system to learn the pattern of Wi-Fi RSS throughout the building while tracking the user.

A vital information for fingerprint-based positioning is that the position associated with each RSS fingerprint has to be accurate, as it is the fundamental reference for positioning. Any bias in the fingerprint position would result in a biased final positioning result. Collaborative positioning improves user positioning accuracy and reliability by applying network constraints. A number of nearby users may form a network and ranging measurements are acquired between each pair of users within the network. Corrections are applied to adjust each user position until they all obey the relative ranging constraint.

A SLAM-like collaborative Wi-Fi fingerprint database training (c-WiDB) approach is introduced here to enable a quicker and more reliable Wi-Fi fingerprint training process. A network of mobile users that are in the same indoor environment achieves positioning estimations through applying the inertial measurements obtained from mobile devices to a PDR model. The PDR solutions of the users are constrained by relative ranging measurements among each other, which reduce the inertial measurements error and biases, improving the positioning accuracy significantly (Chan et al., 2006). Meanwhile, each user collects its observed Wi-Fi RSS and stores the measurement associated with a positioning estimation. GPR is then carried out to generate fingerprints for the whole indoor environment based on the collected data. Positioning accuracy, robustness and flexibility is greatly improved through collaborative positioning, as users have the option of performing PDR, collaborative ranging or Wi-Fi based positioning based on available information and number of users.

Fingerprint positioning is achieved by searching through a database and finding the location of the fingerprint that is most similar to the current RSS vector. Therefore, the fingerprints should cover the floor plan in more detail to achieve more accurate positioning results, i.e. dense TPs increase accuracy. Yet in reality, it is almost impossible to cover the entire floor plan in high density. A common way of selecting TPs is to divide the area into small square grids. The RSS data is collected within each grid and an assumption is made that the RSS is the same within the grid, hence one fingerprint for each grid. Typical grid sizes are 1m$\times$1m, 2m$\times$2m (Liu et al., 2014). Smaller grids generate a more detailed database. However it will be more time consuming. Another way of training the database is to collect data at various selected TPs and apply GPR to generate the fingerprints for each grid of the entire floor plan as described in Chapter 3.

Further collaborative database training will be discussed in this section. Eight Cisco 1142 Series APs with internal omni-directional antenna are located inside the NGB (four on Floor A and two on Floor B and C), as shown in Figure 5.13. Each AP transmits signals in both the 2.4GHz (802.11b/g/n) and 5GHz frequency (802.11a/n) (Convergis and Logicalis, 2011). Radio power is set to auto so that capacity can be adjusted to match traffic patterns in the network, which maximises network coverage and avoid data congestion. Power is normally kept low to gain extra capacity and reduce interference. Radio Resource Management (RRM) provides real time management of the RF controller balance the transmit power by reducing power with the transmit power control algorithm or increase power if a failed AP is detected by the coverage hole detection algorithm. RRM periodically performs radio resource monitoring, transmit power control, dynamic channel assignment and coverage hole detection to improve network efficiency (Cisco Systems, Inc, 2013). As a result, the Wi-Fi signal environment can change and fingerprints may vary over time. Therefore, the fingerprint database should be updated frequently to indicate the most current RSS measurement for different locations. As the signal characteristics are different on the two frequencies, the different frequencies will be treated separately. Hence a full database consists of 16 MAC address groups, each denoted as AP1a - 8a and AP1b - 8b respectively, where *a* indicates the 2.4GHz signal and *b* indicates the 5GHz signal.

Figure 5.13: A Cisco wireless access point located in NGB

5.5.1 Static database density

To examine the database training quality based on different TP density in different environments, a number of different fingerprint databases are generated for Floor A by adjusting the number and location of the TPs. First of all, the total number of TPs throughout the training area is reduced to generate the database and the RSS difference between each database is compared. For a total number of 112 TPs on Floor A, the density is regarded as 1. The density is then reduced to 0.85, 0.5, 0.4, 0.2 and 0.1 respectively. The difference between the RSS of the fingerprints from the GPR generated database and the RSS of the TPs that are within 2m distance of each other are listed in Table 5.2a.

The density is also compared in two different rooms, R1 is a small meeting room with very little obstruction and R2 is the store room with metal shelves. In the set of TPs which generated s-DB described in Chapter 3, four TPs were located in each room. A regional GPR database is generated for each room based on the four TPs so that the resulting database resolution is 1m. A further 56 TPs is selected and trained, 32 TPs located in R1 and 24 TPs in R2, where TPs are 1m apart. Thus the second training density is the same as the GPR generated database. The average difference of the RSS between the high density TP database and the GPR generated databases for each AP is listed in Table 5.2b. An indication of the difference is also plotted in Figure 5.14. Results show that the RSS difference in R1 is quite small, hence density does not affect the quality of the database for R1, which has less obstructions. The database quality for R2 is much worse due to metal shelves inside the room. Therefore, we can assume that in a less obstructed region, the number of TPs can be reduced to minimise the training effort. Furthermore, 5GHz gives relatively better performance in both environments. The histogram of the RSS difference for the two rooms

are plotted in Figure 5.14 and we can see that the bars are more clustered towards 0 in the plot for R1, whereas the bars are more spread out in the plot for R2.

Table 5.2: ΔRSS of different density (dB)

(a) Different density level (dB)

	0.85	0.5	0.4	0.2	0.1
ΔRSS	4.91	4.59	4.95	6.28	5.44

(b) ΔRSS between fingerprints in R1 and R2 (dB)

	AP1		AP2		AP3		AP4	
	a	b	a	b	a	b	a	b
R1	3.24	2.01	2.66	3.15	1.27	2.18	2.65	2.12
R2	3.64	4.98	7.74	4.03	7.05	5.08	10.94	3.77
	AP5		AP6		AP7		AP8	
	a	b	a	b	a	b	a	b
R1	3.19	2.78	2.57	1.67	1.77	3.34	8.92	2.97
R2	8.00	7.65	6.80	4.89	17.68	12.62	8.16	5.89

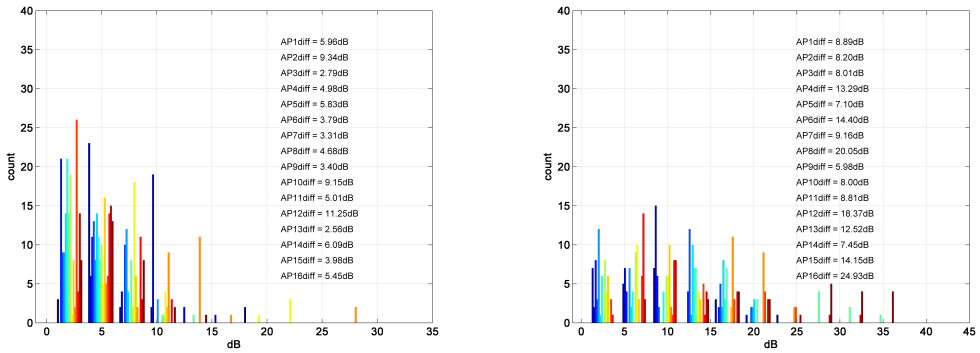

(a) R1 (b) R2

Figure 5.14: ΔRSS between fingerprints generated from GPR and the training data at TPs for two rooms

5.5.2 Dynamic database

5.5.2.1 Training the fingerprints

As c-WiDB builds a dynamic relationship between the RSS of the mobile receiver and its estimated location while the receiver is moving, collaborative positioning is applied to achieve accurate localisation. The ARCP/SARCP is applied to provide positioning for each receiver and train for the Wi-Fi fingerprints simultaneously through multiple users. The signal measurement

noise is assumed to be normally distributed with zero mean.

c-WiDB not only reduces the training effort by providing training during the positioning phase, but RSS is also collected from a number of rovers where all the available information can be integrated into one system. The c-WiDB method gathers the Wi-Fi RSS data during the collaborative positioning phase and stores them as training data. Initially, one set of RSS vector is required for a training area. This data can be used to generate an initial fingerprint database through GPR for areas where training data is available. The GPR predicted value will be used as the fingerprint RSS for each location. As more data is collected by the users, the database can be regenerated and updated from new training data.

However, signal strength fluctuation means that the signal strength could vary over a range of 5dB to 10dB or more at any single location even when the receiver is static. Therefore, a single RSS vector for one training location is barely sufficient for fingerprint training. Furthermore, the receiver is constantly moving during the dynamic training process and because the Wi-Fi scanning rate is slower than the average walking pace, a data "smearing" effect may be observed as the RSS might actually be the signal strength at a previous location but time-tagged to a later time. This will increase uncertainty in the training data hence the dynamic data is always collected for a training area rather than a training point. While ARCP/SARCP builds a link between the collected RSS data through ranging measurements, the training data from different receivers can be combined and applied in three different ways.

If the distance between the two users is above a separation threshold, it would be regarded that the users are not in the same area of interest. Their training data would be stored separately and used to generate individual fingerprint databases or individual parts of the same database. If their distance is within the separation threshold but above the integration threshold, their training data would be considered to be within the same area of interest, but not the same location. These data would be sorted into one set of training data for GPR and used to generate the same database.

Any training data distance that are within the integration threshold would be regarded as correlated data and combined to form one fingerprint for the database. If these data are not collected simultaneously, their time-tag would also be stored in a history database to provide information on signal change over a period of time. If the time difference is fairly small, e.g. seconds or minutes, the change in the signal strength would be regards

as short term signal fluctuation and the signal change would be regarded as the fluctuation variance. If the change is observed extends over days or even longer, it would be regarded that the change is reflecting a change of the hardware or surrounding environment.

The standard deviation of all the history training data σ_{nm} that are within the integration threshold is obtained periodically and acts as a confidence indicator for the fingerprints at the specific location. If the training RSS for any location appears to continuously differ from historical data and σ_{nm} remains above 3, it is considered that the Wi-Fi properties at that location have changed. Previous fingerprints will no longer be reliable and valid information for positioning, hence fingerprints will be replaced by new fingerprints generated from new training data. On the other hand, if the σ_{nm} is high but the RSS fluctuates around the same mean value, we will simply assume that the signal tends to be noisy at the specified location.

While the collaborative users are spread out in various different locations within the same region, the fingerprint database can be generated fairly quickly. The confidence factor for historic fingerprints will be updated based on new data. The procedure is shown in Figure 5.15.

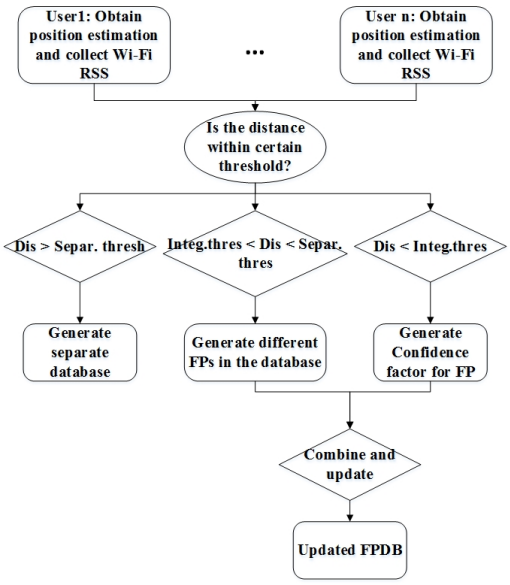

Figure 5.15: Collaborative Wi-Fi fingerprint database generation flowchart

Four different trajectories, denoted as T1, T2, T3 and T4, of varying length and located at different places on Floor A are chosen as the training trajectory where training data will be collected during the collaborative positioning phase. Users follow each of the different routes respectively

and collect RSS data using a laptop. GP is then applied to generate a fingerprint database based on the training data, which will be referred to as the dynamic database (d-DB), denoted as d-DB1a, d-DB1b, d-DB2 and d-DB3 respectively for each trajectory. For experimental purposes, the training data will always be within the separation threshold so that they can be applied to generate one database.

The RSS of the dynamic TPs along the trajectory is compared to the RSS of the static TPs from Chapter 3 that are within a certain distance. The mean and standard deviation of the ΔRSS for TPs that are separated by 1m to 4m are listed in Table 5.3. Signal acquisition is less stable while the receiver is moving and more disturbance occurs from the user himself. On the other hand, the update frequency of the Wi-Fi RSS collection software is relatively low compared to the human walking pace, so there are data gaps in the logged data where there is positioning information but no RSS data. Therefore it can be anticipated that the dynamic training data is noisier. The ΔRSS between TPs up to 3m apart is within 15dB, which is actually within the RSS fluctuation range itself. Once the distance is over 4m, the variance drops and correlation fails, which was also observed between the GPR generated RSS and the RSS of the TPs.

Table 5.3: ΔRSS between dynamic and static training data at TPs (dB)

	1m	2m	3m	4m
ΔRSS	9.85	12.55	13.39	19.36
σ	10.61	10.49	15.91	8.58

Figure 5.16 plots the RSS from AP4 collected along four different training trajectories where the colours specify the actual RSS of the collected data. Red indicates high RSS (with the highest of -30dB) and blue indicates low RSS (with the lowest of -100dB). The full collection of RSS data from AP4, AP5, AP6 and AP7 is plotted in Appendix A.2 for all four d-DBs. These four APs were selected as they are located on Floor A and more signal strength variation could be seen amongst the received data.

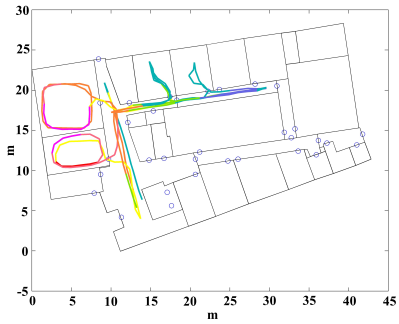

(a) d-DB1a AP4a

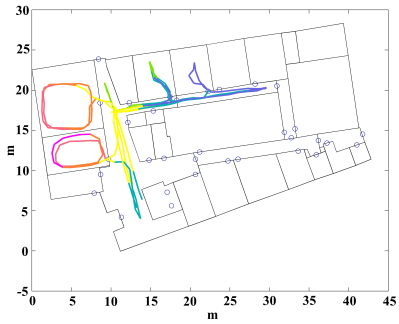

(b) AP4b

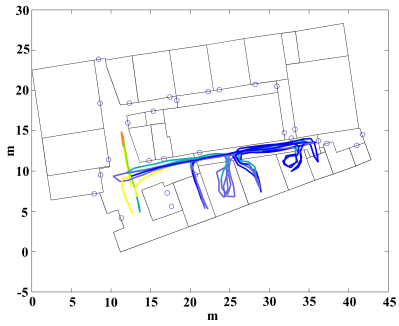

(c) dDB1b AP4a

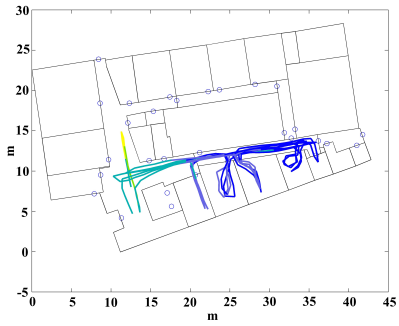

(d) AP4b

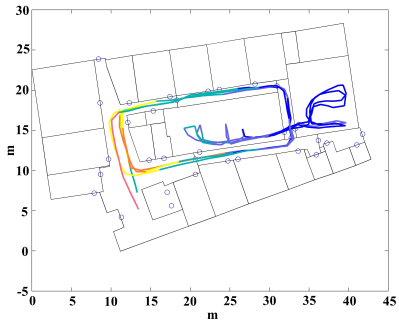

(e) dDB2 AP4a

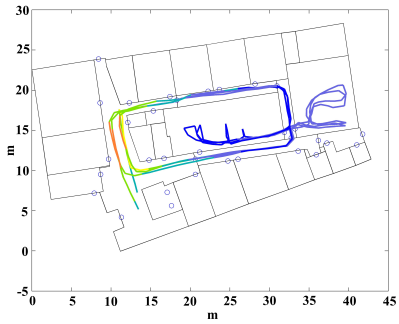

(f) AP4b

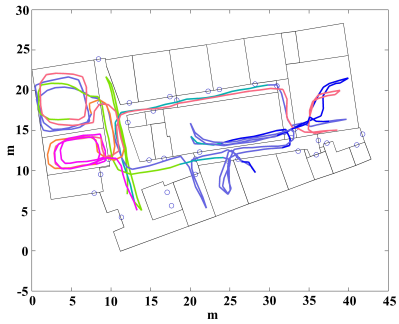

(g) dDB3 AP4a

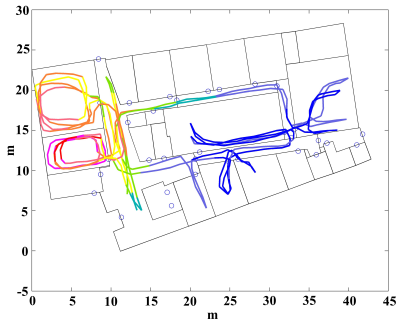

(h) AP4b

Figure 5.16: Training data for each d-DB from AP4 (a indicating 2.4GHz signal, b indicating 5GHz signal)

Due to signal fluctuation, collecting one RSS for each AP during training is insufficient as the single value is always just a random value out of a distribution of RSS with a certain noise level. To generate better knowledge of the RSS distribution at each location, it has to be modelled from collecting a large number of RSS. This is why conventional training requires the receiver to collect RSS data over a long period of time and the standard deviation is sometimes used as an indication of signal fluctuation. However, during dynamic training, it is only possible to collect one RSS data at each location from one rover. This potentially causes a bias in the final database as the signal fluctuation is not taken into account.

Another problem in dynamic training is that the signal from some APs are very weak and unstable at certain locations, e.g. AP1b, whereas no data could be collected during the training period, resulting in a fingerprint vector such as $\{(x_n, y_n)|RSS_{n1}, \sigma_{n1}, AP_1, Null, AP_2, ..., Null, AP_m\}$. In such cases, the empty RSS vectors are set to -100dB. A large amount of empty data at a certain location indicates unstable signal which is usually caused by too much disturbance in between or the AP being too far away, thus should best be ignored during the positioning phase. As we rarely collect -100dB RSS data, therefore any -100dB data will not be taken into account during positioning.

From the training data, we can see that although 5GHz signals appear to be weaker as they are less likely to penetrate walls, but it is actually due to this less penetrable characteristic they are able to reflect the signal strength more accurately throughout the building with respect to each AP. On the other hand, 2.4GHz signals are much better at penetrating obstructions. Due to this, we can see 2.4GHz signals "leak" out of a room unexpectedly. This in result makes the signal noisier and could be misleading during the positioning phase. As shown in Figure 5.16, the training data for d-DB3 from AP4a in one of the rooms varied as much as 30dB.

Figure 5.17 shows the RSS difference between d-DB1a and s-DB for AP4 and AP7 in both the 2.4GHz and 5GHz frequency. Locations that are outside the region covered by the dynamic training data as shown in Figure 5.16 can be ignored. We can see that the RSS from the two training methods are very close. However, signal fluctuation and other disturbances cause the RSS to differ in some areas and interestingly, especially in places nearer to the AP. Furthermore, the difference between the 5GHz signal database is also smaller.

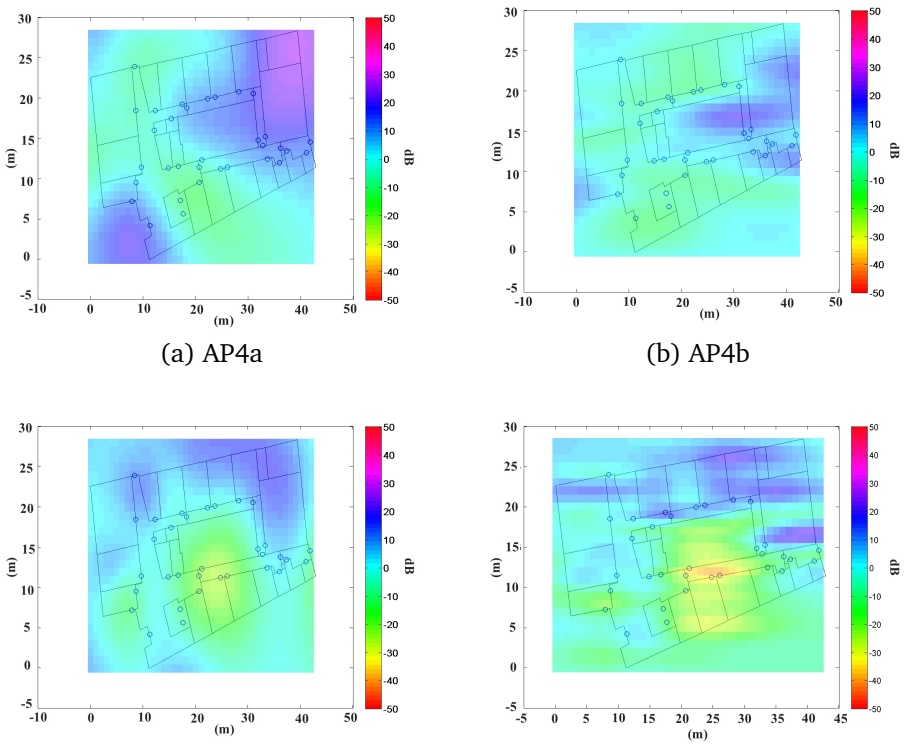

(a) AP4a (b) AP4b

(c) AP7a (d) AP7b

Figure 5.17: Examples of ΔRSS between d-DB and s-DB for dDB1a

To improve the data quality of the dynamic trained database, training data from different paths are integrated collaboratively. This enables the combination of data collected at different locations and also at different periods, denoted as c-DB. c-DB generates the database from more data and longer time span. This in result captures the RSS fluctuation and environment disturbances.

Collaborative training greatly extends the training data coverage. For example, each of the training data, dDB1a and dDB1b, only covers half of the building plan, but would cover the entire floor plan when combined together. It also increases the quantity of RSS data for a small area of interest. Instead of computing the standard deviation of the RSS for one single TP as in the conventional method, a cluster of RSS data within the integration threshold is used to reflect one common location. Therefore, as more collaborative training data is collected, more RSS that are within the integration threshold can be found. This information can then be applied to derive the confidence indicator for a fingerprint vector regarding to a specific location.

5.5.2.2 Database results

To analyse the training quality of the dynamic database, the RSS differences between d-DB, c-DB and s-DB for the same positions are compared. First of all, the fingerprint locations and RSS that are covered by training points are extracted. The difference for AP4 and AP7 was plotted in Figure 5.17. The absolute value of ΔRSS between each d-DB and s-DB for all APs are plotted in Figure 5.18.

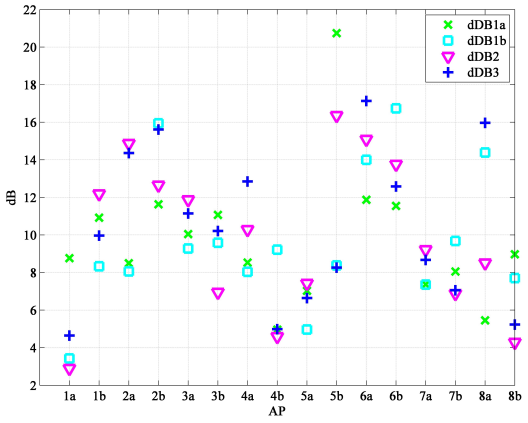

Figure 5.18: ΔRSS between s-DB and each d-DB for each AP and signal frequency

Although the database only covers Floor A, but four APs, i.e. AP1, AP2, AP3 and AP6, are located in four different locations on Floor B and C. Therefore, when data was collected on Floor A, the signal from those four APs pass through more obstructions, such as extra floor obstruction, is also experienced. For those APs that are not on the same floor as TPs, the 5GHz signal RSS difference is larger than the 2.4GHz signal. As 5GHz are less able to penetrate obstructions, thus when signals reach a different floor it would become very unstable and less easy to capture. However, for those APs that are on Floor A, AP4, 5, 7 and 8, the ΔRSS between d-DBs and s-DB is smaller for 5GHz signals.

All the selected TPs for d-DBs are located within Floor A of NGB, therefore lies within the separation threshold and could be combined to generate the same database. The training data for d-DB1a and d-DB1b are combined to generate c-DB1; d-DB1 (consisting d-DB1a and d-DB1b) and d-DB2 are combined to generate c-DB2; d-DB1, d-DB2 and d-DB3 are combined to generate c-DB3. Figure 5.19 plots the average ΔRSS between each c-DB and s-DB.

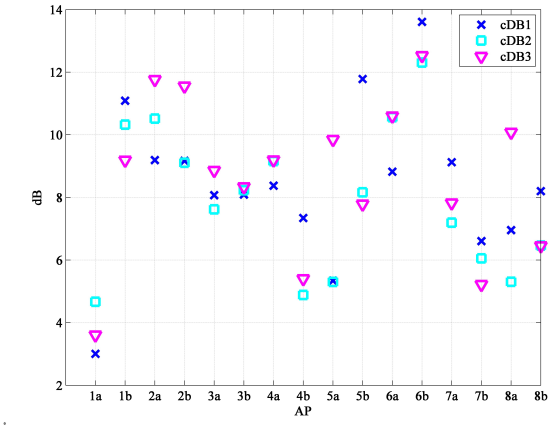

Figure 5.19: ΔRSS between s-DB and each c-DB for each AP

The overall ΔRSS is reduced when the training data from different path are combined. As an example, the ΔRSS between DB1a, DB1b, c-DB1 and sDB for AP5a is plotted in Figure 5.20. The area of the heatmap that is covered by blue grows from d-DB1a to c-DB1. Combining the training data extends the fingerprint coverage and produces fingerprints that agree better with the ground truth, s-DB.

Sometimes, users in a collaborative network may across each other's path and collect training data that lie within the integration threshold. This may happen at the same time when two users come cross each other, or separately when a user enter an area where previous data has already been collected by another user. Nevertheless, these data can be integrated to update the database and produce a confidence factor based on how much variance is seen in the signals. If data are collected within a short period, the variance will be regarded as signal fluctuation. However, if the timespan extends and the RSS difference between new data and history data remains a high level, the system should consider discarding the old data and update the database with new data only. As an example, the training data for d-DB3 are collected in two parts, P1 and P2. P1 consists of data collected during the first round of walking in the building and P2 is collected in the second round. The ΔRSS between the database generated from d-DB3 P1, d-DB3 P2 and s-DB is plotted in Figure 5.21a and 5.21b. Some RSS variance can be identified between the two data as there are changes in the difference pattern between each database.

Figure 5.21c shows the RSS difference between the database generated from the combination of P1 and P2, i.e. d-DB3, and s-DB. The combined database sees a smaller ΔRSS to s-DB. P2-P1 lists the difference between

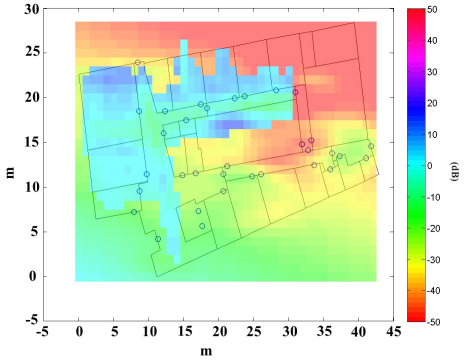

(a) d-DB1a and s-DB

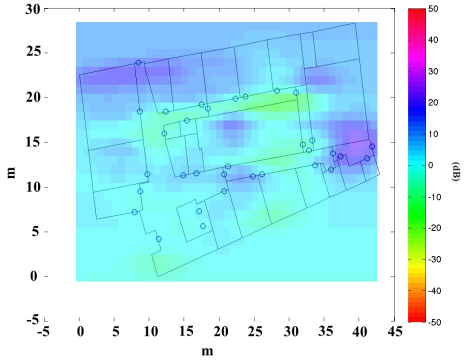

(b) d-DB1b and s-DB

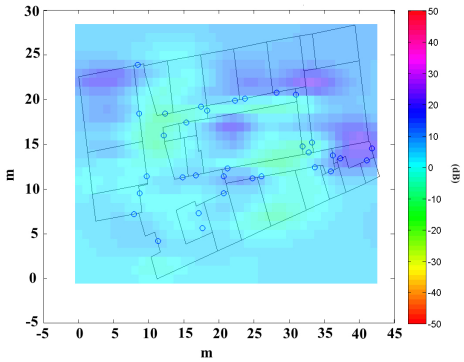

(c) c-DB1 and s-DB

Figure 5.20: ΔRSS between s-DB and d-DB1a, d-DB1b, c-DB1 (AP5a)

the database generated from P1 and P2. When the ΔRSS between P1 and P2 is small, e.g. AP4b, the combination of the two parts produce a database with a smaller difference to s-DB. On the other hand, when the ΔRSS between the two parts is around or over 10dB, e.g. AP8a, the ΔRSS between the combined database and s-DB is also very large.

5.5.3 Training data confidence factor

The comparison between the databases generated from different training data indicates that when the collection of RSS for one training area agrees with each other, the resulting database would be closer to the ground truth. Furthermore, the data collected from different rovers at different locations can be combined to generate the same database. By integrating training data from multiple users, the time and labour for fingerprint database training is greatly reduced. However, as signals are collected dynamically, more instability is brought into the data. To give users more confidence when applying the database for fingerprinting, the system should identify the quality of the generated database and the confidence in the fingerprint

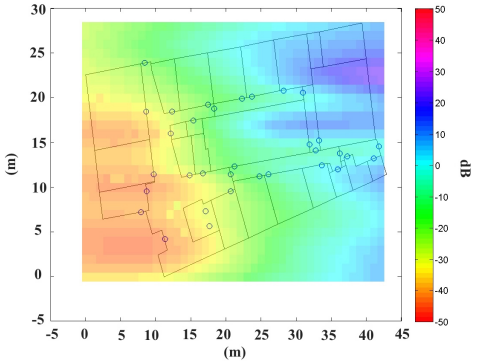

(a) d-DB3 p1 and s-DB

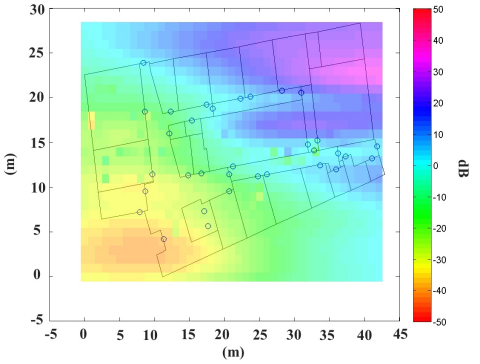

(b) d-DB3 p2 and s-DB

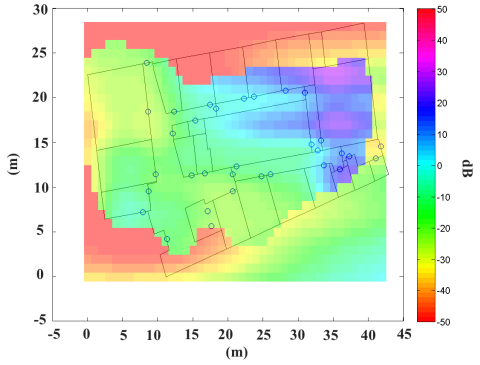

(c) d-DB3 and s-DB

Figure 5.21: ΔRSS between sDB and d-DB3 p1, p2 (AP8a)

data.

The variance of the signals is further analysed from the data collected during different periods. The static training data which was applied to generate s-DB were collected repeatedly within two months and each collection time lasted for at least 30 minutes, thus the database takes into account both short term and long-term signal variance. While short-term signal variance may occur either due to human interference or natural fluctuation, long-term variance may occur from the change in the hardware environment. Moreover, signals also tend to vary slightly at different times of the day (Wang et al., 2003). The static training data from two collection periods are extracted for comparison. Figure 5.23 shows the average ΔRSS for each AP at each TP as well as the average ΔRSS at each TP for each AP. Apart from random noise which can be seen across all APs and TPs, there is no obvious difference in the performance of different APs. There is no obvious noisy AP, but there is also no obvious clean data with no signal fluctuation. The ΔRSS at a few TPs is more obvious. Based on the characteristics of the collected data, we can see that the signal strength

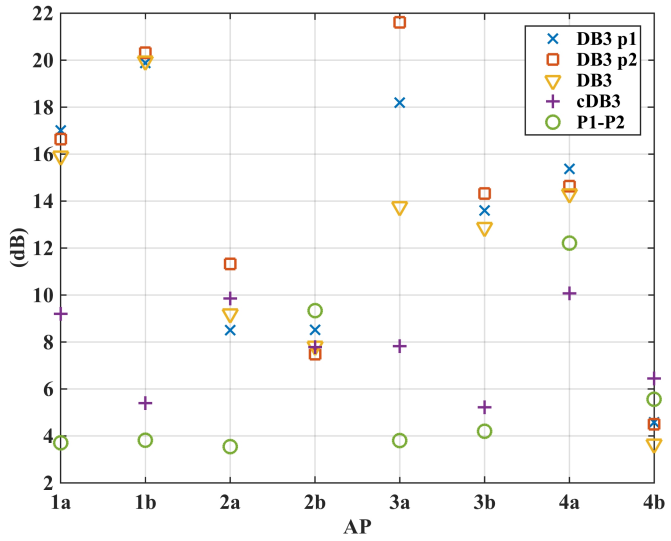

Figure 5.22: ΔRSS between: s-DB and d-DB3 p1, p2, d-DB3, cDB3; d-DB3 p1 and p2 (dB)

varies both temporally and spatially.

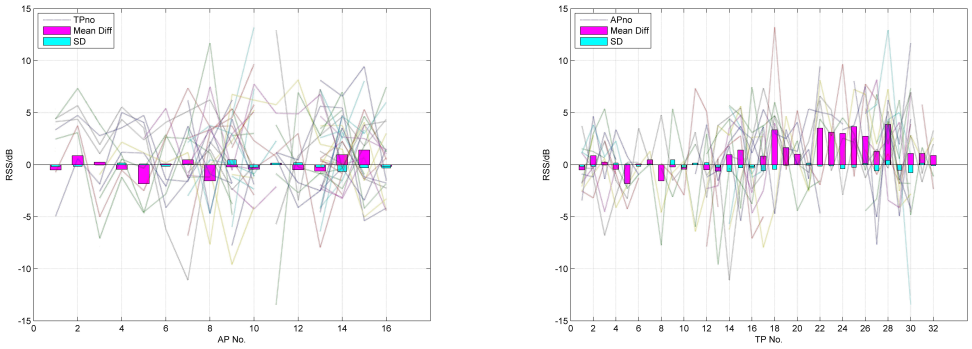

(a) Difference between APs

(b) Difference between TPs

Figure 5.23: ΔRSS between static training points for each AP

Other than signal fluctuation, additional noise is also brought into the dynamically collected data as there may be delays in extracting the collected RSS data in the receiver. Hence a possibility of bias between the actual collected location and the system recognised data logging location. Moreover, when users travel in different directions, the location of the body relative to the receiver and the AP will differ. This will also potentially cause further bias in RSS which again differs from the signal fluctuation seen in static data. Hence new RSS can be different to historical RSS when we return to the same location due to a number of reasons. Due these bias and variance, it is hard for the system to decide which training data

contains less noise. Yet whether the correct training data has been applied has a big influence on the accuracy of the generated database.

To further compare the signal variation over a period of time for dynamic data collection, two sets of training data, T1 and T2, were collected while following the same route inside NGB but at different periods. Two separate fingerprint databases are generated from T1 and T2. Due to the different noise captured over the collection period, the resulting database is not exactly the same. The ΔRSS between the two databases for AP4 and AP7 is computed and shown in Figure 5.24. A larger variation is seen in the 2.4GHz signal, and the 5GHz signal seems to be more stable over the collection period. This reflects that the 5GHz not only shows more stability throughout different locations, but also over a period of time.

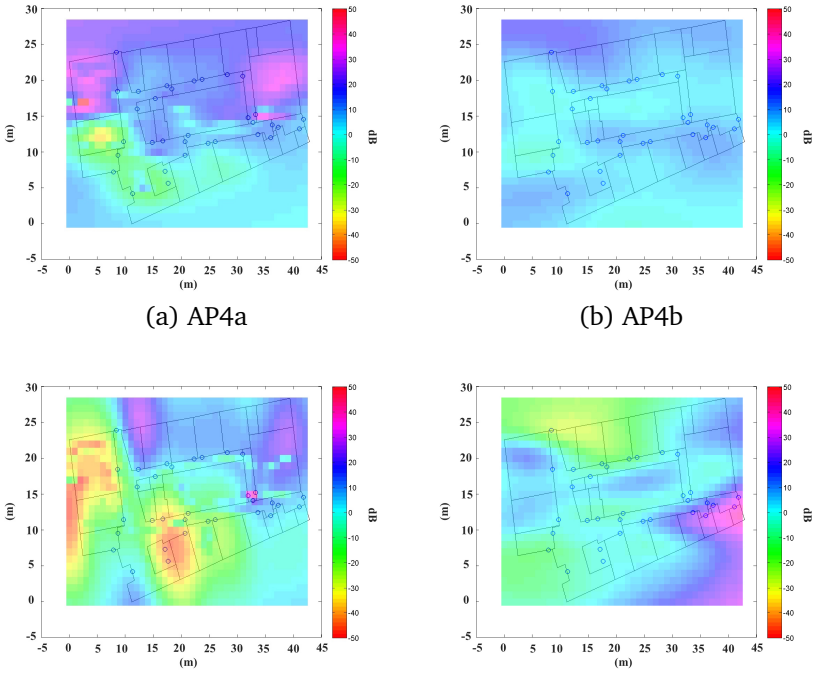

(a) AP4a (b) AP4b

(c) AP7a (d) AP7b

Figure 5.24: ΔRSS between fingerprints from different collection time

To select the appropriate training data from the large amount of datasets in a dynamic collaborative fingerprint training process, the system keeps track of all historical training data by storing them along a timeline and comparing them to the new data. When new RSS data is collected at a repeated location, the variance of the signal strength is measured and applied to generate confidence factors. The confidence factor consists of two vectors, i.e. the training data difference level $diff_{sgn}$ and the confidence level η_{CF}, which is the standard deviation of all previously

collected data. The confidence level η_{CF} for each fingerprint grid in the entire building is generated based on the training data standard deviation, which indicates how much signal strength variance to expect at each specific fingerprint location. Smaller η_{CF} means higher confidence with the current RSS of the fingerprint stored in the database. The difference level $diff_{sgn}$ is updated at each epoch by measuring the sign of the δRSS between the new RSS at a new TP and the mean of all historical RSS that is within 2m of the TP. If the $diff_{sgn}$ for a location is always positive or negative indicates that the RSS is constantly increasing or decreasing. If this is true while the confidence factor goes over the given threshold, old RSS data will be discarded. After replacing an old data with a new RSS, the confidence level η_{CF} for the fingerprint is reset back to the initial value which represents a high confidence level. If $diff_{sgn}$ changes randomly, we would assume that the collected RSS is within the signal strength random fluctuation range. In such cases, the signal fluctuation range is reflected by the confidence level η_{CF}. In general, the difference level $diff_{sgn}$ keeps track of the direction of change along the time scale while the confidence level η_{CF} reflects the actual signal fluctuation based on the collected data.

The generated fingerprint confidence factor of the three APs located on Floor A is plotted in Figure 5.25. The primary data for generating the confidence factor η_{CF} is the training data for d-DB3 P1, which is then updated by the training data of d-DB3 P2, d-DB1 and d-DB2. Blue areas indicate a small η_{CF} which means high confidence in the fingerprint RSS value and red areas vice versa.

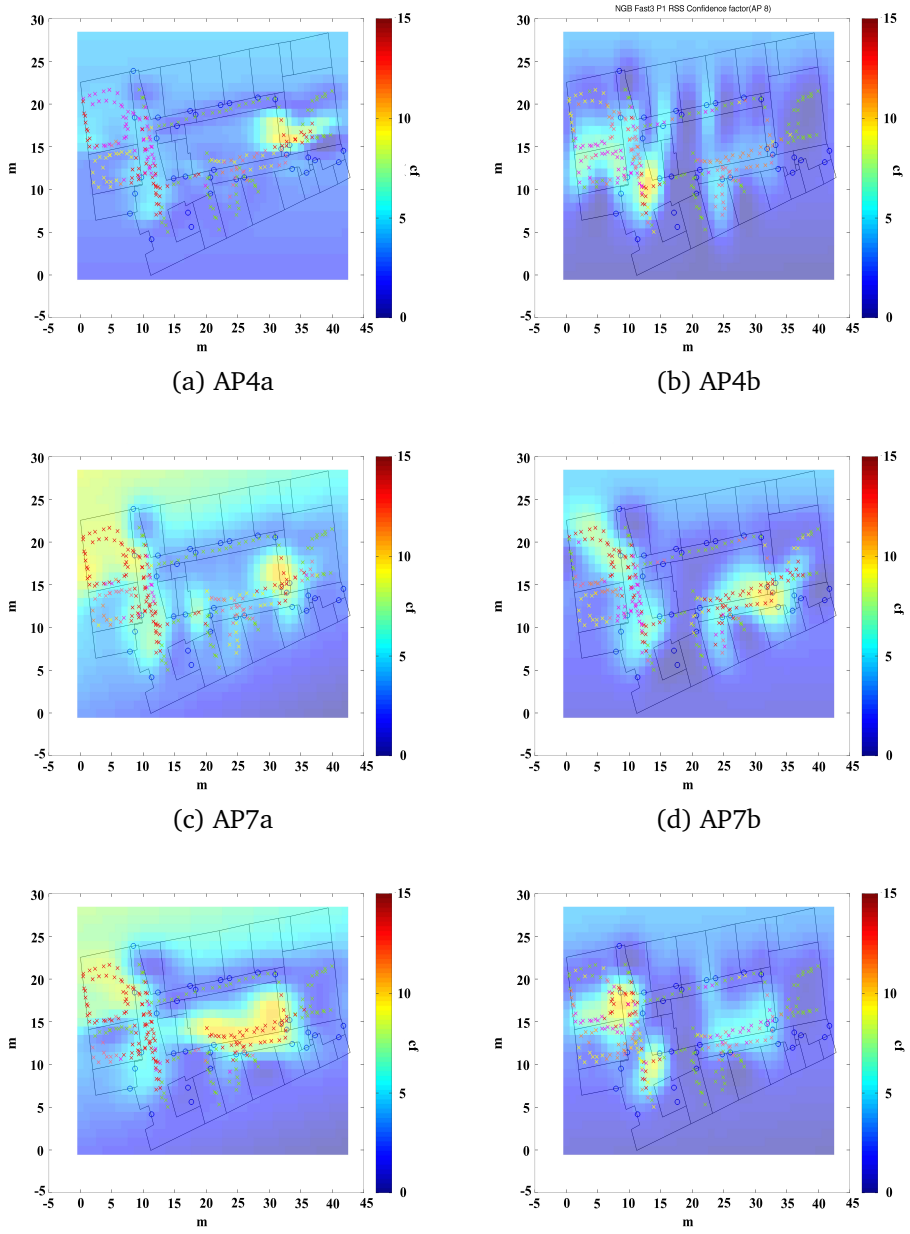

(a) AP4a (b) AP4b

(c) AP7a (d) AP7b

(e) AP8a (f) AP8b

Figure 5.25: Fingerprint confidence factor map for three APs

The RSS of the training data is also plotted on the map and results clearly indicate that the resulting η_{CF} is higher in those areas where the training data changes rapidly. Furthermore, we can see that once again, there is less fluctuation in the 5GHz signal than the 2.4GHz signal. Higher confidence is generated for 5GHz signals. The characteristics of the 5GHz signal generates signal patterns that are more unique for different regions in a building. 2.4GHz wireless signals, on the other hand, have greater ranging distance and penetrate walls better. However this results in noisier

training data, thus lower confidence level of fingerprints.

5.5.4 Improved Wi-Fi fingerprinting

Once the confidence level information is derived, each fingerprint takes the form of $\{(x_i, y_i)|AP_1, (RSS_1, \eta_{CF_1}), ..., AP_n, (RSS_n, \eta_{CF_n})\}$. η_{CF} indicates the range of RSS to search for when looking for possible fingerprints. Therefore large η_{CF} values indicate greater signal variation and vice versa. For example, if RSS_p is collected at the current unknown location and RSS_{FP} are the fingerprints from the database, all fingerprints that follow

$$RSS_{FP} - \tau_{FP} < RSS_P < RSS_{FP} + \tau_{FP} \tag{5.1}$$

is returned as potential fingerprints during the positioning phase, where τ_{FP} is a variance boundary defined by

$$\tau_{FP} = a \cdot \eta_{CF_n} \tag{5.2}$$

where a is a coefficient defining the relationship between the two values depending on the environment. Following such selection procedures, a fingerprint with a large η_{CF} is more likely to be selected than the fingerprints with a small η_{CF}. However, if a fingerprint with a small η_{CF} is selected, then its possibilities of indicating the true location is much higher than when a fingerprint with a high η_{CF} is selected. An improved Wi-Fi fingerprinting method is proposed here based on the improved database, where it is applied within a collaborative positioning algorithm with adaptive ranging constraints, denoted as WARCP.

The procedures of WARCP is a combination of Collaborative fingerprint mapping positioning (CFPM) presented in Section 4.6.1.3 and SARCP. The basic procedures of WARCP is outlined as below:

i. Initialisation: generate N_p particles around the initial position for each rover $[x_i, y_i]$, all particles are assigned an equal weight $w_k^i = \frac{1}{N_p}$, indicating that each particle contributes the same amount in the position estimation at the beginning;

ii. prediction: particles propagate forward based on the PDR prediction model Eq.3.1. The step length is assumed to be a constant value sl with a uniformly distributed random noise $U \sim (-n_s, n_s)$, the heading $\hat{\theta}_{(t|t-1)}$ is simulated with a constant heading bias of b_h and a uniformly distributed random noise $U \sim (-n_h, n_h)$;

iii. Update and weighting: map information can be integrated so that particles which cross walls are "killed", i.e. $w_k^i = 0$; rover search for ranging measurements and Wi-Fi RSS measurements.
If Wi-Fi measurement RSS_p are obtained, it is stored to update the database, potential fingerprints are also extracted for positioning based on Eq.5.1;
If ranging measurements $\hat{r}_{ij}$ are obtained between the rover i and available units j, ranging constraints will be applied to further extract potential fingerprints,

$$\Delta dis = \sqrt{(x_{FP_m} - x_{FP_n})^2 + (y_{FP_m} - y_{FP_n})^2} - r_{ij} \leq thresh_{dis} \quad (m = 1, 2, ..., M; n = 1, 2, ..., N) \quad (5.3)$$

fingerprints that fall within the threshold $thresh_{dis}$ will be kept valid, those that fall outside will be discarded. Particles will then be weighted according to their distance to the valid fingerprints following Eq. 4.28 in CPFM;
If only ranging measurement are obtained, update procedure will continue same as in SARCP, where ranging constraints are applied to constrain particles.

iv. Positioning estimations are achieved from the weighted mean of particles.

v. Resampling: if the number of "live" particles, N_e falls below a threshold ($\frac{N_p}{2}$ is applied), new particles are generated by replicating the live particles with an additional noise to replace the killed particles in order to maintain a total number of N_e particles.

vi. Return to step ii or end iteration.

The confidence factor is generated from the collected data as an indication of the stability of the training data as well as the quality of the generated database. While the database influence the positioning accuracy of Wi-Fi fingerprinting, the quality of the database is affected by the observed training data. This parameter gives both the system and the user an updated knowledge of how trustworthy the database fingerprints are for positioning. As a result, positioning robustness and integrity is improved as users know from confidence information when they can produce a trusted high accuracy positioning result and when the positioning result cannot be trusted.

Moreover, the system would know when the positioning from fingerprinting can no longer be trusted and other positioning methods should be considered as backup. Chapter 6 will demonstrate a fingerprinting-based positioning algorithm with confidence factor updates to restrict the spread of potential fingerprints which enables the final position to gather closer to the true location.

5.6 Summary

This chapter presents two collaborative positioning algorithms that applies the collaborative constraint adaptively based on the actual ranging measurement quality. The measurement quality reflects the detected ranging accuracy, the current network geometry and network size. ARCP is applied when the number of collaborative units is fixed and the rover only decides on the constraint threshold based on the relative measurements from the units. SARCP is applied when more than four units are found in the environment and the rover needs to choose the appropriate units first to include in the collaborative network and then set the collaborative constraint based on the network conditions of the chosen units. The adaptive ranging constraint threshold in ARCP proves to improve collaborative positioning accuracy. SARCP further enhances positioning performance by giving users the freedom to choose the most appropriate collaborative users and anchors to restrict its measurement error. Collaborative positioning error is reduced by 60% by changing the collaborative constraint and choosing the units for the network adaptive. Positioning becomes more efficient by applying SARCP as network is reduced by choosing only the effective units.

Based on the collaboration between rovers, a collaborative Wi-Fi fingerprint database training method is also proposed. With more than one user collecting RSS training data for the same database, collaborative training reduces the required database training time while also improving the database quality by including more historic information on the variation of signal strength. While the RSS data cannot be collected at exactly same location during the dynamic training process, fingerprints are generated based on all collected RSS data in the same training area. In most current Wi-Fi environments, two signal frequencies can be found. However, the two signals have very different properties. 2.4GHz signals travel a longer distance but are also noisier as they are easily affected by the obstructions in the environment. 5GHz wireless signals are less able to penetrate ob-

structions, as a result, its signal is more stable hence more suitable for fingerprinting.

For positioning purposes, the collaborative database treats the data from the two frequencies separately. Yet wireless signals from both frequencies tend to fluctuate, thus the database is stored in a way that it reflects both the short-term and long-term signal variation. WARCP is proposed which integrates both Wi-Fi fingerprinting and relative ranging constraint adaptively to eliminate inertial bias and improve positioning results.

Chapter 6

Trials and discussion

6.1 Introduction

Three trials are discussed in this chapter each based on a positioning algorithm introduced in Chapter 4 and Chapter 5. The adaptive collaborative positioning is carried out in Trial 1 where two rovers each collect inertial measurements with a foot-tracker and ranging measurements with UWB units. The collaborative indoor positioning algorithm is tested in a more complicated scenario in Trial 2 where the environment is changing, relative ranging and Wi-Fi signals are only intermittently available. Hence inertial measurements errors are constrained by them only when they are available. The collaborative fingerprint database training and fingerprinting is carried out in Trial 3.

6.2 Trial 1: Collaborative positioning for low-cost inertial systems

A trial was carried out in the Business School South Building (BSS), University of Nottingham to test the performance of ARCP/SARCP algorithms when dealing with real data. This building was selected because its internal structure is less complicated than NGB so we would receive better UWB measurements. The collaborative network consists of two moving users, Rover 1 (R1) and Rover 2 (R2), and four anchors. Each user is equipped with a MicroStrain foot-mounted IMU, an UWB mobile unit (MU), a Raspberry Pi single board computer and a laptop, as shown in Figure 6.2. The Raspberry Pi is connected to the IMU for logging inertial measurements and the laptop is used to log the ranging data between the UWB units. The IMU and UWB data output rate is 10Hz and 2Hz respectively. Time synchronisation is achieved by tagging the data with the laptop time which is synchronised to the network. A Leica TS30 robotic total station is used to track Rover 1 where its data is synchronised to GPS time and outputs data at a rate of 1Hz. The offset between the GPS time to the current network time is then aligned during post-processing. The walls and doors of the

building were surveyed using the total station to generate the ground truth for the locations inside the building to a local coordinate system with the point of origin set at point next to the building. The point of origin was also surveyed to the WGS84 coordinate so that the collected data could be overlaid on existing datasets. All the position outputs are referenced to the local grid coordinate with the building map as reference.

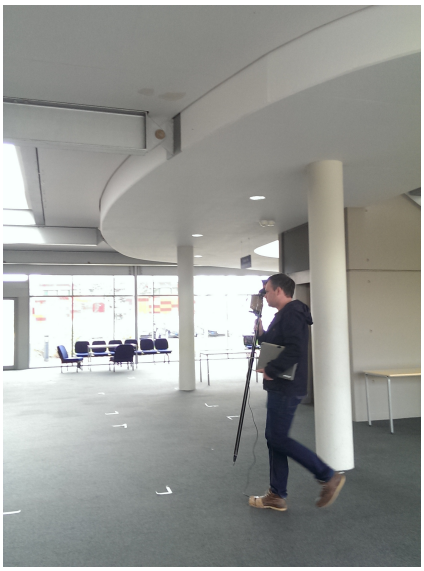

Figure 6.1: Business School South Building experiment environment

Four UWB BUs are setup at four corners of the building only to act as anchors in the collaborative network, no positioning is received from them. The UWB system works on a grid coordinate system so it is setup in the local coordinate system provided by the building map. The ground truth of both rovers are shown in Figure 6.3. The total station is used during the trials to track and provide the ground truth for the trajectory of Rover 1. Due to the limited number of equipments, the ground truth of Rover 2 is provided by UWB. As UWB positioning results are disturbed in some places, especially during the period before Rover 2 enters the building, therefore it only provides a coarse reference for Rover 2's trajectory when indoors and is very inaccurate outside.

(a) MicroStrain 3DM-GX3®-25 IMU attached onto user's foot

(b) Raspberry Pi

(c) UWB unit attached onto a prism pole to be tracked by total station

Figure 6.2: Devices used for data collection

Both rovers start off from just outside the building in the area overlaid by the patch of light green area with black lines indicating rooms and corridors as shown in Figure 6.4 to initialise the IMU and start to walk inside the building with Rover 2 following behind Rover 1 with an interval of 30 seconds. After both rovers enter the building, they each walk separately and randomly around the building. Data was collected for ten minutes consisting of 644 epochs. In every epoch, each rover creates its own collaborative positioning network by integrating the ranging measurement between the two rovers and also between one or two of the available anchors. The anchors are selected using SARCP and the ranging constraint threshold is adjusted based on the received signal characteristics.

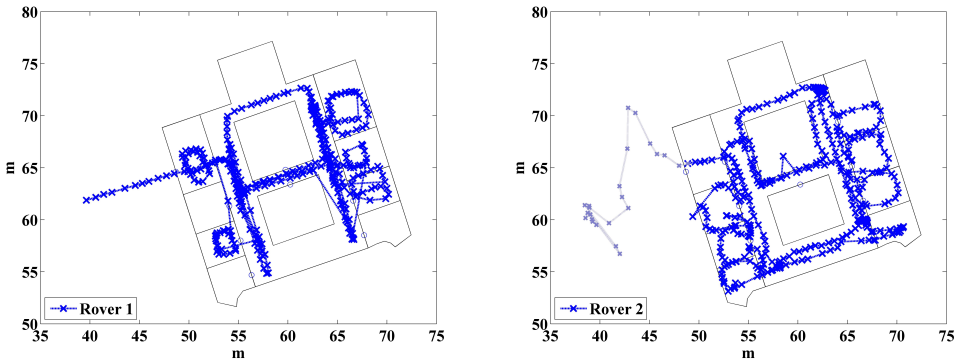

(a) Rover 1 (tracked by TS)

(b) Rover 2 (tracked by UWB full system, light blue indicates noisy data)

Figure 6.3: True trajectory of the two rovers

The IMU data is logged as a binary file and processed in Matlab to extract the required data to a text file, where each row logs the IMU

time, the estimated the longitude and latitude, the acceleration in three directions and the gyro measurement in yaw, pitch and roll. The IMU is always initialised to a reference start location in the WGS84 coordinate system and the estimated longitude and latitude is computed from the inertial measurements relative to the initial position. Figure 6.4 shows the raw IMU measurements after being processed with an extended Kalman Filter with ZUPT. The same data is processed using particle filtering based on PDR model with wall constraints and outputs are shown in Figure 6.5. It can be seen that positions are likely to jump which is caused by particles been trapped in the wrong location and having to regenerated particle clusters.

(a) Rover 1 (b) Rover 2

Figure 6.4: IMU raw output after processed with ZUPT

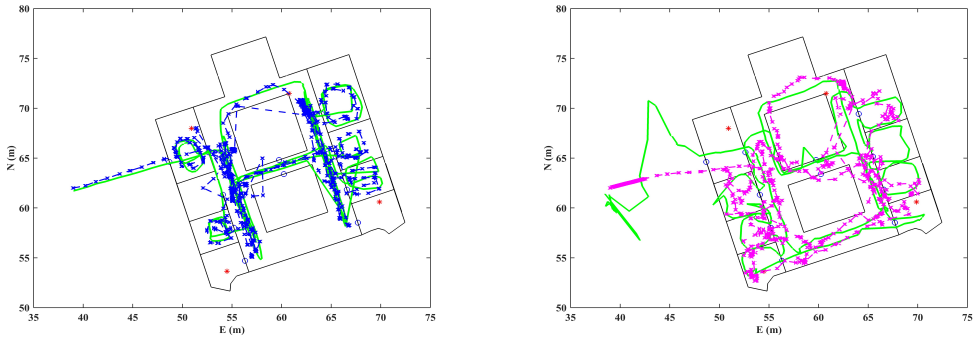

(a) Rover 1 (b) Rover 2

Figure 6.5: Data processed with particle filtering based on wall constrained PDR model only

The UWB ranging measurements between both rovers and each BU (denoted as Tx1, Tx2, Tx3 and Tx4) are plotted in Figure 6.6 and 6.8. The

received data signal strength between both rovers and the BUs are plotted in Figure 6.7 and 6.9.

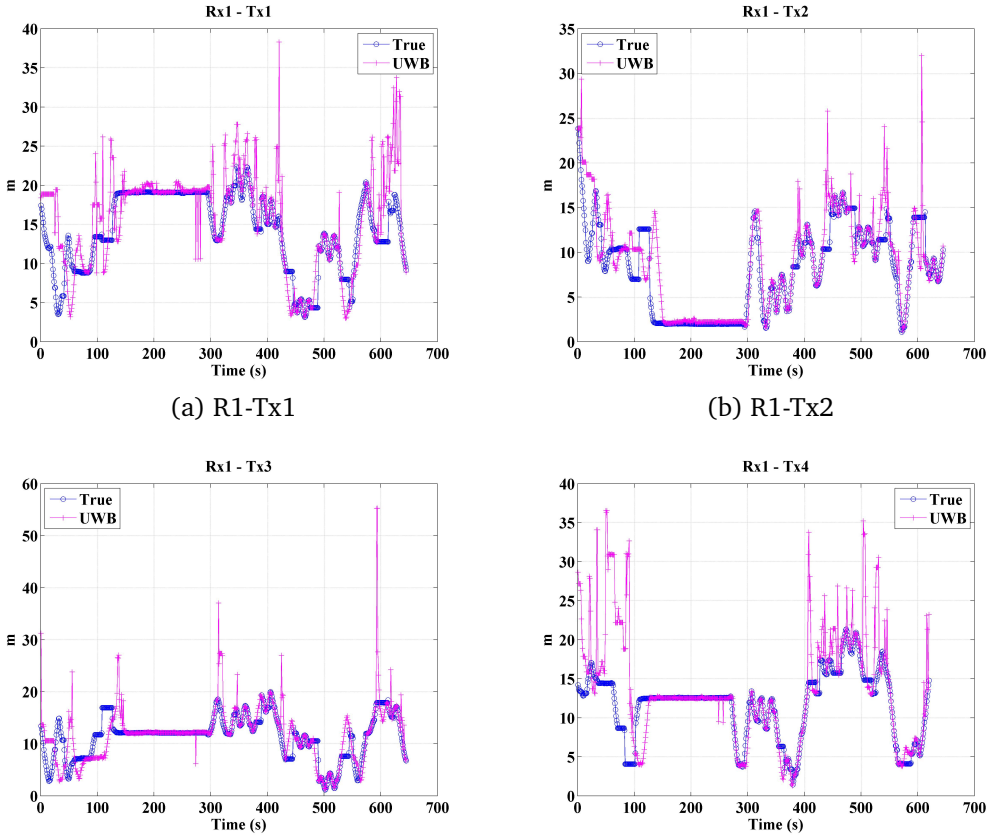

(a) R1-Tx1

(b) R1-Tx2

(c) R1-Tx3

(d) R1-Tx4

Figure 6.6: Rover 1 UWB ranging measurement compared to the true distance

During the beginning of each trial, a very large difference between the ranging measurement and the true distance is observed. This would be caused by the data noise and disturbance seen in the measurements during the period when the MU was outside the building. It would take a while before the units can adjust to a better accuracy after the MU goes inside the building where better measurement can be received between the units. This is also reflected in the data signal strength plots where the signal strength is very low in the first 50 seconds.

While the units are outdoors, the external walls cause a great deal of noise in the measurements and reduce the data quality greatly. The measurements collected while the rovers are inside the building lie close to the truth although occasional spikes can be seen in some periods. These noise could be caused by pedestrian disturbance or system hardware noise, which has been observed in other occasions as well. The overall ranging is

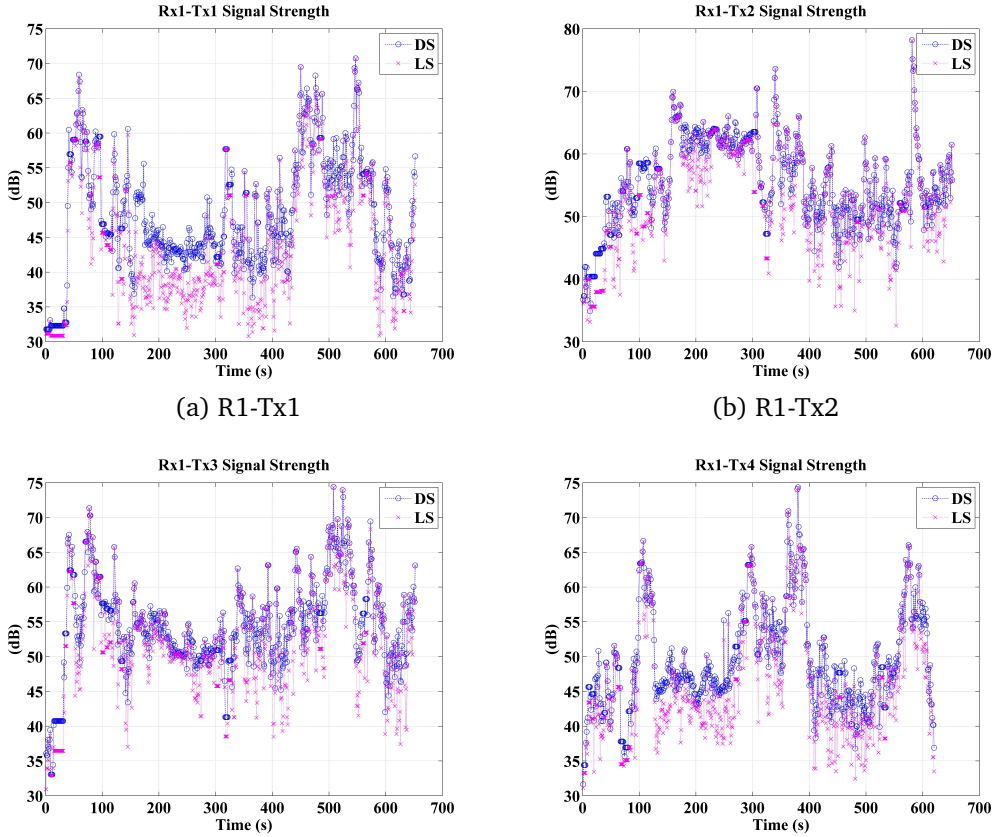

(a) R1-Tx1 (b) R1-Tx2

(c) R1-Tx3 (d) R1-Tx4

Figure 6.7: Rover 1 UWB strongest signal strength (DS) compared to the signal strength of the first arriving signal (LS)

reliable as the average accuracy is within 2m for 75% of the time and 50% within 1m. The lowest accuracy is within 5m, as listed in Table 6.2.

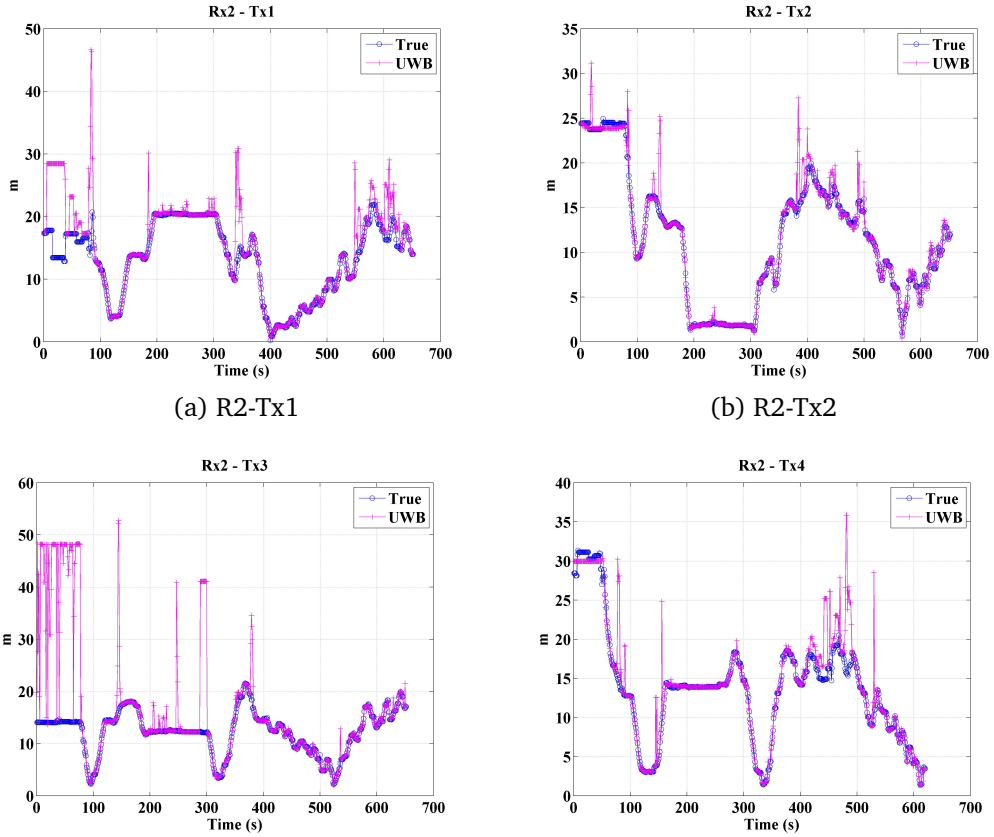

(a) R2-Tx1 (b) R2-Tx2

(c) R2-Tx3 (d) R2-Tx4

Figure 6.8: Rover 2 UWB ranging measurement compared to the true distance

The lowest signal strength in all plots are found within the first 50 seconds where the MUs carried by the two rovers are outdoors. The signal strength increases immediately as the users enter the building. However, as the users walk around the building, the signal strength, both the DS and LS, as well as the difference between DS and LS, changes quite significantly during some periods. The variation pattern of the signal strength is almost a mirror image of the ranging variation pattern. As the distance between the rover and the BU reduces, the corresponding DS/LS increases, e.g. Rover 1 moves closer to Tx1 at time 450-550s as shown in Figure 6.6a, and in the same period, the DS shown in Figure 6.7a increases. However, when the distance increases, as between Rover 2 and Tx2 during time 400-500s shown in Figure 6.8b, the DS reduces significantly as plotted in Figure 6.9b. For many parts of the trial, the difference between DS and LS becomes quite significant. Although we have chosen a relatively quiet location in the campus for trials, but passing pedestrians cannot be avoided. While the ranging distance affects the absolute value of DS, the obstructions and disturbance influence the difference between DS and LS.

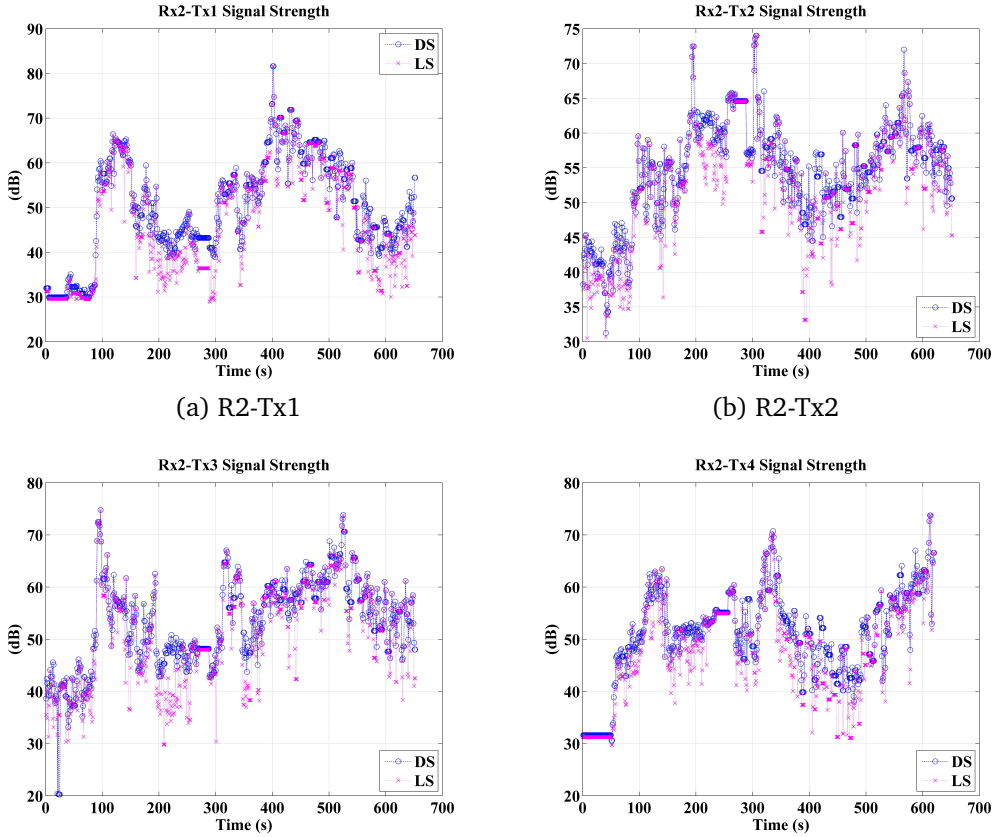

(a) R2-Tx1 (b) R2-Tx2

(c) R2-Tx3 (d) R2-Tx4

Figure 6.9: Rover 2 UWB strongest signal strength (DS) compared to the signal strength of the first arriving signal (LS)

Table 6.1: UWB ranging accuracy (m)

	Tx1	Tx2	Tx3	Tx4
Rx1	1.44	0.99	0.59	2.03
Rx2	1.69	0.24	4.16	0.64

While SARCP has to set the ranging constraint threshold based the ranging accuracy, the actual ranging accuracy is not provided to the positioning algorithm. Instead, the measurement accuracy level is detected based on the signal strength patterns as introduced in Chapter 4. During the update phase of the algorithm, the system produce an RQI which detects the ranging measurement accuracy level from the received DS and LS data in the current epoch. An RQI that is close to 1 indicates an accurate measurement, whereas a value close to 0 indicates inaccurate measurement. During the collaborative ranging constraint procedure, the constraint threshold which defines the allowed maximum $diff_m$ is set based upon the RQI value, such that the threshold $\propto \frac{diff_m}{RQI}$. Therefore, a

larger RQI would lead to a low threshold, where only the particles that lies within a small constraint boundary will be kept alive hence particles which do not represent the true state should be killed.

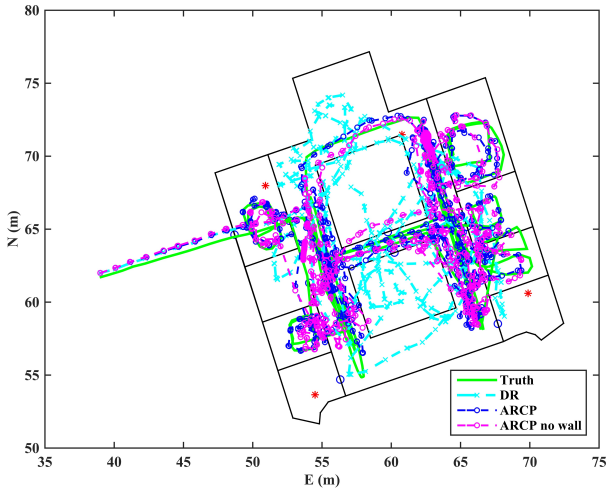

(a) Rover 1

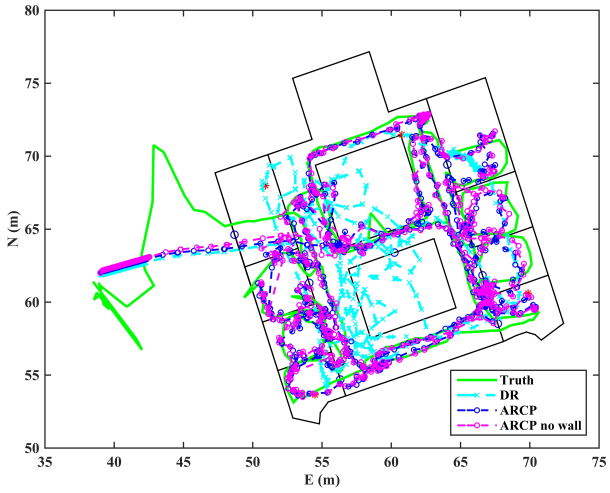

(b) Rover 2

Figure 6.10: SARCP positioning result for Rover 1 and Rover 2 in Business School South Building (For both rovers, SARCP results follow the truth accurately, SARCP without wall constraint results in very similar accuracy)

The SARCP positioning result for both Rover 1 and Rover 2 is shown in Figure 6.10. The green solid line indicates the ground truth for both rovers. The cyan dashed line shows the DR output from raw inertial data. The blue line represents the SARCP result while integrating the wall constraint from the building map information, and magenta line represents the result without integrating the wall constraint.

Table 6.2 lists the mean and maximum positioning error as well as the standard deviation of the positioning error for Rover 1 throughout the whole trial, which is the distance between the positioning estimation and true position. The error of processing the same data using basic CPF is also given for comparison. As the ground truth for Rover 2 is provided by only the UWB positioning system that has a varying accuracy in disturbed environments, therefore it is not sufficient to evaluate the accuracy level of Rover 2 positioning result based on SARCP.

Table 6.2: Rover 1 positioning error in Business School trial (m)

	CPF			SARCP (wall)			SARCP (no wall)		
	mean	max	std	mean	max	std	mean	max	std
R1	5.30	15.99	4.54	2.03	8.61	2.00	2.28	8.98	2.20

Compared to CPF results, SARCP improves positioning accuracy by more than 60%. This improvement is even more obvious compared to the SARCP simulation based in NGB in Chapter 5. While the simulated measurements are more stable as the noise always lies within the simulated standard deviation, the real data in this trial tends to be noisier as they are less predictable and prone to sudden changes caused by disturbance in the environment. The maximum error could be caused by particles being stuck in the wrong room, but the algorithm recovers such problems by resampling. This demonstrates the adaptive ability of ARCP to cope with noisy real data. Moreover, CPF is less able to cope with noisy situations than the simulated noise thus ARCP demonstrates better performance in comparison. Therefore more boundary adjustment is needed to deal with varying noise levels. SARCP contributes to the improvement in positioning by selecting the appropriate units for the network, therefore the best network is always used to provide more effective collaborative constraint, whereas CPF does not have the freedom to select the network and must integrate what is available.

While wall constraint provides slightly better positioning results, we can see that the positioning result when wall constraint is eliminated is not much different. The magenta lines which indicate the result without wall constraint overlap the blue lines, which represent wall constraint results, in most places. Although the estimated positions can jump over walls in places when the wall constraint is not implemented, but there are also situations where it gives better performance than wall constrained results. This is caused by the short periods during navigation where the

propagation patterns of the particles may fit into more than one of the local geometries, or a door may be nearby where particles could accidentally leak through. Once particles enter the wrong location, they will be killed in time when their propagation path no longer fits with the geometry. However if the particles in the wrong location are not killed soon enough, the errors brought in by the particles will accumulate and make it even harder for the system to adjust back to the right location. SARCP results demonstrate a strong adaptiveness to situations without integrating map information. Therefore, the building map information can be eliminated in the ARCP/ARCP algorithm as collaborative ranging between units already provide sufficient constraint on the particles. Without the wall constraint, the particles will have a better chance of returning to the right location when it is not jammed behind the wrong wall. The elimination of wall constraint also means that ARCP/SARCP is able to provide positioning independent of any infrastructure and reference information of the building. This offers users the ability to start navigating in a new environment without prior knowledge of the environment.

6.3 Trial 2: Collaborative positioning for DR and Wi-Fi based systems

One unresolved problem in ARCP/SARCP is the initialisation of particles at the beginning of a navigation process. Most indoor positioning begins when the user enters the building, thus particles can be initialised near the building entrance. However, there will be situations when the user wishes to start positioning once already inside the building. The best option would be to initialise particles based on Wi-Fi fingerprinting estimation.

Another situation collaborative users need to consider is the intermittent availability of collaborative units. Collaborative positioning is designed so that the user does not rely on any pre-installed infrastructure, however each user would need to find local units, either other rovers or anchors, to form an local collaborative network for positioning. If the user fails to find local units, it will not be able to perform collaborative positioning. If the period of insufficient collaborative units is only for a few or tens of seconds, the practical solution would be to continue navigation based on DR. However, if the period continues for any longer, low-cost gyro drift would be badly biased and other absolute positioning solutions should be implemented, e.g. Wi-Fi fingerprinting.

Further trials are carried out in NGB by collecting IMU, ranging and Wi-

Fi measurements while two rovers walk along two individual trajectories. The collaborative ranging information between Rover 1 and Rover 2 is eliminated intermittently on purpose during the positioning process. The first location of the each Rover is initialised by fingerprinting. However, fingerprinting cannot provide an initial heading therefore the particles are propagated in all directions during the start of the navigation. Once it has found the trajectory where the PDR geometry could fit into, the particles which have gone off in the wrong direction would be killed off and the remaining particles will follow the detected "true" direction.

Figure 6.11a shows the positioning result when only intermittent ranging measurement is available and DR is used to complement lack of collaborative units. The Wi-Fi integrated adaptive ranging collaborative positioning (WARCP) is applied to provide continuous positioning in a changing environment. Figure 6.11b plots the result of WARCP which applies ARCP when collaborative ranging is available and Wi-Fi fingerprinting when ranging is not available. Wi-Fi fingerprinting is only implemented when collaborative ranging is not available. Fingerprinting is carried out by comparing the measured Wi-Fi RSS vector at the unknown location to the s-DB obtained in Chapter 3.

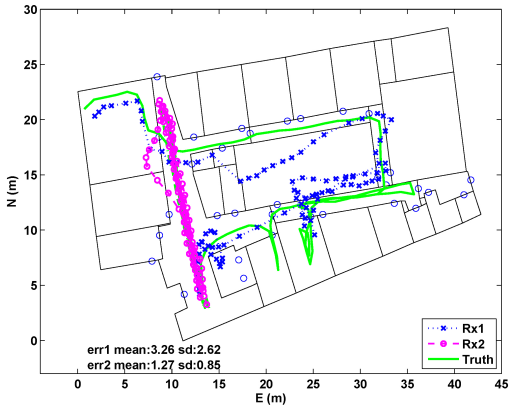

(a) ARCP where ranging constraint is intermittenly available

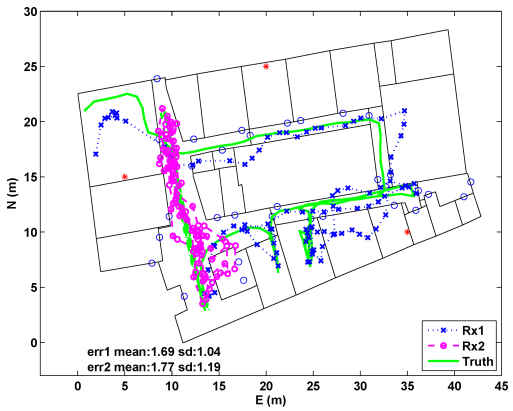

(b) WARCP where Wi-Fi measurements compensate lack of ranging constraint

Figure 6.11: Intermittent ARCP/WARCP Positioning result

Although Wi-Fi fingerprinting results can be noisy and relies on both the accuracy of the fingerprint database as well as the quality of the current RSS, but nevertheless, it provides an absolute positioning result, whereas DR is only able to provide relative position. The simulations discussed in Chapter 3 demonstrated that integrating Wi-Fi fingerprinting improves DR positioning. While heading bias will accumulate as the IMU continues to provide navigation to the rover, Wi-Fi fingerprints will eliminate this error partially by updating the position with a fingerprinting result, which is uncorrelated to IMU errors. However, the accuracy of Wi-Fi fingerprinting is relatively low compared to ARCP/SARCP collaborative positioning. Once a fingerprinting result is produced, further positioning error still needs to be reduced by applying collaborative ranging. Figure 6.12 shows the positioning result of a network that is exactly the same as that shown in Figure 6.11b. However, collaborative ranging is integrated continuously

here without applying Wi-Fi fingerprinting at all. Comparing this result to the positioning estimation in Figure 6.11b, this result demonstrates that the accuracy of Wi-Fi fingerprinting is lower than ARCP. Unless fingerprinting can be improved, there is no need to implement fingerprinting when collaborative ranging can be performed.

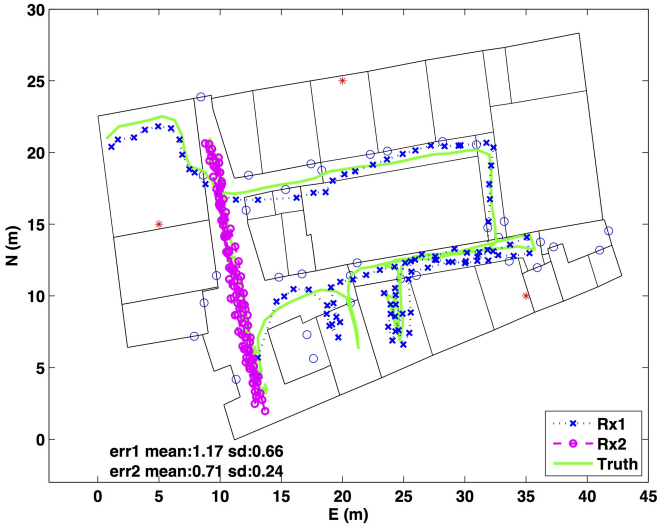

Figure 6.12: ARCP without Wi-Fi

6.4 Trial 3: Collaborative Wi-Fi fingerprinting

This trial addresses the problem of fingerprinting inaccuracy. First of all, as the 5GHz frequency signal outputs more stable signal strength and shows more variance around different locations in the building while generating previous fingerprint databases, the fingerprinting process is evaluated by 2.4GHz and 5GHz signal separately.

To evaluate the fingerprinting performance on the two frequency bands, a user collects Wi-Fi RSS while walking in the building following a designated path and extracts potential fingerprints from the database at each epoch. Fingerprinting is performed individually for each frequency data of d-DB3, one based on the 2.4GHz frequency and the other based on the 5GHz frequency. The average distance between each potential fingerprint to the true location is measured and plotted in Figure 6.13. The advantage of the 5GHz-database is not prominent here as there is no obvious evidence that the fingerprints from the 5GHz is better and closer to the truth than the 2.4GHz database. However, the advantage of the 5GHz-database based fingerprinting is that potential fingerprints can always be found, while for a majority of the time, the 2.4GHz-database based fingerprinting returns

no potential fingerprints. Without potential fingerprinting, the rover can only navigate based on inertial measurements, where the bias will accumulate in no time. Although there is no evident improvement in accuracy, the 5GHz-database fingerprinting does provide improved robustness. To ensure more stable fingerprinting, database from both frequencies will be applied. The mean error between the potential fingerprint location and the true location is listed in Table 6.3.

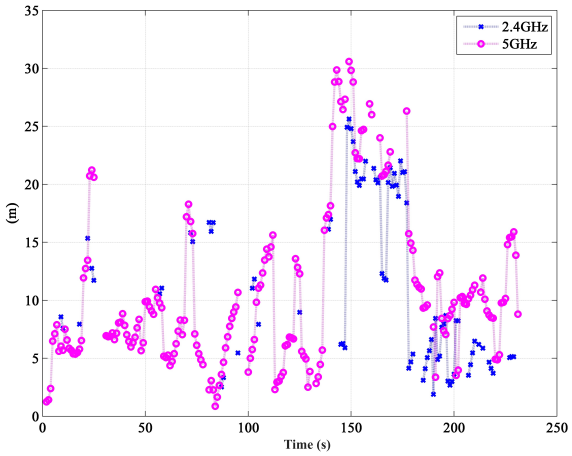

Figure 6.13: 2.4GHz and 5GHz fingerprinting RMSE

Such Wi-Fi fingerprinting performance cannot provide the required accuracy for positioning and navigation as there are many periods during the evaluation test where the potential fingerprints are more than 20m away from the true location, which is almost half way across the building. With such accuracy, fingerprinting is insufficient to provide any aiding to the collaborative positioning results achieved by ARCP/SARCP. The error and instability of fingerprinting fundamentally comes from the fluctuation and variance of the signal strength of Wi-Fi signals. Therefore, the solution to improving fingerprinting accuracy is to learn about the signal fluctuation at each location and know the real time noise of the current received RSS_p so that accurate fingerprinting can be achieved based on the exact variance of the fingerprints and the noiseless current RSS_p. But of course, it is impossible to eliminate the noise from the current RSS. It is also hard to know exactly what the signal variance is at each location as situations could change easily. The signal strength collected at the same location of a fingerprint may differ to the signal strength of the fingerprint RSS_{FP} from the database by a few or even tens of dB. On the other hand, a specific RSS value may refer to a number of different locations which could be

quite far away from the actual location. The best we can do is estimate the variance of each fingerprint before the positioning phase and try to find the best match of fingerprints based on the estimated information.

To overcome the problem of signal variance and noise, the fingerprinting is carried out by defining a variance boundary τ_{FP} based on the trained confidence level. Any fingerprints from the database that fit within $RSS_{FP} - \tau_{FP} < RSS_P < RSS_{FP} + \tau_{FP}$ will be extracted as potential fingerprints. However, the difficult part is usually deciding how large τ_{FP} should be. When the given τ_{FP} is too small, it will be likely that no fingerprints can be extracted as potential fingerprints if either theRSS_p or RSS_{FP} is noisy. Yet if τ_{FP} is too large, too many potential fingerprints may be found covering a very large area. This will cause too much ambiguity in positioning. Therefore, the τ_{FP} should not be set to a constant value. It should be allowed to adjust its value according to each individual situation, as the confidence factor η_{CF} introduced in Chapter 5. By varying the variance boundary τ_{FP} based on the confidence factor of each fingerprint following Eq.5.2, fingerprinting result accuracy can be enhanced.

Different choices of τ_{FP} for extracting potential fingerprints are compared in Table 6.3. τ_{FP} is assigned constant values of $\tau_{FP} = 5$ and $\tau_{FP} = 10$, varying values are also given based on the confidence level following $\tau_{FP} = a \cdot \eta_{CF_n}$. The collected Wi-Fi data used to test the accuracy of 2.4GHz- and 5GHz-database are applied to analyse the accuracy of fingerprinting. Table 6.3 lists the average distance between the extracted potential fingerprints and the true position when different τ_{FP} is selected. Another thing to consider is also the selection of a when choosing τ_{FP} according to confidence level. As introduced in Chapter 5, a is a environmental coefficient. Through trials, it is found that optimal fingerprints are extracted when a is between 1.5 and 3. In an open area, we might choose $a = 1.5$ and in a heavily obstructed area we would choose $a = 3$.

Table 6.3: Fingerprinting error (m)

τ_{FP}	5dB	10dB	η_{CF}		
			2.4&5	2.4	5
Err	16.48	15.51	9.07	11.37	9.69
RMSE σ_{FP}	19.46	17.67	9.63	12.12	10.52

The error for fingerprints from the 2.4GHz- and 5GHz-database is given separately for comparison. The potential fingerprints extracted from the 5GHz-database is slightly better than the fingerprints from the

2.4GHz database, but the most accurate fingerprints are still achieved from the database consisting both frequencies. The errors of the extracted fingerprints seem to be quite large partly due to the location ambiguity in fingerprints. Figure 6.14 shows a comparison of extracting fingerprints when different variance boundary is applied. When $\tau_{FP} = 5$, only very few of the potential fingerprints lie close to the true position while most the extracted fingerprints are spread elsewhere. In such cases, the number of those fingerprints with a small error is not enough to provide significant weight on producing an accurate position estimation. The area around the true position is covered quite thoroughly when $\tau_{FP} = 10$. However as the bound is very large, the number of fingerprints that lie far away from the true location is outweighs those fingerprints that are closer to the truth. This ambiguity in the fingerprints will still cause a large position error. The potential fingerprints found when $\tau_{FP} \propto \eta_{CF}$ is much more appropriate as all fingerprints lie near the true location.

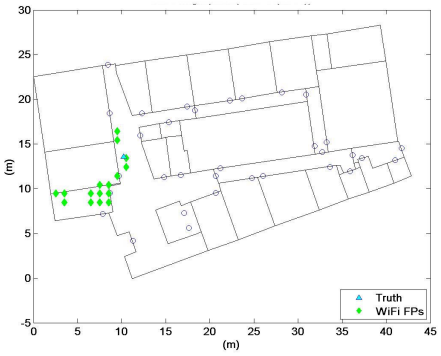

(a) 5dB

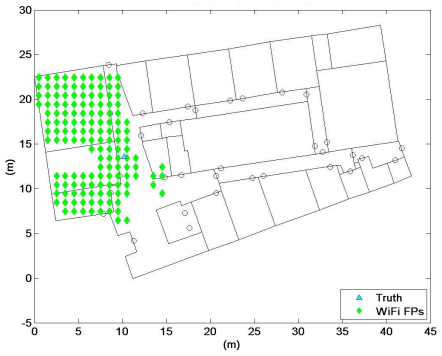

(b) 10dB

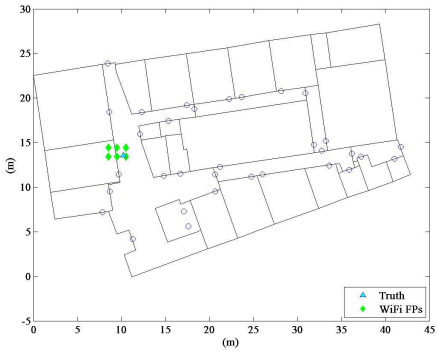

(c) Based on confidence level

Figure 6.14: Potential fingerprints extracted by different boundary settings

Two rovers, i.e. users carrying mobile equipments for data collection, are applied to test the positioning quality of the confidence factor based

fingerprinting. Both users wear the same foot-mounted IMU to obtain inertial measurements. Each user also collect the Wi-Fi RSS and relative ranging measurements while walking inside the building. The only available relative ranging in this trial is the ranging measurement between the two rovers. To enhance collaborative positioning performance, the two rovers do not follow each other so they could travel in different directions. As the space in NGB is limited, the two rovers travel in two opposite directions to start with. Therefore, their paths would not overlap and even if they do come across one another, they would only pass by and continue in different directions. The WARCP is utilised as the positioning algorithm, which integrates the confidence factor based improved fingerprint mapping and relative ranging. The WARCP performance is compared to each of the other positioning methods discussed in earlier chapters, PDR, PDR/Wi-Fi integrated fingerprint mapping and ARCP. The error of the positioning result for both rovers are plotted in Figure 6.15 and 6.16. The orange line plots the error cdf of PDR integrated with wall constraint. Blue lines plot the error cdf of PDR and Wi-Fi integrated positioning, orange lines plot the error cdf of ARCP and purple lines plot the error cdf of WARCP.

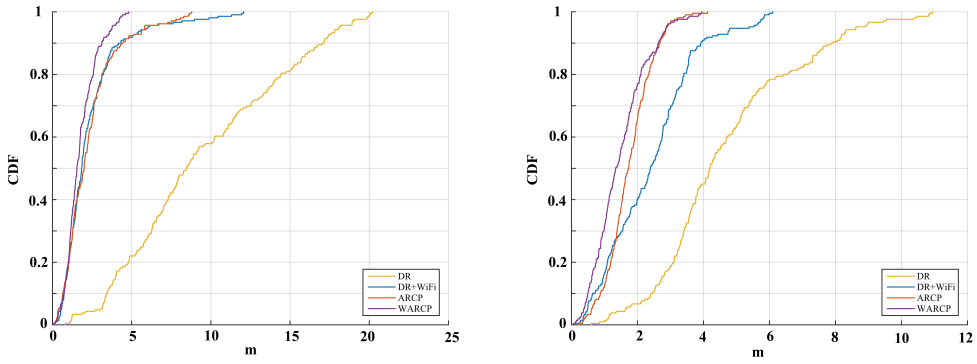

(a) Rover 1 (b) Rover 2

Figure 6.15: Positioning error CDF (wall constraint available)

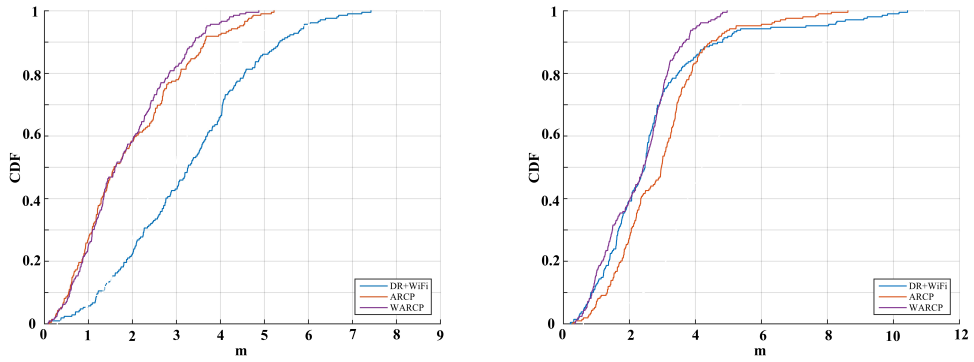

(a) Rover 1 (b) Rover 2

Figure 6.16: Positioning error CDF (no wall constraint)

PDR positioning is not considered when there is no wall constraint as the positioning estimation will be heavily biased, hence the actual accuracy would be meaningless. In the previous trial, integrating Wi-Fi fingerprinting was not able to improve positioning results as the fingerprinting accuracy level is much lower than ARCP. However, once the confidence level based fingerprinting is applied, PDR and fingerprinting integration accuracy improves while WARCP further increase positioning accuracy immensely. The mean positioning error for both rovers when each algorithm is applied is listed in Table 6.4. We can see that in some situations, ARCP does not outperform DR/Wi-Fi fingerprinting. A reason for this would be that there is only two moving rovers in the network thus the constraint from the relative ranging is rather limited. On the other hand, fingerprinting accuracy and reliability is enhanced by applying the confidence level based fingerprinting method. By improving the reliability and accuracy of the extracted potential fingerprints, all methods which implement or integrate fingerprinting will be enhanced. Although the average error for ARCP with only two rovers is not immensely better than DR/Wi-Fi integrated positioning, but ARCP still improves positioning by reducing the maximum error by 20%. This increases positioning robustness as there will be less likelihood for estimation outliers.

The WARCP further reduces the mean error by 20% compared to DR/Wi-Fi integration and ARCP method. The maximum error reduces by 35%. Improved Wi-Fi fingerprinting and relative ranging integration achieves the best possible estimation in this circumstance. Therefore, when both collaborative ranging and Wi-Fi signals are available, integrating the signals adaptively will result in enhanced accuracy.

Table 6.4: Positioning error with improved fingerprinting (m)

	PDR/Wi-Fi		ARCP		WARCP	
	wall	no wall	wall	no wall	wall	no wall
Rover 1	2.35	3.28	2.32	1.94	1.76	1.85
Rover 2	2.41	2.69	1.75	2.94	1.47	2.29

6.5 Result analysis and discussions

This chapter implements all previously proposed positioning and navigation algorithms to real indoor environments so they are tested with real data. SACRP is applied in the trial carried out in BSS, which is the most ideal environment the author could find regarding surveying the building and setting up experimental equipments, as well as collecting ranging measurements. SARCP improves P2P ranging based collaborative positioning by applying the ranging constraint adaptively. As there are two rovers and fours anchors available in the network, each user can choose anchors of its own choice to form the optimal network based on the specific situation. To maintain accuracy with less computation cost, each collaborative network consists at most two rovers and two anchors throughout the trial. The anchors for the network are chosen based on a balance between the predicated accuracy and the position of the anchor relative to the rover. The constraint threshold for each pair of ranging constraint is set according to the MDOP of the collaborative unit. The application of SARCP improved positioning accuracy as well as robustness. Whether single system positioning solutions or simple collaborative positioning (i.e. CPF), positioning solution can easily fail to provide valid results due to the changing environment in an indoor environment. Yet SARCP provides a promising solution by ensuring that there will always be a valid positioning solution regardless of the current situation. Furthermore, a promising accuracy is always achieved when a positioning estimation is obtained. An average positioning accuracy of metre level could be achieved, with the maximum error restricted within 10m.

The other aspect of collaborative positioning is the integration of PDR, ranging and Wi-Fi fingerprinting. As the indoor environment is always changing, therefore the indoor positioning system should always expect changes and be prepared to provide different solutions. The trial in Section 6.3 looks into a situation where relative ranging is not always available and Wi-Fi fingerprinting has to be applied to update positions during such periods. Although fingerprinting cannot provide the same level of accuracy

as ranging based positioning, but it is a good solution to bridging the gap during the intermittent availability of relative ranging. Integrating conventional fingerprinting to a collaborative positioning system has become a backup to ensure the continuity of the positioning solution provided by the system.

An improved fingerprinting algorithm is implemented in Section 6.4 to provide more accurate and reliable fingerprinting results. This improvement is achieved by enhancing information in both phases of fingerprinting. First of all, the confidence of the RSS_{FP} for a specific fingerprint is generated by analysing the collected RSS over a period of time and from different users during the training phase. As a result, the RSS of each fingerprint in the database is defined by a range, characterised by an RSS_{FP} value and a confidence factor η_{CF}. Secondly, during the positioning phase, the potential fingerprints are found by searching for fingerprints whose $RSS_{FP} \pm \eta_{CF}$ range can cover the current RSS_P. By applying the improved fingerprinting method, only those fingerprints that are very likely to be close to the true location will be returned as potential fingerprints. The improved algorithm is applied in all previous algorithms that have involved Wi-Fi fingerprinting, i.e. PDR/Wi-Fi integration, WARCP.

As shown in previous trials, the integration of PDR and ranging outperforms the integration of PDR and conventional Wi-Fi fingerprinting. However, PDR/Wi-Fi integration performance is improved after applying the improved fingerprinting method. It has the potential of providing the same accuracy level positioning results as ARCP. Therefore, the system may choose which algorithm to apply based on whether ranging measurements are available or if Wi-Fi fingerprints are available.

The improved WARCP is the final positioning algorithm given in this thesis. It is able to achieve metre level accuracy with the maximum error reduced to stay within 5m. It implements measurement corrections adaptively from relative ranging constraint and Wi-Fi fingerprinting. The ranging constraint adaptivity comes from the prediction of the ranging accuracy and network geometry which proves to give the optimal result in correcting the gyro bias of the inertial measurements. The fingerprint adaptivity is based on the availability of the confidence factor of each fingerprint based on history data. Improved WARCP enhanced positioning performance in both accuracy and robustness. This algorithm looks at the situation when users start positioning with no prior knowledge of Wi-Fi data and measurement bias is constrained through relative ranging. During

the positioning phase, fingerprints are collected and trained collaboratively by the users in the network. This information will then be available to use when collaborative units cannot be found in the environment.

As positioning solution is needed in much more environments, the continuity of the positioning solution is just as important as the accuracy and reliability of the estimations and the system should be aware that the adaptive information may not always be available. Throughout the discussions in this thesis, we have formed several backup methods to provide continuous positioning even when we lack some information. With full availability, the system should have information on inertial measurements, map information, Wi-Fi signals and relative ranging measurements. Of all the available information, Wi-Fi fingerprinting is the only solution that is able to provide absolute positioning independent to other information, even though very poorly. Inertial measurements and relative ranging measurements are only capable of providing relative navigation based on an initial positioning, yet their relative measurements can be quite accurate. In many previous works and the work in this thesis, we can quite confidently say that improved positioning estimation can be achieved through the integration and collaboration of the different sensors and users, even if just a selection of them.

Chapter 7
Conclusions and recommendations

The problems encountered in indoor positioning calls for more attention as LBS applications are rapidly increasing hence its requirement for indoor positioning is becoming ever more higher. To provide continuous positioning and tracking solutions to such services in all environments, a seamless positioning solution is required which can achieve positioning regardless of the environment and the available sensors. While GNSS positioning in the outdoor environment has become as a mature technology, the search for reliable indoor positioning is still on-going research as different technologies and methods are still been tested. From low-cost IMUs, Wi-Fi and Bluetooth signals, to proximity sensors and RFID tags, a wide range of sensors have been applied to provide indoor positioning in different environments and situations. However, indoor environment is complicated and prone to rapid change, not to mention disturbance. At the moment, there is no single system which is suitable for positioning in all the different indoor environments. This thesis provides a collaborative solution to indoor positioning, where the positioning system can integrate different sensors and data from the current environment based on what is available and which is suitable. The proposed collaborative indoor positioning method integrates low-cost inertial measurements, Wi-Fi fingerprinting, building map and relative ranging measurements depending on which is available.

7.1 Conclusions

The research in this thesis has proposed a collaborative positioning method that looks into two main aspects: the collaboration between a network of units and the the integration of different sensors and signals, especially inertial measurement and wireless signals measurements (Wi-Fi and UWB).

Collaborative positioning brings together multiple users to form a local positioning network by integrating their relative ranging measurements. The theoretical positioning performance of different collaborative networks

and conditions is analysed by Cramer Rao Lower Bound (CRLB). This generates a basic understanding of positioning performance when the network is formed of different geometries and also when the rover is at different locations within the network. The CRLB analysis shows that the positioning performance is affected greatly by three factors: the accuracy of the ranging measurement, the relative geometry of the network and the number of units within the network, i.e. the network size.

Simulations show that positioning is influenced by the position of the units in the network relative to the current rover of interest, which can be reflected by the network horizontal DOP (HDOP). Hence HDOP is applied to analyse the network and predict the network positioning performance. A small HDOP indicates a geometry where the units are more evenly spread out, thus provides more effective constraint on the measurement errors of the rover. This factor is taken into account when designing the constraint boundary. A network with smaller HDOP will have a tighter constraint threshold which restricts the measurement error from increasing, where a network with large HDOP will not such effective constraint on the measurement error.

The size of the network is also reflected by HDOP, where a network with more units will have a smaller HDOP than network with less units. As small HDOP has better effect on relative ranging constraint, a network with more units would be preferable. However, increasing units will increasing computation time. Therefore, the balance for optimal positioning performance and high computation efficiency is to select a network with three to four units.

HDOP reflects the network geometry in a static scenario or the current situation at a certain epoch. However, as the positioning system navigates the user around an indoor environment, users face a dynamically changing environment, where the geometry between the units and ranging measurements is constantly changing. The modified-DOP (MDOP) is developed to take into account all the aspects of the static situation, as well as relative motion of the user and the relative bias of the system measurement. MDOP reflects the geometry and size of the current network, the predicted ranging accuracy and the relative direction of the user to the anchor and other rovers in the network. Particle filter based adaptive collaborative indoor pedestrian positioning algorithms, ARCP/SARCP, are developed for users to select appropriate networks and relative constraint thresholds based on the network MDOP.

UWB units are used to provide ranging measurements between the rovers in the network. UWB ranging accuracy is affected by LOS and NLOS situations, thus to apply the measurements as collaborative constraints the user should have some idea of the actual ranging accuracy. Analysis of the collected data shows that the received signal characteristics, the data strength of the strongest signal and the first arriving signal, correlates with the ranging accuracy. For example, weak data strength and large difference between the two signal strength reflects a higher possibility of NLOS scenario, hence lower ranging accuracy. Therefore the signal strength helps to predict the ranging accuracy of each arriving measurement. A Gaussian process tool is trained to help and predict the accuracy likelihood based on the received signal strength which provides correct prediction up to 90%. The detected ranging accuracy level is fed into MDOP so the network can adjust ranging constraint based the ranging accuracy.

The proposed adaptive collaborative positioning algorithms are simulated, tested in trials and compared to PDR, basic collaborative positioning algorithm. Adaptive collaborative positioning improves positioning accuracy by 60% and achieves metre-level positioning accuracy with a network of two rovers and one anchor.

Improvement on Wi-Fi fingerprinting is also explored in this work. Fingerprinting is firstly integrated with PDR, forming the fingerprint mapping (FPM) algorithm to produce more stable positioning results. A more efficient fingerprint database training method using Gaussian process regression (GPR) is applied to reduce training time and the number of required training points. Training effort is further reduced by introducing collaborative training, where training is carried out during the collaborative training phase. A Wi-Fi RSS training data vector is stored every time the user achieves a positioning estimation. The database can start from only one training dataset and build up as users travel further. Although the receiver is never static at any location, database quality can be enhanced by collecting from different users and also over different periods of time.

From all historic data collected by users, a confidence factor is derived for each fingerprint in the database, indicating the variance of noise to expect at the specific location hence the likelihood of receiving the average RSS at this location and also the long-term signal strength, i.e. whether the RSS is reducing, increasing or stable over the longer period. This improved database reflects the change in the wireless signal environment and enables users to perform fingerprinting based on the latest updated

signal measurements. A Wi-Fi integrated adaptive ranging collaborative positioning (WARCP) is proposed where the user can adjust between integrating relative ranging or Wi-Fi measurements or both to correct inertial measurement error depending on what is available. Relative ranging constraint within the WARCP is applied adaptively according to the network and ranging measurement quality. Fingerprinting is performed based on the improved fingerprint database, thus extracted potential fingerprints are closer to the true location. By applying WARCP, the positioning system maintains metre level positioning accuracy while going through several different positioning phases. The maximum positioning error remains within 10m when relative ranging is available, or 5m when both ranging and improved fingerprinting is available.

For all adaptive collaborative positioning algorithms proposed in this, ARCP, SARCP and WARCP, positioning accuracy and reliability is improved, especially reducing the maximum error. Hence reducing the number of outliers and positioning failure. Furthermore, positioning robustness is enhanced as the system is able to recover from temporary failures. The wall constraint condition, which is required in most particle filter based indoor navigation solutions, is removed, hence giving users the freedom to navigate in new environments where the knowledge of walls and internal structures are unknown. While particle filters improve positioning accuracy in complicated situations, the adaptively integrated measurements reduce the required number of particles and improve positioning efficiency.

7.2 Recommendations and future work

One of the major disadvantages of particle filters is the computation burden. As increasing the particle size reduces estimation error, it will also increase computation load. Collaborative positioning accuracy is improved by integrating relative ranging constraints. However, performing the ranging constraint in the presented collaborative algorithms requires huge computation effort, especially ranging between rovers where each particle pair has to be computed. Further investigation should be carried out to identify the computation cost for different particle size and number of integrated ranging, so that the system can balance between particle numbers, computation cost and positioning accuracy.

The method of choosing the appropriate ranging should also be further examined. While this work focuses on choosing units and ranging measurements to enhance positioning accuracy, further analysis should also be made to ensure computation efficiency when selecting number of

units. In the real world, when a rover enters an indoor environment, there could potentially be tens or hundreds of units and users around. Even though SARCP tries to enhance efficiency by only integrating the units that form the optimal network, but its selection process is carried out by going through all possible combinations first and comparing them. However, when hundreds of different combinations are available, it would be impossible to achieve real time positioning due to heavy computation burden. Therefore, in reality, a more intelligent scheme should be developed to choose units more efficiently.

As Wi-Fi fingerprinting is improved by implementing collaborative positioning, this brings about potentials as well as problems. it is well-known that the actual RSS value is dependent on the data collection hardware. Therefore, when collaborative training analyse the RSS collected from several different equipments, users should be aware of a slight bias or offset between the RSS from each equipment. Although this problem has been avoided in this research by always using the same hardware to collect Wi-Fi RSS, but this bias must be considered and dealt with when used in a real scenario.

Training the fingerprint database collaboratively brings about great potential as it is fundamentally similar to crowdsourcing RSS from a vast number of users in the building. Positioning systems can make use of the large amount of data when sufficient amount of fingerprints are collected. Dense fingerprint database not only provides good indication of the RSS pattern throughout the entire floor plan, but it can also be applied to extract useful environment information, such identifying locations with more pedestrians, locations with higher noise and disturbance, as well as learning about the structure of the building such as identifying walls. Further work can be carried out to analyse such crowd sourced database and apply this information to enhance positioning performance and user experience for LBS applications.

Bibliography

Abdulrahim, K., Hide, C., Moore, T. and Hill, C. (2011) Aiding low cost inertial navigation with building heading for pedestrian navigation. **Journal of Navigation** 64(02):pp.219–233.

Abdulrahim, K., Hide, C., Moore, T. and Hill, C. (2012) Using constraints for shoe mounted indoor pedestrian navigation. **Journal of Navigation** 65(01):pp.15–28.

Abhayawardhana, V., Wassell, I., Crosby, D., Sellars, M. and Brown, M. (2005) Comparison of empirical propagation path loss models for fixed wireless access systems. **2005 IEEE 61st Vehicular Technology Conference,VTC 2005-Spring, Vol.1, 30 May-1 June 2005, Stockholm**. IEEE, pp.73–77.

AEGIS Engineering and Quotient Associates (2013) **Study on the use of wi-fi for metropolitan area applications: Final report for Ofcom**. Technical report. [Online]. Available at: http://stakeholders.ofcom.org.uk/binaries/research/technology-research/2013/wifi-report.pdf [Accessed 1 September 2014].

Afonso, M. (2008) **Particle filter and extended kalman filter for nonlinear estimation: a comparative study**, Instituto Superior Tecnico (IST), the School of Engineering of the Technical University of Lisbon.

Akl, R., Dinesh Tummala and Xinrong Li (2006) Indoor propagation modeling at 2.4 GHz for IEEE 802.11 networks. **Sixth International Association of Science and Technology for Development (IASTED) International Multi-Conference on Wireless and Optical Communications, July 3-5 2006, Banff, Canada**. International Association of Science and Technology for Development.

Alam, N., Balaei, A. T. and Dempster, A. G. (2011) A filtering method for improving the precision of cooperative positioning in VANETs. **International Global Navigation Satellite Systems Society IGNSS Symposium 2011, 15-17 November 2011, Sydney, NSW, Australia**. IGNSS.

Alhmiedat, T., Samara, G. and Salem, A. O. A. (2013) An indoor fingerprinting localization approach for ZigBee wireless sensor networks. **European Journal of Scientific Research** 105(2):pp.190–202.

Alsindi, N., Duan, C., Jinyun Zhang and Tsutomu Tsuboi (2009) NLOS channel identification and mitigation in ultra wideband ToA-based wireless sensor networks. **Positioning, Navigation and Communication, 2009. WPNC 2009. 6th Workshop on, 19 March 2009, Hannover**. IEEE, pp.59–66.

Alsindi, N. and Pahlavan, K. (2008) Cooperative localization bounds for indoor ultra-wideband wireless sensor networks. **EURASIP Journal on Advances in Signal Processing** 2008(1):pp.852509.

Altun, K. and Barshan, B. (2012) Pedestrian dead reckoning employing simultaneous activity recognition cues. **Measurement Science and Technology** 23(2):pp.025103.

Amini, A., Vaghefi, R. M., de la Garza, J. M. and Buehrer, R. M. (2014) GPS-free cooperative mobile tracking with the application in vehicular networks. **Positioning Navigation and Communication (WPNC), 2014 11th Workshop on, 12-13 March 2014, Dresden**. IEEE, pp.1–6.

Arulampalam, M., Maskell, S., Gordon, N. and Clapp, T. (2002) A tutorial on particle filters for online nonlinear/non-gaussian bayesian tracking. **IEEE Transactions on Signal Processing** 50(2):pp.174–188.

Aspnes, J., Eren, T., Goldenberg, D., Morse, A., Whiteley, W., Yang, Y., Anderson, B. and Belhumeur, P. (2006) A theory of network localization. **IEEE Transactions on Mobile Computing** 5(12):pp.1663–1678.

Atia, M. M. M. (2013) **Nonlinear estimation techniques for high resolution indoor positioning systems**. PhD thesis, Queen's University, Ontario, Canada.

Azenha, A. and Carvalho, A. (2008) Dynamic analysis of AGV control under dead-reckoning algorithm. **Robotica** 26(05).

Bahl, P. and Padmanabhan, V. N. (2000) RADAR: An in-building RF-based user location and tracking system. **INFOCOM 2000, Proceedings of Nineteenth Annual Joint Conference of the IEEE Computer and Communications Societies, Vol.2, 26-30 Mar 2000, Tel Aviv**. IEEE, pp.775–784.

Bao, H. and Wong, W.-C. (2013) An indoor dead-reckoning algorithm with map matching. **Wireless Communications and Mobile Computing Conference (IWCMC), 2013 9th International, 1-5 July 2013, Sardinia**. IEEE, pp.1534–1539.

Bao, H. and Wong, W.-C. (2014) A novel map-based dead-reckoning algorithm for indoor localization. **Journal of Sensor and Actuator Networks** 3(1):pp.44–63.

Beauregard, S. (2007) Omnidirectional pedestrian navigation for first responders. **4th Workshop on Positioning, Navigation and Communication, WPNC'07, 22 March 2007, Hannover**. IEEE, pp.33–36.

Benedetto, F., Giunta, G., Toscano, A. and Vegni, L. (2007) Dynamic LOS/NLOS statistical discrimination of wireless mobile channels. **IEEE 65th Vehicular Technology Conference, VTC2007-Spring, 22-25 April 2007, Dublin**. IEEE, pp.3071–3075.

Benford, S. (2005) Future location-based experiences. **JISC Technology and Standards Watch. Available at: http://www, jisc.ac.uk/techwatch** .

Bluetooth (2014) **The low energy technology behind bluetooth smart**, Bluetooth. [Online]. Available at: http://www.bluetooth.com/Pages/low-energy-tech-info.aspx [Accessed 20 October 2014].

Bolliger, P. (2008) Redpin - adaptive, zero-configuration indoor localization through user collaboration. **Proceedings of the first ACM international workshop on Mobile entity localization and tracking in GPS-less environments, 14-19 September, 2008, San Francisco, CA, USA**. ACM, pp.55–60.

Bonenberg, L. K., Hancock, C. M. and Roberts, G. W. (2010) Indoor multipath effect study on the locata system. **Journal of Applied Geodesy** 4(3).

Borre, K. (ed.) (2007) **A software-defined GPS and Galileo receiver: a single-frequency approach**. Applied and numerical harmonic analysis, Birkhauser, Boston, Mass.

Bose, A. and Foh, C. H. (2007) A practical path loss model for indoor WiFi positioning enhancement. **Information, Communications & Sig-**

nal Processing, 2007 6th International Conference on, 10-13 Dec. 2007, IEEE, pp.1–5.

Bouet, M. and dos Santos, A. L. (2008) RFID tags: Positioning principles and localization techniques. **Wireless Days, 2008, WD'08, 1st IFIP, 24-27 Nov. 2008**, IEEE, pp.1–5.

Breed, G. (2005) A summary of FCC rules for ultra wideband communications. **High Frequency Electronics** 4(1):pp.42–44. [Online]. Available at: http://omidi.iut.ac.ir/SDR/2007/WebPages/07_UWB/Refrences/3.pdf [Accessed 15 September 2014].

Casas, R., Marco, A., Guerrero, J. J. and Falco, J. (2006) Robust estimator for non-line-of-sight error mitigation in indoor localization. **EURASIP Journal on Advances in Signal Processing** 2006:pp.1–9.

Cebula III, Stanley L. , Aftab Ahmad, Luay A. Wahsheh, Jonathan M. Graham, Aurelia T. Williams, Cheryl V. Hinds and Sandra J. DeLoatch (2011) Location determination systems for WLANs. **Proceedings of the 2011 International Conference on Wireless Networks, 18-21 July 2011**.

Chan, L.-W., Chiang, J.-R., Chen, Y.-C., Ke, C.-N., Hsu, J. and Chu, H.-H. (2006) Collaborative localization: Enhancing WiFi-based position estimation with neighborhood links in clusters. **Pervasive Computing: Proceedings of 4th International Conference, Pervasive, Vol.3968, Dublin, Ireland, 7-10 May 2006,**, Springer Berlin Heidelberg, Berlin, Heidelberg, pp.50–66.

Chang, C. and Sahai, A. (2004) Estimation bounds for localization. **Sensor and Ad Hoc Communications and Networks, 2004 First Annual IEEE Communications Society Conference on, IEEE SECON 2004, 4-7 Oct. 2004, Santa Clara, CA, USA**. IEEE, pp.415–424.

Chawathe, S. S. (2009) Low-latency indoor localization using bluetooth beacons. **Intelligent Transportation Systems, 2009. ITSC '09. 12th International IEEE Conference on, 4-7 Oct. 2009, St. Louis, MO**. IEEE, pp.1–7.

Chen, C.-S., Chiu, Y.-J., Lee, C.-T. and Lin, J.-M. (2013) Calculation of weighted geometric dilution of precision. **Journal of Applied Mathematics** 2013:pp.1–10.

Chen, Z. (2003) **Bayesian filtering: From kalman filters to particle filters, and beyond**. [Online]. Available at: http://www.dsi.unifi.it/users/chisci/idfric/Nonlinear_filtering_Chen.pdf [Accessed 20 October 2014].

Cheung, K.-W., Sau, J.-M. and Murch, R. (1998) A new empirical model for indoor propagation prediction. **IEEE Transactions on Vehicular Technology** 47(3):pp.996–1001.

Chin, W., Fan, Z. and Haines, R. (2014) Emerging technologies and research challenges for 5g wireless networks. **IEEE Wireless Communications** 21(2):pp.106–112.

Chincholle, D., Goldstein, M., Nyberg, M. and Eriksson, M. (2002) Lost or found? a usability evaluation of a mobile navigation and location-based service. **Mobile HCI 2002, Proceedings of 4th International Symposium on Human Computer Interaction with Mobile Devices, Vol.2411, Pisa, Italy, September 2002**, Springer, Berlin, Heidelberg, pp.211–224.

Choliz, J., Hernandez-Solana, A. and Valdovinos, A. (2011) Evaluation of algorithms for UWB indoor tracking. **Positioning Navigation and Communication (WPNC), 2011 8th Workshop on, 7-8 April 2011, Dresden**. IEEE, pp.143–148.

Cinefra, N. (2012) **Adaptive indoor positioning system based on Bluetooth Low Energy RSSI**. Thesis, Politecnico Di Milano, Italy.

Cisco Systems, Inc (2011) **Wireless LAN design guide for high density client environments in higher education**. [Online]. Available at: http://www.cisco.com/web/strategy/docs/education/cisco_wlan_design_guide.pdf [Accessed 22 October 2014].

Cisco Systems, Inc (2012) **Cisco aironet 1140 series access point data sheet**. [Online]. Available at: http://www.cisco.com/c/en/us/products/collateral/wireless/aironet-1130-ag-series/datasheet_c78-502793.html [Accessed 15 September 2014].

Cisco Systems, Inc (2013) **Cisco wireless LAN controller configuration guide, release 7.4**. [Online]. Available

at: http://www.cisco.com/c/en/us/td/docs/wireless/controller/7-4/configuration/guides/consolidated/b-cg74-CONSOLIDATED.pdf [Accessed 22 October 2014].

Convergis and Logicalis (2011) **UoN-Jubilee-Geospatial WLAN site survey report**. Technical Report Version 1.

Crisan, D., Moral, P. D. and Lyons, T. J. (1999) Interacting particle systems approximations of the kushner stratonovitch equation. **Advances in Applied Probability** 31:pp.819–838.

Curran, K., Furey, E., Lunney, T., Santos, J., Woods, D. and McCaughey, A. (2011) An evaluation of indoor location determination technologies. **Journal of Location Based Services** 5(2):pp.61–78.

Dardari, D., Conti, A., Ferner, U., Giorgetti, A. and Win, M. Z. (2009) Ranging with ultrawide bandwidth signals in multipath environments. **Proceedings of the IEEE** 97(2):pp.404–426.

Dempster, A. (2006) Dilution of precision in angle-of-arrival positioning systems. **Electronics Letters** 42(5):pp.291.

Dempster, A. (2009) QZSS's indoor messaging system: GNSS friend or foe? **Inside GNSS** January/Febuary:pp.37–40.

Ding, W., Wang, J., Rizos, C. and Kinlyside, D. (2007) Improving adaptive kalman estimation in GPS/INS integration. **Journal of Navigation** 60(03):pp.517.

Dissanayake, M., Newman, P., Clark, S., Durrant-Whyte, H. and Csorba, M. (2001) A solution to the simultaneous localization and map building (SLAM) problem. **IEEE Transactions on Robotics and Automation** 17(3):pp.229–241.

Doucet, A., Freitas, N. and Gordon, N. (2001) An introduction to sequential monte carlo methods. **Sequential Monte Carlo Methods in Practice**, Vol. Part 1, Springer New York, New York, NY, pp.3–14.

Doucet, A., Godsill, S. and Andrieu, C. (2000) On sequential monte carlo sampling methods for bayesian filtering. **Statistics and Computing** 10(3):pp.197–208.

Duan, Z., Cai, Z. and Min, H. (2014) Robust dead reckoning system for mobile robots based on particle filter and raw range scan. **Sensors** 14(9):pp.16532–16562.

Dutzler, Roland, Ebner, Martin and Brandner, Robert (2013) Indoor navigation by WLAN location fingerprinting: Reducing trainings-efforts with interpolated radio maps. **UBICOMM 2013, The Seventh International Conference on Mobile Ubiquitous Computing, Systems, Services and Technologies, September 29, 2013, Porto, Portugal**. IARIA, pp.1–6.

Ekahau (2014) **Ekahau**. [Online]. Available at: http://www.ekahau.com [Accessed 27 October 2014].

Evennou, F. and Marx, F. (2006) Advanced integration of WiFi and inertial navigation systems for indoor mobile positioning. **EURASIP Journal on Advances in Signal Processing** 2006:pp.1–12.

Fahed, D. and Liu, R. (2013) Wi-Fi-Based localization in dynamic indoor environment using a dynamic neural network. **International Journal of Machine Learning and Computing** pp.127–131.

Faragher, R. (2012) Understanding the basis of the kalman filter via a simple and intuitive derivation [lecture notes]. **IEEE Signal Processing Magazine** 29(5):pp.128–132.

Faragher, R. and Harle, R. (2013) SmartSLAM - an efficient smartphone indoor positioning system exploiting machine learning and opportunistic sensing. **ION GNSS+ 2013, Proceedings of the 26th International Technical Meeting of The Satellite Division of the Institute of Navigation, 16-20 September 2013, Nashville, TN**. ION, pp.1006–1019.

Faragher, R. M., Sarno, C. and Newman, M. (2012) Opportunistic radio SLAM for indoor navigation using smartphone sensors. **Position Location and Navigation Symposium (PLANS), 2012 IEEE/ION, 23-26 April 2012, Myrtle Beach, SC**. IEEE, pp.120–128.

Farid, Z., Nordin, R. and Ismail, M. (2013) Recent advances in wireless indoor localization techniques and system. **Journal of Computer Networks and Communications** 2013:pp.1–12.

Farshad, A., Jiwei Li, Marina, M. K. and Garcia, F. J. (2013) A microscopic look at WiFi fingerprinting for indoor mobile phone localization in diverse environments. **Indoor Positioning and Indoor Navigation (IPIN),**

2013 International Conference on, 28-31 Oct. 2013, Montbeliard-Belfort. IEEE, pp.1–10.

Farshad, A., Marina, M. K. and Garcia, F. (2014) Urban WiFi characterization via mobile crowdsensing. **Network Operations and Management Symposium (NOMS), 2014 IEEE, 5-9 May 2014, Krakow**. IEEE, pp.1–9.

Faruqi, F. A. and Turner, K. J. (2000) Extended kalman filter synthesis for integrated global positioning/inertial navigation systems. **Applied Mathematics and Computation** 115(2-3):pp.213–227.

Federal Communications Commission (FCC) (2002) **Federal communications commission in the matter of revision of part 15 of the commissions rules regarding ultra-wideband transmission systems**, FCC.

Feng, W., Zhao, H., Zhao, Q. and Li, J. (2013) Integration of GPS and low cost INS for pedestrian navigation aided by building layout. **Chinese Journal of Aeronautics** 26(5):pp.1283–1289.

Ferris, B., Hahnel, D. and Fox, D. (2006) Gaussian processes for signal strength-based location estimation.

Fet, N., Handte, M. and Marron, P. J. (2013) A model for WLAN signal attenuation of the human body. **Proceedings of the 2013 ACM international joint conference on Pervasive and ubiquitous computing, UbiComp '13, September 8-12, 2013, Zurich, Switzerland**. ACM, pp.499–508.

Foerster, J. (2001) The effects of multipath interference on the performance of UWB systems in an indoor wireless channel. **VTC 2001 Spring. IEEE VTS 53rd, Vehicular Technology Conference,Vol.2, 06- 09 May 2001, Rhodes**. IEEE, pp.1176–1180.

Fox, D., Hightower, J., Lin Liao, Schulz, D. and Borriello, G. (2003) Bayesian filtering for location estimation. **IEEE Pervasive Computing** 2(3):pp.24–33.

Fox, J. (2014) **Visible light communications in indoor positioning systems report - 2014**. [Online]. Available at: https://technology.ihs.com/511115/visible-light-communications-in-indoor-positioning-systems-2014 [Accessed 26 November 2014].

Foxlin, E. (2005) Pedestrian tracking with shoe-mounted inertial sensors. **IEEE Computer Graphics and Applications** 25(6):pp.38–46.

Fry, R. H. and Wells, P. J. (1954) Dead reckoning procedures in air navigation. **Journal of Navigation** 7(04):pp.324.

Furey, E., Curran, K. and McKevitt, P. (2012) HABITS: a bayesian filter approach to indoor tracking and location. **International Journal of Bio-Inspired Computation** 4(2):pp.79.

Garello, R., Presti, L. L., Corazza, G. E. and Samson, J. (2012) Peer-to-peer cooperative positioning part I: GNSS-aided acquisition. **Inside GNSS** March/April. [Online]. Available at: http://www.insidegnss.com/node/3150.

Garello, R., Samson, J., Spirito, M. A. and Wymeersch, H. (2012) Peer-to-peer cooperative positioning part II: Hybrid devices with GNSS & terrestrial ranging capability. **Inside GNSS** July/August. [Online]. Available at: http://www.insidegnss.com/node/2980.

Ghavami, M. (2004) **Ultra-wideband signals and systems in communication engineering**. John Wiley & Sons, Chichester.

Godha, S. (2006) **Performance Evaluation of Low Cost MEMS-Based IMU Integrated With GPS for Land Vehicle Navigation Application**. MSc thesis, University of Calgary.

Godha, S. and Lachapelle, G. (2008) Foot mounted inertial system for pedestrian navigation. **Measurement Science and Technology** 19(7):pp.075202.

Gordon, N., Salmond, D. and Smith, A. (1993) Novel approach to nonlinear/non-gaussian bayesian state estimation. **IEE Proceedings of Radar and Signal Processing,** pp.107–113.

Gray, R. and Maybeck, P. (1995) An integrated GPS/INS/baro and radar altimeter system for aircraft precision approach landings. **NAECON1995, Aerospace and Electronics Conference, Proceedings of the IEEE 1995 National, Vol.1, 22-26 May 1995, Dayton, OH**. IEEE, pp.161–168.

Grewal, M. S., Andrews, A. P. and Bartone, C. (2013) **Global navigation satellite systems, inertial navigation, and integration**. Third edition ed., John Wiley & Sons, Hoboken.

Groves, P. D. (2013a) The PNT boom. **Inside GNSS** March/April. [Online]. Available at: http://www.insidegnss.com/node/3442.

Groves, P. D. (2013b) **Principles of GNSS, inertial, and multisensor integrated navigation systems**. GNSS technology and application series, 2nd ed., Artech House, Boston.

Groves, P. D. (2014) The complexity problem in future multisensor navigation and positioning systems: A modular solution. **The Journal of Navigation** 67(02):pp.311–326.

Groves, P. D., Wang, L., Walter, D., Martin, H., Voutsis, K. and Jiang, Z. (2014) The four key challenges of advanced multisensor navigation and positioning. **IEEE/ION Position, Location, and Navigation Symposium (PLANS) 2014, 5-8 May 2014, Monterey, CA**. IEEE, pp.773–792.

GSMA Intelligence (2014) **Measuring mobile penetration**. Technical report, GSMA Intelligence. [Online]. Available at: https://gsmaintelligence.com/files/analysis/?file=2014-05-22-measuring-mobile-penetration.pdf [Accessed 27 November 2014].

Guvenc, I., Chong, C.-C., Watanabe, F. and Inamura, H. (2008) NLOS identification and weighted least-squares localization for UWB systems using multipath channel statistics. **EURASIP Journal on Advances in Signal Processing** 2008(1):pp.271984.

Han, S., Kim, J., Park, C.-H., Yoon, H.-C. and Heo, J. (2009) Optimal detection range of RFID tag for RFID-based positioning system using the k-NN algorithm. **Sensors** 9(6):pp.4543–4558.

Harle, R. (2013) A survey of indoor inertial positioning systems for pedestrians. **IEEE Communications Surveys & Tutorials** 15(3):pp.1281–1293.

Hasani, M., Lohan, E.-S., Sydanheimo, L. and Ukkonen, L. (2014) Path-loss model of embroidered passive RFID tag on human body for indoor positioning applications. **RFID Technology and Applications Conference (RFID-TA) 2014, 8-9 September 2014, Tampere**. IEEE, pp.170–174.

Hata, M. (1980) Empirical formula for propagation loss in land mobile radio services. **IEEE Transactions on Vehicular Technology** 29(3):pp.317–325.

Hide, C., Moore, T. and Hill, C. (2007) A multi-sensor navigation filter for high accuracy positioning in all environments. **Journal of Navigation** 60(03):pp.409.

Hide, C., Moore, T. and Smith, M. (2003) Adaptive kalman filtering for low-cost INS/GPS. **Journal of Navigation** 56(1):pp.143–152.

Hide, C., Moore, T. and Smith, M. (2004) Adaptive kalman filtering algorithms for integrating GPS and low cost INS. **Position Location and Navigation Symposium, 2004. PLANS 2004, 26-29 April 2004, Monterey, CA**. IEEE, pp.227–233.

Hofmann-Wellenhof, B., Legat, K. and Wieser, M. (2003) **Navigation**. Springer Vienna, Vienna.

Honkavirta, V., Perala, T., Ali-Loytty, S. and Piche, R. (2009) A comparative survey of WLAN location fingerprinting methods. **Positioning, Navigation and Communication, 6th Workshop on, WPNC 2009, 19-19 March 2009, Hannover**. IEEE, pp.243–251.

Hossain, A. K. M. M. and Soh, W.-S. (2007) A comprehensive study of bluetooth signal parameters for localization. **Personal, Indoor and Mobile Radio Communications, IEEE 18th International Symposium on, PIMRC 2007, 3-7 September 2007, Athens**. IEEE, pp.1–5.

Huang, J., Millman, D., Quigley, M., Stavens, D., Thrun, S. and Aggarwal, A. (2011) Efficient, generalized indoor WiFi GraphSLAM. **Robotics and Automation (ICRA), 2011 IEEE International Conference on, 9-13 May 2011, Shanghai**. IEEE, pp.1038–1043.

IEEE Computer Society (2012) **Part 11: Wireless LAN medium access control (MAC) and physical layer (PHY) specifications**. IEEE std 802.11-2012. [Online]. Available at: http://ieeexplore.ieee.org/servlet/opac?punumber=6178209 [Accessed 22 October 2014].

Ingram, S., Harmer, D. and Quinlan, M. (2004) UltraWideBand indoor positioning systems and their use in emergencies. **Position Location and Navigation Symposium 2004, PLANS 2004, 26-29 April 2004, Monterey, CA, USA**. IEEE, pp.706–715.

Jacobson, J. (2004) **Lower Bounds on Estimator Error and the Threshold Effect**. Thesis for the degree with honors of bachelor of arts, Harvard College.

Jadhav, V. (2014) A study on LiFi: Light fidelity technology. **International Journal of Scientific & Engineering Research** 5(6):pp.709–710.

Jia, T. and Buehrer, R. (2010) On the optimal performance of collaborative position location. **IEEE Transactions on Wireless Communications** 9(1):pp.374–383.

Julier, S. and Uhlmann, J. (2004) Unscented filtering and nonlinear estimation. **Proceedings of the IEEE** 92(3):pp.401–422.

Julier, S., Uhlmann, J. and Durrant-Whyte, H. (1995) A new approach for filtering nonlinear systems. **American Control Conference, Proceedings of the 1995, Vol.3, 21-23 June 1995, Seattle, WA**. IEEE, pp.1628–1632.

Julier, S., Uhlmann, J. and Durrant-Whyte, H. (2000) A new method for the nonlinear transformation of means and covariances in filters and estimators. **IEEE Transactions on Automatic Control** 45(3):pp.477–482.

Jung, S., Lee, C.-O. and Han, D. (2011) Wi-fi fingerprint-based approaches following log-distance path loss model for indoor positioning. **Intelligent Radio for Future Personal Terminals (IMWS-IRFPT), 2011 IEEE MTT-S International Microwave Workshop Series on, 24-25 August 2011, Daejeon**. IEEE, pp.1–2.

Kaemarungsi, K. and Krishnamurthy, P. (2012) Analysis of WLANs received signal strength indication for indoor location fingerprinting. **Pervasive and Mobile Computing** 8(2):pp.292–316.

Kalliola, K. (2011) **High accuracy indoor positioning based on BLE**, Nokia Research Center Presentation.

Kalman, R. E. (1960) A new approach to linear filtering and prediction problems. **Journal of Basic Engineering** 82(1):pp.35–45.

Kay, S. M. (1993) **Fundamentals of statistical signal processing**. Prentice Hall signal processing series, Prentice-Hall PTR, Englewood Cliffs, N.J.

Kempe, V. (2011) **Inertial MEMS: principles and practice**. Cambridge University Press, Cambridge ; New York.

Kennedy, J. (2005) **Pseudolite positioning system and method**. Google Patents. US Patent 6,952,158. [Online]. Available at: http://www.google.com/patents/US6952158.

Khan, A. M. (2011) **Human Activity Recognition Using A Single Triaxial Accelerometer**. PhD thesis, Kyung Hee University, Seoul, Korea.

Khan, F. A., Rizos, C. and Dempster, A. G. (2010) Locata performance evaluation in the presence of wide- and narrow-band interference. **Journal of Navigation** 63(03):pp.527–543.

Kim, J.-N., Ryu, M.-H., Yang, Y.-S. and Hong, J.-Y. (2014) Estimation of walking direction estimation using a shoe-mounted acceleration sensor. **International Journal of Multimedia and Ubiquitous Engineering** 9(5):pp.215–222.

Kim, J. W., Jang, H. J., Hwang, D.-H. and Park, C. (2004) A step, stride and heading determination for the pedestrian navigation system. **Journal of Global Positioning Systems** 3(1-2):pp.273–279.

King, T., Kopf, S., Haenselmann, T., Lubberger, C. and Effelsberg, W. (2006) COMPASS: A probabilistic indoor positioning system based on 802.11 and digital compasses. **Proceedings of the 1st international workshop on Wireless network testbeds, experimental evaluation & characterization, WiNTECH '06, 29 September 2006, Los Angeles, CA, USA**. ACM, pp.34–40.

Koppanyi, Z., Toth, C., Grejner-Brzezinska, D. and Jozkow, G. (2014) Performance analysis of UWB technology for indoor positioning. **Proceedings of the 2014 International Technical Meeting of The Institute of Navigation, 2014 ION International Technical Meeting (ITM), 27-29 January 2014, San Diego, California**. ION, pp.154 – 165.

Kurazume, R. and Hirose, S. (2000) An experimental study of a cooperative positioning system. **Autonomous Robots** 8(1):pp.43–52.

Ladetto, Q. (2000) On foot navigation: continuous step calibration using both complementary recursive prediction and adaptive kalman filtering. **ION GPS 2000, Proceedings of the 13th International Technical**

Meeting of the Satellite Division of The Institute of Navigation, 19-22 September 2000, Salt Lake City, UT. ION, pp.1735 – 1740.

Langley, R. B. (1999) Dilution of precision. **GPS World** 10(5):pp.52–59.

Lee, J.-Y. and Scholtz, R. (2002) Ranging in a dense multipath environment using an UWB radio link. **IEEE Journal on Selected Areas in Communications** 20(9):pp.1677–1683.

Lei, L. (2014) A method of cooperative localization for multiple moving vehicles. **Journal of Information and Computational Science** 11(3):pp.707–715.

Li, B., Dempster, A. and Tan, Y. K. (2011) Using two global positioning system satellites to improve wireless fidelity positioning accuracy in urban canyons. **IET Communications** 5(2):pp.163–171.

Li, T., Sun, S., Sattar, T. P. and Corchado, J. M. (2014) Fight sample degeneracy and impoverishment in particle filters: A review of intelligent approaches. **Expert Systems with Applications** 41(8):pp.3944–3954.

Liu, W., Chen, Y., Xiong, Y., Sun, L. and Zhu, H. (2014) Optimization of sampling cell size for fingerprint positioning. **International Journal of Distributed Sensor Networks** 2014:pp.1–6.

Lo, C.-C., Chiu, C.-P., Tseng, Y.-C., Chang, S.-A. and Kuo, L.-C. (2011) A walking velocity update technique for pedestrian dead-reckoning applications. **Personal Indoor and Mobile Radio Communications (PIMRC), 2011 IEEE 22nd International Symposium on, 11-14 Sept. 2011, Toronto, ON**. IEEE, pp.1249–1253.

Luo, Y., Hoeber, O. and Chen, Y. (2013) Enhancing wi-fi fingerprinting for indoor positioning using human-centric collaborative feedback. **Human-centric Computing and Information Sciences** 3(1):pp.2.

Mahfouz, M., Cemin Zhang, Merkl, B., Kuhn, M. and Fathy, A. (2008) Investigation of high-accuracy indoor 3-d positioning using UWB technology. **IEEE Transactions on Microwave Theory and Techniques** 56(6):pp.1316–1330.

Marano, S., Gifford, W., Wymeersch, H. and Win, M. (2010) NLOS identification and mitigation for localization based on UWB experimental data. **IEEE Journal on Selected Areas in Communications** 28(7):pp.1026–1035.

Mardeni, R. and Priya, T. S. (2010) Optimised COST-231 hata models for WiMAX path loss prediction in suburban and open urban environments. **Modern Applied Science** 4(9).

Medina, C., Segura, J. and De la Torre, A. (2013) Ultrasound indoor positioning system based on a low-power wireless sensor network providing sub-centimeter accuracy. **Sensors** 13(3):pp.3501–3526.

Merwe, R. v. d., Doucet, A., Freitas, N. d. and Wan, E. (2000) **The unscented particle filter: Technical report**, Cambridge University Engineering Department.

Metageek (2012) **inSSIDer user guide**. [Online]. Available at: http://www.metageek.net/wp-content/uploads/2012/08/MetaGeek_inSSIDer_WiFi-Scanner_UserGuide_2012.pdf [Accessed 20 September 2014].

Minami, M., Fukuju, Y., Hirasawa, K., Yokoyama, S., Mizumachi, M., Morikawa, H. and Aoyama, T. (2004) DOLPHIN: A practical approach for implementing a fully distributed indoor ultrasonic positioning system. **Proceedings of 6th International Conference UbiComp 2004: Ubiquitous Computing,Vol.3205, 7-10 September 2004, Nottingham, UK**. Springer Berlin Heidelberg, pp.347–365.

Mok, E. and Cheung, B. (2013) An improved neural network training algorithm for wi-fi fingerprinting positioning. **ISPRS International Journal of Geo-Information** 2(3):pp.854–868.

Molisch, A., Cassioli, D., Chia-Chin Chong, Emami, S., Fort, A., Kannan, B., Karedal, J., Kunisch, J., Schantz, H., Siwiak, K. and Win, M. (2006) A comprehensive standardized model for ultrawideband propagation channels. **IEEE Transactions on Antennas and Propagation** 54(11):pp.3151–3166.

Molisch, A. F. (2011) **Wireless communications**. 2nd ed., Wiley:IEEE, Chichester, West Sussex, U.K.

Montorsi, F., Pancaldi, F. and Vitetta, G. M. (2011) Statistical characterization and mitigation of NLOS errors in UWB localization systems. **Ultra-Wideband (ICUWB), 2011 IEEE International Conference on, 14-16 September 2011, Bologna**. IEEE, pp.86–90.

Morisue, F. and Ikeda, K. (1989) Evaluation of map-matching techniques. **Vehicle Navigation and Information Systems Conference, 1989. Conference Record, 11-13 September 1989, Toronto, Ontario, Canada**. IEEE, pp.23–28.

Mubaloo Ltd (2014) **Beacons: The technical overview**. [Online]. Available at: http://mubaloo.com/perch/resources/beacons-technical-overviewmibeacons-white-paper.pdf [Accessed 21 October 2014].

Mulloni, A., Wagner, D., Barakonyi, I. and Schmalstieg, D. (2009) Indoor positioning and navigation with camera phones. **IEEE Pervasive Computing** 8(2):pp.22–31.

Multispectral Solutions, Inc. (2006) **Ultra wideband technology for precision indoor personnel location & tracking**, Precision Indoor Personnel Location and Tracking for Emergency Responders. [Online]. Available at: https://www.wpi.edu/Images/CMS/PPL/Multispectral.pdf [Accessed 10 November 2014].

Myers, M., Jorge, A., Mutton, M. and Walker, D. (2012) A comparison of extended kalman filter, particle filter, and least squares localization methods for a high heat flux concentrated source. **International Journal of Heat and Mass Transfer** 55(9-10):pp.2219–2228.

Nguyen, L. T. and Zhang, J. (2013) Wi-fi fingerprinting through active learning using smartphones. **Proceedings of the 2013 ACM Conference on Pervasive and Ubiquitous Computing Adjunct Publication, UbiComp '13 Adjunct, 8-12 September 2013, New York, USA**. ACM, pp.969–976.

Nilsson, J.-O., Zachariah, D., Skog, I. and Handel, P. (2013) Cooperative localization by dual foot-mounted inertial sensors and inter-agent ranging. **EURASIP Journal on Advances in Signal Processing** 2013(1):pp.164.

Nilsson, J., Rantakokko, J., Handel, P., Skog, I., Ohlsson, M. and Hari, K. V. S. (2014) Accurate indoor positioning of firefighters using dual foot-mounted inertial sensors and inter-agent ranging. **Proceedings of the Position, Location and Navigation Symposium (PLANS), 2014 IEEE/ION, 5-8 May 2014, Monterey, CA**. IEEE, pp.631–636.

Nishiguchi, S., Yamada, M., Nagai, K., Mori, S., Kajiwara, Y., Sonoda, T., Yoshimura, K., Yoshitomi, H., Ito, H., Okamoto, K., Ito, T., Muto, S., Ishihara, T. and Aoyama, T. (2012) Reliability and validity of gait analysis by android-based smartphone. **Telemedicine and e-Health** 18(4):pp.292–296.

Niwa, H., Kodaka, K., Sakamoto, Y., Otake, M., Kawaguchi, S., Fujii, K., Kanemori, Y. and Sugano, S. (2008) GPS-based indoor positioning system with multi-channel pseudolite. **Robotics and Automation, IEEE International Conference on, ICRA 2008, 19-23 May 2008, Pasadena, CA**. IEEE, pp.905–910.

Oppermann, I., Hamaainen, M. and Iinatti, J. (2004) **UWB theory and applications**. Wiley, Chichester.

Park, J., Kim, Y. and Lee, J. (2012) Waist mounted pedestrian dead-reckoning system. **Ubiquitous Robots and Ambient Intelligence (URAI), 2012 9th International Conference on, 26-28 November 2012, Daejeon**. IEEE, pp.335–336.

Patwari, N., Ash, J., Kyperountas, S., Hero, A., Moses, R. and Correal, N. (2005) Locating the nodes: cooperative localization in wireless sensor networks. **IEEE Signal Processing Magazine** 22(4):pp.54–69.

Patwari, N. and Hero, A. (2002) Location estimation accuracy in wireless sensor networks. **Signals, Systems and Computers, 2002. Conference Record of the Thirty-Sixth Asilomar Conference on, Vol.2, 3-6 November 2002, Pacific Grove, CA, USA**. IEEE, pp.1523–1527.

Pei, L., Chen, R., Liu, J., Tenhunen, T., Kuusniemi, H. and Chen, Y. (2010) Inquiry-based bluetooth indoor positioning via RSSI probability distributions. **Advances in Satellite and Space Communications (SPACOMM), 2010 Second International Conference on, 13-19 June 2010, Athens**. IEEE, pp.151–156.

Penna, F., Caceres, M. A. and Wymeersch, H. (2010) Cramer-rao bound for hybrid GNSS-terrestrial cooperative positioning. **IEEE Communications Letters** 14(11):pp.1005–1007.

Petovello, M. and Joseph, A. (2010) Measuring GNSS signal strength. **Inside GNSS** (November/ December):pp.20–25.

Priyantha, N. B. (2005) **The Cricket Indoor Location System**. PhD thesis, Massachusetts Institute of Technology, USA.

Priyantha, N. B., Chakraborty, A. and Balakrishnan, H. (2000) The cricket location-support system. **Proceedings of the 6th annual international conference on Mobile computing and networking, MobiCom '00, 06-11 August 2000, Boston, Massachusetts, USA**. ACM, pp.32–43.

Quddus, M. A., Ochieng, W. Y. and Noland, R. B. (2007) Current map-matching algorithms for transport applications: State-of-the art and future research directions. **Transportation Research Part C: Emerging Technologies** 15(5):pp.312–328.

Rai, A., Chintalapudi, K. K., Padmanabhan, V. and Sen, R. (2012) Zee : Zero-effort crowdsourcing for indoor localization. **Proceedings of the 18th annual international conference on Mobile computing and networking, Mobicom '12, 22-26 August 2012, Istanbul, Turkey**. ACM, pp.293–304.

Rainer Mautz (2012) **Indoor Positioning Technologies**. Habilitation thesis for the venia legendi in positioning and engineering geodesy, ETH Zurich.

Rantakokko, J., Stromback, P. and Anderson, P. (2014) Foot- and knee-mounted INS for firefighter localization. **Proceedings of the 2014 International Technical Meeting of The Institute of Navigation, 2014 ION International Technical Meeting (ITM), 27 - 29 January 2014, San Diego, California**. ION, pp.145–153.

Rasmussen, C. E. and Williams, C. K. I. (2006) **Gaussian processes for machine learning**. Adaptive computation and machine learning, MIT Press, Cambridge, Mass.

Ristic, B., Arulampalam, S. and Gordon, N. (2004) **Beyond the Kalman Filter: Particle Filters for Tracking Applications**. Artech House.

Rogers, R. M. (2007) **Applied mathematics in integrated navigation systems**. AIAA education series, 3rd ed., American Institute of Aeronautics and Astronautics, Reston, VA.

Rosa, F. D., Paakki, T., Nurmi, J., Pelosi, M. and Rosa, G. D. (2014) Hand-grip impact on range-based cooperative positioning. **Wireless Commu-**

nications Systems (ISWCS), 2014 11th International Symposium on, 26-29 August 2014, Barcelona. IEEE, pp.728–732.

Saleh, A. and Valenzuela, R. (1987) A statistical model for indoor multipath propagation. **IEEE Journal on Selected Areas in Communications** 5(2):pp.128–137.

Sandeep, A., Shreyas, Y., Shivam Seth, Rajat Agarwal and Sadashivappa, G. (2008) Wireless network visualization and indoor empirical propagation model for a campus WI-FI network. **World Academy of Science, Engineering and Technology** 2.

Schroeder, J., Galler, S., Kyamakya, K. and Kaiser, T. (2007) Three-dimensional indoor localization in non line of sight UWB channels. , **Singapore**. IEEEpp.89–93.

Seeber, G. (1993) **Satellite geodesy: foundations, methods, and applications**. W. de Gruyter, Berlin ; New York.

Serra, A., Carboni, D. and Marotto, V. (2010) Indoor pedestrian navigation system using a modern smartphone. **Proceedings of the 12th International Conference on Human Computer Interaction with Mobile Devices and Services, MobileHCI '10, 07-10 September 2010, New York, NY, USA**. ACM, pp.397–398.

Skulich, M., Bonenberg, L. and Meng, X. (2013) Utilisation of UWB in the mining excavation collapse scenario. **Proceedings of 2nd International Symposium on Deformation Monitoring, 9-11 September 2013, Nottingham, UK**. JISDM.

Skyhook (2014) **Skyhook**. [Online]. Available at: http://www.skyhookwireless.com/products [Accessed 27 November 2014].

Spinella, S. C., Iera, A. and Molinaro, A. (2010) On potentials and limitations of a hybrid WLAN-RFID indoor positioning technique. **International Journal of Navigation and Observation** 2010:pp.1–11.

St-Pierre, M. and Gingras, D. (2004) Comparison between the unscented kalman filter and the extended kalman filter for the position estimation module of an integrated navigation information system. **Intelligent Vehicles Symposium, 2004 IEEE, 14-17 June 2004, Parma, Italy**. IEEE, pp.831–835.

Stirling, R., Collin, J., Fyfe, K. and Lachapelle, G. (2003) An innovative shoemounted pedestrian navigation system. **Proceedings of European navigation conference GNSS, 22-25 April 2003, Graz, Austria**. ENC, pp.110–5.

Subhan, F., Hasbullah, H., Rozyyev, A. and Bakhsh, S. T. (2011) Indoor positioning in bluetooth networks using fingerprinting and lateration approach. **Information Science and Applications (ICISA), 2011 International Conference on, 26-29 April 2011, Jeju Island**. IEEE, pp.1–9.

Suwansantisuk, W., Win, M. and Shepp, L. (2005) On the performance of wide-bandwidth signal acquisition in dense multipath channels. **IEEE Transactions on Vehicular Technology** 54(5):pp.1584–1594.

Tang, S., Kubo, N. and Ohashi, M. (2012) Cooperative relative positioning for intelligent transportation system. **ITS Telecommunications (ITST), 2012 12th International Conference on, 5-8 November 2012, Taipei**. IEEE, pp.506–511.

Tarrio, P., Bernardos, A. M. and Casar, J. R. (2011) Weighted least squares techniques for improved received signal strength based localization. **Sensors** 11(9):pp.8569–8592.

Thompson, B. and Buehrer, R. M. (2012) Characterizing and improving the collaborative position location problem. **Positioning Navigation and Communication (WPNC), 2012 9th Workshop on, 15-16 March 2012, Dresden**. IEEE, pp.42–46.

Titterton, D. H. and Weston, J. L. (2004) **Strapdown inertial navigation technology**. Number 17, 2nd ed., Institution of Electrical Engineers, Stevenage.

Torge, W. and Muller, J. (2012) **Geodesy**. De Gruyter textbook, 4th ed., De Gruyter, Berlin.

Tsai, M.-F., Wang, P.-C., Shieh, C.-K., Hwang, W.-S., Chilamkurti, N., Rho, S. and Lee, Y. S. (2014) Improving positioning accuracy for VANET in real city environments. **The Journal of Supercomputing** .

Tulsyan, A., Huang, B., Bhushan Gopaluni, R. and Fraser Forbes, J. (2013) On simultaneous on-line state and parameter estimation in non-linear state-space models. **Journal of Process Control** 23(4):pp.516–526.

Valentin, R. and Mahesh, M. (2013) HiMLoc: Indoor smartphone localization via activity aware pedestrian dead reckoning with selective crowdsourced WiFi fingerprinting. **2013 International Conference on Indoor Positioning and Indoor Navigation, 28-32 October 2013, Montbeliard, France**. IEEE, pp.658–667.

van den Bos, A. (1994) A cramer-rao lower bound for complex parameters. **IEEE Transactions on Signal Processing** 42(10):pp.2859.

Venkatesh, S. and Buehrer, R. (2006) Multiple-access insights from bounds on sensor localization. **World of Wireless, Mobile and Multimedia Networks, 2006, International Symposium on a, WoWMoM 2006, 26-29 June 2006, Buffalo-Niagara Falls, NY**. IEEE, pp.10–12.

Wang, C.-S., Chen, W.-D. and Chen, C.-L. (2011) Location-based p2p mobile navigation system. **Computer Science and Society (ISCCS), 2011 International Symposium on, 16-17 July 2011, Kota Kinabalu**. IEEE, pp.361–364.

Wang, J. (2002) Pseudolite applications in positioning and navigation: Progress and problems. **Journal of Global Positioning Systems** 1(1):pp.48–56.

Wang, Y., Jia, X., Lee, H. and Li, G. (2003) An indoors wireless positioning system based on wireless local area network infrastructure. **The 6th International Symposium on Satellite Navigation Technology Including Mobile Positioning & Location Services, 22-25 July 2003, Melbourne, Australia**. Global Positioning Systems Society Inc.

Ward, A. (2010) **Ultrawideband (UWB) in-building location systems**, Ubisense.

Ward, A., Jones, A. and Hopper, A. (1997) A new location technique for the active office. **IEEE Personal Communications** 4(5):pp.42–47.

Weimann, F., Abwerzger, G. and Hofmann-Wellenhof, B. (2007) A pedestrian navigation system for urban and indoor environments. **Proceedings of the 20th International Technical Meeting of the Satellite Division of The Institute of Navigation (ION GNSS 2007), 25-28 September 2007, Fort Worth, TX**. ION, pp.1380–1389.

Welch, G. and Bishop, G. (1995) **An introduction to the kalman filter**, University of North Carolina at Chapel Hill. [Online]. Available

at: http://www.cs.unc.edu/ welch/media/pdf/kalman_intro.pdf [Accessed 14 October 2014].

Weninger, B., Bouchain, J., Lukianto, C. and Sternberg, H. (2011) Smartphone-based portable pedestrian indoor navigation: Experiments on visualisation and positioning. **8th Symposium on Location-Based Services, 21-23 November 2011, Vienna**. LBS2011.

Weyn, M. and Schrooyen, F. (2008) A WiFi-assisted-GPS positioning concept. **ECUMICT, 13-14 March 2008, Gent, Beglium**. ECUMICT.

White, C. E., Bernstein, D. and Kornhauser, A. L. (2000) Some map matching algorithms for personal navigation assistants. **Transportation Research Part C: Emerging Technologies** 8(1-6):pp.91–108.

Win, M. and Scholtz, R. (1998) On the robustness of ultra-wide bandwidth signals in dense multipath environments. **IEEE Communications Letters** 2(2):pp.51–53.

Woodman, O. J. and Harle, R. K. (2010) Concurrent scheduling in the active bat location system. **Pervasive Computing and Communications Workshops (PERCOM Workshops), 2010 8th IEEE International Conference on, 29 March-2 April 2010, Mannheim**. IEEE, pp.431–437.

Wymeersch, H., Lien, J. and Win, M. Z. (2009) Cooperative localization in wireless networks. **Proceedings of the IEEE** 97(2):pp.427–450.

Wymeersch, H., Marano, S., Gifford, W. M. and Win, M. Z. (2012) A machine learning approach to ranging error mitigation for UWB localization. **IEEE Transactions on Communications** 60(6):pp.1719–1728.

Yan, J., Tiberius, C. C. J. M., Bellusci, G. and Janssen, G. J. M. (2013) Non-line-of-sight identification for indoor positioning using Ultra-WideBand radio signals. **Navigation** 60(2):pp.97–111.

Yang, C., Nguyen, T., Venable, D., White, M. and Siegel, R. (2009) Cooperative position location with signals of opportunity. **Aerospace & Electronics Conference (NAECON), Proceedings of the IEEE 2009 National, 21-23 July 2009, Dayton, OH**. IEEE, pp.18–25.

Yang, C. and Soloviev, A. (2014) Covariance analysis of spatial and temporal effects of collaborative navigation: Analysis of collaborative navigation. **Navigation** 61(3):pp.213–225.

Yao, J., Balaei, A. T., Hassan, M., Alam, N. and Dempster, A. G. (2011) Improving cooperative positioning for vehicular networks. **IEEE Transactions on Vehicular Technology** 60(6):pp.2810–2823.

Youssef, M. (2008) Indoor localization. ***in* S. Shekhar and H. Xiong (eds), Encyclopedia of GIS**, Springer US, pp.547–552.

Youssef, M. and Agrawala, A. (2005) The Horus WLAN location determination system. **Proceedings of the 3rd international conference on Mobile systems, applications, and services, MobiSys '05, 5 June 2005., Seattle, Washington**. ACM Press, pp.205–218.

Youssef, M. and Agrawala, A. (2008) The horus location determination system. **Wireless Networks** 14(3):pp.357–374.

Zampella, F. J., Jimenez, A. R., Seco, F., Prieto, J. C. and Guevara, J. I. (2011) Simulation of foot-mounted IMU signals for the evaluation of PDR algorithms. **Indoor Positioning and Indoor Navigation (IPIN), 2011 International Conference on, 21-23 September 2011, Guimaraes**. IEEE, pp.1–7.

Zandbergen, P. A. (2009) Accuracy of iPhone locations: A comparison of assisted GPS, WiFi and cellular positioning. **Transactions in GIS** 13:pp.5–25.

Zhao, L., Ochieng, W. Y., Quddus, M. A. and Noland, R. B. (2003) An extended kalman filter algorithm for integrating GPS and low cost dead reckoning system data for vehicle performance and emissions monitoring. **Journal of Navigation** 56(2):pp.257–275.

Zhou, S. and Pollard, J. (2006) Position measurement using bluetooth. **IEEE Transactions on Consumer Electronics** 52(2):pp.555–558.

Zhu, X. and Feng, Y. (2013) RSSI-based algorithm for indoor localization. **Communications and Network** 05(02):pp.37–42.

Zirari, S., Canalda, P. and Spies, F. (2009) Geometric and signal strength dilution of precision (DoP)wi-fi. **IJCSI International Journal of Computer Science Issues** 3.

Ziv, J. and Zakai, M. (1969) Some lower bounds on signal parameter estimation. **IEEE Transactions on Information Theory** 15(3):pp.386–391.

Appendix A

Appendix

A.1 Full data for Section 3.4.2.1

This section shows the Wi-Fi RSS data collected over 24 hours in the three locations indicated.

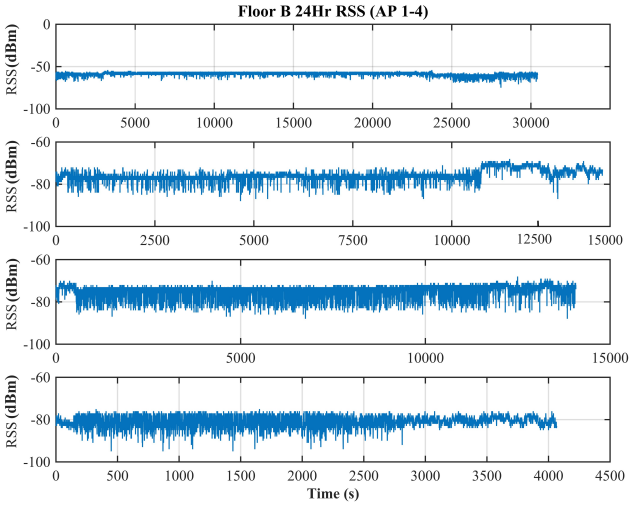

(a) AP1-4

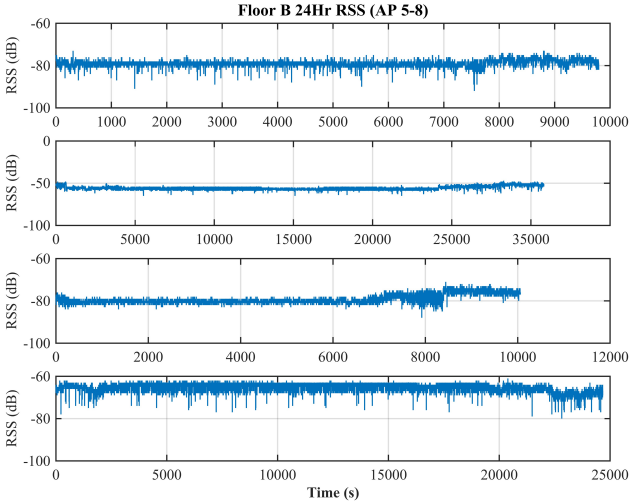

(b) AP5-8

Figure A.1: 24 Hour Wi-Fi RSS data at Location 1

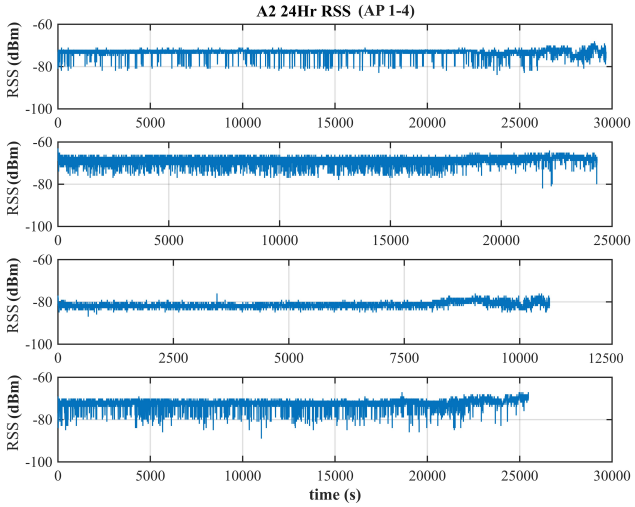

(a) AP1-4

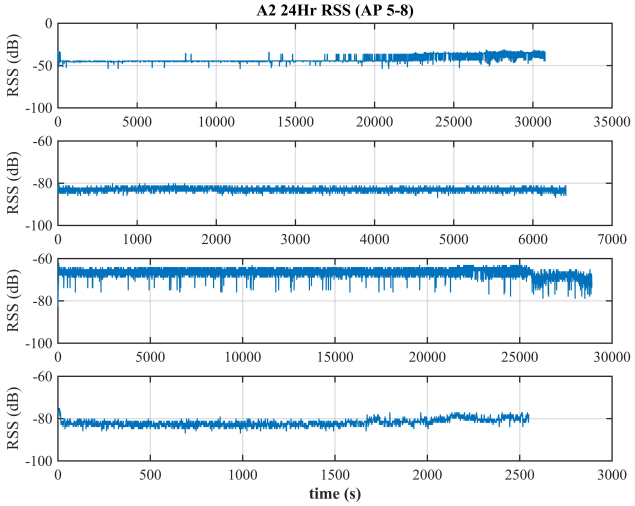

(b) AP5-8

Figure A.2: 24 Hour Wi-Fi RSS data at Location 2

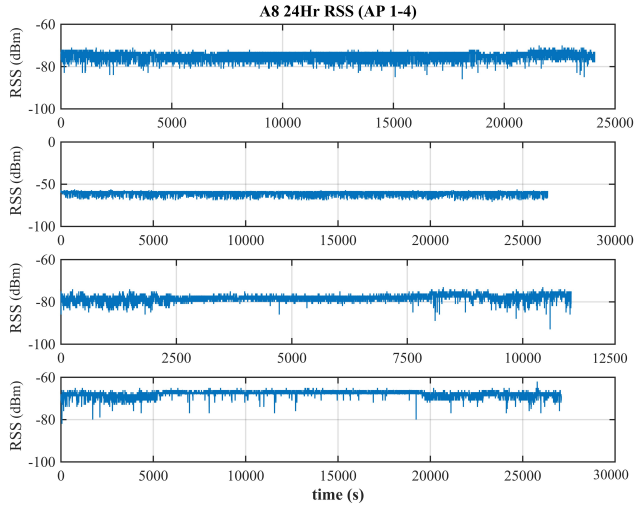

(a) AP1-4

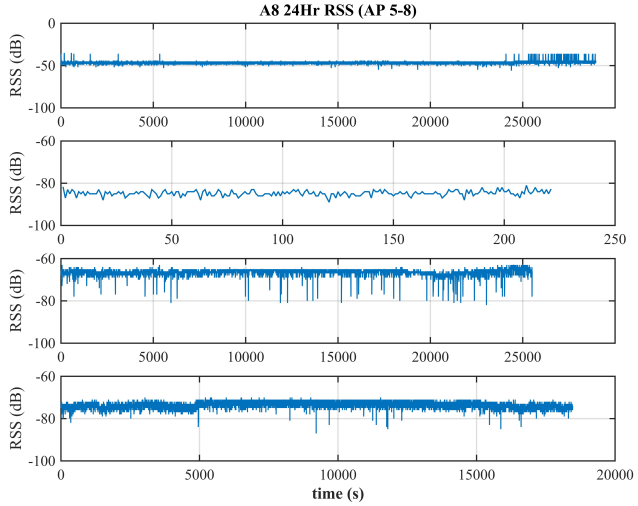

(b) AP5-8

Figure A.3: 24 Hour Wi-Fi RSS data at Location 3

A.2 Mine trial UWB ranging data

This table shows the whole ranging measurement dataset at each receiver location from all BUs.

A.3 Full data for Section 5.5.2.1 Figure 5.16

This section shows the full training data set collected in NGB while walking. The measured RSS along four trajectories is plotted for each AP.

Table A.1: UWB ranging data in mining tunnel

MULocation	Pos 1				Pos 2				Pos 3				Pos 4			
BU No.	97	55	80	84	97	55	80	84	97	55	80	84	97	55	80	84
Dist(m)	19.89	13.75	5.73	61.14	48.61	16.11	30.17	60.70	20.84	12.14	3.38	57.83	20.66	14.51	3.05	52.72
Error (m)	5.13	4.30	0.07	0.61	0.91	0.95	0.30	44.59	0.01	2.62	0.04	0.44	4.28	4.36	0.02	0.48
DS (dB)	33.08	39.28	65.57	41.99	31.34	55.66	41.63	57.89	47.30	65.74	68.48	38.05	32.59	42.21	70.80	40.22
LS (dB)	31.79	36.29	64.92	40.13	30.50	55.09	34.54	57.24	44.89	65.64	68.42	37.57	31.33	40.70	70.33	39.80
ΔDLS (dB)	1.28	2.99	0.65	1.87	0.84	0.57	7.08	0.65	2.41	0.10	0.07	0.48	1.26	1.51	0.47	0.42

MULocation	Pos 5				Pos 6				Pos 7			
BU No.	97	55	80	84	97	55	80	84	97	55	80	84
Dist(m)	28.22	24.93	18.47	37.11	44.92	42.95	38.38	17.19	72.75	71.82	68.07	12.52
Error (m)	Null	8.93	0.13	0.35	Null	9.96	0.38	0.08	60.04	31.45	0.73	0.16
DS (dB)	Null	34.40	56.42	41.59	Null	35.68	51.42	54.94	52.02	46.52	40.02	50.56
LS (dB)	Null	33.71	56.31	41.26	Null	35.31	51.25	54.85	51.91	44.78	39.07	49.47
ΔDLS (dB)	Null	0.69	0.11	0.33	Null	0.37	0.16	0.09	0.11	1.74	0.95	1.08

Note: NLOS cases are Pos1: 97,55; Pos2: 80,84; Pos4: 97,55; Pos6: 97,55; Pos7: 97,55.

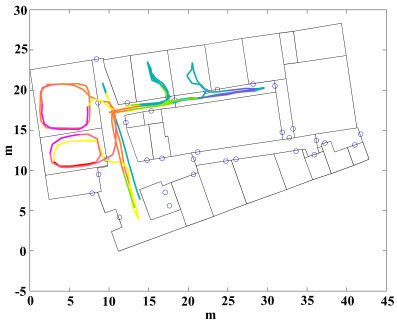

(a) AP4a

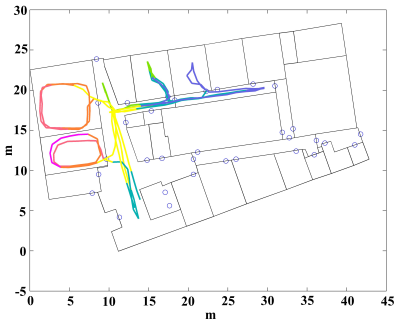

(b) AP4b

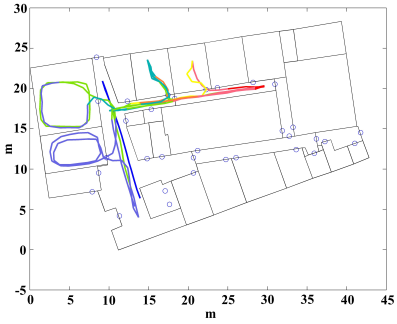

(c) AP5a

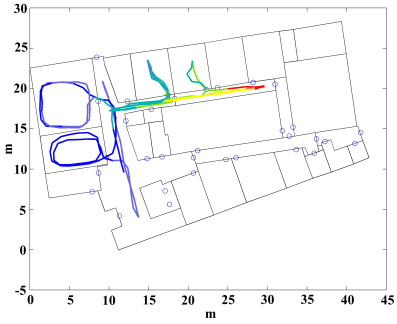

(d) AP5b

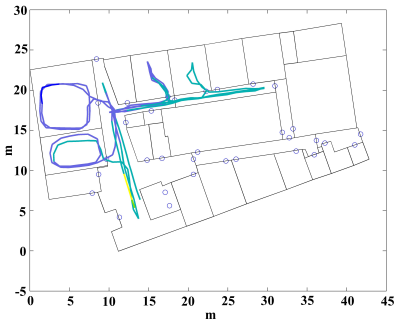

(e) AP7a

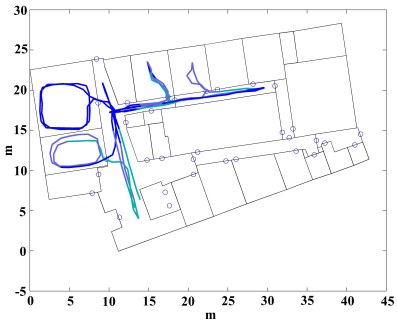

(f) AP7b

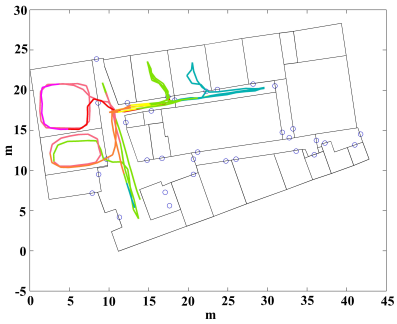

(g) AP8a

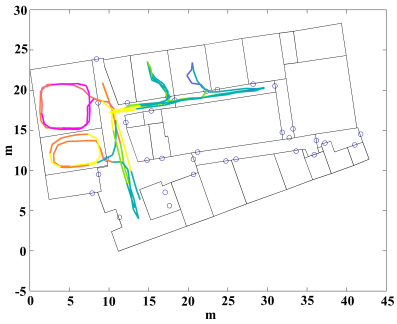

(h) AP8b

Figure A.4: Training data from all AP on Floor A for d-DB1a

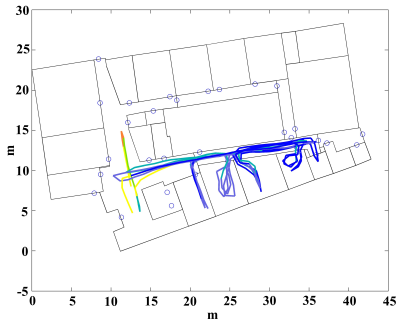

(a) AP4a

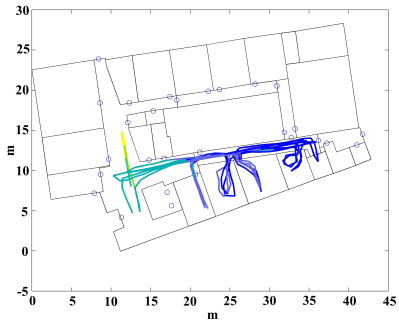

(b) AP4b

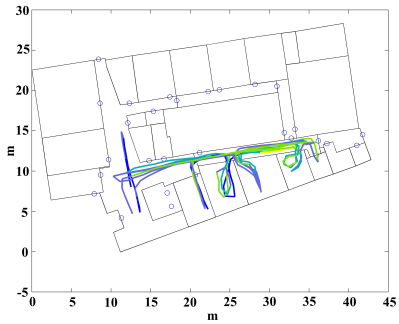

(c) AP5a

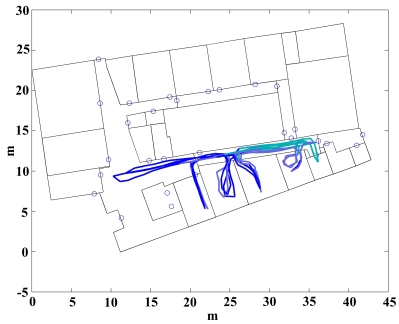

(d) AP5b

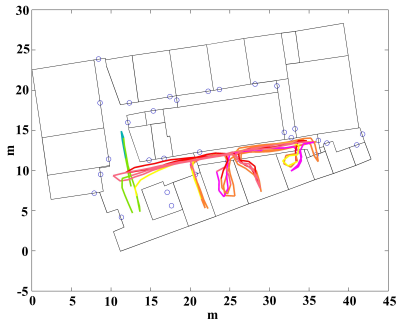

(e) AP7a

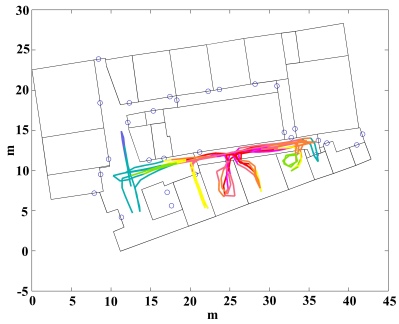

(f) AP7b

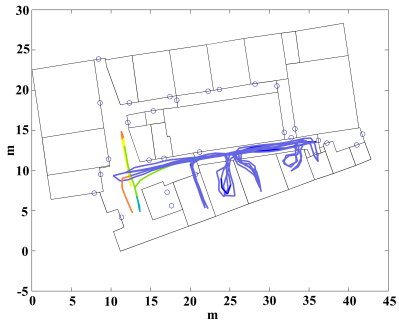

(g) AP8a

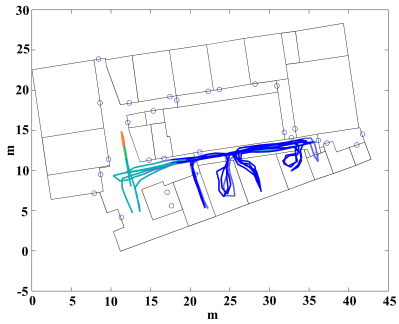

(h) AP8b

Figure A.5: Training data from all AP on Floor A for d-DB1b

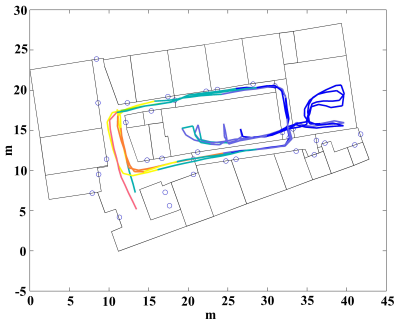

(a) AP4a

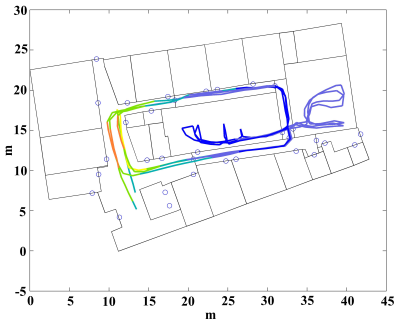

(b) AP4b

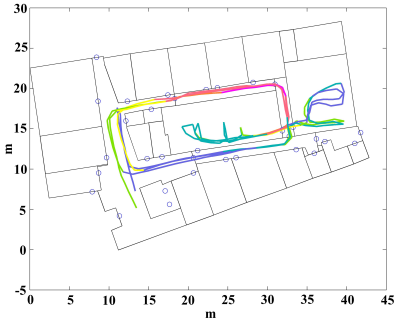

(c) AP5a

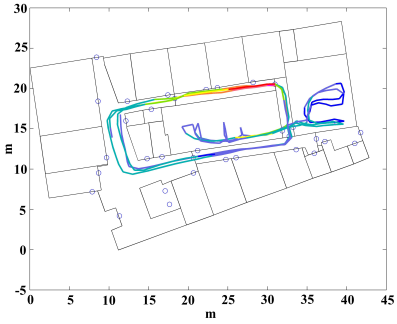

(d) AP5b

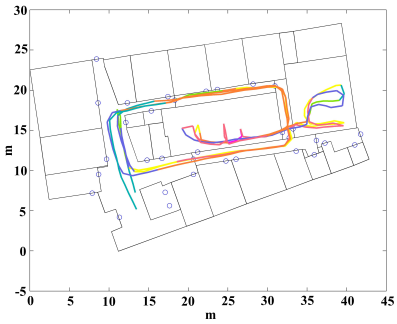

(e) AP7a

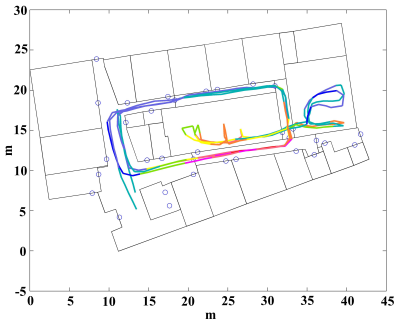

(f) AP7b

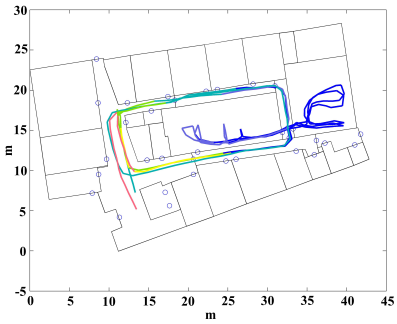

(g) AP8a

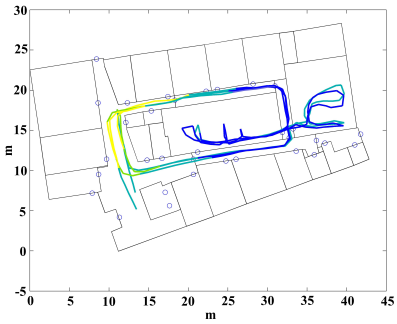

(h) AP8b

Figure A.6: Training data from all AP on Floor A for d-DB2

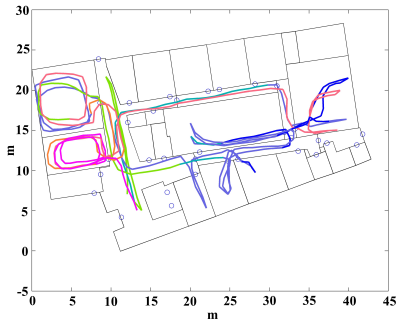

(a) AP4a

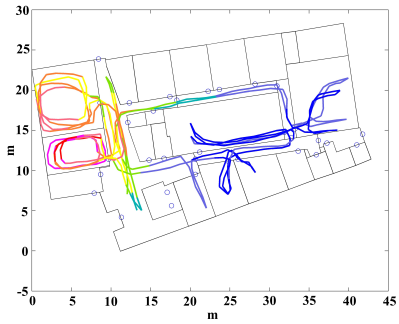

(b) AP4b

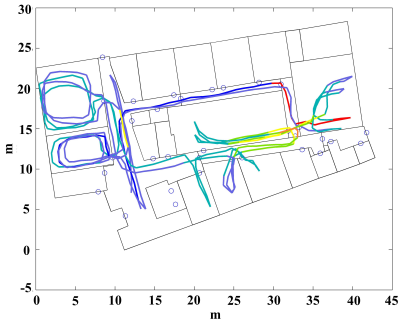

(c) AP5a

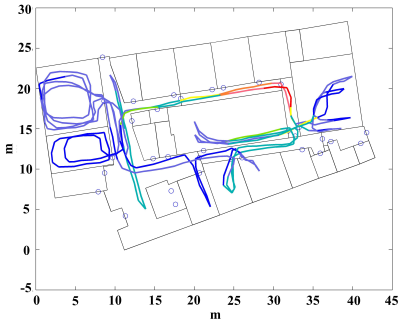

(d) AP5b

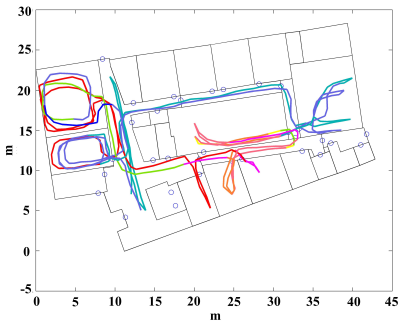

(e) AP7a

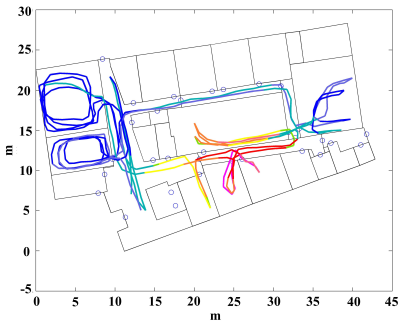

(f) AP7b

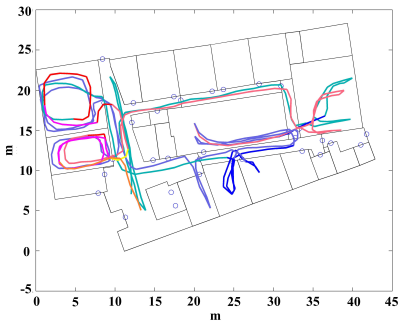

(g) AP8a

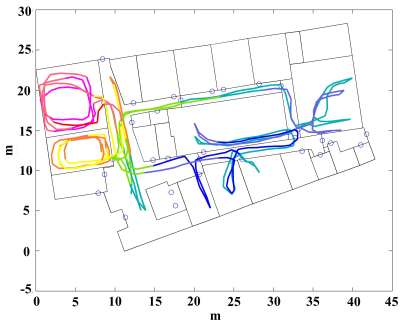

(h) AP8b

Figure A.7: Training data from all AP on Floor A for d-DB3